Universidad de Cantabria

Programa de doctorado en Biología molecular y Biomedicina

RAS SITE-SPECIFIC EFFECTS IN THYROID CANCER

Memoria presentada por

Yaiza García Ibáñez

para optar al título de doctora por la Universidad de Cantabria

Esta tesis se ha realizado bajo la dirección del

Dr. Piero Crespo Baraja

en el laboratorio de Regulación espacial de las señales RAS-ERK en cáncer

en el departamento de Señalización celular y molecular ubicado en el Instituto de Biomedicina y Biotecnología de Cantabria (IBBTEC)

Abril 2019, Santander

Director de tesis	Doctoranda

This thesis work title “RAS site-specific effects in thyroid cancer” has been developed in the Spatial regulation of Ras-ERK signals in cancer laboratory at IBBTEC (Santander) and it has been founded by University of Cantabria with a pre-doctoral scholarship.

During the present work Yaiza García Ibáñez performed one secondment in Deborah Goberdhan laboratory at the University of Oxford thanks to the financial support from University of Cantabria.

Para mi familia

“If everything seems under control, you are not going fast enough”

Mario Andretti

Acknowledgements

Después de cuatro largos y duros años, por fin he logrado acabar la locura que me propuse un día en Barcelona. Pero como bien decía Ray Bradbury "la locura es relativa y depende de quién tiene a quién encerrado en qué jaula" y bien sabe la gente que me conoce que siempre fui de volar cuanto más alto y lejos mejor. Aunque todavía me queda un año para acabar la preciosa carrera de medicina, el capítulo de la tesis ha acabado y no me puedo sentir más feliz. Por supuesto, todo esto no hubiera sido posible sin la ayuda de una larga lista de personas y aunque no puedo nombraros a todos, espero hacer un buen resumen.

En primer lugar, quiero agradecer a mi director de tesis Piero Crespo que me abriera las puertas de su laboratorio a pesar de saber que iba a estar también haciendo medicina a la vez y que, muchas veces, las prácticas, me iban a quitar tiempo de estar en el laboratorio. Por eso tengo que agradecerle que confiara en mí. También quiero darle las gracias por haberme hecho crecer profesionalmente y por haberme enseñado a pensar más críticamente en ciencia. Es un placer haber compartido estos cuatro años de laboratorio y escritura contigo.

I would also like to thank Dr. Deborah Goberdhan from the University of Oxford who gave me the opportunity to explore the exciting world of exosomes, for finding me a place to stay at one of the beautiful colleges, and for being the nicest. Moreover, it would not be fair enough to only say thanks to John. You were incredible welcoming and inspiring. Thanks for caring and getting involve in my project, for your patience teaching me, for all the laughs at the office and the laboratory... you will always make fun of my "august" hahaha… You are one of the nicest and more caring persons I have met in science and I know that your thesis is going to be remarkable. Matt, what can I say about you…thanks for teaching me all I asked you…I know I was a pain in the ass for you and John. Also, for all the good times at the lab, and for the dinners and barbeques at your house and most importantly for not killing me every time I showed you a picture of my dog… or a picture of the dogs I was walking there... You really are an amazing person and I hope that you are happy in your new lab. I would also like to thank Britt for all the dinners, barbeques and table games at her house. I also want to thank Kristie for always being nice to me, it was a shame that you were writing and not that much at the laboratory. Last but not less Shih-Jung Fan. Thanks for always being there every time I had a doubt. You are incredibly smart. Hope you get a PI position soon. You really deserve it.

Hay una persona a la que no puedo dejar de decir gracias durante mi estancia en Oxford…¿Quién me iba a decir que mi primer fin de semana sola en un autobús de viaje a Birmingham iba a conocer a una de las personas más importantes de mi vida? Marina, gracias, gracias y gracias. Gracias por ser de esas amigas que te alegran la vida, que te inspiran y de las que aprendes a cada paso que das. Gracias por esos viajes por Reino Unido, por las cervezas en los fancy places de Oxford y en los que asusta hasta entrar, por los paseos, por las risas y confidencias, en resumen, por hacerme sentir como en casa. Nunca me sentí ni un segundo

sola y eso fue gracias a ti. Me alegro de no haber ido a San Diego solamente por haberme llevado una de esas amigas que sólo puedes contar con los dedos de una mano. Eres un tesoro. A ver cuando organizamos el siguiente viaje.

También me gustaría agradecer a mi primer jefe, Francesc Viñals, la oportunidad que me brindó cuando era simplemente una estudiante de tercero de carrera. Te estaré eternamente agradecida por enseñarme, guiarme y hacerme crecer en esta profesión. Eres excepcional como persona y como científico. También gracias a Oriol Casanovas y a Mariona Graupera por creer en mí desde un primer momento y ayudarme con todas mis aspiraciones. Sin vosotros hoy no estaría aquí.

Otra persona que no quiero dejar de agradecer es Guillem Genové. Gracias por haberme brindado la oportunidad de hacer una estancia después de la carrera en tu laboratorio y por el maravillo año que estuve allí después del máster. Ha sido la mejor experiencia de mi vida.

"Stockholm, du kommer alltid vara min glada plats."

Tian Li and Jonh Hong you are the craziest, in the best way, Asian persons that I know. Thanks for teaching me all about animal work, immunohistochemistry, confocal microscopy and immunofluorescence. I miss the congresses after parties dancing "Sevillanas" with you. Sergey, Marion, Toni… and all the people that was in the MBB at the Karolinska Institutet at that time, thanks for being the best department mates and friends. I miss that times.

No me puedo olvidar de mis chicas…Me ayudasteis en Suecia desde el primer día que nos conocimos hasta hoy mismo. Me habéis enseñado ciencia y vida. Sonia, Patricia, Arancha y Lorena sois lo más bonito que me llevé de Suecia. Por esos momentos en Solna centrum, las cervezas y nachos en S:t Eriksplan, los fika en el trabajo y las cenas en casa. *Tack så mycket.*

Me gustaría también agradecer a todos los profesores del Grado de Medicina que me han ayudado a cambiar de día prácticas, a ofrecerse a tutorías...la Dra. Maite Berciano, el Dr. Miguel Lafarga, la Dra. María Isabel Pérez Núñez, el Dr. Nacho Varela, el Dr. Juan García Lobo, el Dr. Fernando Pazos y a todos los demás. La lista sería interminable. Gracias por ayudarme cuando no teníais la obligación. Os estaré agradecida siempre.

Me faltan también palabras para agradecer a mis compañeros de clase de Medicina. María desde el primer día me brindaste tu amistad. Gracias por pasarme apuntes, por mantenerme informada y por ser una amiga. Fernando muchísimas gracias por ser como eres, por hacerme reír en cada práctica, por preocuparte por mí y por estar siempre dispuesto a ayudar. Eres el mejor amigo que me llevo de la carrera. También quiero agradecer particularmente a Bárbara, Benedetta, Fau, Lisa, Andrea, Dani, Sira, Patri, Ana, nuestro delegado Javi, Celia y todos los

demás por haberme ayudado SIEMPRE que habéis podido, por los apuntes, por las risas en clase y fuera de ellas y por las que nos esperan en nuestra carrera por preparar el MIR y en Tailandia de viaje de fin de carrera. Sois el gran ejemplo de que para brillar no hace falta pisar a nadie. Sin vosotros compaginar las dos cosas hubiera sido imposible.

En la parte más personal no puedo dejar de agradecer a mis amigos, a los de siempre, Zuriñe, Bea, Adhara, Xabi, Ibón, Aitor, Txope, Lauri y las recientes, Janire e Irene. Sin teneros a vosotros en la puerta de casa obligándome a ir a tomar algo para que me diera el aire, creo que no hubiera sobrevivido. Habéis estado en mis mejores y peores momentos y me habéis ayudado a levantarme cuando no veía solución, sois gente extraordinaria. Pasan los años y seguimos y seguiremos estando ahí los unos para los otros. Sois la mejor cuadrilla que hay.

No tengo palabras para agradecer a mis padres, Mº Carmen y Anibal y mi hermano, Imobach, todo lo que han hecho por mí. Por sacrificarse desde que era pequeña para que pudiera cumplir mis sueños. Por estar ahí cada vez que les necesitaba y por hacerme sentir acompañada aunque estuviera a 2780 km de distancia. Esta tesis es para vosotros porque es el fruto de vuestro trabajo también. Espero que estéis igual de orgullosos que yo de vosotros. Me tocó nacer en una gran familia, la mejor. Gracias por vuestra infinita paciencia, por ser como sois, por comprenderme, aguantarme y ayudarme a ser mejor persona cada día. Os quiero mucho.

Carlos, llegaste a mi vida cuando más necesitaba un abrazo. Gracias también por tu infinita paciencia. Creo que en los dos años y medio de relación que llevamos no me has conocido sin tener una obligación ni un solo día y aun así has estado en cado paso que he dado ayudándome en todo lo que podías. Gracias por apoyarme y aguantarme cuando no podía más, cuando estaba insoportable, cuando el agobio me invadía…yo sabía en lo que me metía, pero tú no lo elegiste. Ahora sólo te queda aguantarme el MIR. Ánimo que ya queda poco jajaja. Fuera bromas, gracias por enseñarme a ser mejor persona, a valorar las pequeñas cosas, y sobre todo por hacerme sonreír todos los días. Simplemente soy más yo que nunca y eso te lo debo a ti.

Aunque no sea algo que tenga que entrar en unos agradecimientos de una tesis no quiero dejar de nombrar a mi perro “Ris”. Hace un año y medio que entraste en mi vida para robarme el corazón. Nunca fui una persona apegada o cariñosa. pero tú me has hecho cambiar y ser mejor persona. Me has mantenido cuerda en esta locura y me has dado la desconexión que necesitaba. Me haces sonreír cada mañana.

A mi amiga Sheila. Parece mentira que te conozca hace casi 10 años. Desde el primer año de carrera en Tarragona me abriste las puertas de tu casa. Eres de esas personas que todo el mundo quiere tener en su vida. Gracias por haber estado aguantándome estos últimos meses de escritura. No nos ha venido mal acabar la tesis casi la vez jajaja. Moltes gracies per los

consejos y por ayudarme a desahogarme como nadie más podía. Ets la millor. Y no me animo más con el catalán que te acostumbras jajaja ☺.

No puedo dejarle de agradecer a Gustavo su ayuda con la portada, si no fuera por ti no se que hubiese salido! También gracias a ti y a Bea por haber escuchado más de una vez mis quejas tomando algo.

También quería agradecer a Pilar Santiesteban y Garcilaso Riesco, así como a los miembros de su grupo en Madrid, las discusiones científicas en los meeting anuales de la AECC. Gracias a vosotros he aprendido y me habéis aportado nuevas ideas para mi proyecto.

Por último, quería agradecer a la gente del IBBTEC, tanto los diferentes grupos, los técnicos de laboratorio y la gente de administración. En particular me gustaría agradecer a Charo todo lo que hizo por mí para arreglar todos mis papeles de la estancia y por escucharme. Sé que no tenías por qué y te estaré siempre agradecida.

Me gustaría también agradecer a Maite Berciano y Miguel Lafarga, así como los componentes de su grupo por ayudarme y enseñarme todo sobre microscopia electrónica y por siempre estar dispuestos a una buena discusión científica. Gracias por el ejemplo que dais por vuestro amor a la ciencia. Necesitamos más gente como vosotros.

Quería agradecer también a Fidel, del servicio de microscopía electrónica su ayuda, y a Víctor del servicio de microscopia del IBBTEC por ayudarme con la dificultad de mis muestras y la microscopia confocal.

También querría agradecer al Dr. Ramón merino que me haya prestado su ayuda y me haya dejado invadir su laboratorio de vez en cuando. Pero sobre todo quiero dar las gracias a Iván. Gracias por haberme ayudado a hacer posibles mis experimentos de inmunohistoquímica, a enseñarme la mejor manera de hacer las cosas, por prestarme tu tiempo y materiales. Además de un gran profesional eres una magnífica persona. Ojalá te vaya todo genial.

Me gustaría también agradecer a personas de otros grupos como a Antonio, Jorge, Ruth… por haber hecho los días en el IBBTEC más amenos.

También quería agradecer a algunas personas de mi grupo su ayuda. En primer lugar, quería agradecer a Berta toda su dedicación. Gracias por enseñarme todo lo que sabías y más. Por ayudarme en todo lo que has podido y haberme animado en cada paso. Eres lo mejor que hay en ese laboratorio. Espero que tus metas se cumplan porque te lo mereces de verdad. También me gustaría agradecer a Alicia la alegría que desprende, las ganas de hacer las cosas, su profesionalidad, el haberme ayudado a acabar algunos experimentos de la tesis y por haberme

recibido siempre con una sonrisa. Mucho ánimo con todos tus proyectos. También querría dar gracias a Ana y a Dalia por haber hecho más amenas las horas en el laboratorio y por recibirme siempre con una sonrisa. Sé que os irá todo genial.

También quiero dar gracias a los que me han puesto la zancadilla a cada paso del camino, a los que creían que no lo iba a conseguir, a los que me han criticado y para los que he sido el tema de conversación los último cuatro años. Me he sentido una superestrella de la televisión. De todas maneras, me habéis ayudado a mejorar la seguridad en mí misma, a no depender de la aprobación de nadie para ser feliz, a ayudar a controlar mis impulsos más viscerales y poner una sonrisa allá donde voy. Gracias por el bonito aprendizaje.

RESUMEN:

1. INTRODUCCIÓN:

RAS, es uno de los oncogenes más mutados en cáncer. Hoy en día sabemos que las proteínas RAS de la membrana plasmática están presentes en diferentes microdominios, como en las balsas lipídicas (BL) o en membrana desordenada (MD), y su distribución está modulada por la depalmitoilasa, APT-1. Además, RAS también se localiza en diferentes organelos intracelulares siendo los más comunes el Retículo Endoplasmático (RE) y el Complejo de Golgi (CG) donde también es funcional, contrastando con una idea inicial de una sola fuente de las señales de RAS. Sin embargo, poco se ha sabe de cómo la sublocalización de RAS afectan a su potencial oncogénico.

Es bien conocido que las mutaciones de RAS en distintos tipos de cánceres humanos y el cáncer de tiroides es uno de ellos. De hecho, los carcinomas papilares de tiroides presentan un 26% de mutaciones en RAS, los carcinomas foliculares de tiroides sobre un 40% y los carcinomas anaplásicos, los más agresivos, sobre un 53%. Sin embargo, las mutaciones de RAS también ocurren en un 20-25% de los adenomas benignos tiroideos. En consecuencia, a pesar de que en la última década se ha realizado un esfuerzo considerable en asociar la presencia de RAS con el manejo clínico de los nódulos tiroideos y del cáncer de tiroides. Sin embargo, la gran mayoría de los nódulos tiroideos positivos para RAS son clasificados como indeterminados. Además, debido al papel incierto de RAS en la evolución clínica del cáncer de tiroides, ha sido difícil usar las mutaciones de RAS para ayudar al manejo de estos tumores. En consecuencia, nuevos conceptos son necesarios para descartar la malignidad y predecir la agresividad en los cánceres de tiroides ya que las nuevas guías clínicas se están encaminando a aproximaciones más conservadoras.

Además, en los últimos años ha surgido una nueva faceta de RAS en cáncer, ya que se ha visto que RAS tiene un papel importante en la biogénesis, mantenimiento, secreción y modificación del contenido de los exosomas. Los exosomas son vesículas extracelulares que tienen diferentes tipos de contenido, incluyendo proteínas, mRNA, miRNA, DNA y nlRNA. Estas vesículas afectan fundamentalmente la evolución de diferentes tipos de cáncer como melanoma y colorectal entre otros afectando al crecimiento tumoral, a la angiogénesis, la invasión y la metástasis.

Por tanto, hipotetizamos que el cambiante comportamiento de RAS en el cáncer de tiroides es debido a los efectos diferenciales de RAS en función de su diferente localización en la célula.

2. OBJETIVOS:

-Estudiar cómo RAS en sus diferentes sublocalizaciones contribuye al cáncer de tiroides

-Encontrar nuevos marcadores para descartar malignidad en los nódulos de tiroides mutados en RAS y determinar agresividad en cáncer de tiroides.

- Elucidar la relevancia de los exosomas en la carcinogénesis de tiroides mediada por RAS en sus diferentes sublocalizaciones.

3. MATERIALES Y MÉTODOS:

Para explorar el papel de las sublocalizaciones de RAS en el cáncer de tiroides elegimos las células PCCL3 que no tienen mutaciones conocidas, y las transfectamos con vectores de pCEFL hemaglutinina (HA) que contienen las señales diana M1, LCK, CD8α y KDELr unidas a H-, N- o K-RASv12. Éstas señales dirigen a RAS a retículo endoplásmico, balsas lipídicas, membrana desordenada y aparato de Golgi, respectivamente. Además, usamos el modelo de metástasis espontanea del embrión de pollo para analizar los efectos de estas células en el crecimiento tumoral y metástasis y determinar los efectos de diferentes proteínas. Los exosomas fueron aislado por cromatografía de exclusión por tamaño y sus efectos fueron probados *in vitro* y en el modelo de pollo.

4. RESULTADOS Y DISCUSIÓN:

Para analizar los efectos de las sublocalizaciones de RAS en el cáncer de tiroides utilizamos las células PCCL3 expresando H- o N-RASv12 en retículo endoplasmático (RE), balsas lipídicas (BL), membrana desordenada (MD) y complejo de Golgi (CG). Para K-RASv12 RE y MD. Cuando analizamos sus efectos *in vitro* observamos que no había diferencias entre las sublocalizaciones de RAS en la proliferación, pero sí en la migración, induciéndola RAS en MD y GC. Además, RAS era capaz de inducir apoptosis desde todas las localizaciones celulares excepto desde BL y más notablemente desde CG, lo que puede estar relacionado por los efectos de RAS en la inestabilidad genómica y su posible inducción de una catástrofe mitótica.

Al mirar el papel de RAS *in vivo* en el modelo de metástasis del embrión de pollo, vimos que los tumores más pequeños, generados por RAS en MD y CG, eran los más metastáticos. Además, para confirmar que esto también sucedía en líneas celulares con H-RAS endógeno mutado analizamos la locación de RAS en BL y MD, los cuales exhibieron efectos opuestos, en las células tumorales de cáncer anaplásico de tiroides C643 y HTH83. Fuimos capaces de ver que las células C643 tenían H-RAS en BL y las células HTH83 en MD y que su localización estaba modulada por los niveles de APT-1. Cuando se determinó el potencial tumoral de estas

células en el modelo de pollo pudimos observar que las células HTH83, con H-RAS mutado, esta vez endógeno, en MD, generó tumores más pequeños con mayor potencial metastático en comparación con las células C643. Además, la alteración de APT-1 fue capaz de promover la translocación de H-RAS, modificando los efectos en crecimiento tumoral y metástasis de las dos líneas celulares. Al ver que los niveles altos de APT-1 estaba relacionado con la localización de H-RAS en BL que exhibe mayores tumores, pero con poca capacidad de colonización a distancia, quisimos ver qué sucedía en tumores de pacientes. Para ello usamos la herramienta cBioPortal en la que seleccionamos una base de datos de mutaciones y alteraciones en niveles de mRNA y proteína de 507 pacientes con carcinomas papilares de tiroides. En este caso no encontramos ninguna co-ocurrencia entre las mutaciones de H-RAS y APT-1 aunque todos los pacientes con amplificaciones o ganancias de función en APT-1 exhiben un 100% de supervivencia. Esto sugiere que incluso la modulación de RAS *wt* por APT-1 podría estar ejerciendo un efecto en el proceso carcinogénico. Además, al analizar también alteraciones de APT-1 en melanoma, en el cuál si existían co-ocurrencias con mutaciones en H-RAS, observamos un aumento de supervivencia de casi un año en esos casos con altos niveles de APT-1 mientras que al mirar los efectos de su deleción o perdida de expresión observamos lo contrario. Por tanto, esto sugiere que APT-1 puede ser un buen marcador pronóstico en cáncer de tiroides y melanoma.

Al observar inmunohistologicamente los tumores generados por RAS en sus diferentes sublocalizaciones observamos que RAS en RE y BL, las localizaciones en las que RAS generaba los tumores más grandes, pero con menos capacidad de metastatizar, parecían presentar gotas lipídicas, lo cual confirmamos usando una tinción de red oil. Además, fuimos capaces de relacionar el acúmulo de lípidos con los niveles de VEGF-B, un miembro de la familia de VEGF con poca capacidad angiogénica. Cuando añadimos VEGF-B a los tumores formados por las otras sublocalizaciones de RAS, MD y CG, observamos que esta proteína era capaz de aumentar el tamaño tumoral y disminuir la metástasis. Por tanto, VEGF-B al estar presente a altos niveles en los tumores menos metastáticos podría ser un posible marcador de invasividad en tumores de tiroides.

En cuanto a los efectos de las sublocalizaciones de RAS en la biogénesis, secreción y cargo de los exosomas, fuimos capaces de determinar que las sublocalizaciones de RAS pueden modular diferencialmente el tamaño, la cantidad y el cargo de los exosomas. Sorprendentemente hemos demostrado que los exosomas secretados por células con RAS en MD y CG son capaces de transferir su potencial metastático a otras células lo que sugiere que podrían estar modulando la intravasación, la supervivencia celular en el torrente sanguíneo y/o el nicho pre-metastático.

5. CONCLUSIONES:

En resumen, hemos encontrado que el tamaño de los tumores generados por H-RAS y N-RAS en sus diferentes sublocalizaciones no se correlaciona con su potencial metastático. Además, hemos visto que la modificación de los niveles de APT-1 afecta la proliferación y el potencial metastático de los tumores de tiroides al regular la presencia de RAS en los diferentes microdominios de la membrana plasmática.

Por otro lado, los tumores formados por H-RAS en RE y BL presentan gotas lipídicas cuya acumulación se relaciona con los niveles de VEGF-B el cuál es capaz de aumentar el tamaño tumoral, pero disminuir la metástasis. Debido a ello, tanto APT-1 como VEGF-B podrían ser propuesto como posibles marcadores a estudiar para determinar la posibilidad de colonización a distancia.

Además, los exosomas secretados por células expresando H-RASv12 en sus diferentes localizaciones celulares son diferentes en tamaño, se secretan en diferente cantidad, presentan diferentes marcadores y presentan efectos diferenciales en proceso carcinogénico.

Contents

List of figures

List of tables

Abbreviations

AKT	Protein Kinase B
ALIX	ALG-2-Interacting Protein X
ALK	Anaplastic Lymphoma Kinase
APS	Ammonium Persulfate
APT1 / APT2	Acyl Protein Thioesterase 1 or 2
ARF	ADP-Ribosylation Factor
ARID	AT- rich interacting domain-containing proteins
AT	Acyl thioesterases
ATA	American Thyroid Association
ATC	Anaplastic Thyroid Carcinoma
DNA	Deoxyribonucleic Acid
BSA	Bovine Serum Albumin
CAM	Chorioallantoic Membrane
CCDC6	Coiled-Coil Domain Containing 6
CMFDA	5-chloromethylfluorescein diacetate
CUL3 E3	Cullin 3 E3
DAB	Diaminobenzidine
DHHC MOTIF	Aspartate-Histidine-Histidine-Cystein
DM	Disordered Membrane
DMEM	Dulbecco´s Modified Eagle Medium
DNA	Deoxyribonucleic acid
EGF	Epidermal Growth Factor
EGFR	Epidermal Growth Factor Receptor
EIF1AX	eukaryotic translation initiation factor 1A in chromosome X
EMT	Epithelial-Mesenchymal Transition
eNOS	Endothelial Nitric Oxide Synthase
ER	Endoplasmic Reticulum
ESCRT	Endosomal Sorting Complex Required for Transport
EVs	Extracellular Vesicles
EXOs	Exosomes
Gαi	Inhibitory G-protein alpha subunit
G	Gauge
GAPs	GTPases-Activating Proteins

GC	Golgi Complex
GDNF	Glial Derived Neurotropic Factor
GDIs	Guanosine Nucleotide Dissociation Inhibitor
GEFs	Guanine-Nucleotide-Exchange factors
GFP	Green Fluorescent Protein
GRB2	Growth-factor-Receptor-Bound protein 2
H_2O_2	Hydrogen Peroxide
HCL	Hydrochloric Acid
H-RAS	Harvey-Rat Sarcoma
HRP	Horseradish Peroxidase
HVR	Hypervariable Region
ICMT	Isoprenyl-Carboxymethyl Transferase
IHC	Immunohistochemistry
ILVs	Intraluminal Vesicles
K-RAS	Kirsten-Rat Sarcoma
LB	Lysogeny Broth
LCFAs	Long-Chain Fatty Acids
LR	Lipids Raft
LZTR1	Leucin Zipper like Transcription Regulator 1
MAPK	Mitogen Activated Protein Kinase
MIF	Migration Inhibitory Factor
MLBs	Multilamellar bodies
mRNA	messenger Ribonucleic Acid
mTOR	Mammalian Target Of Rapamycin
MVBs	Multivesicular Bodies
MVs	Microvesicles
NCOA4	Nuclear Receptor Co-Activator 4
NIS	$2Na^+/I^-$ symporter
N-RAS	Neuroblastoma-Rat Sarcoma
NTRK	Neurotrophic Receptor Tyrosine Kinase
FTC	Follicular Thyroid Cancer
O/N	Over-Night
PAT	Palmytoil Acyltransferase
PAX8/*PPARγ*	Paired box gene 8 / Peroxisome proliferator-activated receptor gamma-1

PBS	Phosphate-Buffered Saline
PCNA	Proliferation Cell Nuclear Antigen
PCR	Polymerase Chain Reaction
PDE6δ	Delta subunit Phosphodiesterase 6
PDK1	Phosphoinositide-Dependent Kinase 1
PDTC	Poorly Differentiated Thyroid Carcinoma
PFA	Paraformaldehyde
PH	Pleckstrin Homology
PI3K	Phosphatidylinositol-3 Kinase
PIP_2	Phosphatidylinositol (4,5)-bisphosphate
PIP_3	Phosphatidylinositol (3,4,5)-trisphosphate
PKC	Protein Kinase C
PLCε	Phospholipase C Epsilon
PM	Plasma Membrane
PMN	Premetastatic Niche
PPT1	Palmitoyl Protein Thioesterase 1
PTC	Papillary Thyroid Cancer
PTEN	Phosphatase and Tensin Homolog
PTH	Parathyroid Hormone
PTPRκ	Tyrosine Phosphatase Receptor κ
RAB	Ras-like proteins in brain
RAD	Ras Association Domain
RAI	Radioactive Iodine
RAL	RAS-Like
RAN	Ras-like nuclear
RAP	RAS Proximal
RBD	Ras Binding Domain
RCE1	RAS Converting Enzyme 1
RET/PTC1/3	Rearranged during transfection / Papillary carcinoma type I and III
RHO	Ras homologous
RIN1	RAF Interactor 1
RIN	Ras like protein In Neurons
RT	Reverse Transcription
RTK	Receptor Tyrosine Kinase

siRNAs	Small Interfering RNAs
SNAP-23	Synaptosomal-Associated Protein 23
SNAREs	N-ethylmaleimide-sensitive Factor Attachment Protein Receptors
STAT3	Signal Transducer and Activator of Transcription 3
T4	Thyroxine
TBS	Tris Buffered Saline
TBS-T	Tris Buffered Saline-Tween
TCGA	Cancer Genome Atlas of the Thyroid
TDEs	Tumor Derived Exosomes
TEMED	Tetramethylethylenediamine
TERT	telomerase reverse transcriptase
TIAM1	T Cell Lymphoma Invasion and Metastasis 1
TGF	Transforming Growth factor
TSG101	Tumor Suspectibility 101
TSH	Thyroid Stimulating Hormone
TTF1	Thyroid Transcription Factor
VEGF-A	Vascular Endothelial Growth Factor -A
VEGF-B	Vascular Endothelial Growth Factor -B

1. Introduction

1. INTRODUCTION

1.1 Ras superfamily of small GTPases

The Ras superfamily are small G proteins of approximately 21 kDa that share a main biochemical feature that defines them. This property is their ability to act as molecular binary switches cycling between an active GTP bound form and inactive GDP-bound form, being able to couple extracellular signals to intracellular signaling networks.

The research about these proteins began in 1964 when Jennifer Harvey discovered that a leukemia virus isolated from a rat, was able to produce sarcomas in young rodents (1). The oncogene behind the tumorigenic activity was named Harvey *RAS*, from "Rat sarcoma", nowadays known as H-*RAS*. Moreover, in 1974 another sarcoma virus, the Kirsten murine sarcoma virus, was identified and named K-*RAS (2).* In addition, by 1983, N-*RAS* was described as the third member of the *RAS* gene family after being isolated from two human sarcoma cells lines (3, 4). These proteins were found to have intrinsic capacity to bind guanine nucleotides and were reported to be GTPases. It was also described that their ability to maintain their GTP-bound state was higher in the proteins encoded by transforming alleles than normal ones and H-*RAS* was isolated as the first oncogene in a bladder cancer cell line (5-8). In 1993, 50 proteins similar to RAS had been described and they were all reported to have key functions regulating processes such as proliferation and cell cycle control (9). Nowadays, in humans, there are more than 160 members of the Ras superfamily identified. Conserved orthologs are found throughout the evolutionary scale (10).

The Ras superfamily is divided, depending on their sequence and function, into five major subfamilies: Ras, Rho, Rab, Ran and Arf **(Fig.1.1)**. (From now on lowercase will be used to refer to the families, capital letter will denote specific proteins and italics will be used to refer to genes).

Ras family is composed by 36 members that regulate multiple cytoplasmic signaling networks and control cell proliferation, survival and differentiation among other cellular functions (11). (it will be further described in section 2)

Rho (Ras homologous) family has 20 members being RHOA, RAC1 and CDC42 the best studied. They mainly regulate the actin cytoskeleton, regulating cell movement, shape as well as vesicular mediated processes. RHOA is particularly involved in focal adhesion dynamics and mainly regulates actomyosin, RAC1 controls lamellipodium assembly and membrane ruffing, and CDC42 promotes the formation of actin structures such as filopodia and micro spikes. However, they all have been implicated in a wide variety of function such as regulation of phagocytosis or polarity regulation. Moreover, RHO GTPases mutations have been proposed to be pro-tumorigenic since they are linked to cell survival, metabolism control as well as with metastasis (11-13).

Rab (Ras-like proteins in brain) subfamily is the largest one, with 61 members. RAB GTPases are key regulators of membrane endocytic and secretory processes and membrane budding by controlling actin- and tubulin-dependent vesicle movement and membrane fusions (11, 14).

Ran (Ras-like nuclear) family is involve in nucleus-to-cytosol protein trafficking and its function, unlike the others depends, on the spatial gradient of its active form (11).

Arf (ADP-ribosylation factor) subfamily is involved in coated vesicles biogenesis, vesicular trafficking and actin regulation (11).

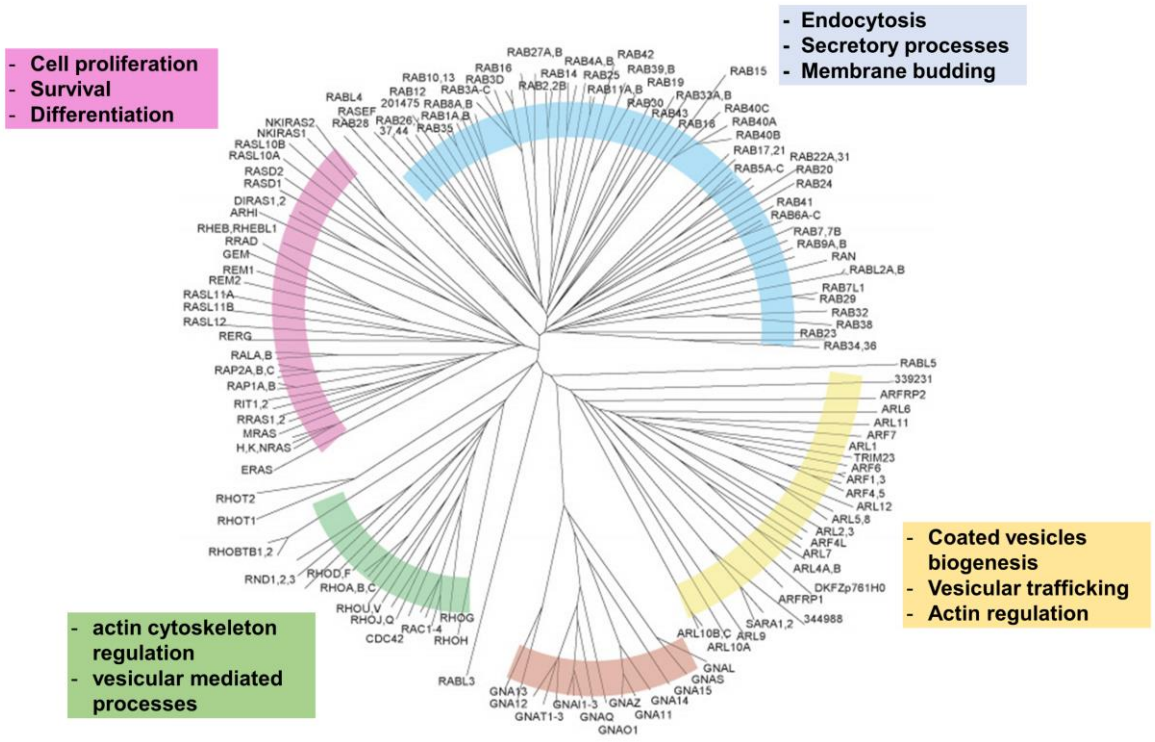

Figure 1.1: Cladogram of human Ras superfamily members and functions. Subfamilies of proteins are indicated by colored arcs: RAS (pink), RHO (green), Gα (brown), ARF (yellow), and RAB (blue). Adapted from Colicelli J. Human RAS superfamily proteins and related GTPases. *Sci STKE.* 2004;2004(250):RE13. Published 2004 Sep 7. doi:10.1126/stke.2502004re13

1.1.1 STRUCTURE AND FUNCTION OF RAS GTPASES

RAS small GTPases act as biological switches cycling between GTP-bound and GDP-bound state affecting almost all cellular processes **(Fig 1.2 B)**. Their protein structure is conserved among all Ras subfamilies, as well as other GTPases. They share a five α-helix surrounding a six-stranded β-sheet structure in a Rossman-type fold structure (15, 16). The structure of H-RAS p21 protein in the triphosphate conformation (17) shows that is made up of five conserved motifs (G1-G5): The G1 motif (I), GXXXXGKS/T, containing the P-loop that is the phosphate binding site. This motif also binds to the purine nucleotide. The G2 motif E, T,

is the major effector binding component. The G3 motif (III), DXXGQ/H/T, is the one that recognize the nucleotide-related Mg^{2+}; G4 motif (IV), T/NKXD, brings close the guanine ring and the G5 motif (V), C/SAK/L/T, makes indirect associations with the guanine nucleotide (11) (18) **(Fig. 1.2 A)**. However, despite this common structure some members of the family exhibit some differences in their structure. For instance, ARF proteins present additional N-terminal sequences (19), whereas RAN has them in the C-terminus determining conformational changes during the GDP/GTP binding cycle (20).

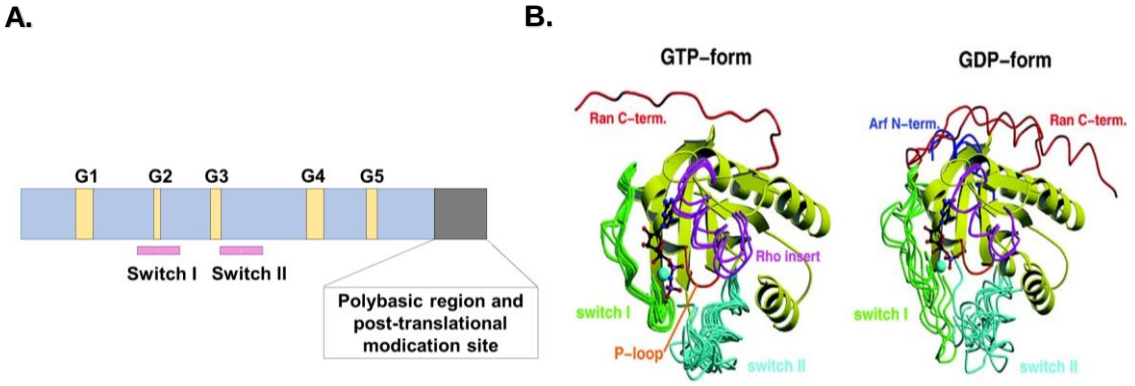

Figure 1.2: Ras family protein sequence and structure. (A) Ras superfamily functional domains representation. The core G-domains, corresponding to RAS residues 4-166 contains the nucleotide binding domains (G1-G5) and the switch regions. **(B)** Small GTPases crystal structure in their active GTP-form and inactive GDP-form. Figure adapted from (21).

Small GTPases activity depends on their GTP/GDP binding status. When they bind GDP they are in their inactive form and are unable to trigger any signaling pathway. To become activated they need to exchange GDP for GTP. This causes a conformational change in their *switch I* (30-40 residues) and *switch II* (60-76 residues) regions allowing the repositioning of the terminal extension enabling regulator/effector interactions (22).

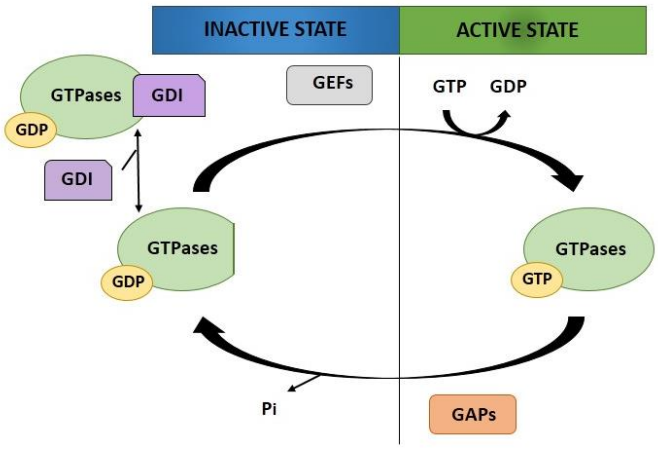

Figure 1.3: Small GTPases activation cycle. RAS proteins function as molecular switches, cycling between the GDP-bound ('off') and the GTP-bound ('on') states and exist predominantly in the GDP-bound state. Upon exogenous stimulation, GEFs catalyze the exchange of GTP for GDP. RAS proteins are inactivated by GAPs, which accelerate the cleavage of the terminal inorganic phosphate (P_i) group of GTP(23).

This cycle is regulated by Guanine-Nucleotide-Exchange factors (GEFs) that promote formation of the active, GTP-bound form (24), and GTPases-Activating Proteins (GAPs), which enhance the intrinsic GTPase activity promoting hydrolysis of GTP, leading to the inactive GDP-bound form (25). Moreover, there is another group of proteins, called Guanosine Nucleotide Dissociation Inhibitors (GDIs), which kidnap GTPases in the cytosol avoiding them to anchor to the membrane and to bind to different effectors (26) **(Fig. 1.3)**.

1.2 RAS family

1.2.1 GENERAL OVERVIEW AND DESCRIPTION

Besides RAS classical proteins (H-RAS, N-RAS, K-RAS4A and K-RAS4B), R-RAS (R-Ras2/TC21, R-RAS3/M-RAS) is the only one with transforming capability. There are several non-transforming members such as RAS-Like (RAL) proteins (RAL-A y RAL-B) and RAS Proximal (RAP) proteins (RAP1A, RAP1B, RAP2A and RAP2B), RHEB, RAS like protein In Neurons (RIN) and RAS like protein in tissue (RIT) (27). This thesis will only be referring to the classical RAS proteins (H-Ras, N-Ras, K-Ras4A and K-Ras4B).

These proteins are encoded by three different genes (*H-RAS, N-RAS* and *K-RAS*) located in chromosome 11 (11p15.1-p15.5), chromosome 1 (1p22-p32) and chromosome 12 (12p12.1-p-terminal) respectively. All of them are composed by four coding exons and a non-codifying fifth one, giving rise to the different RAS proteins. For *K-RAS* there is an exon four alternative splicing that encodes for two different K-RAS isoforms (K-RAS4A and K-RAS4B) (28, 29). K-RAS4B is a 188 amino acid protein whereas the other isoforms are 189 amino acids. These proteins, as they are GTPases, are comprised of two main domains: the G domain and the hypervariable region (HVR). In the N-terminus the G domain (residues 1–166) presents an effector lobe (residues 1–86) and an allosteric lobe (87–166). RAS effector lobe is crucial for the interaction with its effectors such as RAF, PI3K and RalGEFs, whereas the allosteric lobe allows intra-protein communication, where it connects the active site of the effector lobe to membrane-interacting residues (22, 30-32). When RAS is activated, conformational changes occur in the switch I (aa 30–40) and switch II (aa 60–76) regions to allow for effector interactions and signalling **(Fig. 1.2 B)**. The RAS proteins, share 90% identity in their G domain, with conserved structural and biochemical properties (22). More importantly, each protein has a unique HVR **(Fig. 1.4)** containing specific sites for posttranslational modifications resulting in differences in membrane trafficking, localization and function (32, 33).

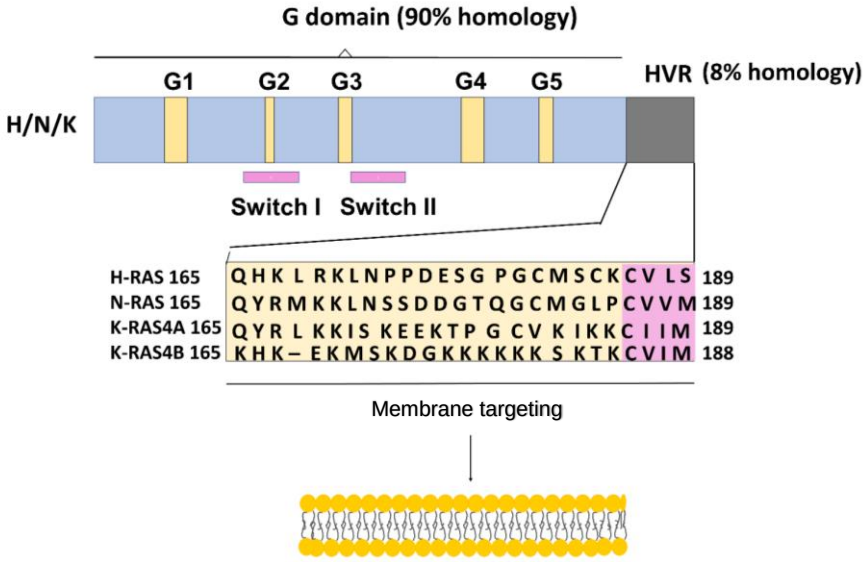

Figure 1.4: Divergent C-terminal membrane targeting domains in RAS proteins. The four RAS proteins: N-RAS, H-RAS, K-RAS4A and K-RAS4B share a conserved core domain ('G-Domain') which confers GTPase and effector binding. However, they diverge in C-terminal where they present a hypervariable region ('HVR'), that contains different membrane targeting signals such as a (CAAX) motif (denoted by pink box).

1.2.2 RAS POSTTRANSLATIONAL MODIFICATIONS

RAS proteins are all synthesized on free polysomes, as hydrophilic proteins that remain scattered throughout the cytoplasm. However, it is well known that these proteins need to be anchored to different membranes by their carboxy-terminus in order to be active. Therefore, a variety of posttranslational modifications in their HVR are necessary in order to increase their hydrophobicity and binding to different types of membranes (33).

All nascent RAS isoforms are firstly farnesylated at Cysteine (C)186 (C185 in K-Ras4B), in the cytosol on their CAAX motif (where C is cysteine, A is an aliphatic amino acid, and X is serine or methionine) by farnesyl protein transferases (34) forcing them to transiently accumulate on the cytoplasmic face of the Endoplasmic Reticulum (ER). They are further modified at the ER by RAS Converting Enzyme 1 (RCE1), a protease that eliminates the last three amino acids, AAX (35) to form, a carboxy-terminal S farnesyl cysteine carboxylmethyl ester. Also, at the ER, the Isoprenyl-Carboxymethyl Transferase (ICMT) adds a carboxymethyl group on the C-terminal cysteine residue (36-38). This allows RAS to weakly bind the plasma membrane, but it also needs a second modification to strengthen membrane interactions that it is takes place at the Golgi Complex (GC). It is been proposed that RAS, once it leaves the ER, enters into the cytoplasmic fluid phase, rebinding then to Golgi membranes (39).

The second mandatory anchor component results of the mono-palmitoylation, that is the addition of palmitate, a satured (acyl) fatty acid, to N-RAS at C181 and K-RAS4A at Cys180, or a bi-palmitoylation of H-RAS at C181 and C184, through the covalent attachment of a 16-carbon palmitoyl chain (40). RAS palmytoilation is catabolized by a Palmytoil Acyltransferase (PAT) localized at the GC, which consist in a heterodimeric complex formed by DHHC9 and GCP16, transmembrane proteins that have a conserved aspartate-histidine-histidine-cysteine (DHHC) motif **(Fig. 1.5)**. However, the possibility that some of the other 20 members of the DHHC family can perform this task at other sublocations cannot be discarded. K-RAS4B, the most prevalent splice form of K-RAS has a polybasic region (residues 175-180) that allows it to bind to membranes enriched acidic phospholipids (41-44).

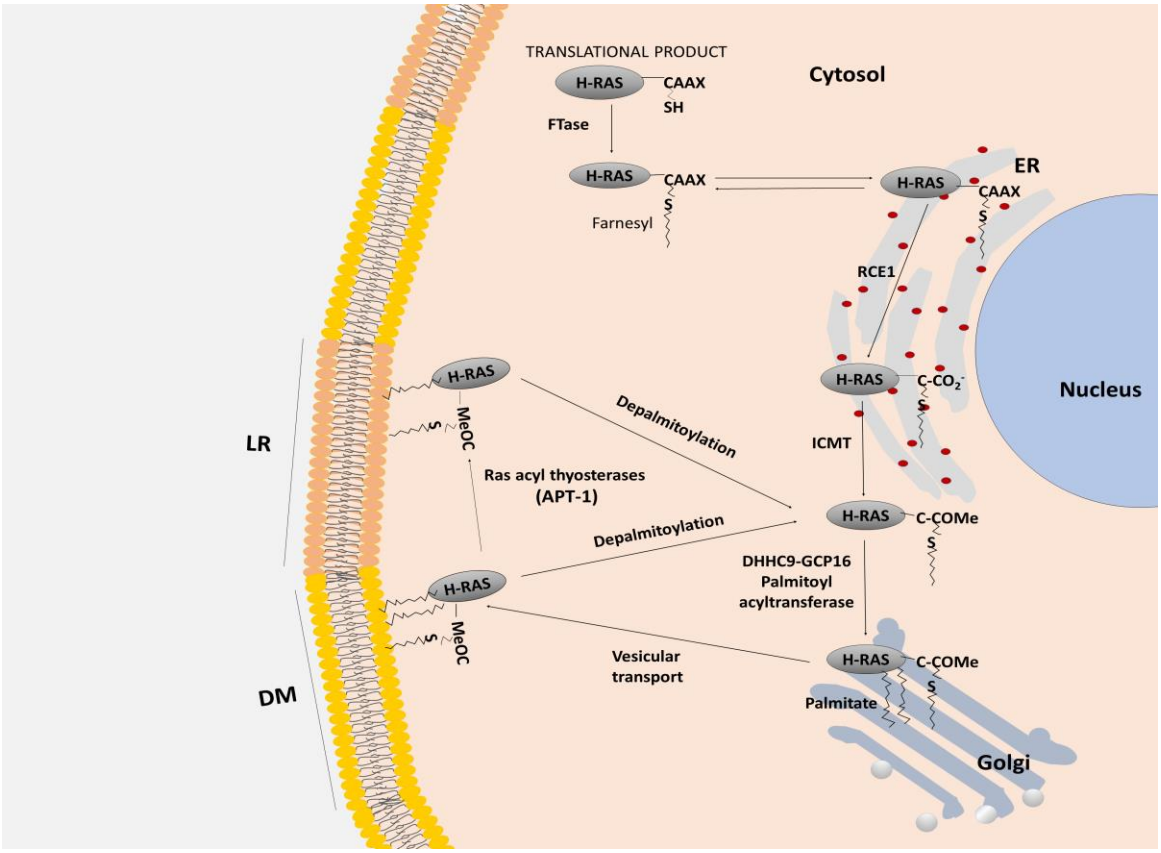

Figure 1.5: H-RAS posttranslational modifications and palmitoylation cycle. H-RAS is synthesized on cytosolic free polysomes as a globular hydrophilic protein. Nascent RAS is farnesylated by a farnesyltransferase (FTase) in the cytosol and transported to membranes of the endoplasmic reticulum (ER) where it encounters the subsequent CAAX-processing enzymes RAS-converting enzyme 1 (RCE1) and isoprenyl cysteine carboxylmethyl transferase (ICMT). Following CAAX modification H-RAS proceed to the cytosolic face of the Golgi apparatus, where is duo-palmitoylated by DHHC9–GCP16 allowing it to traffic via vesicular transport to the plasma membrane, locating at disordered membrane (DM). Then, duo-palmitoylated H-RAS can be partially depalmytoilated by APT-1 provoking H-RAS segregation to lipids rafts (LR). Duo- and mono-palmitoylated H-RAS can also be dissociated from the membrane by depalmitoylation, which translocates it by retrograde transport to the Golgi for another round of palmitoylation.

Additionally, RAS proteins are subject to other posttranslational modifications including phosphorylation, ubiquitination, acetylation, and S-nitrosylation. The G-P peptidyl-prolyl bond of H-RAS at position 178–179 undergoes *cis-trans* isomerization catalyzed by FKBP12 (45). Protein kinase C (PKC) phosphorylates K-RAS4B on serine 181 negatively regulating its association with the plasma membrane (46). Cysteine 118, which is conserved in all RAS isoforms, can be S-nitrosylated facilitating guanine nucleotide exchange and therefore promoting efficient RAS activation (47). RAS proteins can also be acetylated at lysine 104 decreasing RAS activity (48). Furthermore, H-RAS and K-RAS can be mono- and di-ubiquitinated on several lysines (K), K117, K147 and K170, by the E3 ligase Rabex-5 affecting the activation state of the GTPase and the subcellular localization of the proteins, that it is also modified by phosphorylation (49). In addition, monoubiquitinated RAS in lysine 147 impairs GTP dependent binding interactions with the p120 GAP catalytic domain, PI3K and both CRAF- and RALGDS RBDs, but displays significantly enhanced binding to the CRAF RBD in its GDP bound state what it is thought to promote RAF signaling (50, 51). Finally, last year was described that RAS proteins can be modified by SUMOylation in Lysine 42 by SUMO-E3 ligase PIASγ but little is known about its implications yet (52).

1.2.3 RAS PALMITOYLATION CYCLE

RAS palmitoylation, unlike farnesylation, is a reversible labile process creating a cycle of palmitoylation/depalmitoylation that controls H-RAS and N-RAS membrane attachment and maintenance on their specific sub-cellular localizations. As a result, when farnesylated N-RAS and H-RAS are palmitoylated in the Golgi, they become stably associated with membranes and packaged into transport vesicles for delivery to the cell surface. RAS proteins palmitoylation affects their distribution in GC. N-RAS and K-RAS4A, which are monopalmitoylated, are polarized toward the cis Golgi whereas H-RAS, that is duopalmitoylated, is found to be homogeneously distributed throughout the Golgi stacks. The differential palmitoylation states of N-RAS and H-RAS determine their distinct Golgi Sub-compartment localizations (53). This, has been proposed to affect Golgi mediated transport to the plasma membrane of N-RAS but no H-RAS (53, 54), suggesting that N-RAS might be transported through a pathway consistent with the recently proposed 'rapid partitioning' model of Golgi trafficking (55, 56). On the other hand, H-RAS seems to traffic by the classical *trans*-Golgi vesicular transport to the plasma membrane. Once in the plasma membrane, their half-lives of residency are estimated to be <30 min for N-RAS, which has just a single palmitoyl-modification therefore cycling faster; and <1 h for H-RAS, which must undergo a double depalmitoylation (57).

Acyl thioesterases (ATs) are the enzymes that control depalmitoylation and subsequently H-RAS, N-RAS and K-RAS4A translocation from the plasma membrane to the GC. Furthermore, Acyl Protein Thioesterase 1 (APT1) (originally designated lysophospholipase I (LYPLA1)), previously thought to be a lysophospholipase, was found to depalmitoylate H-

RAS and Gαi (inhibitory G-protein alpha subunit) *in vitro* (58, 59). APT1 is a conserved *α/β* hydrolase that contains a S-H-D catalytic triad and a G-X-S-X-G motif (59, 60). It has a wider variety of substrates such as the Endothelial Nitric Oxide Synthase (eNOS), the Synaptosomal-Associated Protein 23 (SNAP-23) and some viral proteins (61-64) and is in charge for H-RAS segregation between plasma membrane microdomains, from disordered membrane to lipids rafts **(Fig. 1.5)**.

The phosphodiesterase delta (PDEδ), acting as a chaperone, has been found to increase the diffusion of farnesylated RAS, via a non-vesicular route, in the cytosol facilitating its recycling back to the Golgi complex (GC) where it undergoes re-palmitoylation, permitting a new palmitoylation cycle of trafficking back to the plasma membrane (65). Besides them, FKBP12, a *cis-trans* prolyl isomerase, has been recently shown to be involved in depalmitoylation, specifically of H-RAS but nor N-RAS or K-RAS (45). In addition, for N-RAS, ABHD17 proteins have been proposed as novel protein depalmitoylases (66).

Since Golgi and PM pools of H/N-RAS activate different downstream signaling cascades (67), the regulation of their localization affects signaling. Thus, RAS depalmitoylation cycle is crucial for its correct localization since it regulates both RAS macro-localization, and its localization within plasma membrane subdomains. Overall, this cycle affects different cellular processes and its inhibition can be exploited for therapeutic approaches in different human cancers (68).

1.2.4 RAS SIGNALING AND ITS REGULATORS

1.2.4.1 RAS effectors and signaling pathways

1.2.4.1.1 RAS effectors

For a protein to be considered a RAS effector needs to be able to mainly associate to RAS active form (RAS-GTP) through regions called the Ras Binding Domain (RBD) and Ras Association Domain (RAD), with a βαβαβ structure (69). There are several RAS effectors such as RAF Interactor 1 (**RIN1**), T Cell Lymphoma Invasion and Metastasis 1 (**TIAM1**), Phospholipase C Epsilon (**PLCε**) and **AF6** but the best characterized are **RAF** family kinases, the p110 catalytic subunit of class I phosphatidylinositol-3 kinase (**PI3K)** and a **RAL-GEFs** exchange factors (70-72) **(Fig. 1.6)**.

1.2.4.1.2 MAPK pathway

The MAPK (Mitogen-Activated Protein Kinase) pathway is one of the primordial signaling systems that exists in all eukaryotes, and controls such fundamental cellular processes as proliferation, differentiation, survival and apoptosis. Mammalian MAPK can be divided into

four groups based on their structure and function: Extracellular signal-Regulated Kinases (**ERK**), **p38** MAPKs , c-Jun NH2-terminal Kinases (**JNKs**) and Extracellular signal-Regulated Kinase-5 (**ERK-5**) (73, 74). Activation of these MAPKs occurs through a cascade of upstream kinases; a MAPKKKs (MAPK Kinase Kinase) first phosphorylates a dual-specificity protein kinase MAPKK (MAPK Kinase), which in turn phosphorylates the MAPK. This set-up provides not only for signal amplification, but, maybe even more importantly, for additional regulatory interfaces that allow the kinetics, duration and amplitude of the activity to be precisely tuned (74, 75).

The MAPK /ERK is one of the best characterized and its signaling cascade is activated by a wide variety of receptors involved in growth and differentiation including GPCRs (G-Protein Coupled Receptors), RTKs (Receptor Tyrosine Kinases), Integrins, and Ion channels. The specific components of the cascade vary greatly among different stimuli, but the architecture of the pathway usually includes a set of adaptors like SHC and GRB2 (Growth Factor Receptor Bound protein-2), linking the receptor to a GEF, like SOS (Son of Sevenless) or CDC25, transducing the signal to RAS which in turn activate the core unit of the cascade composed of a MAPKKK (**RAF**), a MAPKK (**MEK1/2** (MAPK/ERK Kinase-1/2)) and MAPK (**ERK**). An activated ERK dimer can regulate targets in the cytosol and ERK also translocate, as monomer, to the nucleus where it phosphorylates a variety of transcription factors regulating gene expression (74, 76-78).

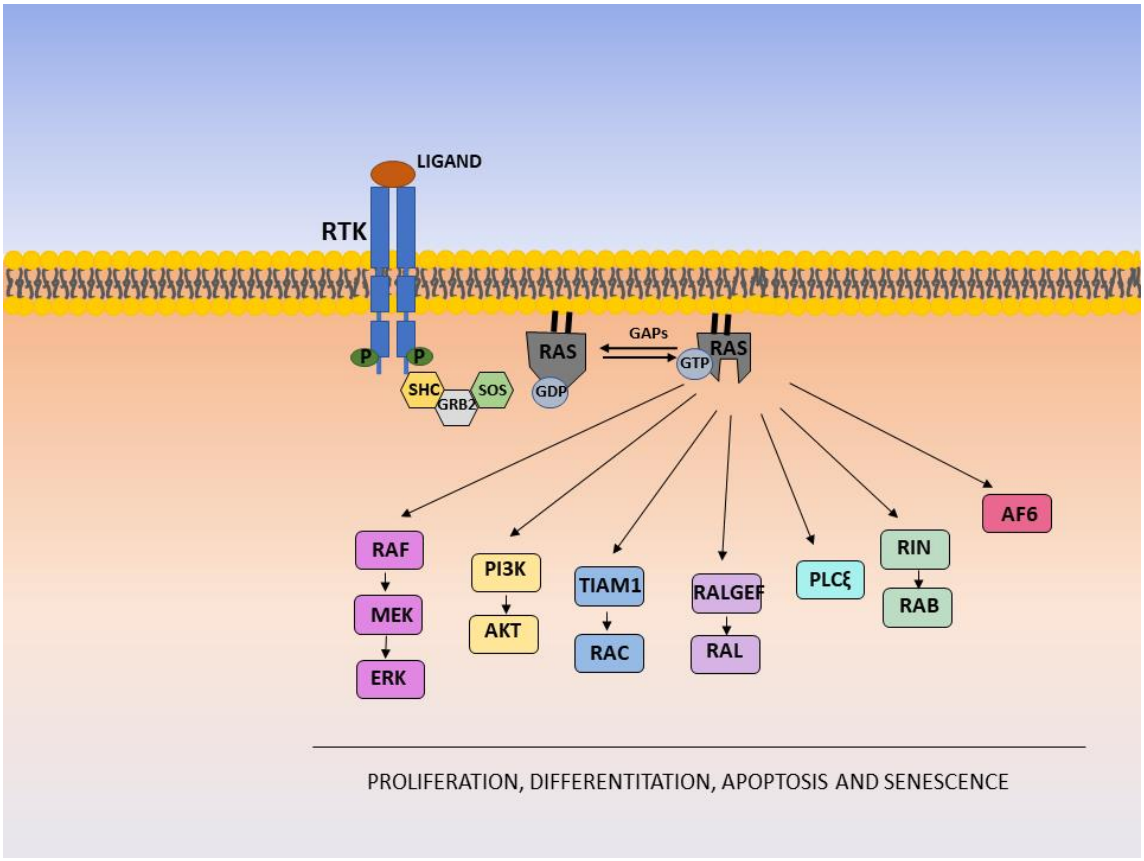

Figure 1.6: RAS effectors.

1.2.4.1.3 PI3K/AKT signaling pathway

Another well studied signaling pathway is the PI3K/Protein Kinase B (AKT), which plays important roles as modulator of RAS-mediated cell survival and proliferation (70, 79). Upon ligand stimulating of a Receptor Tyrosine Kinase (RTK) RAS interacts with lipid kinases, like Class I PI3K 110 subunits (p110α, p110β, p110γ, and p110δ) independently of its p85 regulatory subunit. This interaction allows the conversion of phosphatidylinositol (4,5)-bisphosphate (PIP_2) into phosphatidylinositol (3,4,5)-trisphosphate (PIP_3). PIP_3 then binds the Pleckstrin Homology (PH) domain of Phosphoinositide-Dependent Kinase 1 (PDK1), which allows PDK1 mediated activation of AKT by its phosphorylation at residue threonine 308 (80-82). AKT can promote cell survival by inhibiting proapoptotic Bcl-2 family members BAD and BAX (83, 84), negatively regulating the transcription factor NF-κB which leads to antiapoptotic and pro-survival signals (85). Moreover, AKT also promotes RHEB activation which in turn stimulates the Mammalian Target Of Rapamycin (mTOR), leading to increased p70 S6 kinase activity. This finally results in an increase in protein synthesis by phosphorylation of the eukaryotic initiation factor 4E and the ribosomal S6 protein (86). Moreover, mTORC2 contributes to complete AKT activation by phosphorylating AKT on serine 473 (87, 88) **(Fig. 1.7)**.

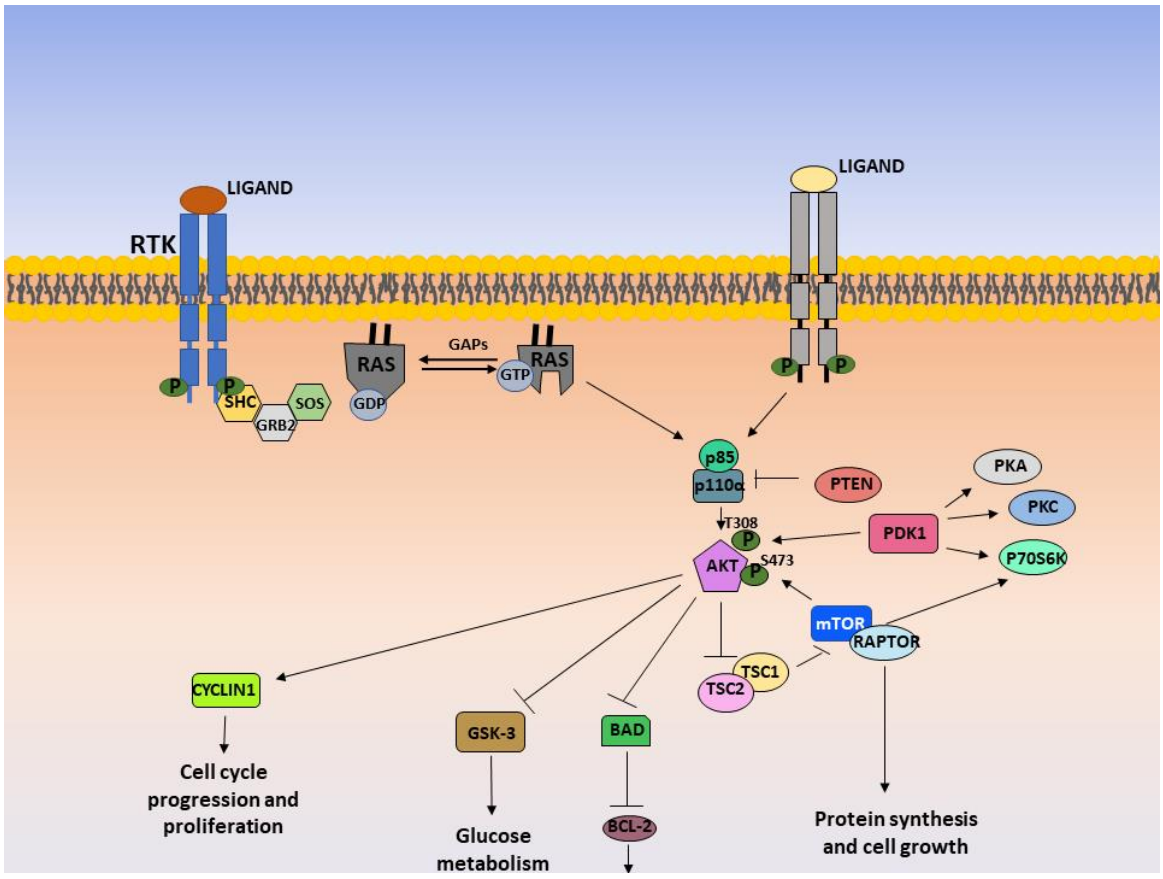

Figure 1.7: Schematic diagram of the most representative signaling of the PI3K/AKT pathway.

The tumor suppressor phosphatase and tensing homolog (PTEN) meanwhile dephosphorylates PIP_3 to PIP_2, thereby terminating PI3K-dependent signaling (80).

Additionally, RAS also interacts with the RAS GTPase family RALGEF (RalGDS, RGL, RGL2 and RGL3) promoting activation of the RALA and RALB small GTPases (89). The biological function of these proteins is not yet fully understood, although there is evidence that they play a role in RAS-mediated transformation and tumorigenesis *in vivo (90)*.

1.2.4.2 RAS sub-cellular localizations

Initially, it was thought that RAS proteins, in order to be functional, needed to be in the inner leafled of the plasma membrane where GEFs would be active (91). However, today we know that RAS is also present and functional in different subcellular localizations, contradicting the initial concept of a single source of RAS signals.

For instance, in 1980 when Willigham and colleagues first pointed that RAS needed to be in the plasma membrane (PM) in order to be active, they were considering PM as a simple and homogeneous lipid bilayer, the "fluid mosaic model"(92). Nowadays, we are aware that the plasma membrane is highly asymmetric and laterally compartmentalized (93, 94). Due to its different lipid components, the plasma membrane can be divided into lipid rafts, defined as liquid-ordered domains enriched in sphingolipids, cholesterol and in caveolin proteins; and disordered membrane, also known as bulk membrane, a liquid disordered domain, due to the high concentration of highly unsaturated phospholipids and lacking caveolin (95, 96). It was years later that Hancock and colleagues showed that RAS proteins are in different microdomains within the plasma membrane. It was then shown that at a steady-state H-RAS and N-RAS localized mainly in caveolin rich lipids raft from where they diffuse to the bulk plasma membrane after activation, on the other hand K-RAS was located in disordered membrane but not lipids rafts (57, 97-99) **(Fig. 1.8)**.

Years later, our group described that the presence of H-RAS at different PM microdomains was not only due to H-RAS activation state, but also regulated by its palmitoylation levels. This depends on the level of palmitoylation in a specific cell type. It was proposed that H-RAS double palmitoylation (C181, C184) will direct H-RAS to disordered membrane but when single palmitoylated H-RAS (C181) will be present in lipids rafts. Moreover, we saw that double palmitoylated H-RAS can loss one of its palmitic groups, at C184, due to high levels of APT-1 activity, causing H-RAS lateral diffusion from disordered membrane to lipids raft. Also, fully depalmitoylation of H-RAS causes its diffusion back to the Golgi complex (100) **(Fig. 1.5)**.

RAS isoforms can also be present in different endomembranes where they display different degrees of association (N-RAS>H-RAS>K-RAS) to the Golgi Apparatus, ER, mitochondria and a variety of endosomes (101) **(Fig. 1.8)**. For instance, non-palmitoylated RAS proteins can be found in ER where they can trigger different signaling pathways. Moreover, once N-RAS

RAS isoforms can also be present in different endomembranes where they display different degrees of association (N-RAS>H-RAS>K-RAS) to Golgi Apparatus, ER, mitochondria and a variety of endosomes (101) **(Fig. 1.8)**. For instance, non-palmitoylated RAS proteins can be found in ER where they can trigger different signaling pathways. Moreover, once N-RAS and H-RAS are steadily palmitoylated they can also be found in GC coming from either ER or through the retrograde pathway from the PM, closing the palmytoilation cycle (102). Additionally, as pointed before N-RAS seems to be only in cis-Golgi whereas H-RAS is thought to be dispersed throughout the whole complex (103-105).

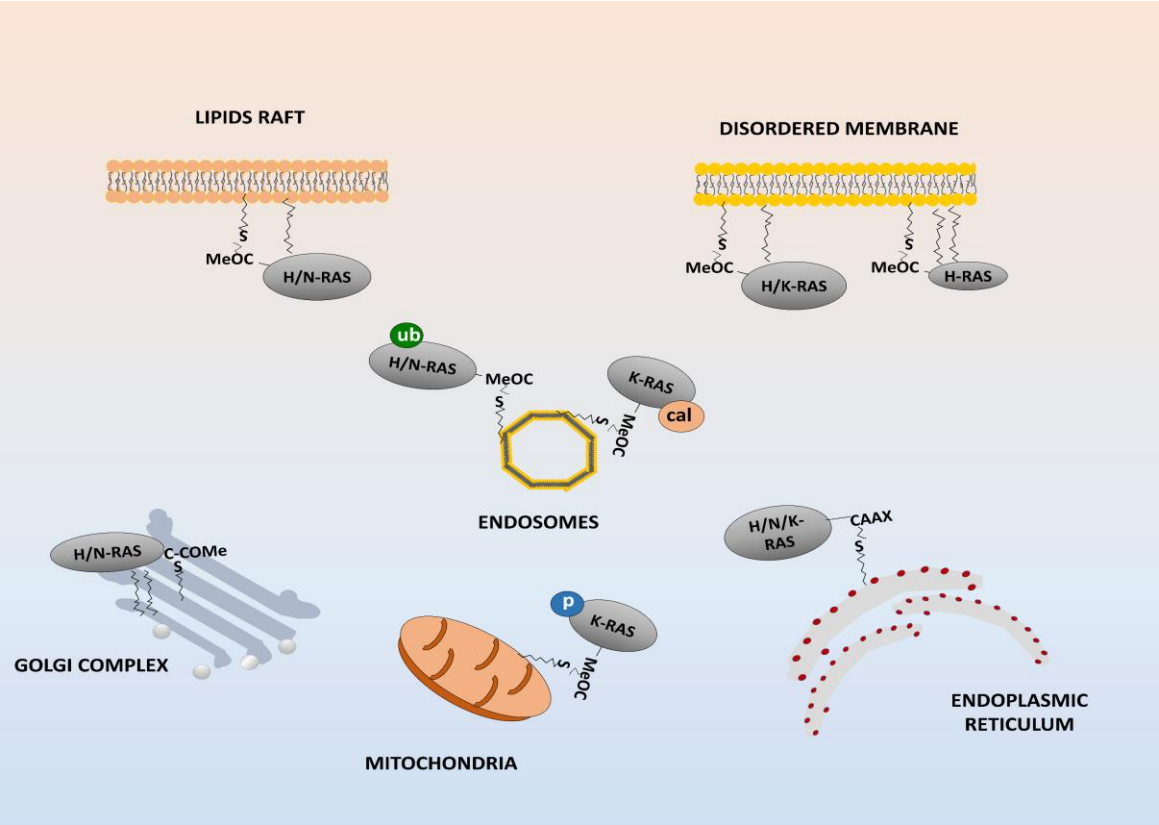

Figure 1.8: RAS locations within the cell. In the plasma membrane, H- and N-RAS can be located at lipids rafts and disordered membrane, whereas K-RAS is only present at disordered membrane. H- and N-RAS can be present and signal from the Golgi Complex but K-RAS is not found in this organelle. Moreover, H- and N-RAS once ubiquitinated can locate at endosomes and K-RAS needs to bind calmodulin in other to locate in them. Moreover, phosphorylated K-RAS can be found at mitochondria.

Besides from being substrate to depalmytoilation, RAS proteins at the PM can be translocated to endomembranes (endosomes/ER/Golgi) by endocytosis. Strikingly, H-RAS, in order to be present in the recycling endosomes (RE), needs to be bi-palmytoilated, and H-RAS mono and diubiquitination seems to stabilize endosomal interactions and impedes reclycling (51, 106, 107). Therefore, this locates H-RAS and N-RAS to endosomes regulating RAF-1 activation (108). Additionally, K-RAS was shown to be internalized in a clathrin-dependent fashion and to be transported along early endosomes, late endosomes and eventually into lysosomes, displaying only a minor and transient association with endosomes (109).

1.2.4.2.1 Effectors in different RAS sublocalizations

Since RAS is present in different locations is not a surprise that RAS sublocalizations has functional consequences.

Previous studies from our group using H-RASv12 constructs specifically tethered to the different compartments where RAS is known to be active (Disordered membrane, lipids raft, Endoplasmic Reticulum and Golgi Aparatus) showed that RAS compartmentalization determines effector usage **(Fig. 1.9)**. This way, RAS is able to activate different effector signaling pathways and tightly regulate their amplitude, intensity and substrate specificity consequently affecting gene expression patterns. Our group showed that H-RASv12 at lipids rafts and ER was able to strongly activate ERK and the PI3K/AKT pathway, while from disordered membrane it displayed lower ERK and AKT activation. The activation of these pathways was almost negligible from the Golgi Complex. However, RAL-GDS was mainly activated at this organelle. Consequently, H-RASv12 could induce NIH3T3 cells proliferation and transformation from all sublocalizations except from the Golgi Complex. Conversely, other groups have found that RAS from GC is also able to strongly induce ERK and PI3K/AKT activation (104, 110-113). These site-specific differences are thought to be mediated by different space related mechanism that probably include kinase tiers (GEFs and GAPs), scaffold proteins and protein dimerization.

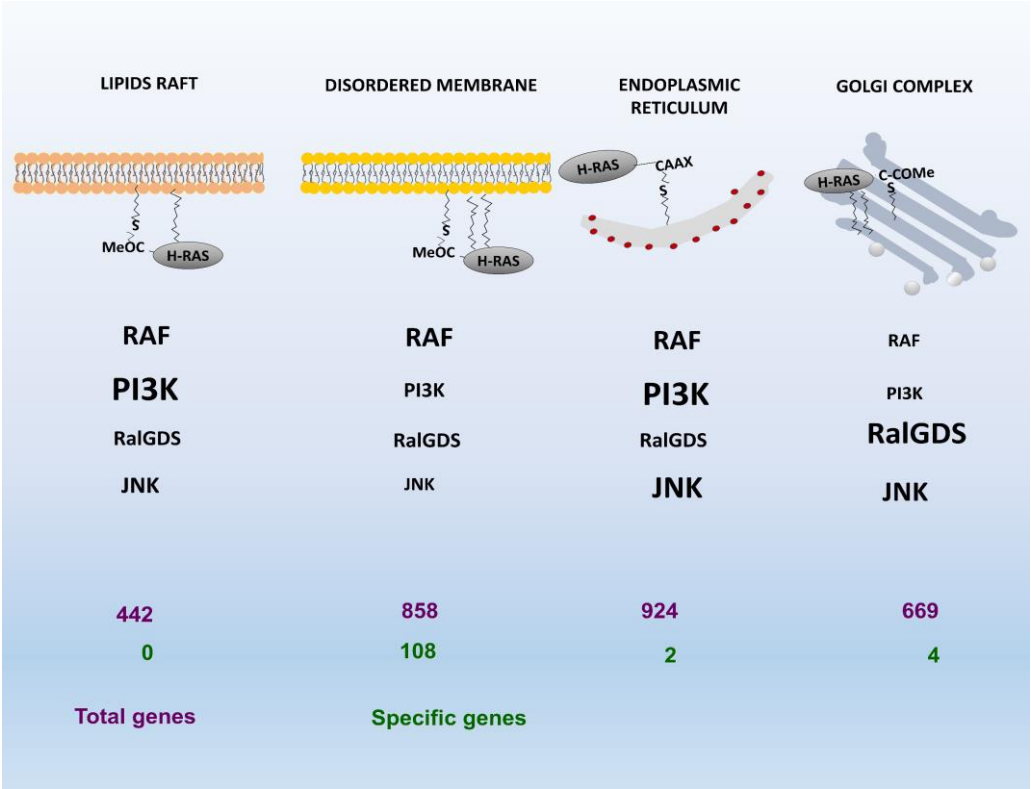

Figure 1.9: RAS site-specific signals. Main signaling pathways activated by RAS at its different subcellular locations (Bigger letters represents more activation) and the total and specific number of genes regulated by RAS from the different sublocalizations.

These site-specific differences are thought to be mediated by different space related mechanism that probably include kinase tiers (GEFs and GAPs) (114, 115), scaffold proteins (116-118) and protein dimerization (119, 120).

1.2.4.2.2 Role of RAS sublocalizations *in vivo*

RAS sublocalizations role in *in vivo* carcinogenesis has been mostly explored in melanoma. In this respect, H-RASv12 signals emanating from all locations but GC are able to induce tumors in a zebrafish melanoma model. In this model H-RASv12 signals from GC, specifically from cis Golgi, strongly induce apoptotic signals and is not able to induce tumor formation. These results are related with TP53 mutated status and PTPRk levels (121). However, little is known about their effects in other tumoral types.

1.3 VEGF FAMILY

The human vascular endothelial growth factor family is composed by VEGF-A, VEGF-B, VEGF-C, VEGF-D, VEGF-E and placental growth factor (PLGF), that bind a family of cognate protein tyrosine kinase receptors (VEGFRs)(122, 123). For instance, VEGF-A binds to VEGFR2 and VEGFR1; VEGF-B to VEGFR1 and NEUROPILIN-1; VEGF-C and VEGF-D to VEGFR2 and VEGFR3; VEGF-E only to VEGFR2; and PLGF to VEGFR1 and NEUROPILIN-1 and -2 (122-125).

Human *VEGF* genes are characterized by a highly conserved seven exon structure, with the exception of *VEGF-A*, which has eight exons that gives rise to at least six different transcripts and *VEGF-B* that gives rise to two transcripts (78, 124). VEGF-B_{167} and VEGF-B_{186} are two VEGF-B isoforms. Both bind VEGFR1 and its coreceptor neuropilin-1 and are expressed in most tissues and organs (126).

VEGF-A is the best studied member. VEGF-A is crucial for angiogenesis and therefore for embryonic vascular development. A single VEGF-A allele in mice causes embryoinic death (127, 128). Moreover, many tumors have taken advantage of VEGF-A, which promotes formation of new vessels from pre-existing ones feeding the tumor. Nowadays, an specific humanized monoclonal antibody to this molecule, Avastin (Bevacizumab), is approved for treatment of metastatic colorectal cancer, metastatic renal cell carcinoma, recurrent glioblastoma and non-squamous non-small cell lung, cancer among others (129-133).

In contrast to VEGF-A, VEGF-B genetic deletion in mice seemed to be harmless. However, these mice have trouble recovering from ischemic myocarditis. Although substantial efforts have been focused to relate VEGF-B to angiogenic activities little has been found in this matter (134, 135). Nevertheless, VEGF-B_{167} can increase blood vessel

density in ischemic and infarcted hearts but not under normal conditions, and VEGF-B_{186} induced myocardium specific angiogenesis and arteriogenesis. This suggest that VEGF-B has only angiogenic activity in the heart (126, 136).

More surprisingly, Eriksson´group has recently showed that VEGF-B is crucial for energy metabolism, by regulating fatty acid uptake and transportation across the endothelium, using fatty acid transporter proteins (FATPs) (135, 137, 138). Moreover, VEGF-B was shown to induce blood vessel stabilization and survival and to inhibit VEGF-A induced pathological angiogenesis (136). Although VEGF-B has been seen to promote cancer metastasis through a VEGF-A independent mechanism in human melanomas (139), and its expression is associated with lymph node metastasis in human primary breast cancers (140), little is known about its effects in cancer.

1.4 Extracellular vesicles

Besides all these types of RAS signalling modulators regulating its role in cancer development and metastasis, there is a new aspect in the control of RAS-mediated cancer effects. A new hot topic in cancer has emerged in the last years, focusing on Extracellular Vesicles (EVs). These were initially considered to be extracellular debris but have been identified as key mediators in cell-to-cell communication. This has added a new layer of complexity to our still poor knowledge of tumor cell physiology.

1.4.1 EVS DEFINITION

EVs are lipid bilayer-enclosing membranes containing a variety of cargoes protected from enzymatic degradation and serve as vehicles of biological information. The term EVs was proposed as a generic term for all types of secreted membrane vesicles, regardless of their differences in biogenesis and composition. Although EVs have been differently defined by different criteria, the general and accepted one classify EV subpopulations based on their biogenesis. EVs are then broadly classified into: Exosomes (EXOs), Microvesicles (MVs) and apoptotic bodies (141).

1.4.2 EXOSOME BIOGENESIS

Exosome biogenesis is initiated as an endocytic event driven by the Endosomal Sorting Complex Required for Transport (ESCRT), including: ESCRT I-III, ALG-2-Interacting Protein X (ALIX), which connects the *SYNTENIN*–SYNDECAN complexes to the ESCRT machinery, and Tumor Suspectibility 101 (TSG101), involving inward invagination of the plasma membrane. This leads to the formation of early endosomes that after maturation, promote Intraluminal Vesicles (ILVs) formation in late endosomal Multivesicular Bodies (MVBs) (142-144). These vesicles size is 40-120 nm and are composed of a wide variety of

cytosolic components, containing molecules from the phospholipid bilayer, endoplasmic reticulum, cytosol, and Golgi apparatus; including transmembrane proteins as tetraspanins, such as CD81, CD63 and CD9; signal transduction proteins; biogenesis factors such as TSG101, ALIX and SYNTENIN; nucleic acids (messenger Ribonucleic Acid (mRNA), microRNA (miRNA), other non-coding RNA, Deoxyribonucleic acid (DNA) (and histones)); enzymes, chaperones and several lipids (Table 1.1). The exosomal membrane cargoes are known to reach endosomes from the Golgi Apparatus, or are internalized from the plasma membrane before being sorted to ILVs, during endosome maturation (145-147). RAB GTPases, among others, modulate lysosomal MVBs degradation in a ubiquitin-dependent manner and their secretion in an ubiquitin-independent manner (148-150). After that, and among other proteins, N-ethylmaleimide-sensitive Factor Attachment Protein Receptors (SNAREs), orchestrate the fusion of MVBs with the plasma-membrane, releasing exosomes to the extracellular space. However, this is a not a fully-understood process yet (151, 152). Alternatively, another ESCRT-independent mechanism for exosome biogenesis, dependent on sphingolipid ceramide has been proposed. Ceramide contributes to the inward budding of the plasma membrane, generating another ILV population destined for secretion as EXOs (153).

EV type and Size	Biogenesis	Enriched Markers	Content
Exosomes (40-120 nm)	Endosomal pathway vesicle maturation in MVB	ALIX, Syntenin, TSG101, CD63, CD9, CD81	Proteins (cytoplasmic and membrane), mRNA, miRNA, DNA, noncoding RNA
Microvesicles (120-1000 nm)	Outward budding of plasma membrane	Integrins, metalloproteinases, CD-40 ligand, ARF6 phosphatidyl-serine	Proteins (cytoplasmic and membrane), mRNA, miRNA, DNA, noncoding RNA
Apoptotic bodies (50-5000 nm)	Cell surface. Release from cellular blebs during apoptosis	Phophatidyl-serine	Nuclear fractions, cell organelles

Table 1.1. Extracellular vesicles characteristics, biogenesis, content and useful markers for their detection.

1.4.3 MICROVESICLES

Microvesicles (120-1000 nm) originate by an outward budding of the plasma membrane and are released to the extracellular space (154). During membrane budding, lipid rafts containing ceramide, regulatory proteins, and cytoskeleton elements, can promote membrane curvature and extensive cytoskeletal changes, promoting the formation of MVs (155, 156). Due to its origin, they have different lipid, cytoplasmic and membrane components, only presenting tetraspanins CD9, CD81 and CD82 but not CD63; biogenesis factors as ALIX, TSG101 but not SYNTENIN, nucleic acids and signaling molecules; also presenting cytoleskeletal molecules such as ACTIN and TUBULIN and extracellular matrix adhesion proteins **(Table 1.1)** (145, 157).

1.4.4 APOPTOTIC BODIES

Apoptotic bodies, containing fragmented nuclear and cytoplasmic components from the dying cell, range from 50-5000 nm and are formed during programmed cell death, and have been shown to promote apoptosis of adjacent cells **(Table 1.1)** (141, 158).

1.4.5 EVs IN CANCER

The nature and abundance of extracellular vesicle cargoes are cell-type-specific and are often influenced by the physiological or pathological state of the donor cell, the stimuli that modulate their production and release, and the molecular mechanisms that leads to their biogenesis (157). When EVs are released to the extracellular space they can exert their functions in proximity or they can travel in different biofluids such as blood. Moreover, they can be internalized by cells delivering their cargo, by either fusion (159, 160), energy-dependent receptor-mediated endocytosis (161, 162), macropinocytosis (163) or phagocytosis (164), thus participating in cell-to-cell communication (165).

Several studies have recently pointed out that cancer cells are able to secrete a high amount of EVs and that they are critical messenger in tumor progression and metastasis, contributing to the acquisition of all of the cancer hallmarks delineated by Hanahan and Weinberg such as tumor growth, angiogenesis, invasion and metastasis (166) **(Fig. 1.10)**. Cancer cell-derived EVs have been found to transfer oncogenic molecules among the cells in the primary tumor as well as to neighbouring stromal cells. These cells can also intervein secreting EVs mediating bi-directional communication, thus, influencing tumor progression and shaping of tumor microenvironment (157). Moreover, tumor-derived EVs from several types of tumors such as melanoma (167), renal cancer (168) and breast cancer (169) among others, are able to shape distant organs environment. This process, known as premetastatic niche (PMN) conditioning, allows primary tumor survival and outgrowth once tumor cells scape blood circulation. Moreover, due to surface protein specific composition, tumor-derived EVs may be directed to specific tissues (170, 171). Furthermore, tumor-derived EVs could be future targets for

anticancer therapies, since they are found in blood and urine, and are promising emerging biomarkers to monitor cancer progression and treatment response (157, 172).

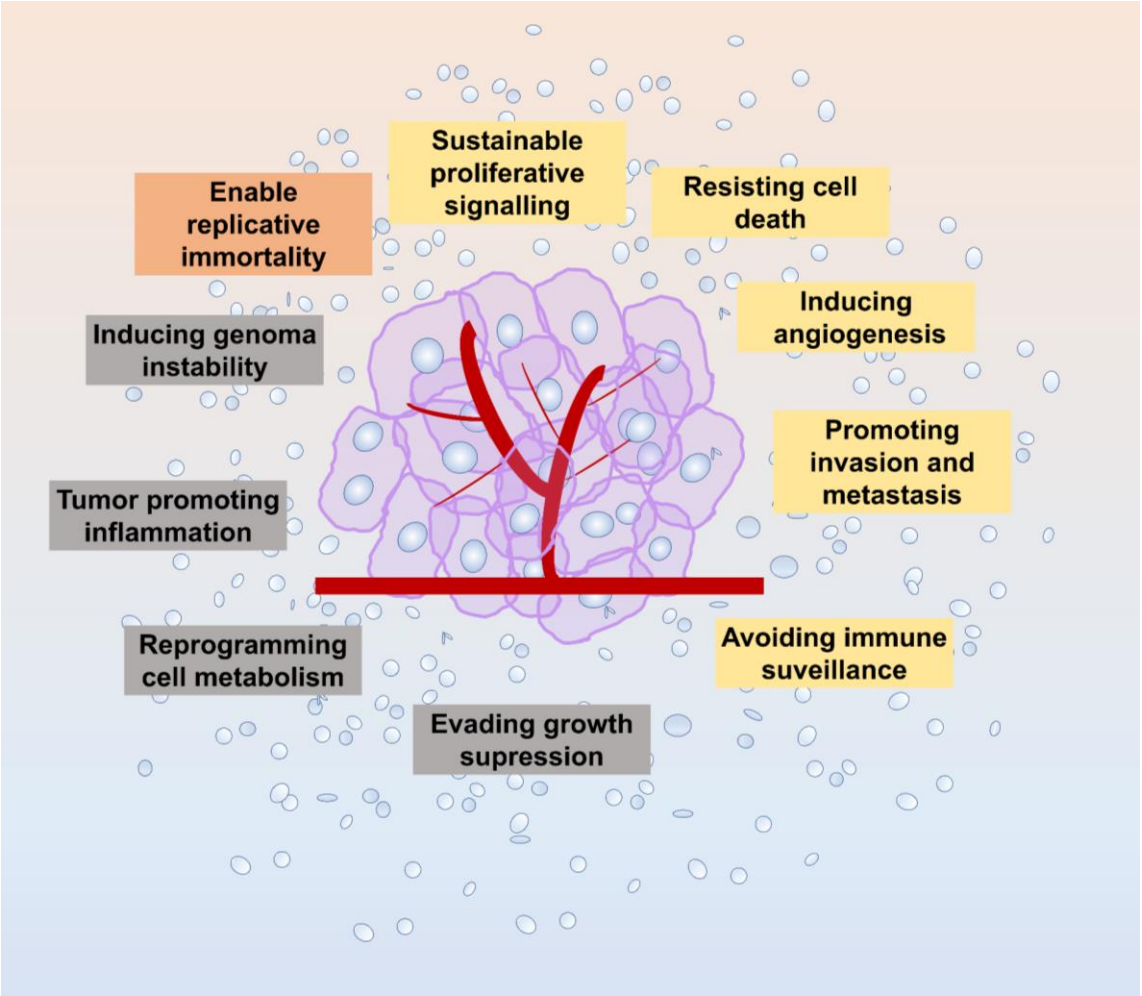

Figure 1.10: Representation of the hallmarks of cancer acquired during tumor progression. by Hanahan and Weinberg, Cell 2011. The hallmarks of cancer where EVs have been shown to participate are marked in yellow. The functions marker in grey are the ones where EVs effects are still poorly understood. In red, we show that enabling replicative immortality has not been related to EVs yet.

1.4.6 RAS AND EXTRACELLULAR VESICLES

Since cancer-derived EVs can mediate in horizontal transformation of normal cells, it is not a surprise that RAS presence in EVs, as well as RAS mutated cells derived EVs, have risen researcher´s attention.

RAS networks have been shown to play a critical role in exosome biogenesis, maintenance, secretion and even cargo loading (173) **(Fig. 1.11)**. Some studies have shown that tumor cell-derived EVs can functionally transfer fragments of genomic DNA (174). Indeed, double stranded genomic DNA for mutated *K-RAS* (^{G12V} and ^{G12D}) has been found in serum isolated EVs from patients with colon cancer and pancreatic cancer (175, 176). Moreover, Shi and

Colleagues have also found genomic *RAS* in exosomes isolated from the blood of a cervical cancer mouse model and that it was related with higher tumor aggressiveness (177). Also, rat epithelial cells transformed by H-RASv12 secreted EVs containing chromatin-associated double-stranded genomic DNA for *H-RASv12*, which in turn were able to transiently transform fibroblast and endothelial cells (178). Furthermore, apoptotic bodies have been found to mediate *H-RAS* genomic DNA transfer, inducing tumor formation of non-tumorogenic fibroblasts (179, 180).

Additionally, farnesylated RAS proteins have been found in Glioblastoma extracellular vesicles associated with ESCRT proteins, what suggests that RAS plays a crucial role in exosomes biogenesis (181). K-RAS has also been found in non-small cell lung cancer-derived EVs (182).

In addition, RAS can modulate EVs cargo by promoting the packing of different molecules. For instance, H-RAS overexpression in Madin-Darby canine kidney epithelial cells leads to the incorporation of different mesenchymal markers such a as vimentin and MMPs into EVs that are thought to induce epithelial to mesenchymal transition (EMT) in recipient cells (183). Furthermore, MK4 cells transformed by H-RASv12, increased exosome-like microvesicle release compared with their normal counterparts (184).

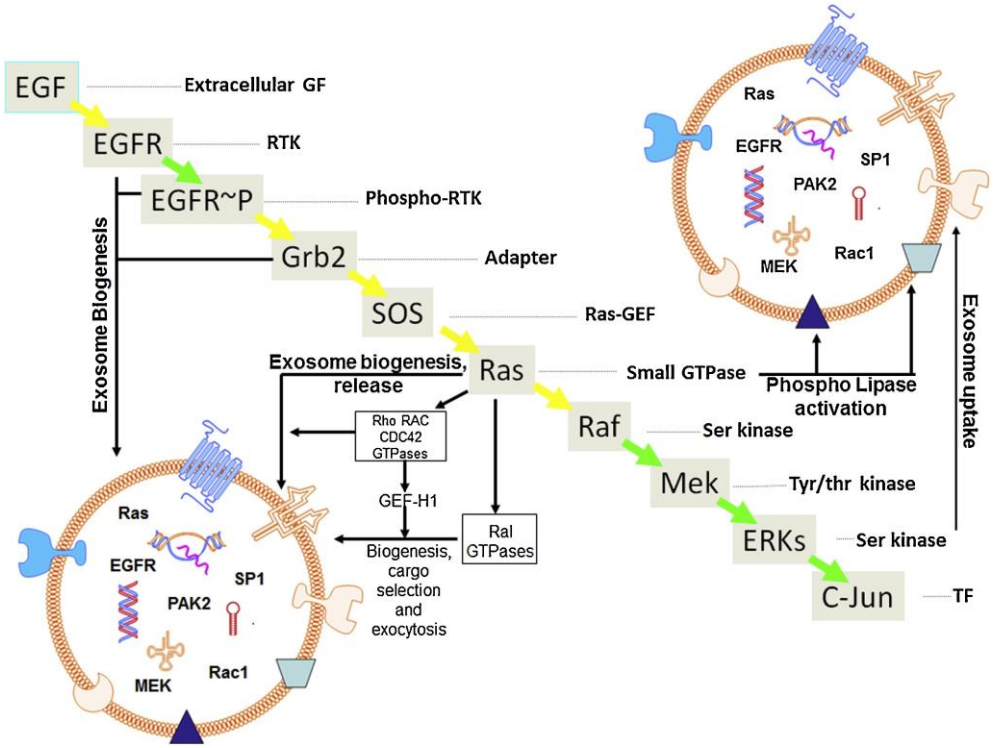

Figure 1.11: Role of RAS pathway proteins in exosome biogenesis, cargo selection and release. Adapted from (173).

Other group has seen that mutant *K-RAS* CRC cells exosomes contained higher levels of the EGFR ligand amphiregulin (AREG) than *K-RAS wild type* ones, enhancing invasiveness by

recipient cancer cells (185). Moreover, Beckler and colleagues showed that exosomes isolated from mutant K-RAS^{G13D}-expressing colon cancer cells enhanced the invasiveness of recipient cells in comparison to exosomes purified from *wt* K-RAS-expressing cells which leads to hypothesize that mutant *K-RAS* might affect neighboring and distant cells by regulating exosome composition and behavior (186) **(Fig. 1.11)**.

Finally, active RAS isolated from human and mouse glioblastoma extracellular nanovesicles lysates coprecipitates with ESCRT-associated exosome proteins VSP4a and ALIX (181). Furthermore, H-RASv12 expression in fibroblasts was associated with higher levels of tetraspanins, involved in vesicle formation (187). There are also several RAS effectors, such as RHO family GTPases or RAL GTPases that have been shown to promote protein sorting into exosomes and to be regulators of MVB formation and exosome release (173, 188, 189). Additionally, Small GTPases have also been documented in stabilizing the phospholipases present in the exosome bilayer and ERKs have been reported to play a role in facilitating exosome uptake (173).

1.5 Thyroid lesions and cancer

1.5.1 THE THYROID GLAND

The thyroid is a highly vascularized gland located anteriorly in the lower neck. It has two symmetrical lobules connected by an isthmus. These lobules are irrigated by the superior thyroid artery, that arises from the external carotid artery, and the inferior thyroid artery that is a branch of the subclavian artery (190, 191). The thyroid is covered by a thin true capsule that penetrates the parenchyma of the gland dividing it into several lobules containing 20-40 follicles. These follicles are the structural units of the gland and consist of a colloid-filled cavity surrounded by a layer of polarized epithelial cells, also called follicular cells, that are the main component of the gland **(Fig. 1.12)** (191, 192). The colloid serves as a storage for the thyroid hormones precursor, iodo-thyroglobulin, while follicular cells are able to incorporate iodine, through a $2Na^+/I^-$ symporter (NIS) located in their basolateral membrane (193), in response to the Thyroid Stimulating Hormone (TSH) (194). This process finally results in the synthesis of the two thyroid hormones, triiodothyronine (T3) and thyroxine (T4), which are crucial for children growth and nervous system maturation and for a correct metabolism control in adults (191, 194).

Parafollicular cells, also known as C cells, are the other component of the gland. They are found among follicles and their main function is the production of Calcitonin, a hormone that decrease ionic calcium and phosphorus in blood preventing bone resorption (191, 192, 195).

A broad plethora of diseases affect this gland, the most common ones being autoimmune diseases (196, 197), followed by inflammatory diseases (198) and cancer, which can arise from alterations on follicular and C cells (199).

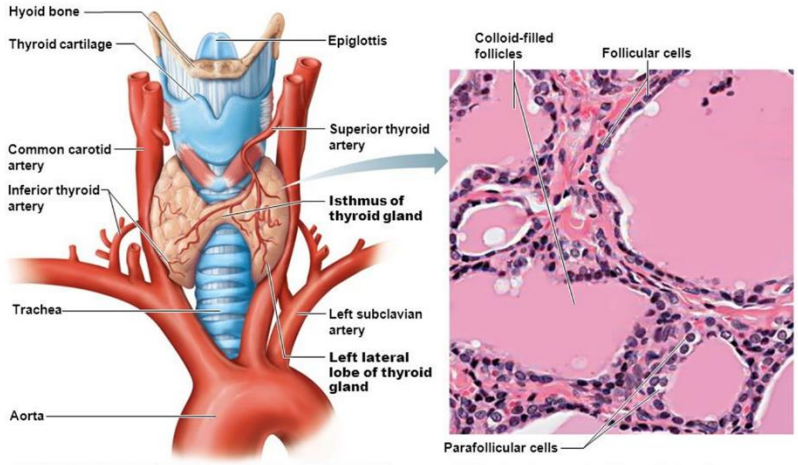

Figure 1.12: Thyroid gland anatomy and histology showing the structural units of the gland, the follicules, and its epithelial cells, follicular cells and parafollicular cells.

1.5.2 THYROID CANCER INCIDENCE

Thyroid cancer is the most common endocrine malignancy worldwide accounting for ~ 2.1% of all cancer diagnoses. Almost 3 out of 4 cases are women. Last year, the American Cancer Society accounted an estimated 53 990 new diagnoses in the United States, a figure significantly higher than 10 years ago (200). Thyroid cancer incidence continues to rise, mostly due to overdiagnosis as a consequence to an increased use of improved diagnostic imaging and surveillance (201) **(Fig. 1.13)**. However, big tumors diagnosis suggests that other factors besides overdiagnosis, such as an increase in the most prevalent environmental factors, obesity and cigarette smoking, could drive the initiation of new tumors (202-204). Noticeably,

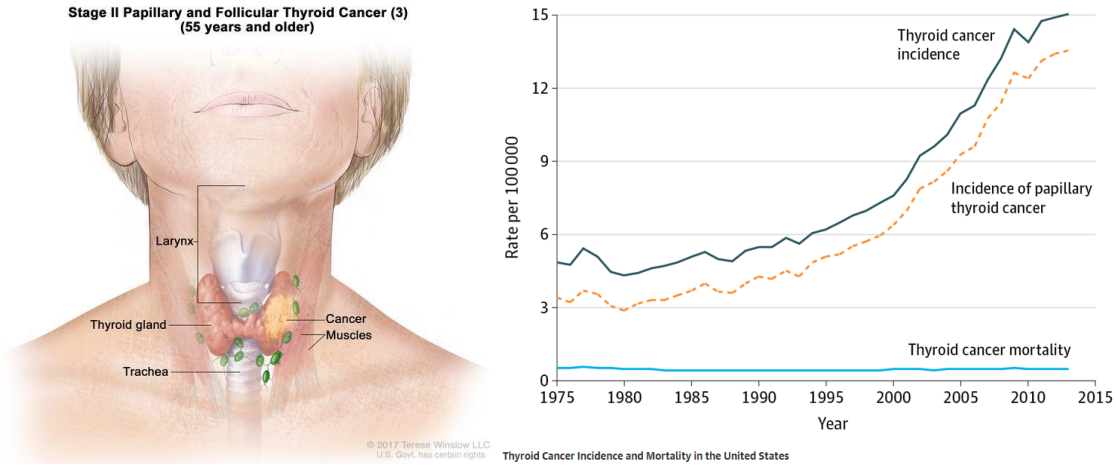

Figure 1.13: Thyroid cancer incidence and mortality. For the National Cancer Institute © *(2019)* Terese Winslow LLC, U.S. Govt. has certain rights

although incidence is rising steadily, mortality has not changed significantly over the past fifty years (205) **(Fig. 1.13)**. This is thanks to the standard Radioactive Iodine (RAI) ablation, TSH suppressive therapy and surgery that allow thyroid cancer patients to have an overall survival rate of 95% after 5 years. However, locoregional recurrence is frequent, affecting up to 20% of patients, and 10% of them will also develop distant metastasis after 10 years (206, 207). Right now, there are several challenges that face clinicians, but the main goal is not to overtreat patients with low risk disease or benign thyroid nodules, and to identify those patients with a high risk disease, in order to treat them fast and more aggressively (201).

1.5.3 CLINICAL PRESENTATIONS

1.5.3.1 Thyroid nodules

Thyroid nodules are defined as any lump within the thyroid gland that is ultrasonographically distinct from the surrounding parenchyma (207). The vast majority, around 90%, are small, non-palpable, benign lesions that have no clinical significance. Their size or the presence of more than one nodule are not predictive of malignancy. For example, cancer is no less frequent in nodules smaller than 10 mm, or when there are several nodules. However, generally, only nodules >1 cm are evaluated, since they are consider to harbor a greater potential to be clinically significant cancers (208).

Nowadays, to be able to discern between low-risk and high-risk patients, a good familiar history, a proper physical examination, neck ultrasonography (US) **(table 1.2)**, TSH laboratory determination and Fine-Needle Aspiration (FNA), in > 1cm suspicious nodules or > 2 cm low suspicion sonographic pattern nodules, in the correct patients, are fundamental (201).

US feature	Relative risk
Microcalcifications	4.97
Hypoechogenicity	1.92
Irregular margins or no halo	16.83
Solid	4.2
Intranodule vascularity	14.29
More tall than wide	10.5

Table 1.2. Summary of key ultrasonographical (US) features in thyroid nodules and their relative risk for thyroid cancer.

FNA cytology is classified by the 2017 Bethesda System for Reporting Thyroid Cytopathology **(Table 1.3)**, into seven different categories that predict their risk of malignancy and posterior management (209).

Diagnostic Category	Risk of malignancy	Management
I.Nondiagnostic/unsatisfactory	5-10%	Repeat FNA under US guidance
II. Benign	0-3%	Clinical and US follow-up until two negative
III. Atypia of undetermined significance/follicular lesion of undetermined significance	10-30%	Repeat FNA, molecular testing or lobectomy
IV. Follicular neoplasm/suspicious for a follicular neoplasm	25-40%	Molecular testing and lobectomy
V. Suspicious for malignancy	50-75%	Lobectomy or near total thyroidectomy
VII. Malignant	97-99%	Lobectomy or near total thyroidectomy
Papillary thyroid carcinoma		
Follicular thyroid carcinoma		
Poorly differentiated carcinoma		
Anaplastic carcinoma		
Squamous cell carcinoma		
Carcinoma with mixed features		
Metastatic malignancy		
Non-Hodgkin lymphoma		
Others		

Table 1.3: Bethesda System for Reporting Thyroid Cytopathology

Although the Bethesda system is able to determine the risk of malignancy, about 15-40% of FNA samples are included in Bethesda group III or IV which are indeterminate lesions (210, 211). As pointed in table 1.3 10-40% these lesions are malignant and originally, repeat FNA and diagnostic lobectomy were recommended for these lesions (210). Nevertheless, around 80% of samples from lobectomy patients classified as Bethesda III and IV lesions are ultimately benign.
Therefore, much research has been centered on better identifying high risk patients classified as Bethesda III and IV, to avoid unnecessary surgery or to perform more aggressive treatment in case they are predicted to be an aggressive tumor.

The 2015 ATA guidelines have proposed three novel molecular diagnostic tools in order to further stratify the risk of those patients with undetermined lesions. One of the most affordable molecular testing, consists in the evaluation of a seven gene panel of mutations and rearrangements that includes *$BRAF^{v600e}$, H-RAS, N-RAS* and *K-RAS* as well as *Rearranged during transfection / Papillary carcinoma type I and III*, (*RET/PTC1, RET/PTC3)* and *Paired box gene 8 / Peroxisome proliferator-activated receptor gamma-1* (*PAX8/PPARγ) rearrangements* (207, 212). In indeterminate cytology nodules, the sensitivity of the seven-gene mutational panel testing is variable, with reports ranging from 44% to 100% (213-215). For instance, using the 7-gene panel *RAS* and *BRAF* mutations were the most commonly detected. Interestingly, in a series of 67 prospectively identified RAS-positive thyroid nodules, cytology was malignant in 3%, benign in 3%, and indeterminate in 94% of the cases. Positive testing for *BRAF, RET/PTC* or *PAX8/PPARγ* was specific for a malignant outcome in almost 100% of cases, although *BRAF* mutation sensitivity is too low to reliably rule out the presence of malignancy. Therefore, only these last nodules are classified as cytologically-diagnosed thyroid carcinoma (207).

Regarding *RAS* mutations, it has been seen that their presence relates to an 80% risk of cancer and a 20% chance of benign follicular adenoma in Bethesda III and IV patients, which makes difficult to determine their risk of malignancy. In consequence, they are considered in a similar risk category to cytologically suspicious for malignancy, which can lead to an undertreatment of patient with highly aggressive *RAS* mutations, or to an overtreatment of other more benign forms (207, 216). There is evidence that the risk of malignancy varies with the *RAS* isoform that is mutated. One group demonstrated that the specific isoform of *RAS* that was mutated in follicular neoplasms (Bethesda IV) determined the relative risk of malignancy, being greatest with *H-RAS* (80-90%), compared to *N-RAS* (75-85%) and *K-RAS* (41-61%) (217) (218). By contrast, there are several series demonstrating predominance of *N-RAS* mutations (219-221).

Nowadays, no genetic test is able to discern between high or low risk *RAS* mutations, since the same mutation can lead to the development of a thyroid carcinoma or not. Neither this is an indicator that will define their risk of distant spreading. If molecular testing is either not

performed or inconclusive, surgical excision may be considered for removal and definitive diagnosis of these thyroid nodule. Nodules lacking all of these mutations still have a substantial cancer risk (222). To assess nodules risk of malignancy, another tests have been tried, such as the 167 GEC, that analyzes the mRNA expression of 167 genes (223) and galectin-3 immunohistochemistry (224) but, currently, there is no single optimal molecular test that can definitively rule in or rule out malignancy in those cases of indeterminate cytology, and, importantly, in *RAS* mutated ones. Therefore, long-term outcome data with clinical utility is necessary to draw conclusions.

1.5.3.2 Thyroid cancer

Thyroid malignant lesions can mainly arise from either follicular cells, being the most common ones, or from C cells. Tumors that have other origin are exceptional.

There are different follicular-derived thyroid cancers that include: differentiated thyroid cancer, poorly differentiated carcinoma and anaplastic thyroid cancer, the most aggressive form (225) **(Fig. 1.14)**. Tumors arising from C cells of neuroendocrine origin are known as medullary thyroid carcinomas (226). This thesis will focus exclusively in follicular-derived thyroid cancers.

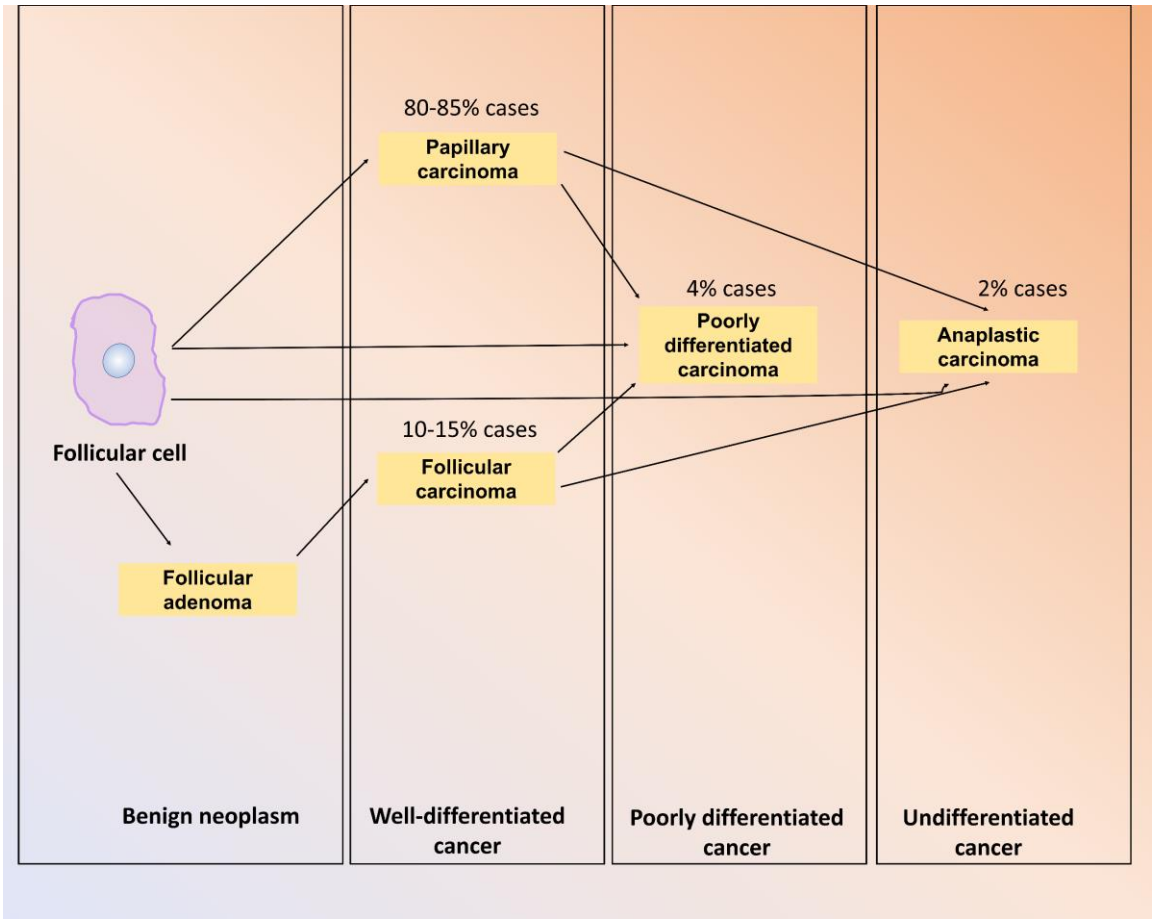

Figure 1.14: follicular-derived thyroid cancers and incidence.

1.5.3.2.1 Differentiated thyroid cancers

These types of thyroid cancers are the most common, accounting for more than 95% of the cases. They can be divided depending on their level of differentiation into well differentiated, under this category are Papillary Thyroid Cancer (PTC) and Follicular Thyroid Cancer (FTC), where we can include its less common variant: the Hürthle cell thyroid cancer (227).

1.5.3.2.1.1 Papillary carcinoma

PTC is a well-differentiated adenocarcinoma, often multifocal (20%) and is the major subtype accounting for 80-85% of thyroid cancers (228). There are different variants, including: papillary carcinoma, follicular variant of PTC, encapsulated variant of PTC, papillary microcarcinoma, columnar cell variant of PTC and oncocytic variant of PTC (229). They have been highly associated to ionizing radiation and they have the best overall prognosis as they tend to grow and metastasize slowly and generally in cervical lymph nodes (20-50%), and, more exceptionally, in lungs. Moreover, unlike other tumors PTC excellent prognosis is not affected by the extension of this cancer to lymph nodes, where micrometastases (<2 mm) can be present in 90% cases, and more than 95% of patients diagnosed with this cancer are alive after 10 years (201, 230, 231).

These tumors are histologically complex, branching with papillary structures, a fibrous tail surrounded by neoplastic tissue, and display characteristic nuclear alterations such as; eosinophilic intranuclear inclusions; finely dispersed optically clear chromatin also called ground glass and Orphan Annie nuclei or micronucleoli. Moreover, Psammoma bodies, present in 50% of tumors, are round concentric collections of calcium and are almost pathognomonic for PTC (229).

1.5.3.2.1.2 Follicular thyroid carcinomas (FTC)

FTC is defined as a differentiated, malignant, follicular epithelial tumor that does not have the PTC typical nuclear alterations. It represents 10–15% of all the thyroid carcinomas and its overall survival is around 85% in 10 years. Rarely they are multifocal and they do not usually colonize locoregional ganglion, although they are more likely to spread to distant organs, mainly lungs and bones in around 70% of the cases. Their main risk factor is insufficient dietary iodine and due to that their incidence, unlike PTC, is decreasing (201, 206, 232). There are three types that are: minimally invasive follicular carcinoma (with capsular invasion only), encapsulated angioinvasive and widely invasive. Patients diagnosed with FTC are mainly women (75%) and the peak age is higher than in papillary carcinoma. Histologically, they are highly variable (from well-formed follicles to solid or trabecular growth) not being their cellular characteristics or cytoarquitecture exclusive for malignant lesions. Then, the only difference between them is their invasive capacity (capsular and/or vascular) (229).

Hürthle cell carcinoma derives from oncocytic follicular cells, that are polygonal cells with granular and eosinophilic cytoplasm, full of mitochondria. These tumors can be poorly or highly invasive. Nevertheless, it is usually more aggressive than other differentiated cancers and is associated to higher rates of distant metastases (233, 234).

1.5.3.2.1.3 Differentiated thyroid cancer treatment

The basic goals of initial therapy for patients with DTC are to improve overall and disease-specific survival, reduce the risk of persistent/recurrent disease and associated morbidity, and permit accurate disease staging and risk stratification, while minimizing treatment-related morbidity and unnecessary therapy.

The new 2015 American Thyroid Association (ATA) guidelines have changed the surgical management recommendations of patients with biopsy proven for differentiated thyroid cancer (DTC). In the old guidelines all patients with a >1 cm nodule diagnosed with DTC were recommended to undergo total thyroidectomy as the primary treatment option. However, since thyroid surgery is not without risk, the mostly indolent course of these tumors and some recent studies demonstrating that in properly selected patients, clinical outcomes are very similar after hemithyroidectomy and total thyroidectomy (235-238), the new 2015 ATA guidelines have suggested hemithyroidectomy as an acceptable option for malignant nodules 1–4 cm in diameter without extrathyroidal extension, and without clinical evidence of any lymph node metastases (cN0) (207). This measure has been the most controversial change since they suggest that hemithyroidectomy is equivalent to total thyroidectomy for low risk cancer between 1-4 cm in diameter (239).

1.5.3.2.2 Poorly differentiated and anaplastic thyroid carcinomas

Poorly Differentiated Thyroid Carcinoma (PDTC) and Anaplastic Thyroid Carcinoma (ATC) account 5-10% of thyroid cancers and represent a major clinical challenge since they are very aggressive and have a mean survival of 3.2 and 0.5 years, respectively, from the time of diagnosis. Particularly, anaplastic cancers have an almost 95% mortality in 5 years and have no available treatment options (240, 241).
PDTC is a malignant follicular neoplasm with limited follicular cell differentiation and with an intermediate clinical behavior between well differentiated and anaplastic carcinoma (62) (242). It is more common in older patients, mean age 55-63 years, and it is relatively more usual in Europe and South America than in Unites States. These tumors usually extend to perithyroidal soft tissue, 60-70% of cases; undergo vascular invasion in 60-90% cases; with a distant metastasis rate of 40-70%, mainly to lungs and bone, and nodal invasion rate between 15-65%. This results in 3 years survival rate of the 38% of patients with nodal and hematogenous metastases (62).

The histology description follows the Turin consensus diagnostic criteria that includes: solid, trabecular or insular growth pattern, no nuclear features of papillary carcinoma and the presence of at least one of the following: convoluted nuclei, >3 mitotic figures/10 high power field or tumor necrosis. It stains positive for keratin, Thyroid Transcription Factor (TTF1) and Ki67 (10-30%) and negative for calcitonin and Parathyroid Hormone (PTH) (64).

ATC is an undifferentiated, high grade, follicular cell carcinoma of the thyroid gland and it usually presents as a rapidly enlarging, bulky neck mass that invades adjacent structures causing hoarseness, dysphagia and dyspnea. The mean age is 70 years and it is often presented with local and distant metastases in lungs, bone and with lower frequency in liver and brain, being all considered since diagnosis high stage (IV) tumors (243). The etiology is unknown although 50% arise from prior multinodular goiter suggesting a possible relationship with iodine deficiency.
Histologically there are three patters that can be seen singly or in any combination:

- Sarcomatioid: Malignant spindle cells are present, and it resembles high grade pleomorphic sarcoma.
- Giant cell: highly pleomoporphic tumors with some tumor giant cells and might have blood vessel structures that resemble aneurysmal bone cysts.
- Epithelial: squamous tumors nests with occasional focal keratinization are present.

Moreover, necrosis, vascular invasion, high mitosis, heterologous differentiation, acute inflammation and some other less common variants such as the paucicellular one can be found. It stains positive for Paired Box Gene 8 (PAX8), Keratin, vimentin, p53, increased KI-67 and Proliferation Cell Nuclear Antigen (PCNA). It is negative for calcitonin, thyroglobulin and TTF1 (64).

1.5.3.2.2.1 PDTC and ATC treatment

Patients with PDTC and ATC must undergo total thyroidectomy and neck dissection in order to remove any lymph node affected. Moreover, RAI is used when possible and suppressive thyroxine therapy is fundamental too (244).

1.5.4 Thyroid cancer genetics

Thyroid cancer it is thought to undergo a multistep carcinogenesis model, accumulating mutations, that promote progression through a dedifferentiation process. Firstly, this causes well-differentiated carcinomas as PTC and FTC eventually giving rise to PDTC, thought to be an intermediate tumor that can derive later to the most aggressive form, the ATC (245, 246). However, some evidences supporting ATC arising *de novo* has nurtured a novel less studied theory: the fetal cell carcinogenesis theory. This theory propose that cancer cells arise from fetal thyroid cells remnants instead of normal adult thyroid follicular cells (247).

The Cancer Genome Atlas of the Thyroid (TCGA) shows that PTC has 11 non-synonymous mutations per tumor, that is: 0.41 mutation per Mb on average, which is one of the lowest among solid tumors (248). In contrast, ATC shows 90 non-synonymous mutation per tumor, around 3 per Mb, that is a much higher mutation rate supporting the multistep carcinogenesis model (249, 250).

The DNA sequencing studies in thyroid carcinomas have disclosed accumulation of mutations affecting genes encoding: growth factors and cell cycle regulators plus genetic and epigenetic alterations of multiple genes. However, there is a signaling pathway that harbor most of thyroid cancer mutations and drives nearly 70% of thyroid tumors, the well-known RAS-ERK signaling pathway. This pathway, key for thyroid cancer initiation, is essential to transmit growth factor external signals from the plasma membrane to the nucleus, a process that is crucial for regulating cellular proliferation (166, 250, 251). Another pathway that has seen to be crucial is the PI3K/AKT, which is fundamental for thyroid cancer progression along with P53 alterations and TERT mutations (201) **(Fig. 1.15)**.

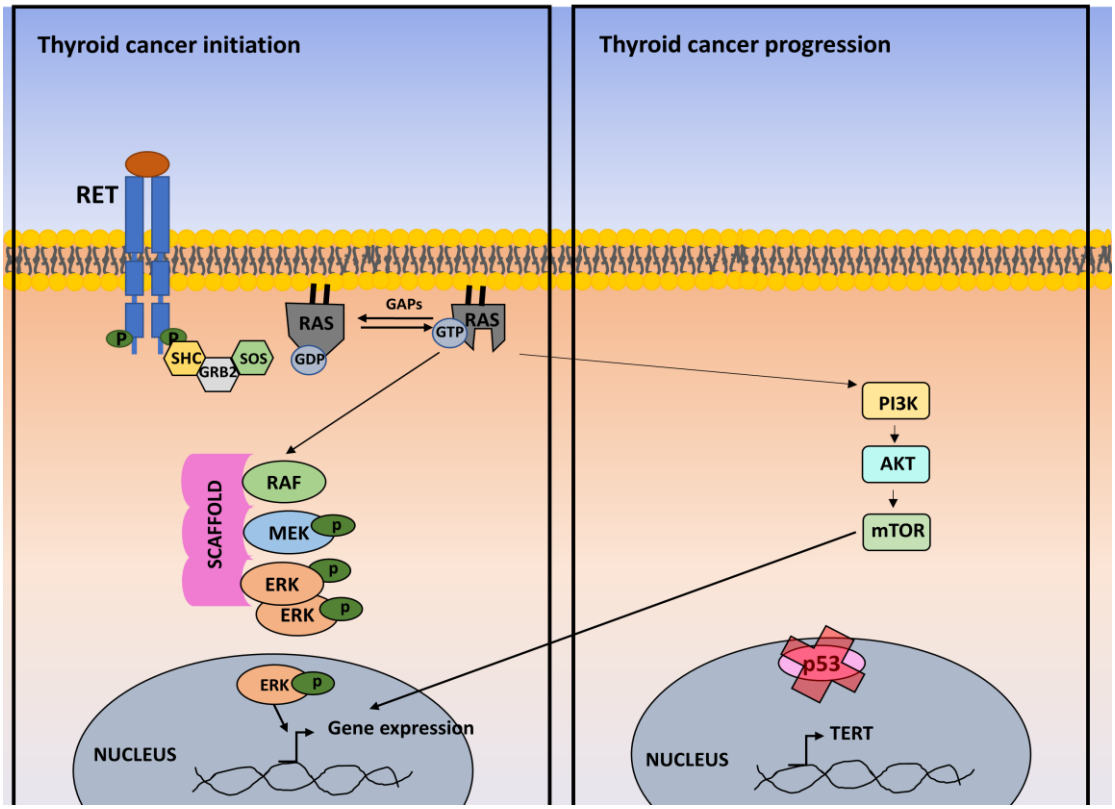

Figure 1.15: Thyroid cancer pathways. Image shows the fundamental signaling pathways involved in thyroid cancer. The left box shows the most mutated one, that is the MAPK signaling pathway, which has been thought to initiate thyroid cancer development by altering gene expression, which promotes cell proliferation, cell growth, angiogenesis, and loss of differentiation. The right box shows pathways that promote tumor progression and are altered in advanced thyroid cancers. This includes the PI3K–mTOR pathway and alterations in p53 tumor suppressor, and in the promoter for TERT (201). mTOR=mammalian target of rapamycin. PI3K=phosphatidylinositol-3-kinase. TERT=telomerase reverse transcriptase.

Many **PTC** tumor initiating events have been identified and all of them involve a single pathway: the RTK/RAS/RAF/MAPK pathway, obeying an exclusion principle where only one component of the pathway is mutated in a given tumor. *RET* rearrangements, mainly, and less frequently, *Neurotrophic Receptor Tyrosine Kinase* (*NTRK*) and *Anaplastic Lymphoma Kinase* (*ALK)* rearrangements or *RAS* (26%) *(252)* and *BRAF* activating point mutations are some of the main alterations, although *BRAF* accounts mostly 60% of the mutations.

FTC main drivers are *RAS* mutations accounting around 40% of them (252), mostly activating PI3K/AKT signalling pathway to promote tumorigenesis and *PAX8/PPARγ* rearrangements.

PDTC and **ATC** have a high mutation rate for *RAS* (53%) (252) that together with other alterations such as *telomerase reverse transcriptase* (*TERT)* (253) and *eukaryotic translation initiation factor 1A in chromosome X* (*EIF1AX*) (254) mutations confer worse prognosis, which also occurs in **PTCs**. ATC has also *TP53* frequently mutated, which confer aggressiveness if co-occurring with *RAS*. Moreover β-catenin is also frequently mutated in these tumors together with mutations in genes encoding components of the SWI/SNF chromatin remodeling complex, mostly in ATC (36%), including *AT- Rich Interacting Domain-containing proteins 1A, 1B, 2 and 5B* (*ARID1A*, *ARID1B*, *ARID2* and *ARID5B*) (245, 248).

Mutations in genes encoding members of the PI3K/AKT/mTOR pathway were also seen more frequently in ATCs than PDTCs mainly in *PIK3CA* and *PTEN* genes, which could also be epigenetically regulated altering its function in thyroid cancer (245). Moreover, loss of expression of thyroid differentiation markers, such as *PAX8*, is one of the hallmarks of advanced thyroid cancers causing loss of *NIS* expression leading to resistance to radioiodine therapy (245, 255).

1.5.4.1 Oncogenic rearrangements

RET is a versatile receptor tyrosine-protein kinase that binds ligands from the Glial Derived Neurotropic Factor (GDNF) family, triggering the phosphorylation of several proteins such as SRC, Signal Transducer and Activator of Transcription 3 (STAT3), Phospholipase C Gamma (PLCγ) and ENIGMA, plus the common RAS/ERK and PI3K/AKT signaling pathways. Therefore, it participates in numerous cellular processes such as proliferation, migration and differentiation (256, 257). *RET* rearrangements, mainly *RET/PTC1* and *RET/PTC3*, that are a fusions of the tyrosine kinase domain of *RET* to *Coiled-Coil Domain Containing 6 (CCDC6)* or *Nuclear Receptor Co-Activator 4 (NCOA4)* respectively, the later being of worse prognosis (258). As pointed before, RET rearrangements are very common in PTC, although they can also be found in thyroid adenomas (259), in FTC but in a less prevalence, in 14% of PDTC and are completely absent in ATCs (245).

RET, NTRK and ***ALK*** rearrangements are genetic events that occur mainly in PTC. Although they have the potential to activate pathways such as the PI3K-AKT axis, their oncogenic potential in the thyroid has been mostly related to the activation of the RAS-ERK pathway (260, 261).

Another common rearrangement is the ***PAX8/PPARγ*** which is mainly found in FTC (262, 263).

1.5.4.2 Mutations

1.5.4.2.1 BRAF

The most common *BRAF* mutation, accounting for 95% of the total, is a Valine 600 (V) change to a glutamic acid (E) ($BRAF^{V600E}$) in the activation loop, promoting BRAF constitutive activation independent of RAS and with no requirement for dimerization. The V600E mutation also increases BRAF kinase activity up to 500-fold as compared to wild-type BRAF (264, 265). Data from the TCGA network surveying a large panel of PTC, confirmed that PTC with $BRAF^{V600E}$ mutations are associated with a undifferentiation state and higher ERK activation than tumors harboring RAS mutations (248). Co-occurrence of *BRAF* and *TERT* synergistically increase the aggressiveness of the tumor (266). It must be said that *TERT* mutations are found at a relatively low prevalence in PTC (around 11%), but its higher in metastatic PTC, PDTC (30–40%) and ATC (30–70%) (267, 268). A less common *BRAF* mutation, *K601E*, has been detected in benign thyroid adenomas and in the follicular variant of PTC, strikingly showing a RAS-like behavior (269, 270).

1.5.4.2.2 PI3K/AKT

PI3K/AKT activation is thought to be critical in FTC initiation through mutations in *RAS* or inactivating mutations in the tumor suppression gene *PTEN*, or by activating mutations in the *PIK3CA* and *AKT1* genes. Some patients with PTC and FTC may progress to RAI-refractory metastatic disease, and these tumors are particularly enriched with mutations in *BRAF* and *RAS* coexisting with *PIK3CA* or *AKT1* (271, 272). Moreover, thyroid cancer progression and dedifferentiation to PDTC and ATC also involve a number of additional mutations that affect other cell signaling pathways such as p53 and WNT/β-CATENIN (273, 274).

histo-types	RET/PTC Gene fusion	BRAF (V600E) mutations	RAS mutations	PAX8/PPARγ Gene fusion	CTNNB1 (B catenin) mutation	TERT mutations	TP53 mutations
FA	0%	0%	17-43%	8%	0%	0%	0%
PTC	13-43%	30-69%	0-21%	0.3%	0%	9%	0-5%
FTC	0%	0%	40-53%	39%	0%	15%	0-9%
PDC	0-13%	0-13%	18-55%	0%	25%	40%	17-38%
ATC	0%	10-35%	4-60%	0%	66%	73%	60-88%

Table 1.4. Thyroid cancer histological types and their frequency of some of their most common mutations. Adapted from *Kakudo et al* "Thyroid Follicular Cell Neoplasms in Multistep Carcinogenesis" *Journal of Basic & Clinical medicine 2015 4(1):13-21*

1.5.4.2.3 RAS

RAS is one of the most frequently mutated oncogenes in cancer and is activated in one-third of all human tumors. *RAS* activating mutations in thyroid epithelial cells were first reported in the 1980s and have been directly implicated as early frequent events in transformation and proliferation of thyroid carcinoma (275). *RAS* represents the second most common genetic mutation identified in thyroid cancer and includes the 3 isoforms: N-RAS, K-RAS, and H-RAS. Single base missense mutations, leading to a constitutively activation of RAS by locking it in a GTP-bound active form, are mainly in codons 12/ 13 which affect the guanosine triphosphate (GTP)-biding domain, and in 61, which alters the GTPase domain (252).
N-RAS mutations in codon 61 are the main RAS alterations found in thyroid cancers, and substitution from a glutamine (Q) to an arginine (R) is the most common. It is followed by *H-RAS* mutations in codon 61, *K-RAS* mutations in codons 12/13 and *H-RAS* mutations in codon 12. However, N-RAS has been mainly found in well-differentiated carcinomas whereas *K-RAS* mutated in codon 12/13 and *H-RAS* mutated in codon 12 have been found mainly in PDTC and ATC, although they can also be found in PTC and FTC. Overall this suggest that different mutations can be related to some extent with patient outcomes (252, 276). There are some discrepancies related to the overall frequency of *RAS* mutations (ranging from 7 to 62%) and their prevalence in specific thyroid tumors (219, 277, 278). It is well accepted that *RAS* mutations, although common in follicular adenomas or in well-differentiated carcinomas (follicular or papillary), have higher prevalence in poorly differentiated and anaplastic carcinoma. See (table 1.4).
In thyroid cells, RAS mainly activates PI3K/AKT, a critical event in FTC initiation, rather than RAS-ERK signalling that is more related with BRAF driven oncogenicity (279).

Several studies have related RAS with high rates of mortality (276, 280) and distant metastasis (281, 282). However, a high number of follicular adenomas (FA) have *RAS* mutations and some of them will never progress to thyroid cancer, which makes difficult to propose RAS as a risk factor and further research is necessary to elucidate this baffling behavior. Although some research has been done in this matter, showing RAS co-occurrence with *TERT* promoter and EIF1AX mutations frequently associated with a worse prognosis than tumors harboring only *RAS* mutations (245). However, not all RAS mutated ATC co-occur together with TERT or EIF1AX mutations and therefore are unable to fully explain RAS seemly changing behavior.

2. Objectives

2. OBJETIVES

RAS is commonly mutated in thyroid cancer. In consequence, considerable efforts have been made in order to apply RAS mutations as molecular markers to the clinical management of thyroid nodules and cancer, as new guidelines are heading to more conservative treatments. However, no good marker has been found yet. Moreover, due to RAS presence in benign adenomas and its uncertain role in the clinical outcome of thyroid cancer more research is needed. Since RAS has recently been found to be present and functional in different subcellular localizations as at lipids rafts, disordered membrane, the Golgi Complex and endoplasmic reticulum and has been shown to modulate exosomes biogenesis and cargo, we wanted to explore their implications in thyroid tumorigenesis. Thus, the aims of this thesis are:

1. **Study how RAS at its different subcellular locations contribute to thyroid tumorigenesis**

2. **Find new markers to rule out indeterminate thyroid nodules risk of malignancy and thyroid cancer aggressiveness**

3. **Adress the relevance of exosomes in thyroid cancer tumorigenesis mediated by RAS at its different sublocalizations**

3. Material and Methods

3. MATERIAL AND METHODS

3.1 DNA purification and plasmid description

3.1.1 Plasmidic DNA purification from bacterial cultures

A bacterial competent colony (DH5α, a *E. Coli* strain engineered to maximize transformation efficiency) containing the plasmid of interest was inoculated in four 5 ml Lysogeny Broth (LB) containing tubes with their specific resistance antibiotic, ampicillin or kanamycin. They were left shaking at 200 rpm at 37ºC Over-Night (ON). The bacterial culture was harvested by centrifugation at 8000 rpm for 2 minutes at room temperature and we Plasmidic DNA was extracted using GeneJET Plasmid Miniprep Kit (Thermo Fisher). In order to resuspend the cells we added 250 μL of Resuspension Solution and vortexed, 250 μL of Lysis Solution was then used to lyse bacteria then 350 μL of Neutralization Solution was added and centrifuged at 13,000 rpm for 5 minutes.
The supernatant was then transferred to a Thermo Scientific GeneJET Spin Column and centrifuged at 13,000 rpm for 1 minute. After that, columns were washed twice with 500 μL.
To elute the purified DNA 40 μL of Elution Buffer was added to the column and incubated 2 minutes. Finally, it was centrifuged for 2 minutes at 10,000 rpm and the flow-through containing the Plasmidic DNA was collected.

3.1.2 Plasmids

Plasmid	Brief description
pCEFL	Plasmid used as an expression vector
pCEFL-HA*-HRAS-G12V	H-RASv12 construct presents H-RAS mutated in Glycine 12, presenting a valine instead and its located in every compartment of the cell. HA HA was used as a Tag to detect protein expression by western blotting.
pCEFL-M1-HA*-HRAS-G12V SS	This construct tethers H-RASv12 to ER. HA was used as a Tag to detect protein expression by western blotting.
pCEFL-LCK-HA*-HRAS-G12V SS	This plasmid locates H-RASv12 in Lipids Rafts. HA was used as a Tag to detect protein expression by western blotting.

pCEFL-CD8-HA*-HRAS-G12V SS	This construct directs H-RASv12 to disordered membrane, also known, al bulk membrane. HA was used as a Tag to detect protein expression by western blotting.
pCEFL-KDELN-HA*-HRAS-G12V SS	Thanks to this plasmid H-RASv12 is located in *cis* face of Golgi Complex. HA was used as a Tag to detect protein expression by western blotting.
pCEFL-HA*-NRAS- G12V	This plasmid present N-RAS mutated at position 12 (G>V). HA was used as a Tag to detect protein expression by western blotting.
pCEFL-M1-HA*-NRAS- G12V S	This construct tethers N-RAS mutated at position 12 (G>V) to ER. HA was used as a Tag to detect protein expression by western blotting.
pCEFL-LCK-HA*-NRAS- G12V S	This plasmid locates N-RAS mutated at position 12 (G>V) in Lipids Rafts. HA was used as a Tag to detect protein expression by western blotting.
pCEFL-CD8-HA*-NRAS- G12V S	This construct directs N-RAS mutated at position 12 (G>V) to disordered membrane, also known, al bulk membrane. HA was used as a Tag to detect protein expression by western blotting.
pCEFL-KDELN-HA*-NRAS- G12V S	Thanks to this plasmid N-RAS mutated at position 12 (G>V) is tethered to the *cis* face of Golgi Complex. HA was used as a Tag to detect protein expression by western blotting.
pCEFL-HA*-KRAS-G12V	This plasmid presents K-RAS mutated at position 12 (G>V). HA was used as a Tag to detect protein expression by western blotting.
pCEFL-M1-HA*-KRAS-G12V	This construct tethers K-RAS mutated at position 12 (G>V) to ER. HA was used as

	a Tag to detect protein expression by western blotting.
pCEFL-CD8-HA*-KRAS-G12V	This construct directs K-RAS mutated at position 12 (G>V) to disordered membrane, also known, al bulk membrane. HA was used as a Tag to detect protein expression by western blotting.
pCEFL-FLAG-CDC25	RASGRF1 CDC25 domain, known to specifically activate endogenous H-RAS (283). FLAG was used as a Tag to detect protein expression by western blotting.
pCEFL-M1-FLAG-CDC25	RASGRF1 CDC25 domain, known to specifically activate endogenous H-RAS (283). M1 protein tethered it to endoplasmic reticulum. FLAG was used as a Tag to detect protein expression by western blotting.
pCEFL-LCK-FLAG-CDC25	RASGRF1 CDC25 domain, known to specifically activate endogenous H-RAS (283). LCK protein tethered it to lipids raft. FLAG was used as a Tag to detect protein expression by western blotting.
pCEFL-CD8-FLAG-CDC25	RASGRF1 CDC25 domain, known to specifically activate endogenous H-RAS (283). CD8 protein tethered it to disordered membrane. FLAG was used as a Tag to detect protein expression by western blotting.
pCEFL- KDELN-FLAG-CDC25	RASGRF1 CDC25 domain, known to specifically activate endogenous H-RAS (283). KDELN protein tethered it to Golgi Complex. FLAG was used as a Tag to detect protein expression by western blotting.
pCEFL-FLAG-APT1	This construct carries the acyl-protein thioesterase-1, APT1, an enzyme that

	removes palmitate for diverse palmitoyl protein substrates, as N-RAS and H-RAS. FLAG was used as a Tag to detect protein expression by western blotting.

Table 3.1: Plasmid names and description.

To investigate whether RAS subcellular locations affects thyroid tumorigenesis we used a wide number of constructs that tether H-RAS-G12V (For now on H-RASv12), N-RAS-G12V (For now on N-RASv12) or K-RAS-G12V (For now on K-RASv12) to its different subcellular locations. All these constructs have a resistance for geneticin.

Constructs were already described and used in our laboratory (110, 284) and have the following characteristics:

SS and S: In order to tether RAS to its different locations, we generated palmitoylation-deficient H-RASv12, N-RASv12 and K-RASv12 by mutating cysteines 181 and 184 in H-RAS, cysteine 181 in N-RAS or 180 in K-RAS to serines. In consequence, RAS is not longer efficiently retained at the PM and exists in a dynamic equilibrium shuttling between the ER and cytoplasmic pools. The palmitoylation signal was then substituted by the following cues at RAS N-terminus that specifically direct H-RASv12 SS, N-RASv12 S or K-RASv12 S to the desired locations:

- **The avian infectious bronchitis virus M protein (M1):** When RAS is fused in its N-terminus amino acids 1 to 66 of M1 is delivered to the ER (3)(285).

- **KDEL receptor (KDELr) N193D:** N193D was introduced in KDELr in order to avoid its recycle to the ER. This mutation then prevents KDELr redistribution to the ER and renders it a resident Golgi protein (110, 286).

- **CD8α:** The transmembrane domain of the CD8α receptor directs proteins to bulk membrane (DM) (284, 287).

- **LCK:** LCK myristoylation signal that when placed in RAS N-terminus is able to anchor it effectively to lipids rafts (110).

CDC25 constructs: All CDC25 constructs are composed of RASGRF1 CDC25 domain fused to the sub-localization-defining cues. Herrero A. and colleagues determined that the CDC25 domain has a high specificity for activating endogenous HRAS (HRAS-GTP) but not NRAS and KRAS (283).

Moreover, apart from these tethering signals all of our constructs have a tag epitope that can be the amino acids 98-106 of the Human influenza hemagglutinin (HA), or FLAG that consist of eight amino acids, DYKDDDDK, to enable the detection of these proteins (288, 289). When HA presents * means that HA ATG initiation codon has been deleted in order to avoid reading lecture frame errors.

3.2 Tissue Culture

3.2.1 IMMORTALIZED CELL LINES

3.2.1.1 Wild type cells

PCCL3 are well differentiated rat thyroid follicular cells that were firstly isolated from 18 months donor rats and were spontaneously immortalized. Their doubling time is 24 hours (290).

Culture Medium:

- 1 L of sterile milliQ water mixed with one vial of Nutrient Mixture F-10 Ham powder (Sigma).
- 2,69 g of sodium bicarbonate (Sigma)
- 5% Calf Serum (Gibco)
- Hormones and their working solutions:
    - Gly-His-Lys acetate Salt (Sigma) (20 ng/ml)
    - Hydrocortisone (Sigma) (10 ng/ml)
    - Somatostatin (Sigma) (10 ng/mL)
    - Insulin from bovine pancreas (Sigma) (10 μg/mL)
    - Human apo-Transferrin (Sigma) (5 μg/mL)
    - TSH (Sigma) (0.5U/μL)
- 1% Penicillin-Streptomycin (10,000 U/mL) (Sigma)
- 1% MEM Non-essential amino acid solution (100X)
- 1% Amphotericin B (250 μg/mL) (Gibco)
- 1% Glutamine 100X (Gibco)

Final pH should be 7.4. The whole media is passed through a 22 μm filter vacuum cup in order to avoid any contamination.

Basal media:. This media does not contain any hormones, calf serum, glutamine and MEM Non-essential amino acids.

Since there are no untransformed cell lines from human origin and several groups have been using them extensively to explore the effects of different oncogenes *in vitro* (291-293), we have chosen PCCL3 as our reference cell line to study RAS sublocalizations effects.

3.2.1.2 Human Anaplastic thyroid cancer cell lines

- C643 is a human anaplastic thyroid cancer cell line isolated from a 76-year-old male. They have mutations in H-RAS in position 13 (G13C) and it is heterozygous for *TERT* (228 C>T). This last mutation is located at its promoter (268, 294, 295).

- HTH83 is another human anaplastic thyroid cancer cell line isolated from a male age 66. They have a mutation in H-RAS changing a Glutamine in 61 position for an Arginine. Moreover, it is heterozygous for *TERT* (228 C>T) (268, 294, 295).

Culture Medium: They both were grown in Dulbecco´s Modified Eagle Medium (DMEM) (Thermo Fisher) supplemented with 10% Fetal Bovine Serum (Gibco) and 1% Penicillin-Streptomycin (10,000 U/mL) (Thermo Fisher).

Basal medium: DMEM culture media without Fetal Bovine Serum.

All cells were grown at a 37ºC and 5% CO_2 incubator.

3.2.2 CELLULAR TRANSFECTIONS

3.2.2.1 Lipofectamine LTX

PCCL3 were transfected with the different plasmids described before, using Lipofectamine LTX (Thermo Fisher). Cells were seeded to be 80% confluent at transfection. 14 μL of LTX was diluted in 500 μL Opti-MEM medium (Thermo Fisher). Then, 3.5μg of DNA was diluted in another eppendorf tube containing 500 μL Opti-MEM medium and 18 μL of PLUS Reagent was added. DNA was added to the Lipofectamine LTX Reagent tube and was incubated at room temperature for 5 minutes. Meanwhile PCCL3 cells were washed twice with Phosphate-Buffered Saline (PBS) 1X and the DNA-lipid complex was added to cells. Next day, media was completed and cells were incubated for 3 days at 37ºC. A control plate of PCCL3 transfected with a Green Fluorescent Protein (GFP) was analyzed under a Leica microscope to determine transfection efficiency. Generally, a 70% efficiency was achieved. Cells were then selected with Geneticin (G418 (Sigma) 200 μg/ml.

3.2.2.2 Lipofectamine 3000

SiRNA transfection was done using lipofectamine 3000 (Thermo Fisher). PCCL3, C643 or HTH83 cells were plated so they were around 80% confluent at the time of transfection. 12μL of Lipofectamine 3000 Reagent was added to Opti-MEM medium (Thermo Fisher). Then, diluted Small Interfering RNA (siRNA) (10 μM/ml) was added to the lipofectamine 3000 tube (1:1 ratio) and incubated for 10 minutes. During that time, cells were washed twice in PBS 1X and mixture was added. Cells were left ON with the mixture and media was completed. At 36 hours transfected cells were collected to perform the chick embryo assays or they were left 3 days for other *in vitro* assays.

SiRNA	Company (Catalog)
LYPLA1 siRNA (Human) 10 μM	Santa Cruz Biotechnology (sc-77637)

Table 3.2: SiRNA description and Company.

3.2.3 PROLIFERATION ASSAYS

3.2.3.1 AlamarBlue proliferation assay

To perform proliferation assays we used AlamarBlue Cell Viability Reagent (Thermo Fisher) that has as active component a non-toxic, cell-permeable non-fluorescent blue compound called Resazourin. This molecule can be reduce by several mitochondrial reductases (NADPH, NADH, FADH) as it acts as an intermediate electron acceptor in the electron transport change and as well by cytochromes and other enzymes as flavin reductase or NAD(P)H: quinone oxidoreductase. This indicates viability and indirectly number of cells by giving rise to a red highly fluorescent compound that is Resorufin. In consequence this change of color can be measure using absorbance-based place readers using 600 nm as a reference wavelength and monitoring reagent absorbance at 570 nm (296).

We plated 6,000 cells per well in a corning 96-well plate in 100 μL complete medium and led them seat overnight. Then, complete medium was changed to 90 μL starving medium for 12 hours. After that time, 10 μL of room temperature AlamarBlue Reagent was added and incubated in the dark at 37ºC, in the same cell incubator, for 12 hours. Then, absorbance was read as explained above.

3.2.3.2 IncuCyte proliferation Assays

In a 96-well plate, 3 x 10^3 PCCL3 cells transfected with the different HRASG12V constructs in 100 µl of starving medium were mixed with 10^4 freshly prepared EVs isolated by size exclusion (material and methods 3.8.1.1) in starving medium per cell (about the same number

of EVs secreted by each PCCL3 cell in 24 hour) for 30 minutes at 37ºC. Growth was followed over a period of three days by live image acquisition using the IncuCyte ZOOM® analysis system (10x magnification; Essen Bioscience) to automatically detect cell edges and to generate a confluence mask for cell coverage area calculation. Each biological replicate is represented as mean of at least 8 technical replicates.

3.2.4 *IN VITRO* MIGRATION ASSAY

Cell migration was measured using transwell chambers (Corning, USA) containing 24 well inserts with 8 μm pores. 10,000 cells were dyed with 10μM Green Cell Tracker (Thermo Fisher) for 30 minutes and placed in transwell chambers with 100 μL of basal medium. Wells containing transwell chambers were filled with 100 μL of complete media. After 24 hours cells in the upper chamber were removed and the remaining cells were seen using a Leica fluorescence microscope. Cells were quantified in five randomly selected fields for three independent experiments. The average of cell count per field was presented and compared between the different cells.

3.2.5 Electron microscopy

We first removed media from a 100 mm plate and washed cells twice with 1X PBS. After that, we fixed them with 5 ml of 3% glutaraldehyde in Phosphate Buffer 0.12 M (Buffer 3) for 30 minutes at room temperature.
After, 4 ml were removed, and cells were collected and centrifuged 5 minutes at 7,000 rpm at 4ºC. We then leaved cells in post-fixation for 1-2 hours and centrifuged them at 14,000 rpm at 4ºC. Supernatant was then removed and 1 ml of Phosphate buffer 0.12 M (Buffer 2) was added. Three 15 minutes changes were done (it can be stored at 4ºC in this solution several days). Supernatant was again removed. and pellet was fixed with Osmium Tetroxide 2-4 hours with agitation at room temperature protected from light.
Then, pellets were washed with wash solution pH 4,5-4,6 twice for 15 minutes at 4ºC. Pellets were contrasted with uranyl acetate 90 minutes at 4ºC. Again, two 15 minutes washes at 4ºC were done with wash solution.
The next step is dehydration:

-Acetone 15%.....5 seconds
-Acetone 30%.....10 minutes
-Acetone 50%.....10 minutes
-Acetone 70%.....10 minutes
-Acetone 80%.....15 minutes
-Acetone 95%.....4 times for 15 minutes
-Acetone 100% without water ...3 times for 15 minutes

The last acetone was then substituted by 50% acetone 100% and B mixture. Pellets are there for several hours. After, this is changed to ascendant concentrations of B mixture. (25% (100% acetone) and 75% mixture B, 10% (100% acetone) and 90% mixture B) every 2-3 hours. Then they are left in mixture B over-night. The following morning, mixture B is renewed and is left for 2 hours and we proceeded to pellet inclusion.

Buffers

1. **Phosphate solution (pH 7,2-7,4)**
   $NaH_2PO_4H_20$……..2,4g
   K_2HPO_4……...4g
   H_20 (distilled)…….100 ml

2. **Phosphate solution 0,12 M (pH 7,2-7,4)**
   Phosphate solution 0,4 M…….3ml
   Distilled water……...7ml

3. **3% glutaraldehyde in 0,12 M Phosphate solution**
   25% Glutaraldehyde 25% (Merk ZC755239546)…….1,2ml
   Phosphate solution 0,4M……..3 ml
   0,5% Cl_2Ca (Sigma)…….....40μg
   Distilled water until reach……...10 ml

3.3 Protein analysis

3.3.1 SDS-PAGE AND WESTERN BLOTTING

Cells were collected, washed twice in 1X PBS and lysed with the following lysis buffer:
20 mM HEPES pH 7.5, 10 mM EGTA, 40 mM β-Glycerophosphate, 1% NP40, 2.5 mM MgCl2, 1 mM orthovanadate, 1 mM DTT and 10 μg/ml of aprotinin and leupeptin.
Then, to remove cell debris lysates were centrifuged at 13,000 rpm for 10 minutes at 4ºC. After that, proteins samples were quantified using the Bradford Method. A Bovine Serum Albumin (BSA) standard curve was used to calibrate unknown concentrations.

Laemli 5x tampon (100 mM Tris pH 6.8, 4% SDS, 20% glycerol, 20 mM DTT and 0.005% bromophenol) was added to 40 μg of proteins and heated at 95ºC for 5 minutes.

Antibody	Species	Dilution	Company (Catalog)
HRAS	rabbit	1:4000	Abcam #ab96548
TRANSFERRIN Receptor	mouse	1:1000	Zymed 13-6890
CAVEOLIN	Mouse	1:1000	BD-transduction 610058
APT1 (LYPLA1)	rabbit	1:500	Protein Tech Europe 16055-AP
TUBULIN	mouse	1:4000	Sigma #T8328

Table.3.3: Primary antibodies used for immunoblotting.

Proteins were resolved on sodium dodecyl sulfate-polyacrylamide (SDS) poli-acrylamide gels. SDS-PAGE gel was composed of a stacking part (4% acrylamide, 125 mM Tris-HCl pH 6.8, 0.4% SDS, 0.1% Ammonium Persulfate (APS) and 0.1% Tetramethylethylenediamine (TEMED) in H_20) and a resolving part (acrylamide, 375 mM Tris-HCl pH 8.8, 0.4% SDS, 0.1% APS and 0.1% TEMED in H_20) Then, proteins were electrophoretically transferred to Nitrocellulose membranes (Thermo Fisher) at 400 mA amperage (1 minute for each 1 kDa of the protein) at 4ºC in a Trizma base 25 mM and 192 mM Glycine solution. Membranes were then blocked in Tris Buffered Saline-Tween (TBS-T: 20 mM Tris, pH 7.4, 137 mM NaCl and 0.05% tween) containing 5% BSA for 1 hour at room temperature. Blots were incubated O/N at 4ºC with the different antibodies **(table 3.3)** prepared in blocking solution. The day after, blots were washed (3 x 10´) with TBS-T and incubated for 1 hour with anti-rabbit Immunoglobulin (Ig) (Amersham Pharmacia) or anti-mouse Ig (Amersham Pharmacia) secondary antibodies (1:5000) in 1% milk in TBS-T. After that, membranes were washed with TBS-T 3 times for 10 minutes and blots were developed with an enhanced chemiluminescent system (ECL) and an autoradiography with Konica films was performed to detect proteins.

3.3.2 EVS SDS-PAGE AND WESTERN BLOT

EV preparations for western blot were assessed after normalization based on the amount of proteins in the EV-secreting cells from where they were isolated using cold RIPA buffer (10 mM NaF, 40 mM β-glycerophosphate, 200 μM sodium orthovanadate, Benzamidine 0,1 μg/μl, 100 μM phenylmethylsulfonyl fluoride, 1 μM pepstatin A, 1% NP-40, 0.1% SDS, 0.5% sodium deoxycholate in PBS 1X pH 7.4) supplemented with protease and phosphatase inhibitors (1 μg/ml leupeptin, 4 μg/ml aprotinin) (Sigma). Protein concentration was measured by bicinchoninic acid (BCA) assay (Pierce, Thermo Scientific).

The standardized amount of EVs and total lysates were ultimately dissolved in either reduced 4x Laemmli Sample Buffer (Bio-Rad) with 5% 2-mercaptoethanol or non-reducing sample buffer to asses CD63. Then, samples were heated to 95ºC for 10 minutes before loading. A

pre-stained protein ladder (Bio-Rad) was used for protein size control. Both cell lysates and EV preparations were electrophoretically separated using 10% mini-PROTEAN® precast gels (BioRad) at 140 Volts (V) by sodium dodecyl sulfate–polyacrylamide gel electrophoresis (SDS–PAGE). Protein preparations were ultimately dissolved in either reduced (containing 5% β-mercaptoethanol) or non-reduced (for CD63 detection) sample buffer and were heated to 90-100°C for 10 min before loading with a pre-stained protein ladder (Bio-Rad). Proteins were wet-transferred in cold to Polyvinylidene difluoride (PVDF) membranes at 100 V in 25 mM Tris–HCl, 0.19 M glycine and 10% methanol for 1 hour using a Mini Trans-Blot Cell (Bio-Rad). The membranes were then blocked with either 5% milk (optimal for CD63 detection) or 5% BSA in TBS buffer with Tween-20 (TBST) for 45 minutes and incubated overnight at 4°C with primary antibody **(Table 3.4)** diluted in blocking buffer. After 3 x 10 min washing steps with TBST, the membranes were probed with the relevant secondary antibodies for 1 h at 22°C (anti-mouse IgG (H+L) HRP conjugate (Promega #W4021, 1:10000), anti-rabbit IgG (H+L) HRP conjugate (Promega #W4011, 1:10000) following 3 x 10 min wash steps. The signals were detected using the enhanced chemiluminescent detection reagent (ClarityTM, BioRad) and the Touch Imaging System (BioRad).

Antibody	Species	Dilution	Company (Catalog)
TUBULIN	mouse	1:4000	Sigma #T8328
SYNTENIN	rabbit	1:500	Abcam #ab133267
TSG101	rabbit	1:500	Abcam #ab125011
CD63	mouse	1:1000	Abcam #ab108950
ALIX	mouse	1:500	Abcam #ab117600

Table 3.4: Primary antibodies used to detect Extracellular Vesicles by immunobloting.

3.3.3 GUAVA NEXIN ANNEXIN V ASSAY (APOPTOSIS ASSAY)

The Guava Nexin Annexin V assay relies on a two-dye strategy to detect early and late apoptosis. To detect early apoptosis Annexin V is used due to its high affinity to phosphatidyl serine (PE) a component normally localized to the internal face of the cell membrane that after apoptotic signals translocates to the outer surface, when Annexin V can bind to it. The other dye is 7-AAD that is impermeable and capable to enter late-stage apoptotic and dead cells due to their impairment of their membranes.

200,000 cells were seeded in 60-mm plates and after 48 hours adhered cells and medium containing cells was collected and centrifuged at 1200 rpm for 5 minutes. 1 μM of Staurosporine was added for 5 hours as a positive control, and we proceeded the same. Cells were then resuspended in 1% BSA in 1X PBS to achieve $4x10^5$ cells/mL concentration. Then, 100 μL of these suspensions were transferred to a dark tube containing 100 μL of guava Nexin Reagent (Millipore) thawed to room temperature. After that, samples were stained for 20

minutes at room temperature in the dark. Then, samples were acquired on a Guava Nexin System.

Total apoptosis (Annexin V-PE (early) and 7-AAD + (late)) was determined and analyzed.

3.3.4 PLASMA MEMBRANE FRACTIONATION TO DETECT ENDOGENOUS RAS LOCATION

Four 100-mm dishes of C643 and HTH83 cells were grown to an 80-90% confluence.
Cells were then washed with 1x PBS and were scraped with 1 ml PBS by centrifugation at 1500 rpm for 5 minutes.

Pellet was resuspended in 500 μL of TNET buffer (25 mM Tris-HCL pH 7.4, 150 mM NaCl, 5mM EDTA, 0.01% Triton and 10μg/ml aprotinin and leupeptin) and homogenized, avoiding harsh conditions to limit breakage of lipids rafts microdomains, using a 25 Gauge (G) needle (15 passages) and maintained for 30 minutes at 4ºC in constant agitation.

A discontinuous sucrose density gradient was prepared by layering successive solutions of decreasing sucrose densities upon one another in a 5 mL tube. The lysate was added to one volume of 90% sucrose made in TNET buffer without triton and mixed properly. This new (45%) solution was placed on the bottom of a 5 mL tube. Next, 3,4 mL of 35% sucrose-TNET buffer without triton was loaded slowly and steadily without disturbing the bottom fraction. After that, 1 mL of 16% sucrose-TNET was loaded on top of the gradient. Then, the tube was centrifuge using a MLS-50 Beckman swinging bucket rotor for 18 hours at 41,000 rpm. Twelve 0,4 mL fractions were collected and prepared for analysis by SDS-PAGE and western blotting as described above.

3.4 ANIMAL ASSAYS

3.4.1 CHICK EMBRYO SPONTANEOUS METASTASIS MODEL

Fertilized chicken eggs are incubated on their side in a rotating incubator at 37ºC and 65% humidity for 10 days, rotating three times per hour. On day 10 eggs were placed on their side on an egg rack and using a 30-gauge syringe needle a hole was made in the air sack which is located at the blunt end of the egg. Another hole was made near the allantoic vein, which was firstly localized using a light source contacting the eggshell, using a Dremel rotary tool kit without injuring the Chorioallantoic Membrane (CAM). Then, a third small hole was made using a 20-gauge syringe needle with a small hook made on the end. In order to drop the CAM from the shell, a mild vacuum was applied to the air sack hole working with an automatic pipette with a Tygon tube. Then, a square window around 1 cm^2 was made with a cut off wheel

(Dremel) close to the bifurcation of the allantoid vein. After that, 25μL of the cell suspension containing 1x10^6 cells in starving medium were grafted nearby the allatoid vein bifurcation with a laboratory pipette without touching the CAM. Egg´s window was then sealed with tape and were left to grow for 6 days (C643 and HTH83) or 7 days (all PCCL3-derived cells) or 4 days for all siRNA experiments on a stationary incubator. Then, tumors were excised and weighted and portions of distal CAM, liver and lungs were harvested and analyzed by quantitative Polymerase Chain Reaction (PCR) to determine the number of rat (in case of PCCL3 cells) or human (C643 and HTH83) cells intravasated to the CAM and metastasized to the internal organs (297, 298).

When tumors were treated with VEGF-B (LSBIO LS-G11679), 10 nM concentration was used. Treatment started at day 2 after cells were grafted and was renewed every 2 days.

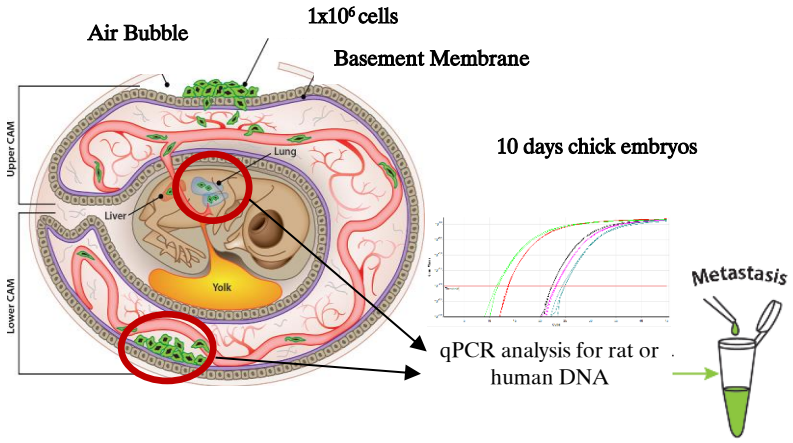

Figure 3.1: Graphic representation of the chick embryo spontaneous metastasis assay. Adapted from Liu, et al. (2013). "The Histone Methyltransferase EZH2 Mediates Tumor Progression on the Chick Chorioallantoic Membrane Assay, a Novel Model of Head and Neck Squamous Cell Carcinoma" Translational oncology. 6. 273-81. 10.1593/tlo.13175.

3.4.2 *EX OVO* CAM MICROTUMOR MODEL

Eggs were incubated lying horizontally in an incubator with a moving tray, rotating three times per hour. Humidity was kept at 65% and temperature at 37ºC. After 3 days of incubation, eggs were removed from the incubator and the content of the eggs were transferred to sterile plastic weigh boats, checking that the embryo is visible and on the top of the yolk sac. They are then covered with a square Petri dish and placed in a stationary incubator until day 10 when embryos were grafted on several places (4-6), always close to small vessels, with 20,000 cells drawing on the square Petri dish the site of inoculation. The cells at a 90% confluence in 100-mm plates were previously labeled with 10 μg of green cell tracker CMFDA (5-chloromethylfluorescein diacetate) dye (Thermo Fisher) for 30 minutes with new media. After 5 days Rhodamine (Thermo Fisher) was injected into the main CAM vessel in order to

visualize vessels and pieces of CAM containing the microtumors were harvested and fixed for 10 minutes with 4% Paraformaldehyde (PFA). After that, CAM was immediately visualized under a 25% water objective using a Leica microscope.

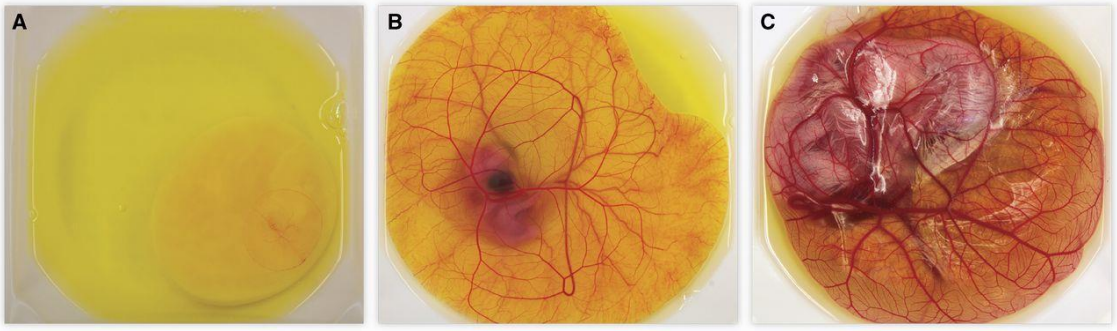

Figure 3.2: Ex ovo CAM microtumor model. (A) 3 days embryo **(B)** 7 days embryo (day of grafting) **(C)** 12 days embryo (harvest day).

3.5 DNA and RNA analysis

3.5.1 GENOMIC DNA EXTRACTION FROM CHICK EMBRYOS AND QUANTIFICATION

To extract genomic DNA from the different organs we used the Gentra PureGen Tissue Kit from QUIAGEN. Following manufactures instructions 600 μL of lysis buffer from CAM or 400 μL for lungs, liver or brain containing 1 μg/ml Proteinase K was added to every organ harvested and was homogenize using a Polytron and was incubated over night at 65ºC. Next day, 200 μL protein precipitation buffer was added and properly mixed. Then, samples were centrifugated at 13,000 rpm for 5 minutes. The supernatant was then collected and transfer to a tube containing 1 volume of Isopropanol and was allowed to settle for 5 minutes in order to allow DNA precipitation. Afterwards, a 13,000 rpm 5 minutes centrifugation was performed, and the pellet was kept and washed twice with 200 μL of ethanol 70% (13,000 rpm 5 minutes). Pellet was then dried for 5 minutes and resuspended with 200 μL hydration buffer.

In order to quantify the amount of DNA contained in each sample we used NanoDrop™ 2000c (Thermo Fisher) making sure that 260/280 ratio was around 1.8.

3.5.2 *REAL TIME* qPCR

In order to detect rat or human cells in the different tissues harvested we used primers (Sigma) for rat β-actin or for human *Alu* sequence (299) **(Table 3.5)**, which are transposable elements,

around 300 nucleotides in length, that account for more than 10% of human genome and are not present in chicken.

Primers name	Sequence
Forward rat primers (light myosin chain)	5´CAAAAATGGAGCTGCGCAGGC 3´
Reverse rat primers (light myosin chain)	5´CGCCAGCTGGTGGGGATTTTA 3´
Forward *Alu* (human) primers (299)	5' ACGCCTGTAATCCCAGGACTT 3'
Reverse *Alu* (human) primers (299)	5´TCGCCCAGGTGGCTGGGGCA 3´

Table. 3.5: Primers and sequence used to assess rat or human cells presence in chick tissues.

PCR reaction contained generally 30 ng of genomic DNA as template in a 20 μL reaction containing 10 μL of 2X PowerUp SYBR Green Master Mix (Thermo Fisher), 100 nM per primer (Alu primers) or 200 nM per primer (Rat primers) and DNAase free Water. PCR conditions were the following: 4 minutes 95ºC followed by 40 cycles of 30 seconds at 95ºC to denaturate DNA, 63ºC during 30 seconds for primers annealing and 30 seconds at 72ºC to allow DNA polymerase to start amplification.
The number of human or rat cells were determined by the measurement of the triplicated Ct values against a standard curve generated by DNA extraction of a specific known number of human or rat cells (100, 1000 and 10,000 cells).

3.5.3 Tumoral RNA extraction and quantification

To analyzed gene expression frozen tumors were harvested and cut in really small pieces, on dry ice to avoid RNA degradation, and RNA extraction was done using the RNeasy Mini Kit (Quiagen). To do so, we introduced tumor pieces into 500 μL of RLT buffer and we homogenized them using a 20 G syringe. Then, samples were centrifuged for 3 minutes at 13,000 rpm and the supernatant was removed and transferred to a new eppendorf tube containing 500 μL of 70% ethanol. After that, 700 μL of the samples were transferred to a RNeasy spin column and centrifugated for 15 seconds at 12,000 rpm discarding the flow through. 700 μL of buffer RW1 were later added and centrifuged, as before. Then, 500 μL of Buffer RPE were added to the column and centrifuged. This step was done twice. The column was placed into a new 1.5 mL collection tube and 30 μL RNase-free water were added to elute RNA by centrifugation. RNA was then quantified using NanoDrop 1000 (Thermo Fisher).

3.5.4 CDNA SYNTHESIS AND QUANTITATIVE REVERSE TRANSCRIPTION (RT) PCR

cDNA was produced from 1 μg of RNA using iScript^{tm} Reverse Transcription Supermix (BioRad). Briefly, 4 μL of iScript RT supermix was added to a 20 μL final volume reaction containing 1 μg of RNA and a variable amount of Nuclease free water. Then the complete reaction mix was incubated in a thermal cycler using the following conditions:

- **Priming** (5 minutes at 25ºC)
- **Reverse Transcription** (20 minutes at 46ºC)
- **RT inactivation** (1 minute at 95ºC)

After that, qPCR was performed as described in **3.5.1** using the following primers:

Primers name	Sequence
Forward VEGF-B primers rat (300)	5´GATCCAGTACCCGAGCAGTCA 3´
Reverse VEGF-B primers rat (300)	5´TGGCTTCACAGCACTCTCCTT 3´
Forward VEGF-A primers rat (300)	5´TAACGATGAAGCCCTGGAGTG 3´
Reverse VEGF-A primers rat (300)	5´ AGGTTTGATCCGCATGATCTG 3´

Table 3.6: VEGF-A and -B primers and sequence.

3.6 Immunohistochemistry of chicken samples

3.6.1 TISSUE INCLUSION IN PARAFFIN

Tissues were fixed ON with 4% Paraformaldehyde (PFA) at 4ºC, washed in 1X PBS (3 times 10´) and embedded in paraffin. Paraffin blocks were then prepared in a paraffin embedding station.

Solution	Time
70% Ethanol	2 x 1 hour
80% Ethanol	1 hour
95% Ethanol	1 hour
100% Ethanol	3 x 1 hour
Xylene	3 x 1 hour
Paraffin (60ºC)	2 x 1.5 hours

Table 3.7: Paraffin processing of tissues.

3.6.2 IMMUNOHISTOCHEMISTRY (IHC)

Once embedded in paraffin, 5μm sections were cut at the microtome and placed on Poly-L-Lysine treated microscopes slides.
Previous any staining, slides were deparaffinize and tissue was rehydrated. Firstly, slides were dried for 1 hour at 60ºC or O/N at 37ºC.

Solution	Time
Xylene	3 x 5´
Tap water	5´
100% Ethanol	5’
90% Ethanol	5´
80% Ethanol	5´
70% Ethanol	5´
Tap water	5´

Table 3.8: Standard procedure to rehydrate histological sections.

In order to allow the antibody to enter more easily to each cell, a permeabilization step was done, incubating specimens for 10 minutes with 0,1% IGEPAL (Sigma) in 1x Tris Buffered Saline (TBS). Then, slides were washed twice for 5 minutes with 1x TBS, and we procced to eliminate non-specific bindings using a serum free blocking reagent, background punisher (BIOCARE Medical) for 8 minutes. After that, a 1% Bovine Serum Albumin (BSA) 0.05% IGEPAL in 1x TBS solution containing a mouse anti-rat CD44 antibody (1:100) (Antibodies Online) or not (negative control), was incubated O/N at 4ºC in a humid chamber (to avoid evaporation). Next day, slides were washed in 1x TBS (3 x 10´) and endogenous peroxidase was quenched using 3x Hydrogen Peroxide (H_2O_2) in 1x TBS for 20 minutes.

Then, specimens were washed in 1x TBS (3 x 10´) and incubated with an anti-mouse biotinylated secondary antibody (Vector Labs) diluted in 1% BSA 0.05% IGEPAL in 1x TBS (1:400) for 1 hour in a humid chamber. After that, slices were washed, as before, and specimens were incubated with Horseradish Peroxidase (HRP) Avidin D diluted in 1x TBS (1:500) for 30 minutes in a humid chamber. Slices were washed again and incubated with the substrate diaminobenzidine (DAB) (Gibco) for 5 minutes or until brownish color started to appear. Chromogenic reaction was stopped with H_20. To finish specimens were stained with Hematoxylin (Sigma), dehydrated, cleared and mounted with DPX. Images were taken at a Zeiss Axio Scope A1 microscope using 10x, 20x or 40x objectives.

3.7 Oil red staining

Fresh harvested tumors were snap-frozen, embedded in OCT (Thermo Fisher) and stored at -80ºC.

Blocks were cut at the cryostat to obtain 10μm and placed on Poly-L-Lysine treated microscope slides. Then, sections were air dried, fixed with 4% PFA for 5 minutes and washed with tap water for 2 minutes. They were rinsed with 60% isopropanol and stained with freshly prepared Oil Red working solution for 5 minutes. They were again rinsed with 60% isopropanol and nuclei were stained with hematoxylin for 2 minutes and mounted using an aqueous mounting media.

Reagent formulae:

Oil Red stock: 0,5 g……...Oil Red (Sigma)
100ml……... Isopropanol
Oil Red was dissolve using a gentle heat.

Oil Red working solution: 30 ml from the stock was diluted in 20 ml of distilled water. It was allowed to settle for 10 minutes and it was filtered into a Coplin jar and covered immediately.

3.8 EXOSOME ISOLATION, DETERMINATION AND ANALYSIS

3.8.1 Extracellular Vesicle Isolation

PCCL3 cells were changed to its serum-free basal medium without hormones or essential amino acids, this time supplemented with 1% ITS (Insulin-Transferrin-Selenium; #41400045 Life 429 Technologies) for 24 h. Generally, about 7 x 10^6 PCCL3 cells were seeded per 15 cm cell culture plate using 12 plates per condition. They were allowed to settle for 72 h in complete medium until they reach 80-90% confluence before changed to 1% ITS depleted medium for 24 h to then proceed to EV collection. After that, culture medium was collected and pre-cleared by centrifuging at 500g for 10 minutes at 4ºC and they were further centrifuge at 2000g for another 10 minutes at 4ºC to remove any cells, debris and large vesicles. The supernatant obtained was then pass through a 0.22 µm filter (Milex®). Thereafter, EV-containing filtrate was concentrate using a tangential flow filter (TFF) set-up with a 100 kDa membrane (Vivaflow 50R, Sartorius) using a 230V pump (Masterflex). After that, size exclusion specific protocol was followed.

3.8.1.1 Size exclusion

Filtrate was concentrated to 5 ml and PBS was added to the TFF machine in order to collect the maximum of EVs that could have been left in the process getting 20 ml final volume. After that, it was further concentrated in 100kDa Amicon filters by sequential centrifugation at 4000g for 10min at 4ºC to a final volume of 1 ml. This volume was then injected into a size-exclusion column (column size 24 cm x 1 cm containing Sepharose 4B, 84nm pore size) set up in an AKTA start system (GE Healthcare Life Science) and eluted with PBS, collecting 30 x 1 ml fractions. Fractions corresponding to the initial "EV peak" (fractions 3-5 for PCCL3) were pooled in 100kDa Amicon tubes by centrifuging at 2000 rpm at 4ºC to a final volume of approximately 100 µl for analysis and later fractions found before the protein peak (6-8), were also pool in 100 µl.

3.8.2 Nanoparticle Tracker Analysis (NTA) (NanoSight®)

NTA is a technique that allows EVs size and concentration distribution measurement in liquid suspension combining the properties of both laser light scattering microscopy and Brownian motion. We used the NS500 NanoSight® (Malvern Instruments Ltd, Malvern, UK) that allows to characterize particles from 10-2000 nm visualizing them by the light they scatter upon laser illumination. Thirty seconds videos were captured 3-5 times per EV sample at known dilution (normalized to protein mass of secreting cells). Particle concentrations were measured within the linear range of the NS500 between about 1-6 x 108 particles ml^{-1}. Equipment settings for data acquisition were kept constant between measurements: camera level 14, threshold 5, minimum expected particle size 80 nm and screen gain 10. Particle movement was analyzed by NTA software 2.3 (NanoSight Ltd.) to obtain particle size and concentration (301).

3.9 BIOINFORMATIC ANALYSIS

cBioPortal database for cancer genomics was used to perform an analysis of APT-1 alterations in thyroid cancer. We chose a 507 sample set from papillary thyroid carcinomas (TCGA) (302) and looked for APT-1 (LYPLA1), H-RAS and N-RAS alterations. We searched for mutations, amplifications, gains, shallow deletions, deep deletions and changes in mRNA levels. To define low mRNA expression levels we selected samples that have them less than -2 standard deviations (SD) below the mean. To define high mRNA expression levels we select samples 2-fold greater than 2 SD above the mean.

3.10 STATISTICAL ANALYSIS AND IMAGES PROCESSING

Data was processed and analyzed using GraphPad Prism Software (GraphPad Software, Inc., San Diego, CA). Data is given as Mean ± SEM (bar graphs) or Mean ± SD (scatter graphs)

from a representative experiment or several normalized experiments. Two tailed unpaired Student's *t*-test or Mann-Whitney test were used to determine differences between data sets and significance (*p<0.05, **p<0.01, ***p<0.001 and ****p<0.0001)

The number of chick embryos and tissue samples analyzed, as well as the number of experiments performed, are indicated in the figure legends.

Confocal images were processed and analyzed using Fiji-Image-J software.

4. Results

4. RESULTS

4.1 Role of RAS sublocalizations in thyroid tumorigenesis

The first aim of this study was to investigate the tumorigenic potential in thyroid cells of RAS activated at its main subcellular locations; Disordered Membrane (DM), Lipids Rafts (LR), Endoplasmic Reticulum (ER) and Golgi Complex (GC); both *in vitro* and *in vivo*.

For this purpose, we choose PCCL3 cells, which are spontaneously immortalized rat thyroid follicular cells; they do not have any known mutations; and have been widely used to study, *in vitro,* RAS, BRAF or RET/PTC signalling (291, 293, 303, 304).

We generated different PCCL3 stable cell lines expressing RAS proteins at their different sublocalizations in the cell. To do so, we transfected them with pCEFL hemagglutinin (HA)-tagged vectors harboring the targeting signals M1 (285), LCK, CD8α (287) or KDELr (286) placed N-terminal to H- , N- or K-RAS (In this case only M1 or CD8α), mutated in position 12 (Gly>Val) **(Fig. 4.1)**. M1 is the avian infectious bronchitis virus M protein that can deliver RAS to ER; LCK is a myristoylation signal that can anchor RAS to LR; CD8α is a receptor that can direct RAS to DM; and KDELr mutated in N193D which avoids KDEL receptor, recycling to ER making it a permanent resident at GC. These constructs have been successfully utilized in previous studies (110, 284, 305). PCCL3 were also transfected with an empty pCEFL plasmid to be used as a control (From now on we will refer to it as control cells).

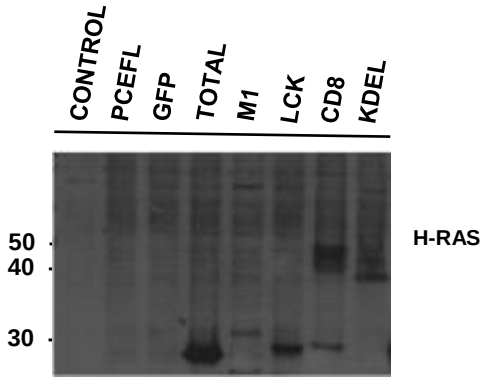

Figure 4.1: Expression levels of the targeted RAS proteins as determined by anti-H-RAS immunoblotting in total lysates from the PCCL3 cells lines stably expressing the RAS constructs.

4.1.1 RAS ISOFORMS ACTIVATED AT DIFFERENT SUBCELLULAR LOCALIZATIONS DO NOT AFFECT THYROID CELLS PROLIFERATION BUT AFFECT APOPTOSIS

Since mutant RAS has been widely described as a thyroid cancer driver, we wanted to know: i) if the different constitutively activated RAS proteins mutated in position 12 (Gly>Val)

could promote cell proliferation in PCCL3 cells and ii) if the effects were different depending on RAS localization within the cell. To asses this, we used the PCCL3 stable cell lines described above, which express mutant H-, N- or K-RAS targeted to the different subcellular locations where they are usually found under physiological conditions: ER, LR, DM and GC for H- and N-RAS and ER and DM for K-RAS.

Cell proliferation, analyzed at 24 and 48 h using AlamarBlue Viability Assay, did not show substantial differences either compared to control cells or among RAS sublocalizations. Results were similar among the three RAS proteins **(Fig. 4.2 A, C and E)**. Although, no major differences were seen in this respect, a high number of floating cells were observed in every RAS PCCL3 stable cell line suggesting some degree of cell death. Indeed, several groups have shown that H-RAS can induce apoptosis in PCCL3 cells by increasing genomic instability (291, 306-308). Additionally, our laboratory recently described that H-RAS signals from the GC were able to induce apoptosis in MCF-7 mammary epithelial cells (121). Therefore, to explore if GC RAS signals, as well as those from, ER, DM and LRs, could also induce apoptosis in thyroid PCCL3 cells, we performed a Guava Nexin Annexin V assay, using Staurosporine as a positive control. This cytometry assay is based in a two-dye strategy, where Annexin V binds to phosphatidyl serine (PE) to detect early apoptosis, and 7-AAD, which detects late-stage apoptotic and dead cells. In line with previous studies (291, 306-308), every RAS protein induced apoptosis, compared to control cells, particularly from the GC, as expected **(Fig. 4.2 B, D and F)**. The exception was LR signals that showed the same percentage of death as control cells in the case of N-RAS, or even reduced apoptotic rates, in the case of H-RAS **(Fig. 4.2 B and D)**.

These results indicate that RAS proteins promote apoptosis in PCCL3 thyroid cells when active mainly at the GC but not from LR.

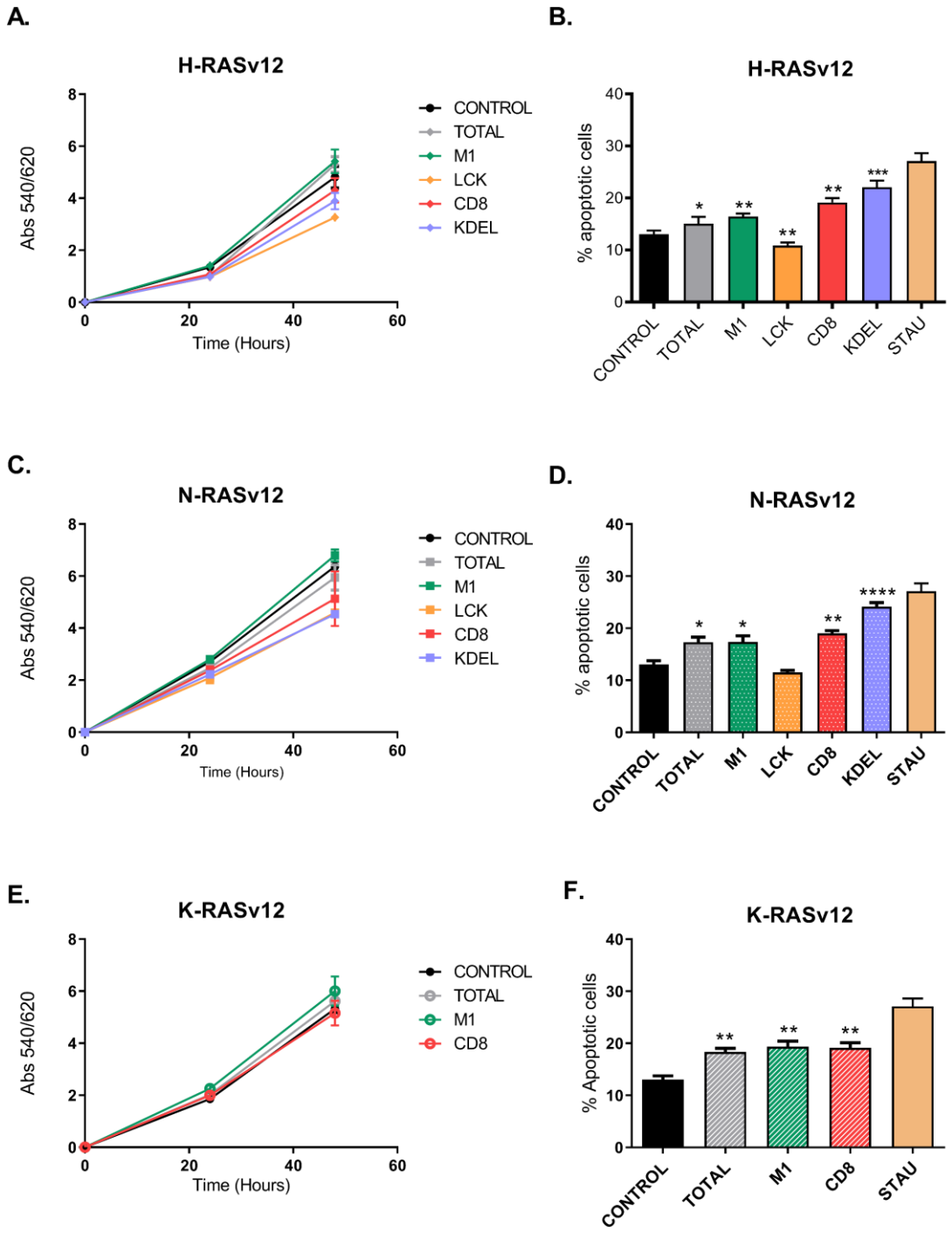

Figure 4.2: Cell proliferation and apoptosis responses to mutant RAS activation at its different subcellular locations in PCCL3 cells. (**Control:** pCEFL; **Total:** H-RASv12; **M1:** H-RASv12 at ER, **LCK:** H-RASv12 at LR; **CD8:** H-RASv12 at DM; **KDEL:** H-RASv12 at GC). Cell proliferation is presented as the rate of AlamarBlue Assay Reagent reduction at 24 and 48 h in **(A)** PCCL3 cells transfected with H-RASv12 **(C)** N-RASv12 or **(E)** KRASv12 constructs tethered to their different subcellular locations. Apoptosis was evaluated by annexin V detection using the Guava/nexin assay **(B)** Apoptosis in response to H-RASv12; **(D)** N-RASv12; or **(F)** KRASv12. Staurosporine (STAU) was used as a positive control. Results show Mean ± SEM (n=3) using two-tailed unpaired Student T-Test (*p<0.05, **p<0.01, ***p<0.001 and ****p<0.0001).

4.1.2 H-RAS AFFECTS MIGRATION DIFFERENTLY DEPENDING ON ITS LOCALIZATION

Since H-RAS oncogenic mutations have been widely related to migration and invasiveness (292, 309, 310), we sought to determine whether this could be differently modulated depending on its subcellular location. Using transwell assays to monitor migration we determined that RAS was able to promote migration from all its locations. It was found that when active in DM and GC H-RAS shower higher rates of migration, three to four times, than those detected from LR and ER **(Fig. 4.3)**.

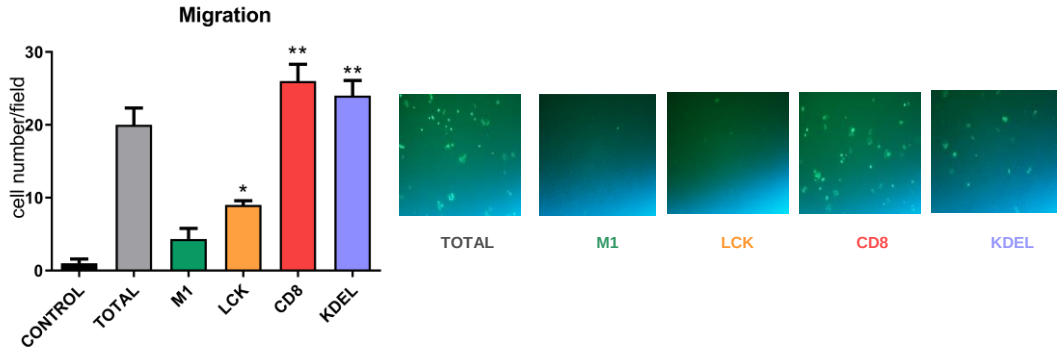

Figure 4.3: Transwell migration assay. The different PCCL3 stable cell lines (**Control:** pCEFL; **Total:** H-RASv12; **M1:** H-RASv12 at ER, **LCK:** H-RASv12 at LR; **CD8:** H-RASv12 at DM; **KDEL:** H-RASv12 at GC). were dyed with 10 μM cell Green tracker and 10,000 cells were placed in 8μm pores transwells. Migrated cells were observed after 24 hours using a 20x objective in a Leica fluorescence microscope. Data shows Mean ± SD of cells per field of three independent experiments. A double tailed unpaired Student T-test was utilized. *p<0.05, **p<0.01.

4.1.3 SPATIALLY-DEFINED H-RAS AND N-RAS POOLS EXHIBIT DIFFERENT SPONTANEOUS METASTASIS POTENTIAL

The chick embryo has been widely used to study tumor growth, intravasation and dissemination of different types of tumor cells (311-313).

Since we did not see major changes in proliferation but observed differences in migration among H-RAS subcellular locations, we wanted to determine whether our cells could generate primary tumors and if they had the ability to metastasize *in vivo*. The chick embryo model overcomes many limitations for studying the metastatic process, thanks to the accessibility of the Chorioallantoic Membrane (CAM), the outermost, highly vascularized, extra-embryonic tissue located under the eggshell, where mammalian or rodent tumor cells can be xenografted. The chick embryo is naturally immunodeficient, so the CAM can support the engraftment of tumor cells, and most of the characteristics of the carcinogenic process such as: growth, invasion, angiogenesis and metastasis, can be recapitulated (299, 314-316).

$1x10^6$ cells were grafted onto the CAM of 10-days chick embryos and were left for 7 days, when sizable primary tumors were observed. Strikingly, although *in vitro* we were not able to see differences in proliferation, H- and N-RAS LR and ER pools evoked three- or two-fold bigger tumors, respectively, in comparison to the DM and GC ones. (Fig. 4.4 A and 4.6 A). We also analyzed whether tumor cells could intravasate into the CAM vasculature or colonize distant organs, such as the liver, the first organ cells reach once intravasation has occurred, and lungs, the most common place for thyroid cancer metastases.

To analyze CAM intravasation, cells in distal CAM were detected by qPCR using specific rat primers. Surprisingly, the RAS sublocalizations yielding the smaller tumors (DM and GC), were the ones that presented higher number of embryos with cells in the distal CAM. However, irrespective of the % of chicks that exhibited distal CAM colonization, the total number of cells in the CAM was not different among the different subcellular locations **(Fig.4.4 B,C and 4.6 B, C)**, although, N-RAS evoked almost twice the number of invading cells than H-RAS.

Similarly, signaling from DM and the GC displayed a 2-3-fold increase in the % of chick embryos showing colonization in lungs, in comparison to ER or LR sublocalizations **(Fig. 4.5 C and 4.7 C)** both from H- and N-RAS. Moreover, irrespective of the sublocalization H-RASv12 showed almost six-fold more cells metastazing the lungs when compared to N-RASv12 **(Fig. 4.5 D and 4.7 D)**. In addition, H- and N-RASv12 DM and GC pools induced liver colonization **(Fig. 4.6 A and 4.8 A)**, though, to a lesser extent than lungs and also half the number of invading cells **(Fig. 4.5 B and 4.5 B)**. In striking contrast, cells with H-RASv12 at LR showed the same % of liver colonization as DM and GC **(Fig. 4.5 A and 4.7 A)**.

Altogether, our results show that H- and N-RAS sublocalizations play different roles in tumor growth and dissemination and suggest that small RAS positive thyroid nodules and tumors could be highly metastatic.

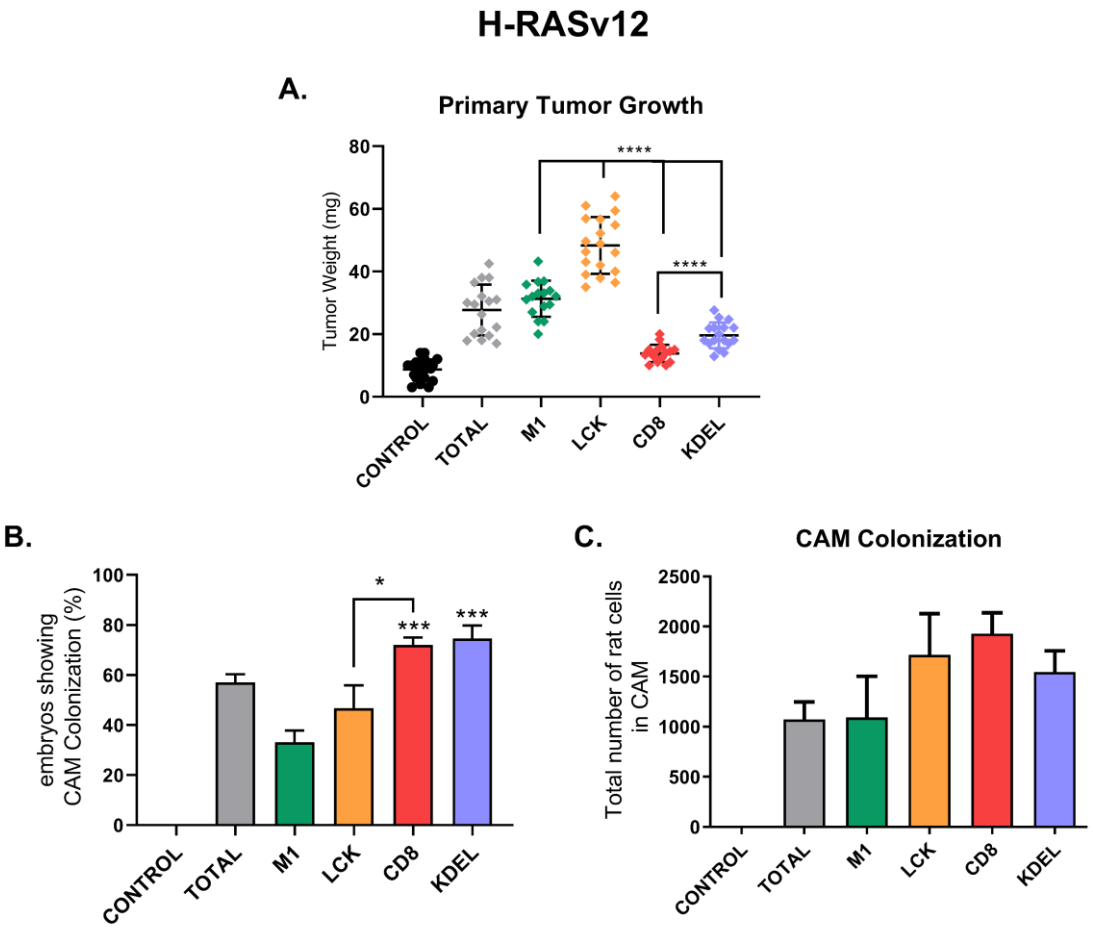

Figure 4.4: Metastatic potential of H-RAS sublocalizations in the chick embryo spontaneous metastasis model. PCCL3 cells:(**Control:** pCEFL; **Total:** H-RASv12; **M1:** H-RASv12 at ER, **LCK:** H-RASv12 at LR; **CD8:** H-RASv12 at DM; **KDEL:** H-RASv12 at GC). 1x10^6 cells from each PCCL3-derived cell lines were grafted on 10-days chick embryos. After seven days, the primary tumors were collected and weighed (mg) (Mean ± SD) **(A),** and the presence of rat cells in distal portions of the CAM were analyzed by qPCR showing the % of chicken displaying intravasation (distal CAM colonization) (Mean + SEM) **(B).** In those cases, the relative numbers of rat cells (MEAN ± SEM) per 10^6 chicken cells was determined **(C)**. Data from three independent experiments with 9 to 15 embryos per case. Statistical significance was determined in comparison to the lower value, when not specified. Groups were analyzed by a double tailed unpaired student T-test. *p<0.05, ***p<0.001 and ****p<0.0001.

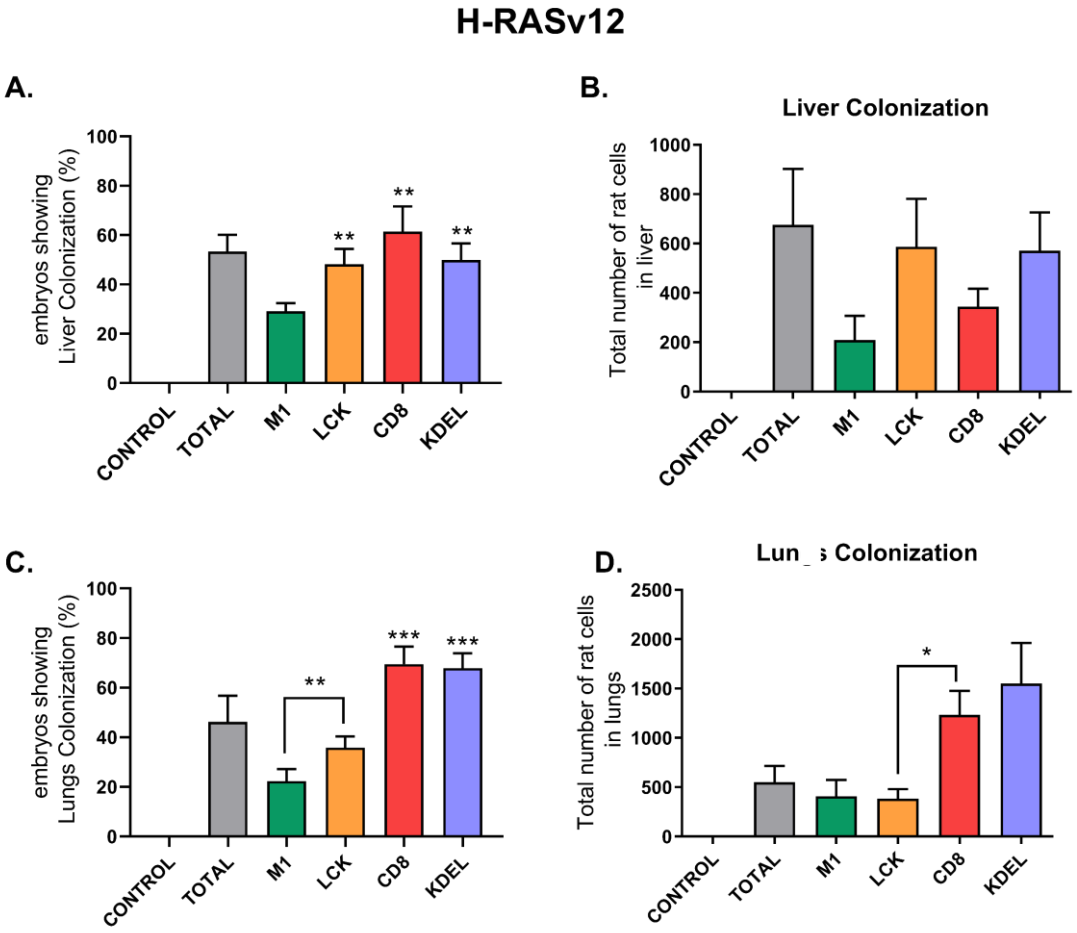

Figure 4.5: Liver and lung colonization in the chick embryo spontaneous metastasis model by PCCL3 stable cell lines expressing site-specific H-RASv12. PCCL3 cells:(**Control:** pCEFL; **Total:** H-RASv12; **M1:** H-RASv12 at ER, **LCK:** H-RASv12 at LR; **CD8:** H-RASv12 at DM; **KDEL:** H-RASv12 at GC). $1x10^6$ cells from each cell line were grafted on 10-days chick embryos. After seven days, liver and lungs were collected and the presence of rat cells was analyzed by qPCR showing **(A)** the % of chick embryos (Mean + SEM) exhibiting liver colonization or **(C)** lung colonization. **(B)** Average number (Mean + SEM) of rat cells found in liver or **(D)** in lungs. Data is from three independent experiments employing from 9 to 15 embryos per cell variant. Statistical significance was determined by a double tailed unpaired student T-test. *p<0.05, **p<0.01 and ***p<0.001.

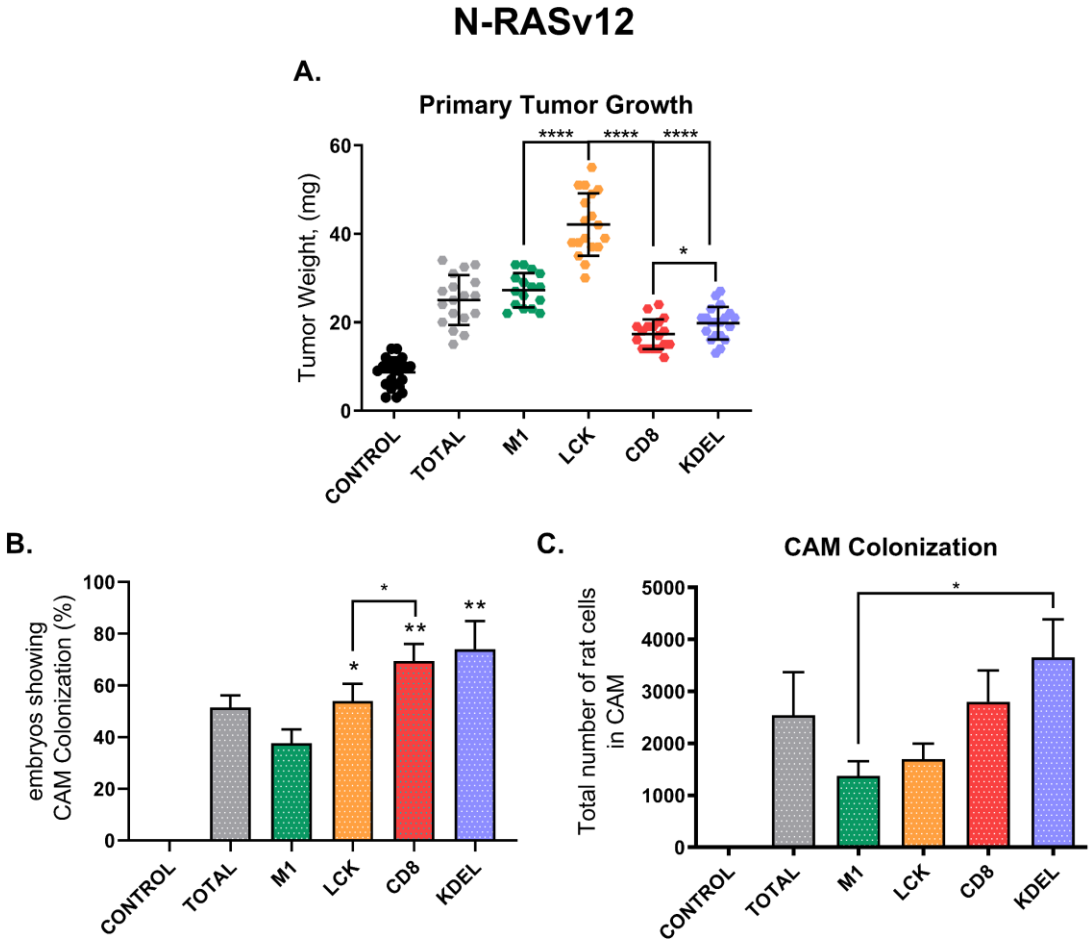

Figure 4.6: Metastatic potential of N-RAS sublocalizations in the chick embryo spontaneous metastasis model. PCCL3 cells: (**Control:** pCEFL; **Total:** N-RASv12; **M1:** N-RASv12 at ER, **LCK:** N-RASv12 at LR; **CD8:** N-RASv12 at DM; **KDEL:** N-RASv12 at GC). 1x10^6 cells from each PCCL3-derived cell lines were grafted on 10-days chick embryos. After seven days, the primary tumors were collected and weighed (mg) (Mean ± SD) **(A),** and the presence of rat cells in distal portions of the CAM were analyzed by qPCR showing the % of chicken displaying intravasation (distal CAM colonization) (Mean + SEM) **(B).** In those cases, the relative numbers of rat cells (MEAN ± SEM) per 10^6 chicken cells was determined **(C)**. Data from three independent experiments with 8 to 15 embryos per case. Statistical significance was determined in comparison to the lower value, when not specified. Groups were analyzed by a double tailed unpaired Student T-test. *p<0.05, ***p<0.001 and ****p<0.0001.

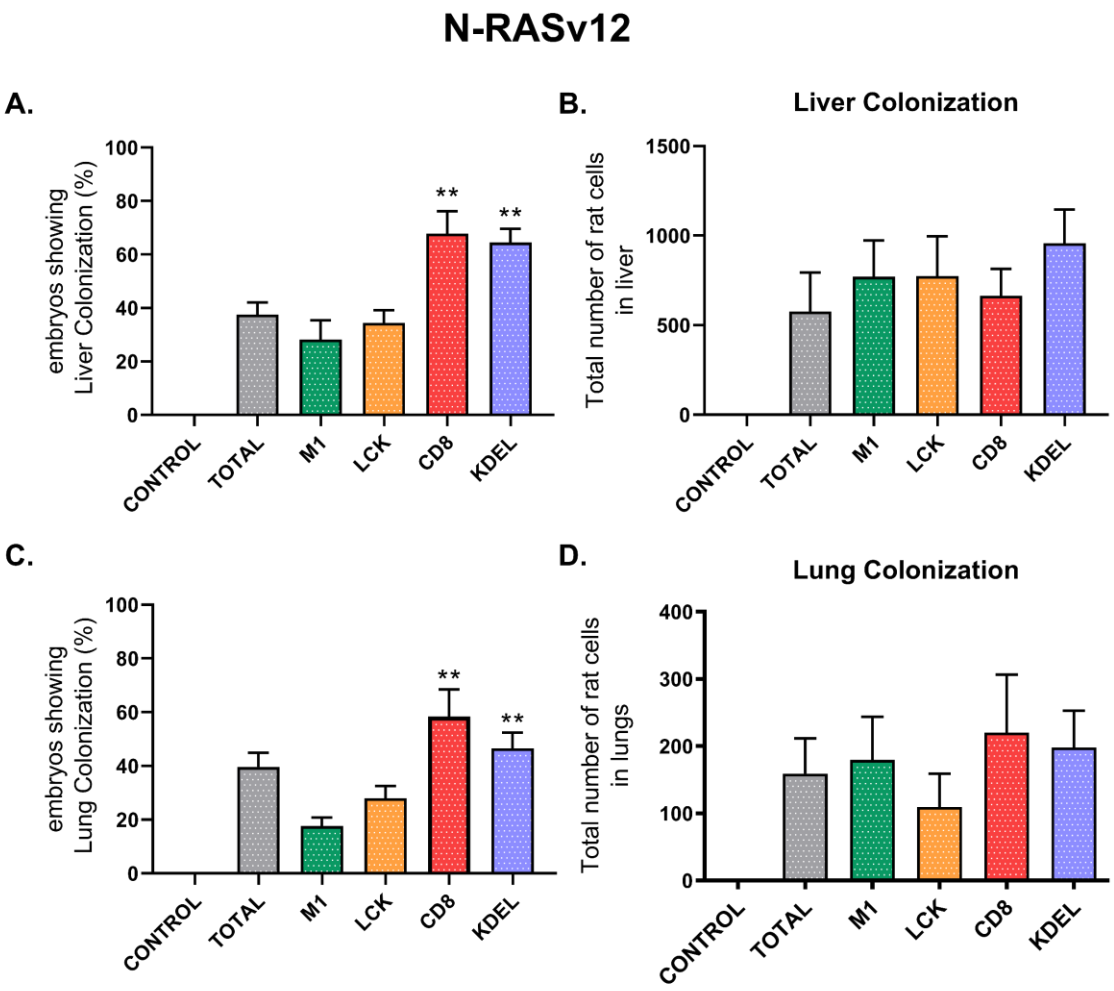

Figure 4.7. Liver and lung colonization in the chick embryo spontaneous metastasis model by PCCL3 stable cell lines expressing site-specific N-RASv12. PCCL3 cells: (**Control:** pCEFL; **Total:** N-RASv12; **M1:** N-RASv12 at ER, **LCK:** N-RASv12 at LR; **CD8:** N-RASv12 at DM; **KDEL:** N-RASv12 at GC). $1x10^6$ cells from each cell line were grafted on 10-days chick embryos. After seven days, liver and lungs were collected and the presence of rat cells was analyzed by qPCR showing **(A)** the % of chick embryos (Mean + SEM) exhibiting liver colonization or **(C)** lung colonization. **(B)** Average number (Mean + SEM) of rat cells found in liver or **(D)** in lungs. Data is from three independent experiments employing from 9 to 15 embryos per cell variant. Statistical significance was determined by a double tailed unpaired Student T-test (**$p<0.01$).

4.1.4 K-RAS SUBLOCALIZATION EFFECTS IN SPONTANEOUS METASTASIS

K-RAS is mainly located at ER and DM (112). Since we saw opposing effects in growth and metastasis when looking at H- and N-RAS signals emanating from these sublocalizations, we hypothesized that this could also be case for K-RAS. However, KRAS ER and DM pools exhibited the same capacity for tumor growth **(Fig. 4.8 A)**, intravasation and liver colonization **(Fig. 4.8 B, C left)**. Strikingly, K-RAS signals from DM promoted more lung colonization, showing high amounts of invading cells **(Fig. 4.8 B, C right)**.

This data indicates that all RAS isoforms signaling from disorder membrane can induce high rates of lung metastases in our thyroid cancer model.

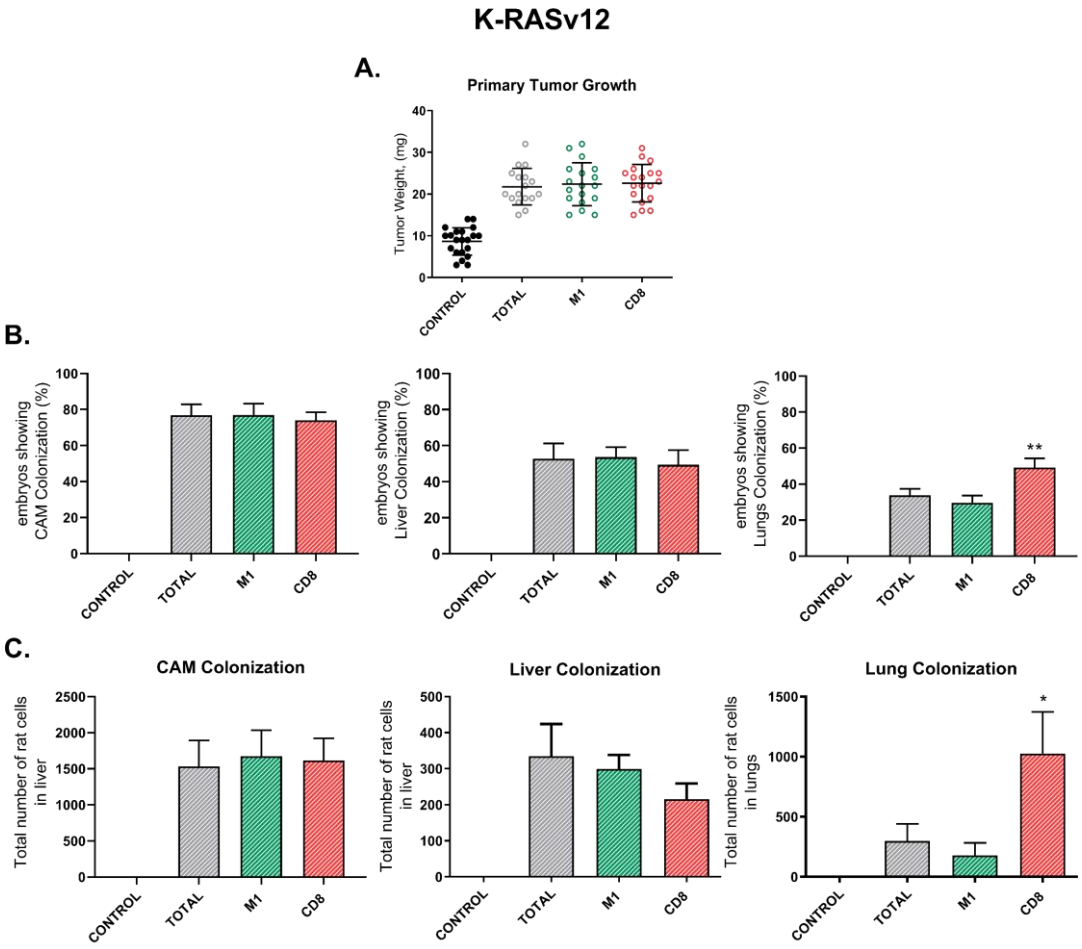

Figure 4.8: Metastatic potential of K-RAS sublocalizations in the chick embryo spontaneous metastasis model. PCCL3 cells: (**Control:** pCEFL; **Total:** K-RASv12; **M1:** K-RASv12 at ER, **CD8:** K-RASv12 at DM). 1x10^6 cells from each PCCL3-derived cell lines were grafted on 10-days chick embryos. After seven days, the primary tumors were collected and weighed (mg) (Mean ± SD) **(A),** and the presence of rat cells in distal portions of the CAM were analyzed by qPCR showing the % of chicken displaying intravasation (distal CAM colonization) (left), liver (middle) or lung (right) colonization (Mean + SEM) **(B).** In those cases, the relative numbers of rat cells (MEAN ± SEM) per 10^6 chicken cells was determined **(C)**. Presented data is from three independent experiments employing from 8 to 16 embryos per cell variant. Statistical significance was analyzed by a double tailed unpaired T-test. *p<0.05 and **p<0.01.

4.1.5 IMMUNOHISTOCHEMICAL ANALYSIS OF CAM, LIVER AND LUNG COLONIZATION

Immunohistochemical staining with an anti-rat CD44 antibody was undertaken in order to study histologically PCCL3 colonization of distant organs.

7 days after grafting only a small number of chick embryos grafted with cells expressing H-RASv12 at ER, showed CAM invasion, consistent with the results obtained by qPCR (Fig. 4.4). Strikingly, the few ones showing cells in distal CAM exhibited high vasculotropism (Fig. 4. 9 B). Conversely, almost all tumors formed by H-RAS at DM (Fig. 4. 9 A) and at GC presented cell agregates that appeared to be expanding into the CAM mesoderm and all were close to blood vessels. Cells with H-RAS at LR showed distal CAM colonization in 50% of the chick embryos assessed, and their immunohistological characteristics were similar to H-RAS at DM and GC.

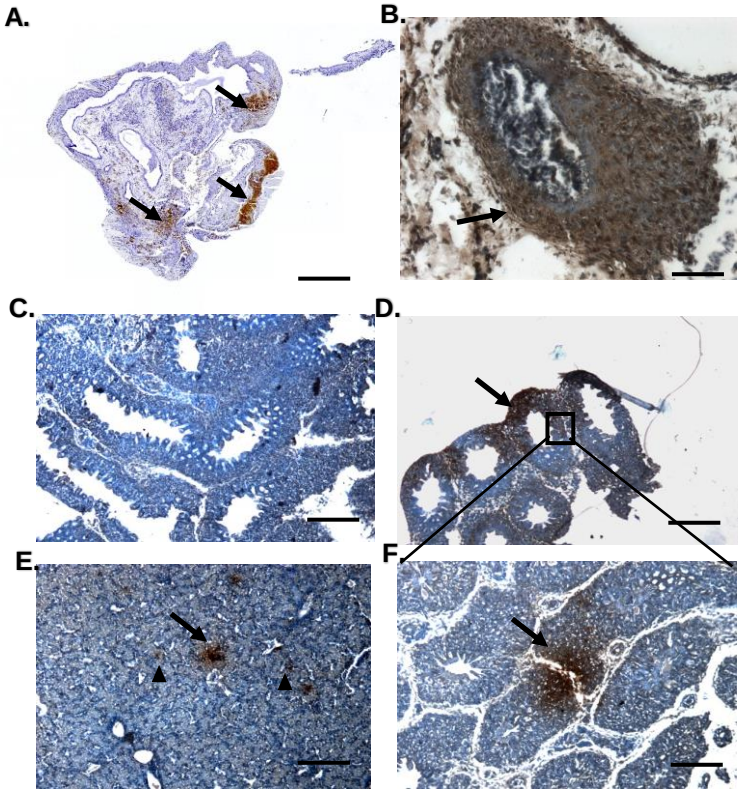

Figure 4.9: Immunohistological analysis of colonized organs. 1x 10^6 cells were grafted onto the CAM of 10 days old chick embryos. After 7 days distal CAM, liver and lungs were collected and processed for immunohischemical analysis of rat cells. Rat cells were stained with an anti-RAT CD44 antibody (brown staining)(arrows) and tissues were counterstained with hematoxylin. **(A)** distal CAM showing big cell aggregates (arrow) in a chick embryo grafted with PCCL3 cells expressing H-RASv12-CD8. Picture was taken with an Axio Scanner microscope in order to see all the sample (5x) **(B)** PCCL3 cells expressing H-RASv12-M1 gathered around a vessel (arrow) in distal CAM (40x) **(C)** lungs of a chick embryo grafted with PCCL3 cells expressing RAS at LR (20x). **(D and F)** Lungs showing high amount of rat PCCL3 cells (arrows) expressing RAS in DM (D 10x) (G 20x) **(E)** Liver showing micrometastasis (arrow) and scattered H-RAS-LCK transfected PCCL3 cells (arrowhead) (20x). Scale bars are: 160μm in **(A)**, 80μm in **(D)**, 40μm in **(C)**, **(E)** and **(F)**, 20μm in **(B)**.

All H-RAS sublocalizations, with exception of the ER, generated microfoci in livers composed of 8-20 cells, as well as scattered cells **(Fig. 4.9 E)**. This suggests, together with qPCR data indicating small number of invading cells, that invading cells are not abundant and have a low potential to proliferate and form macroscopic metastasis in this organ.

When lung immunostaining was analyzed we found that mainly H-RAS at DM and at the GC showed cells in this organ, including large metastatic foci, as opposed to the other H-RAS sublocalizations that did not evoke significant colonization **(Fig. 4.9 D and F)**.

Therefore, our immunohistological studies reinforce our previous qPCR results and confirm the high levels of metastasis induced by DM and GC H-RAS signals. In addition, the histological analyses suggested the close relationship between H-RAS-expressing cells and the CAM vasculature, surprisingly high in tumors with H-RAS active at the ER.

4.1.6 ENDOGENOUS H-RAS ACTIVATION AT ITS DIFFERENT SUBCELLULAR LOCATIONS INDUCES TUMORS BUT NOT METASTASIS

In order to ascertain that the observed effects were not a consequence of some artifact resulting from the expression of artificially-tethered RAS proteins at the different sublocalizations, it was necessary to analyze the effects of endogenous RAS activation at its different sublocalizations. We have developed constructs where the CDC25 domain of RASGRF1 was fused to the site-specific tethers (M1, LCK, CD8α and KDELr) to send it to the different cellular compartments where RAS resides, thereby activating the endogenous RAS pools (283).

Therefore, we transfected PCCL3 cells with the different CDC25 constructs (CDC25, M1-CDC25, LCK-CDC25, CD8-CDC25 and KDEL-CDC25) in order to activate endogenous RAS at ER, LR, DM or GC, respectively, and determine whether its site-specific activation mirrored the H-RASv12 effects observed in our model. To assess so, we grafted $1x10^6$ cells onto the CAM of 10-days-old chick embryos and after 7 days we collected and weighted the tumors and analyzed distal CAM, liver and lungs by qPCR. We saw that the CDC25 constructs elicited similar effects in tumor formation as HRAS constructs **(Fig. 4.10 A)** but they caused little if any-CAM, liver and lung colonization. Only PCCL3 cells expressing CD8-CDC25 or KDEL-CDC25 showed some degrees of intravasation and lung colonization **(Fig. 4.10 B, C).**

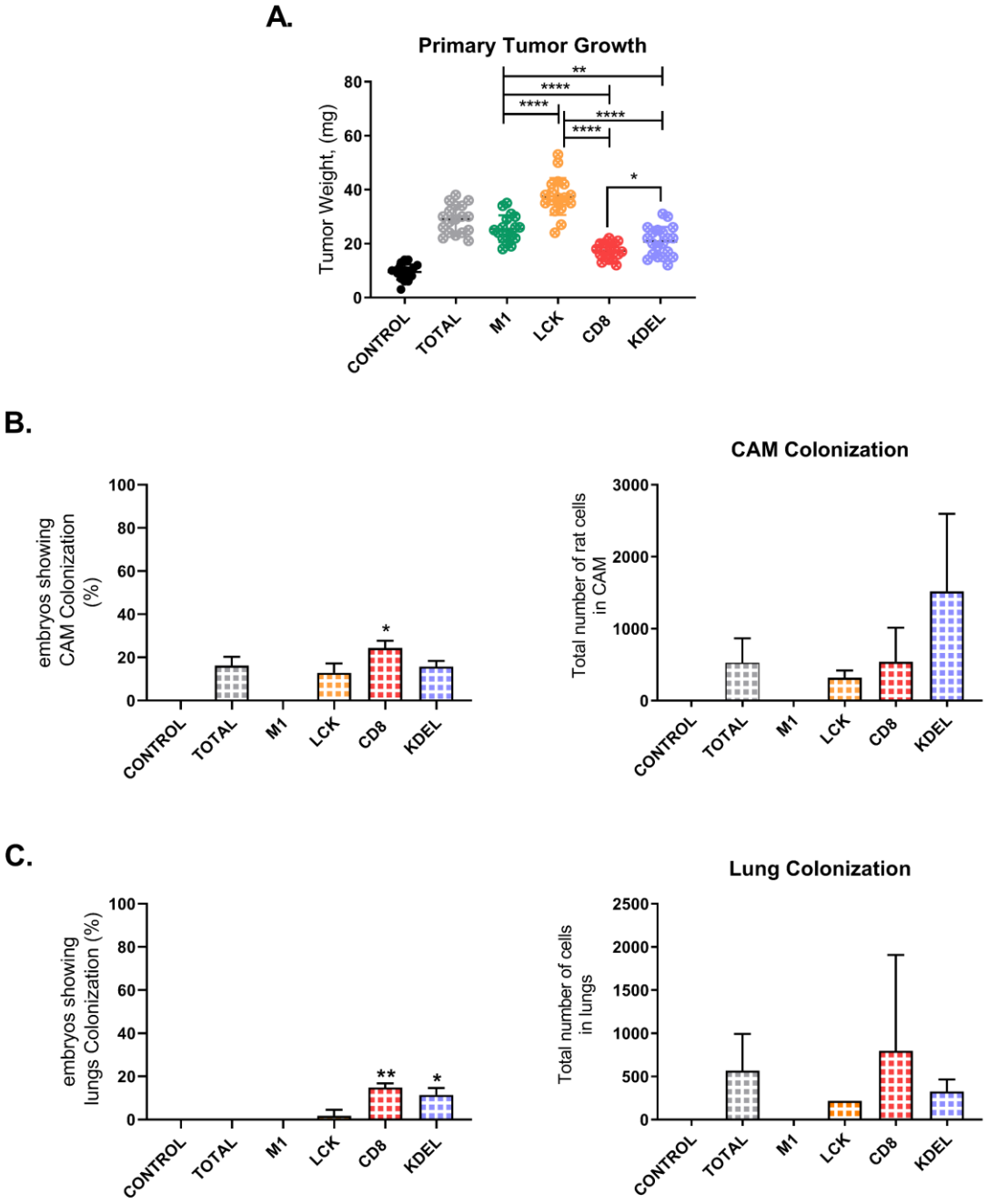

Figure 4.10: Metastatic potential of PCCL3 cells expressing site-specific CDC25 domain in the chick embryo spontaneous metastasis model. PCCL3 cells: (**Control:** pCEFL; **Total:** H-RAS-CDC25; **M1:** H-RAS-CDC25 at ER, **LCK:** H-RAS-CDC25 at LR; **CD8:** H-RAS-CDC25 at DM; **KDEL:** H-RAS-CDC25 at GC). $1x10^6$ cells from each PCCL3-derived cell lines were grafted on 10-days chick embryos. After seven days, the primary tumors were collected and weighed (mg) (Mean ± SD) **(A),** and the presence of rat cells in distal portions of the CAM were analyzed by qPCR showing the % of chicken displaying intravasation (distal CAM colonization) (left), liver (middle) or lung (right) colonization (Mean + SEM) **(B).** In those cases, the relative numbers of rat cells (MEAN ± SEM) per 10^6 chicken cells was determined **(C).** Data is from three independent experiments employing from 7 to 12 embryos per cell variant. Groups were analyzed by a double tailed unpaired Student T-test. *p<0.05, **p<0.01 and ****p<0.0001.

4.2 APT-1 levels modify thyroid tumoral cells behavior

4.2.1 APT-1 OVEREXPRESSION CORRELATES WITH BETTER PROGNOSIS IN THYROID CANCER

Since high levels of APT-1 activity will result in RAS localizacing at LR (119), it was interesting to determine how APT-1 levels related to the evolution of thyroid tumors. Using the cBioPortal for Cancer Genomics database, we choose a 507 sample set from papillary thyroid carcinomas (TCGA) (302) and looked for APT-1 (LYPLA1) alterations, H-RAS and N-RAS alterations. We found that APT-1 was altered in 7% of the tumors, these were mainly showing high mRNA levels. Some tumors showed underexpression of APT-1 and only a few of them showed amplications or shallow deletions **(Fig. 4.11)**. Moreover, some tumors over-expressing APT-1 also had missense mutations in N-RAS, but H-RAS alterations did not co-occur with APT-1 ones **(Fig. 4.11)**.

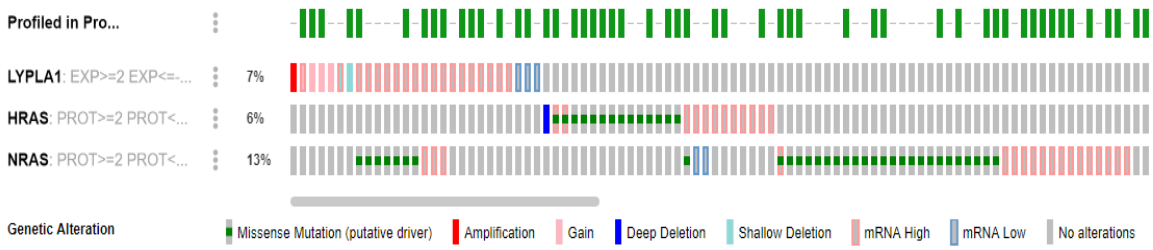

Figure 4.11: APT-1 (LYPLA1), H-RAS and N-RAS mutations, amplifications, gains, deletions and mRNA expression. Data is been extracted from "cBioPortal for cancer genomics" using a database of 507 samples of papillary thyroid carcinomas (TCGA) (302).

When we looked at the overall survival of patients with either amplifications of high levels of APT-1 (5%). Interestingly, all of these patients (22) survived, whereas patients without APT-1 alterations, exhibit a 80% survival after 14 years **(Fig. 4.12 A)**. We also checked the survival of patients showing low levels of APT-1 mRNA and shallow deletions (6) without detecting differences **(Fig. 4.12 B)** although not significant due to the low amount of samples.

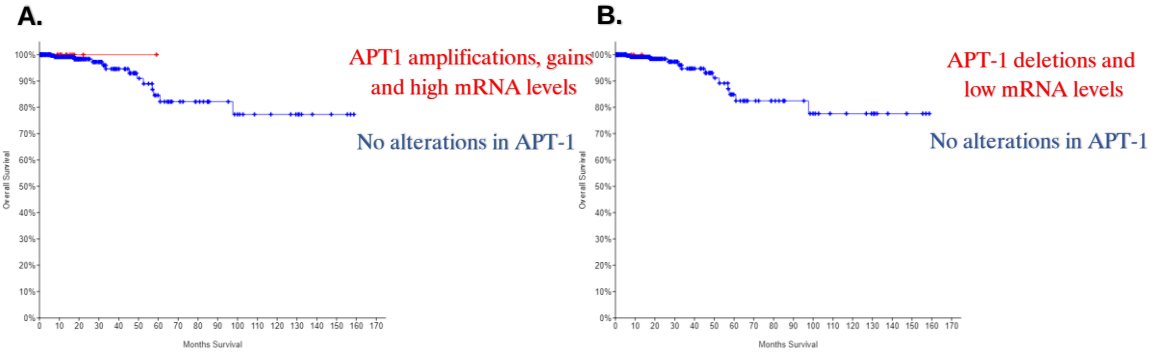

Figure 4.12: Overall survival Kaplan-Meier Estimate. Using data extracted from "cBioPortal for cancer genomics" using a cohort of 507 samples of papillary thyroid carcinomas (TCGA) (302) we selected the samples with APT-1 overexpression, amplification and gains (22 samples) and checked for overall survival **(A)** or the samples with low levels of APT-1 mRNA or deletions (6 samples) and checked again for overall survival **(B).**

4.2.2 H-RAS LOCATION AT PLASMA MEMBRANE MICRODOMAINS IS RELATED TO APT-1 EXPRESSION LEVELS

Since PCCL3 thyroid cells transfected with H-RAS tethered to LR and DM exhibit opposed effects in tumor proliferation and dissemination, we sought to determine if this was also the case in thyroid tumor cells harboring endogenous H-RAS at these different sublocalizations. We utilized C643 and HTH83 cell lines, both are derived from thyroid anaplastic carcinomas and have *H-RAS* mutations in position 13 (G13C) in C643 and in position 61 (Q61R) in HTH83 together with a mutation in *TERT* promoter (C228T) (294, 317). We monitored if H-RAS sublocalizations differed in these cell lines, by membrane fractionation analyses. It was found that C643 cells harbored H-RAS at LR (Fig. 4.11 A) whereas in HTH83 cells H-RAS was located in DM **(Fig. 4.13 B)**. This is a consequence of APT-1, an acyl thioesterase involved in H-RAS depalmitoylation (119), which is more expressed in C643 cells **(Fig. 4.13 C).**

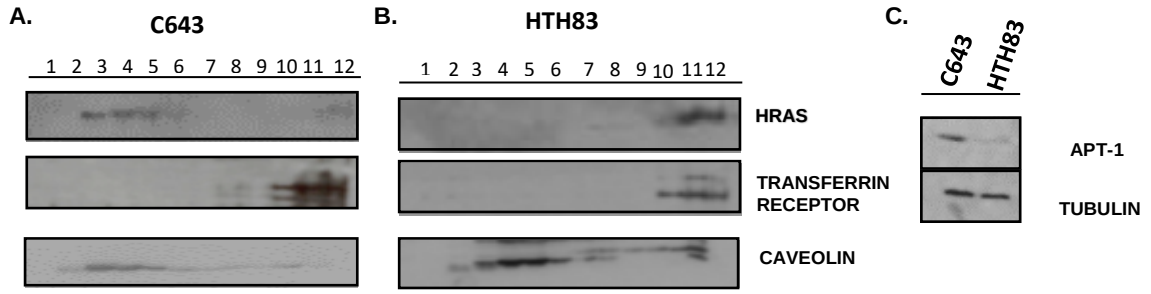

Figure 4.13: H-RAS segregation in plasma membrane microdomains. H-RAS location at detergent-resistant membrane domains (LRs, enriched in Caveolin-1) and detergent-soluble fractions (DM, enriched in transferrin receptor) in C643 **(A)** or HTH83 **(B)** human thyroid anaplastic carcinoma cell lines. **(C)** APT-1 expression levels in lysates from C643 and HTH83 determined by immunoblotting. Protein levels were equalized using Bradford assay.

4.2.3 OPPOSING EFFECTS ON TUMORIGENESIS BY ENDOGENOUS H-RAS AT LR AND DM

To assess C643 and HTH83 cells tumorigenic behavior, we grafted 10^6 cells onto the CAM of 10-days chick embryos and after 6 days we analyzed their tumor weight and distal CAM, liver and lung colonization. Interestingly, even though both cell lines are derived from anaplastic thyroid carcinomas they exhibited some crucial differences: C643 cells generated bigger tumors than HTH83 cells **(Fig. 4.14 A)**, but induced less CAM intravasation and lung colonization, though, more liver colonization **(Fig. 4.14 B)**. Even though, in all the positive cases the number of invading cells did not vary substantially **(Fig. 4.14 C)**. These results are in consonance with the behavior of PCCL3 cells expressing H-RAS at LR or DM.

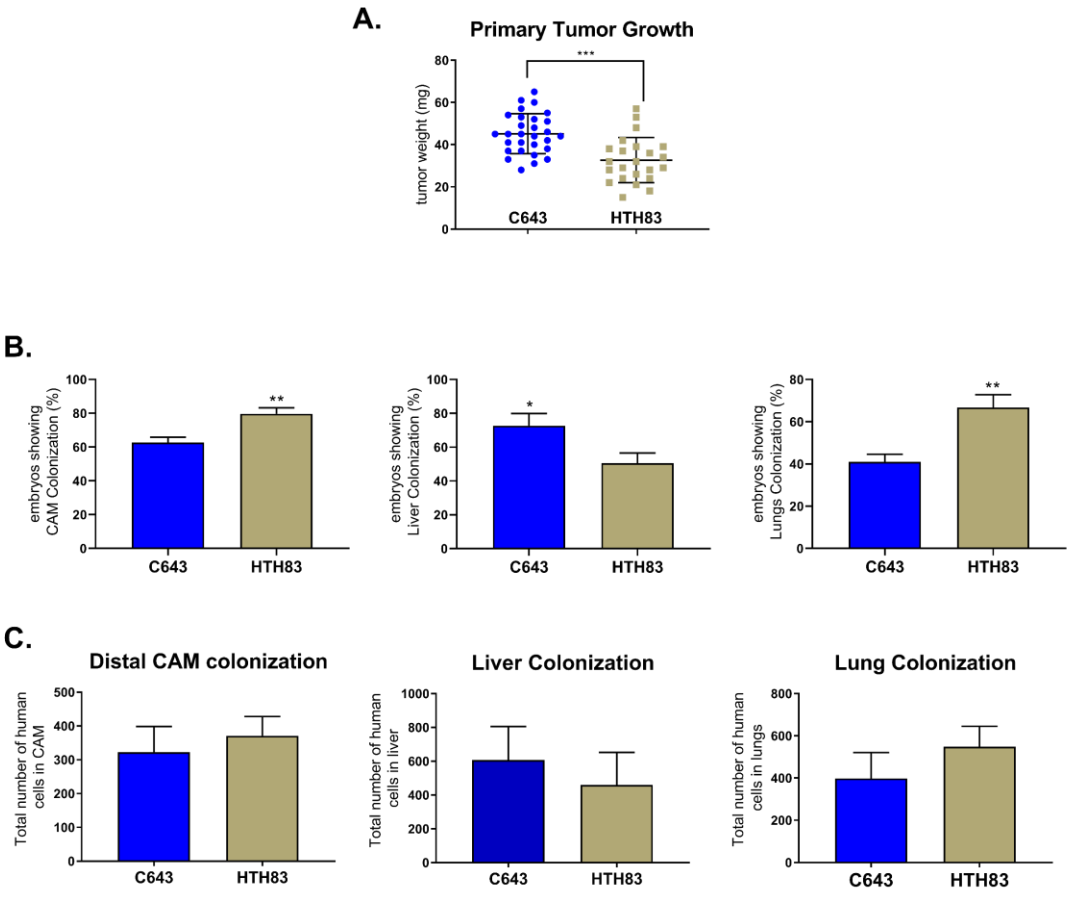

Figure 4.14: Tumorigenic behavior of the human anaplastic thyroid cancer cell lines, C643 and HTH83, in the chick embryo spontaneous metastasis model. $1x10^6$ cells from each cell line were grafted on 10-days chick embryos. After six days, the primary tumors were collected and weighed (mg) (Mean ± SD) **(A)** and the distal portions of the CAM were analyzed by qPCR showing the % of tumors that underwent spontaneous intravasation (Distal CAM) and liver and lung colonization **(B)**; allowing us to determine the relative numbers of human cells (Mean ± SEM) per 10^6 chicken cells in distal CAM, liver and lungs **(C)**. Data is from three independent experiments using from 8 to 16 embryos per cell variant. Statistical significance was analyzed by double tailed unpaired Student T-test. *$p<0.05$, **$p<0.01$ and ***$p<0.001$.

4.2.4 APT-1 KNOCKDOWN IN C643 CELLS TRANSLOCATES H-RAS TO DM AND GENERATES SMALLER TUMORS WITH HIGHER METASTATIC POTENTIAL

To further substantiate the above findings, we downregulated APT-1 in C643 cells using a siRNA. We confirmed its knockdown **(Fig. 4.15 A)** and we performed a membrane fractionation and sucrose gradient to analyze H-RAS location at the plasma membrane. As we expected, APT-1 knockdown caused a H-RAS translocation from LR **(Fig. 4.15 B)** to DM **(Fig 4.15 C).**

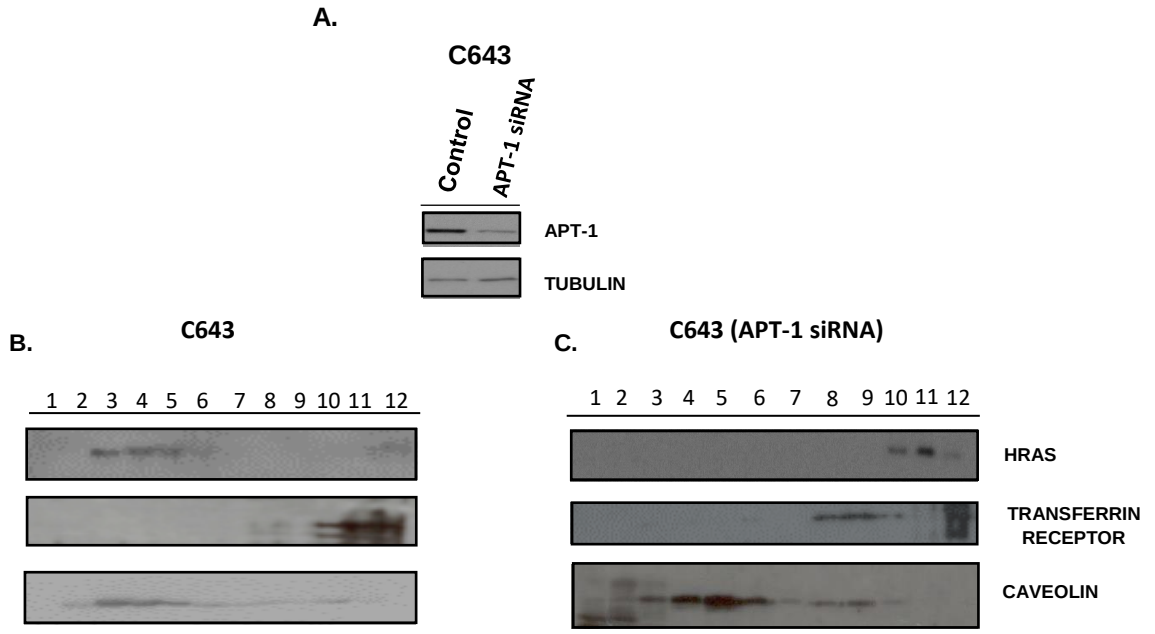

Figure 4.15: APT-1 siRNA knockdown effects in H-RAS micro localization in C643 cells. (A) siRNA-mediated knockdown of APT-1 in C643 cells. APT-1 expression levels determined by immunoblotting. Protein levels were normalized by Bradford assay. **(B)** H-RAS distribution at detergent resistant membrane domains (LRs, enriched in caveolin-1) and detergent soluble fractions (DM, enriched in transferrin receptor) in C643 cells **(C)** H-RAS distribution after APT-1 siRNA-mediated knockdown.

We then, tested whether H-RAS diffusion from LR to DM in C643 cells was able to recapitulate HTH83 characteristics in tumor growth and dissemination. To do so, we grafted 10^6 cells onto the CAM of 10-days chick embryos and after 5 days we collected the tumors and the different organs. We confirmed that APT-1 knock-down in C643 cells, matched HTH83 behavior in tumor growth and metastasis, as they created smaller tumors **(Fig.4.16 A)** with higher rates of intravasation, with higher number of cells **(Fig. 4.16 C)**, and colonized lungs but not liver **(Fig. 4.16 B)**. Therefore, we can conclude that targeting APT-1 in C643 cells, resulting in RAS translocation to DM, generates smaller but more aggressive tumors than the parental cells.

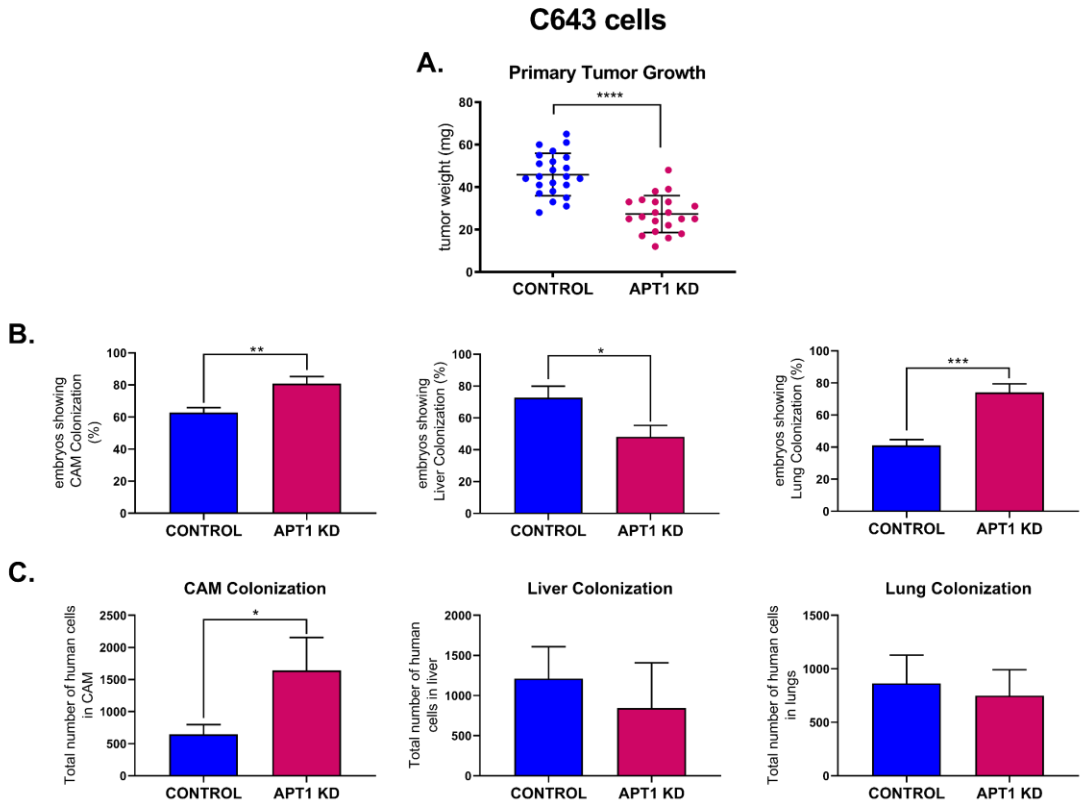

Figure 4.16: Metastatic potential of C643 APT-1 knockdown (KD) cells in the chick embryo spontaneous metastasis model. (**Control:** C643 (blue); **APT-1 KD:** C643 cells with APT-1 knockdown (garnet)) C643 cells were transfected with an APT-1 siRNA and a day after $1x10^6$ cells from each condition (Control and APT-1 KD) were grafted on day 10 chick embryos. After 5 days, the primary tumors were collected and weighed (mg) (Mean ± SD) **(A)** and the distal portions of the CAM were analyzed by qPCR showing the % of embryos that underwent spontaneous intravasation (distal CAM colonization) (MEAN ± SEM) **(B)**; allowing us to determine the relative numbers of rat cells per 10^6 chicken cells (MEAN ± SEM) **(C)**. Data is from three independent experiments employing from 6 to 12 embryos per cell variant. Statistical significance was analyzed by a double tailed unpaired T-test. *p<0.05, **p<0.01, ***p<0.001 and ****p<0.0001.

4.2.5 APT-1 OVEREXPRESSION IN HTH83 CELLS TRANSLOCATES H-RAS FROM DM TO LRS GENERATING BIGGER TUMORS WITH LESS METASTATIC POTENTIAL

After seeing the effects of APT-1 knockdown in C643 cells we sought to investigate whether APT-1 overexpression in HTH83 cells was able to recreate the opposite situation.

To do so we transfected pCEFL-FLAG-APT-1 in HTH83 cells and we corroborated the increase of APT-1 protein levels by immunoblotting **(Fig. 4.17 A)** and analyzed the endogenous H-RAS location in the different membrane microdomains using a membrane fractioning in sucrose gradient by ultracentrifugation. Again, the modification of APT-1 levels, in this case overexpression, was able to partially redistribute, H-RAS from DM to LR. **(Fig. 4.17 B and C)**.

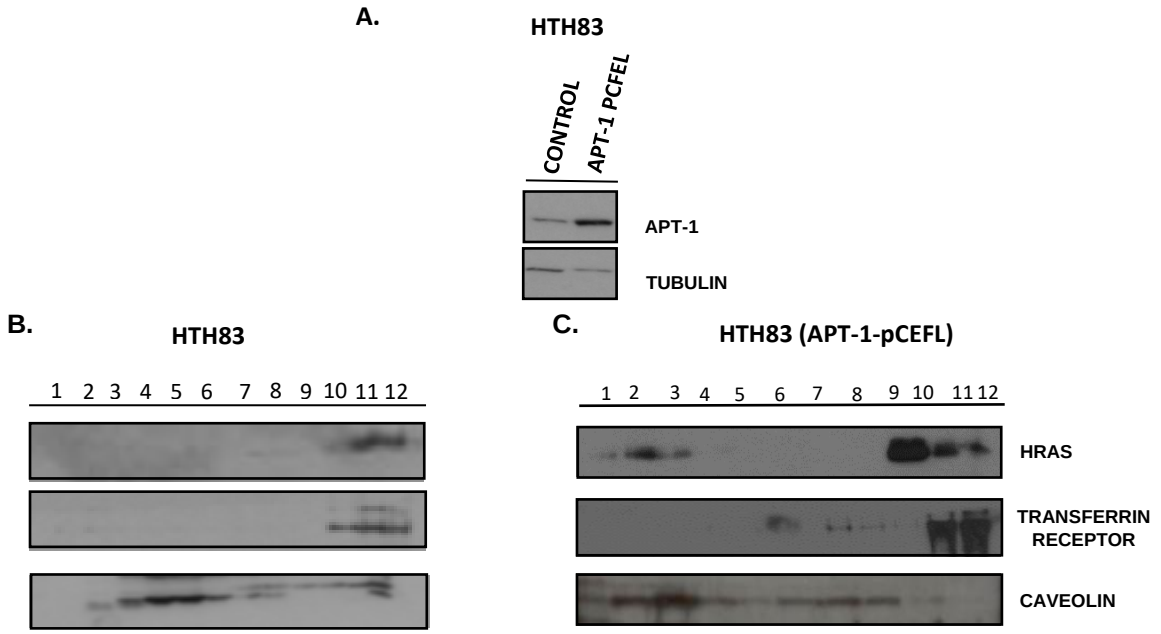

Figure 4.17: APT-1 overexpression effects in H-RAS plasma membrane microdomains distribution in HTH83 human thyroid anaplastic carcinoma cells. (A) pCEFL-FLAG-APT-1 was transfected in HTH83 cells with lipofectamine 3000 following manufacturer instructions. APT-1 proteins expression levels were then assessed by immunoblotting. **(B)** Oncogenic H-RAS distribution at detergent resistant membrane domains (LRs, enriched in caveolin-1) and detergent soluble fractions (DM, enriched in transferrin receptor) in HTH83 cells **(C)** H-RAS distribution in HTH83 cells with APT-1 overexpressed.

Although in HTH83 cells endogenous H-RAS did not fully diffuse to LRs after APT-1 overexpression, this was sufficient to elicit a significant increase in tumor weight compared to HTH83 parental cells (control) **(Fig. 4.18 A)** and a decrease in distal CAM and lung colonization, but not liver **(Fig. 4.18 B)**. No changes in the number of invading cells were seen in the positive cases **(Fig. 4.18 C)**. Altogether, our data demonstrate that H-RAS sublocalizations critically influences thyroid cell oncogenic behavior.

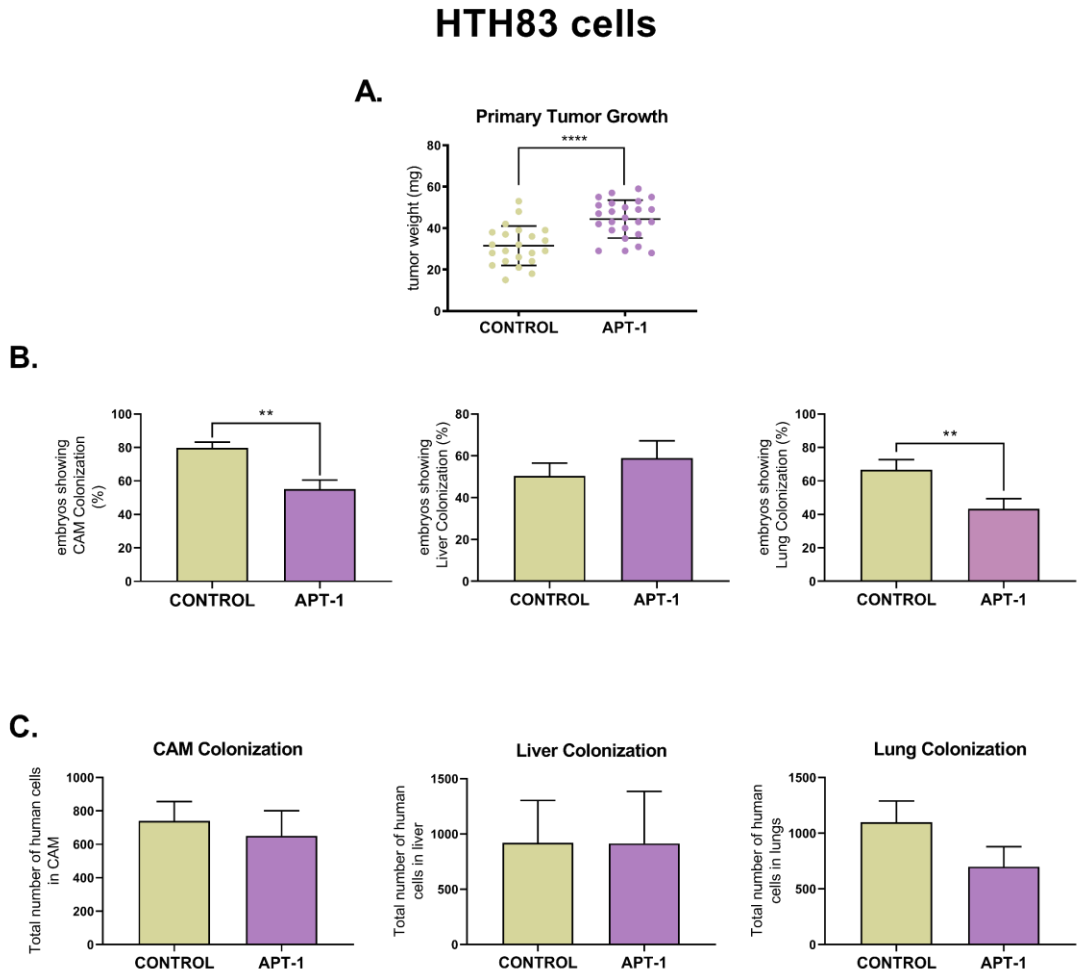

Figure 4.18: Metastatic potential of HTH83 cells, overexpressing APT-1, in the chick embryo spontaneous metastasis model. (**Control:** HTH83 (greenish brown); **APT-1:** HTH83 cells stably expressing ectopic APT-1 (lilac)) 1x10^6 HTH83 cells were grafted on day 10-chick embryos. After 7 days, the primary tumors were collected and weighed (mg) (Mean ± SD) **(A)** and the distal portions of the CAM were analyzed by qPCR showing the % of embryos (MEAN ± SEM) that underwent spontaneous intravasation (distal CAM colonization) and liver and lung colonization **(B)** allowing us to determine the relative numbers of human cells per 10^6 chicken cells (MEAN ± SEM) **(C)**. Data is from three independent experiments employing from 6 to 9 embryos per cell variant. Statistical significance was analyzed by a double tailed unpaired T-test. **p<0.01 and ****p<0.0001.

4.3 H-RAS sublocalizations notably affect tumor phenotype

Given that H-RAS sublocalization can dramatically affect tumor growth and aggressiveness it was interesting to study their histological phenotype. To this end we grafted at several sites of the CAM of 7-days-old chick embryos grown since day 3 *ex ovo,* 20,000 green labeled PCCL3 cells with H-RAS at its different sites. We also looked at C643 or HTH83 cells. After 5 days, Rodhamine was injected to visualized CAM blood vessels and the parts of the CAM containing tumors were fixed in 4% PFA and mounted.

We found that cells transformed by H-RAS ER signals generated big round tumors in the proximity of major vessels, which reinforced previous results pointing out this cells vasculotropism, but few to-non cells were found intravasating **(Fig. 4.19 A)**. H-RAS LR signals yielded the biggest tumors, as expected, showing a roundish shape with some cells migrating from the tumor core. Some necrotic areas were also present (arrow), which can be related to the high rate of proliferation **(Fig. 4.19 B)**. Strikingly, tumors generated by C643 cells showed a similar phenotype to that one elicited by PCCL3 cells expressing H-RAS at LR, although more necrotic parts where observed **(Fig. 4.19 C)**, in consonance with our previous results that demonstrated that C643 cells present H-RAS in LR **(Fig. 4.13 A)**.

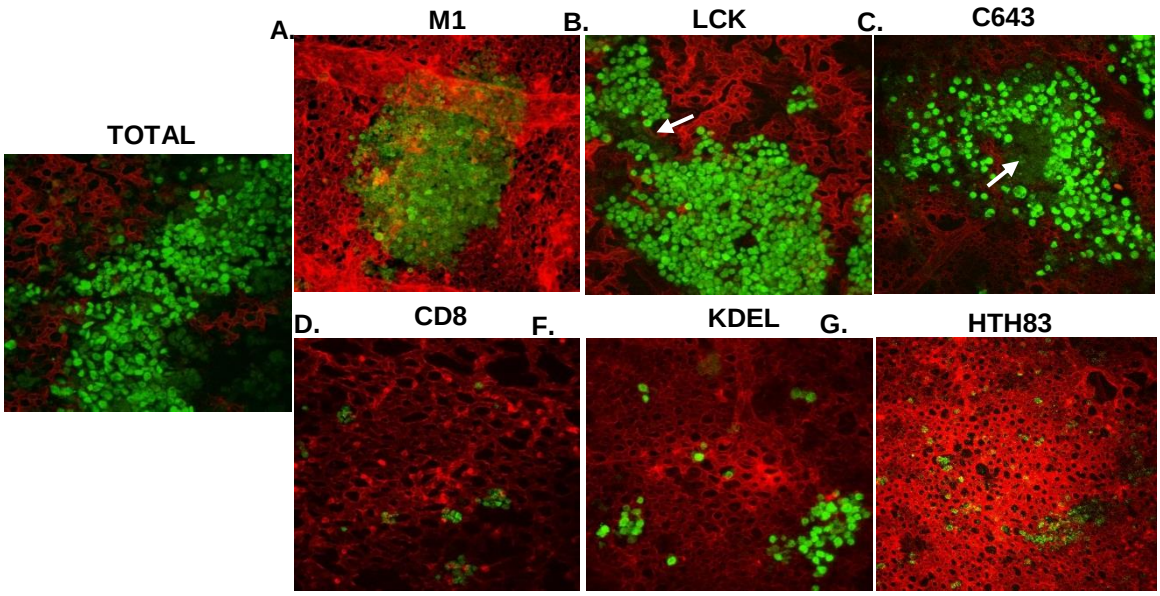

Figure 4.19: Phenotype of the different microtumors formed by H-RAS at its different subcellular locations. C643, HTH83 or PCCL3 cells with total H-RAS or H-RAS activated at either ER (M1), LR (LCK), DM (CD8) or GC (KDEL) were pre-labeled with green fluorescence CellTracker and 20,000 cells were placed on several parts of the CAM of live chick embryos grown *ex ovo* for 3 days. After 5 days CAM vasculature was highlighted by injecting Rodhamine and CAM containing microtumors was fixed with 4% PFA. Then, samples were visualized in a Leica Confocal Microscope using a 25x water objective. 1 μm stacks were captured to visualize the whole thickness of the CAM and images were later reconstructed using Fiji Software. Cells (green), vessels (red), intravasated cells (yellow). Arrows show necrotic zones.

Regarding H-RAS DM-induced tumors they displayed some microfoci as well as high amounts of scattered cells, some of them already in the vessels lumen or intravasating, indicating high rates of invasion and intravasation **(Fig. 4.19 D)**. This is in full agreement with our results in the chick embryo spontaneous metastasis model that identified this H-RAS sublocalization as the most metastatic. These results suggest that the small tumors found in the chick model could be due their highly ability to: i) migrate and scatter throughout the CAM and ii) intravasate. With respect to H-RAS at the GC, it also evokes microtumors but a high amount of scattered cells were also found. As before, some of these cells were already intravasated **(Fig.4.19 E)**. Moreover, HTH83 cells which have mutant H-RAS active at DM showed the same phenotype as H-RASv12-CD8 expressing tumors, presenting mostly scattered cells, some of them intravasating **(Fig. 4.19 F)**.

These results suggest that H-RAS can differentially modulate tumor phenotype, cell invasion and vasculotropism depending on where it is activated within the cell.

4.4 VEGF-B implications in H-RAS mediated tumorigenesis

4.4.1 TUMORS GENERATED BY MUTANT H-RAS AT ER AND LR PRESENT LIPID DROPLETS

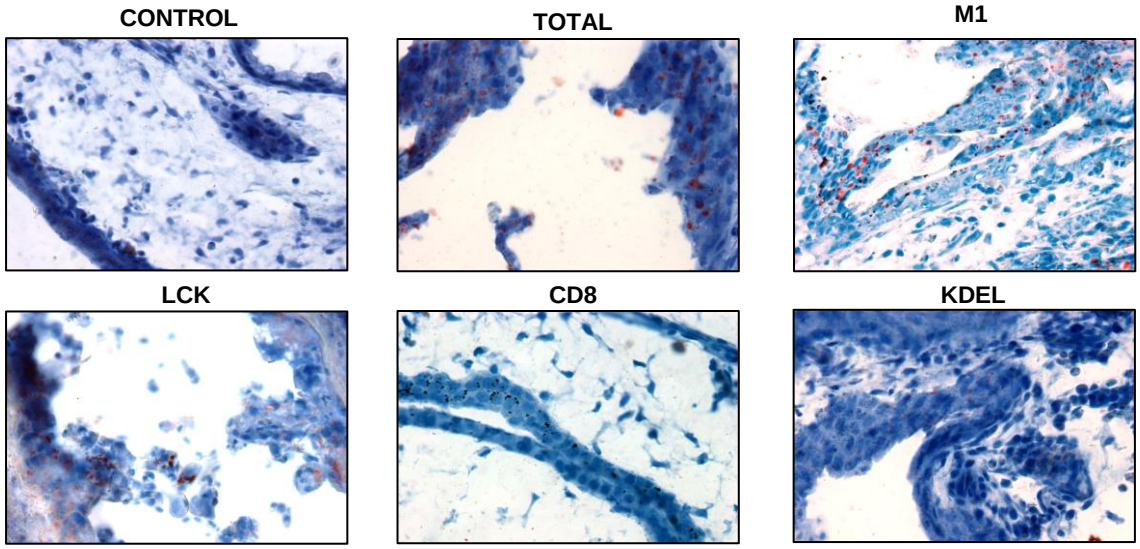

Figure 4.20: Oil red lipid staining of tumor sections. (PCCL3 cells transfected with: **Control:** pCEFL; **Total:** H-RASv12; **M1:** H-RASv12 at ER, **LCK:** H-RASv12 at LR; **CD8:** H-RASv12 at DM; **KDEL:** H-RASv12 at GC).

When tumors generated by H-RAS at its different sublocalizations were stained with hematoxylin we observed particularly in the case of ER and LR H-RAS, empty rounded spaces inside some of the cells, which resembled lipids droplets, which are known to be dissolved by Xylene processing. To explore this possibility an oil red Staining was performed to reveal the

existence of neutral triglycerides and lipids. Strikingly, we found that mainly H-RASv12-M1 and H-RASv12-LCK-expressing tumors stained positive por oil red **(Fig.4.20)**. That made us wonder if H-RAS active at ER and LRs could regulate lipid uptake and storage.

4.4.2 H-RAS ACTIVE AT ER AND LR GENERATES TUMORS EXPRESSING HIGH LEVELS OF VEGF-B

VEGF-B is a poorly angiogenic member of the VEGF family that signals through VEGFR1 and its coreceptor, neuropilin-1 (135). Recently, this growth factor has been related to energy metabolism, instructing endothelial cells to take up Long-Chain Fatty Acids (LCFAs) from the circulation, that are then uptaken by surrounding cells for use and storage as lipid droplets (137). Therefore, we hypothesized that this molecule could be responsible for the accumulation of the lipids shown in our tumors.

To test our hypothesis, we extracted mRNA from the different tumors and we checked for VEGF-B mRNA levels using rat primers that recognized both VEGF-B isoforms. Interestingly, VEGF-B was upregulated in H-RASv12-M1 and H-RASv12-LCK-expressing tumors which correlates with the presence of lipid droplets in the cells **(Fig 4.21 A)**. Moreover, C643 cells, that have H-RAS mainly in LRs also exhibited significantly higher levels of VEGF-B when compared to HTH83 cells **(Fig 4.21 B)**. Since VEGF-B is able to modulate VEGF-A-induced pathological angiogenesis in some situations (136), we also tested for VEGF-A mRNA expression using primers that recognize all VEGF-A isoforms. We saw that H-RASv12-CD8 and H-RASv12-KDEL-expressing tumors exhibited higher levels of VEGF-A compare to tumors generated by H-RAS active at LR and ER **(Fig. 4.21 C)**. Indeed, VEGF-A is known to promote angiogenesis and increase vessels leakage and permeability thus favoring metastasis (124) in agreement with our results showing that H-RASv12-CD8 and H-RASv12-KDEL-expressing PCCL3 cells induced more metastatic tumors. In consequence our results suggest that VEGFs expression could be modulating tumor behavior.

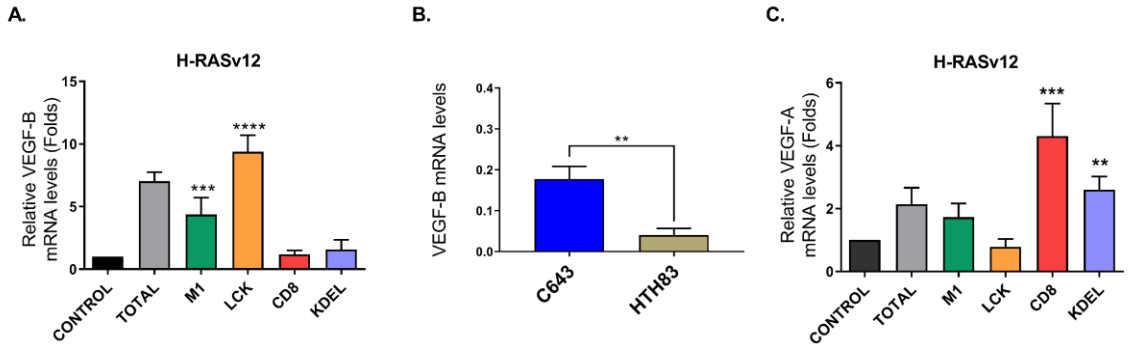

Figure 4.21: Fold changes of the relative mRNA levels of VEGF-B and VEGF-A in the different tumors. (A) and **(B)** represent VEGF-B mRNA expression levels analyzed by qPCR in tumors with H-RAS at its subcellular locations or C643 and HTH83 tumors, respectively, grown using the chick embryo spontaneous metastasis model **(C)** VEGF-A mRNA expression levels analyzed by qPCR. Data **(A,C)** are expressed as the fold change relative to CONTROL.

4.4.3 VEGF-B ADDITION TO H-RAS DM AND GC TUMORS ALTERS THEIR METASTATIC POTENTIAL

Since H-RAS activated in LR and ER induces big tumors with low ability to colonize distant organs, and presents high levels of VEGF-B expression, we sought to elucidate whether VEGF-B was impairing tumor the ability to metastasize.

We grafted $1x10^6$ cells with active H-RAS present at either DM or GC, onto the CAM of 10-days old chick embryos. After two days, rat VEGF-B was added and renewed every two days. At day 7 tumors were collected and weighted and distant organ colonization was analyzed by qPCR. Interestingly we found that VEGF-B was capable of increasing the tumor size of H-RAS DM and GC-generated tumors **(Fig. 4.22 A)** and of decreasing to a substantial extent, about 20%, their ability to intravasate **(Fig. 4.22 B)** and to colonize lungs **(Fig. 4.22 D)**, though, no effects in liver colonization were observed **(Fig 4.22 C)**. These results demonstrate that VEGFB impairs tumor cells ability to intravasate and invade distant organs.

Altogether these results point out VEGF-B as a new possible biomarker to further stratify the risk of H-RAS-positive nodules or to assess the ability of already stablished tumors to colonize distant organs. Therefore, as for APT-1, a prospective or retrospective analysis of H-RAS mutant nodules and tumors should be carried out in order to relate the levels of VEGF-B in immunohistochemistry to the aggressiveness of tumors and thus, confirm our assumptions.

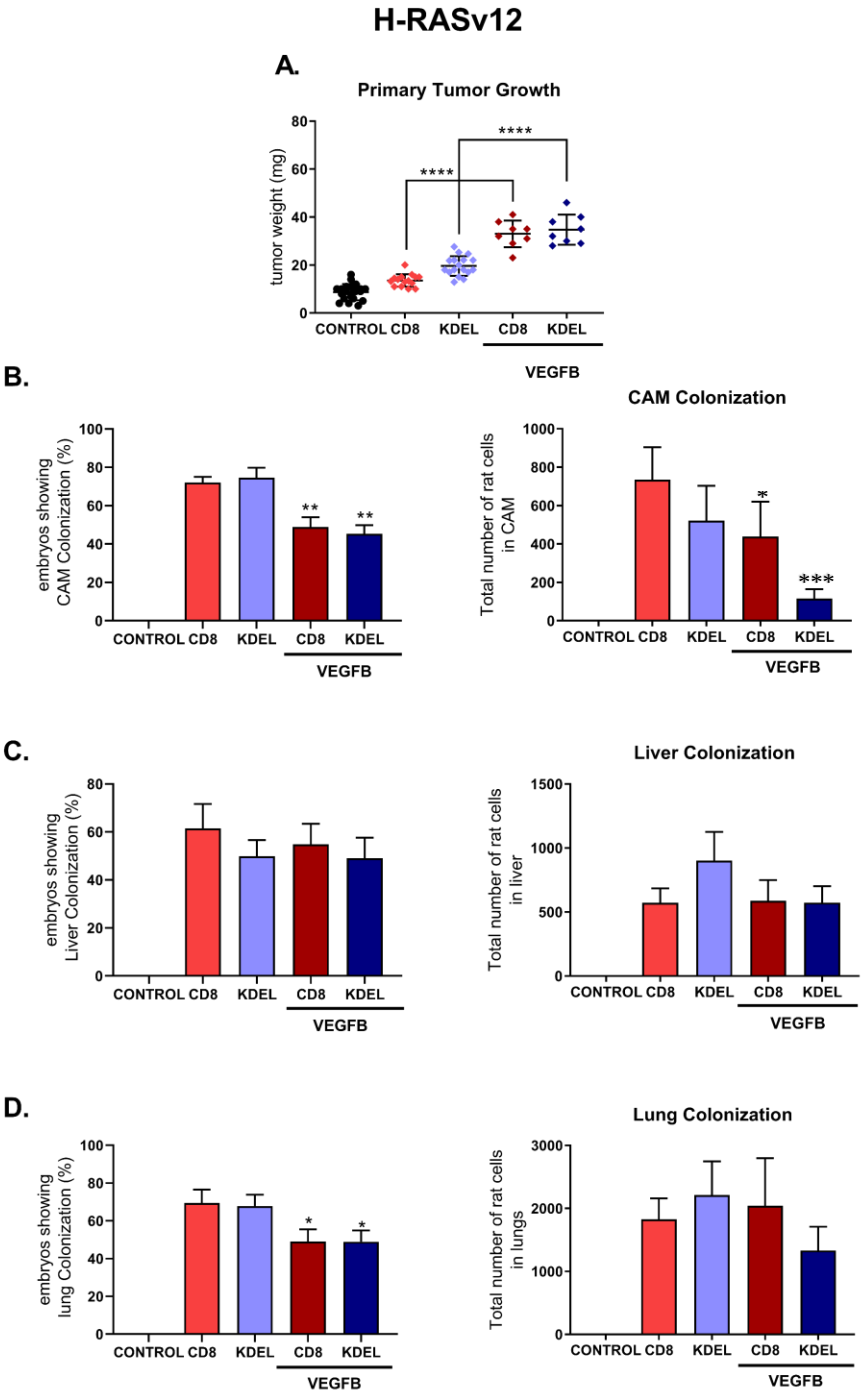

Figure 4.22: Effects of VEGF-B in tumor growth and metastasis. 1x10^6 cells were grafted on 10-days chick embryos. 10 nM of VEGF-B was added at day 2 and every two days it was renewed. After 7 days, primary tumors were collected and weighed (mg) (Mean ± SD) **(A)** and the distal portions of the CAM were analyzed by qPCR showing the % of embryos (MEAN ± SEM) that underwent spontaneous intravasation (distal CAM colonization) **(B left)**, liver **(C left)** or lung colonization **(D left)** allowing us to determine the respective relative numbers of rat cells per 10^6 chicken cells **(B,C, D right)**. Data is from three independent experiments employing from 5 to 10 embryos per cell variant. Statistical significance of cells treated with VEGF-B was determined in comparison with their respective non-treated counterparts. Groups were analyzed by a double tailed unpaired Student T-test. *p<0.1, **p<0.01, ***p<0.001 and ****p<0.0001.

4.5 RAS sublocalizations implications in exosome secretion and its effects

4.5.1 PCCL3 CELLS HAVE MULTIVESICULAR BODIES

Exosomes are nanovesicles having a maximum size of 150 nm, that carry specific cargos, such as, DNA, RNA, proteins and lipids. The vast majority are formed in multivesicular bodies that release them once fused to the plasma membrane, although some of them can arise directly from the plasma membrane budding as microvesicles (150 nm-1 μm) (152). H-RASv12 has been shown to promote exosome secretion (173, 318), and it has also been found in them (177, 319), conferring exosomes the ability to transform other cells. Therefore, to explore whether PCCL3 cells were able to secrete extracellular vesicles and if H-RASv12 sublocalizations could affect their formation or secretion, we looked for multivesicular bodies (MVBs) using transmission electron microscopy. We found MVBs in PCCL3 cells whether expressing H-RAS or not, and independently of its sublocalizations **(Fig. 4.23 B)**. Moreover, we saw high amount of plasma-membrane budding, a key step in microvesicles biogenesis and release so we could confirm that PCCL3 cells induce microvesicles formation and secretion **(Fig. 4.23 C)**.

In addition, we found interesting features in the different cell lines:

PCCL3 parental cells, as expected, showed a polarized state and since they are thyroid follicular cells, which are highly active transcriptomically, we found high amounts of free polyribosomes and a moderate plasma membrane budding **(Fig. 4.23 A)**.

PCCL3 cells expressing H-RAS showed high amounts of free polyribosomes and more compacted chromatin.

H-RASv12-M1-expressing PCCL3 cells have high amounts of free polyribosomes multilamellar bodies, which are membrane-bound organelles. They vary in size from 100-2400 nm, are composed of concentric membrane layers, and frequently exhibit an electron-dense core. Their main function is lipid storage and secretion and they have a lysosomal nature (320) **(Fig. 4.23 C)**. In addition, heterochromatin is more condensed than the other cell lines **(Fig. 4.23 D)**.

PCCL3 cells expressing H-RAS at LR presented high amount of membrane budding, have lots of free polyribosomes and they are still polarized **(Fig. 4.23 F)**. PCCL3 cells with H-RAS at DM exhibited i) high membrane activity ii) high amounts of free polyribosomes iii) big and highly condensed nucleolus and iv) little heterochromatin **(Fig. 4.23 G)**. These results coincide with the reduction in the levels of heterochromatin and an increase in nucleolar size in cancer cells (321, 322) pointing out again that cells with H-RAS at DM show characteristics of aggressive cancers.

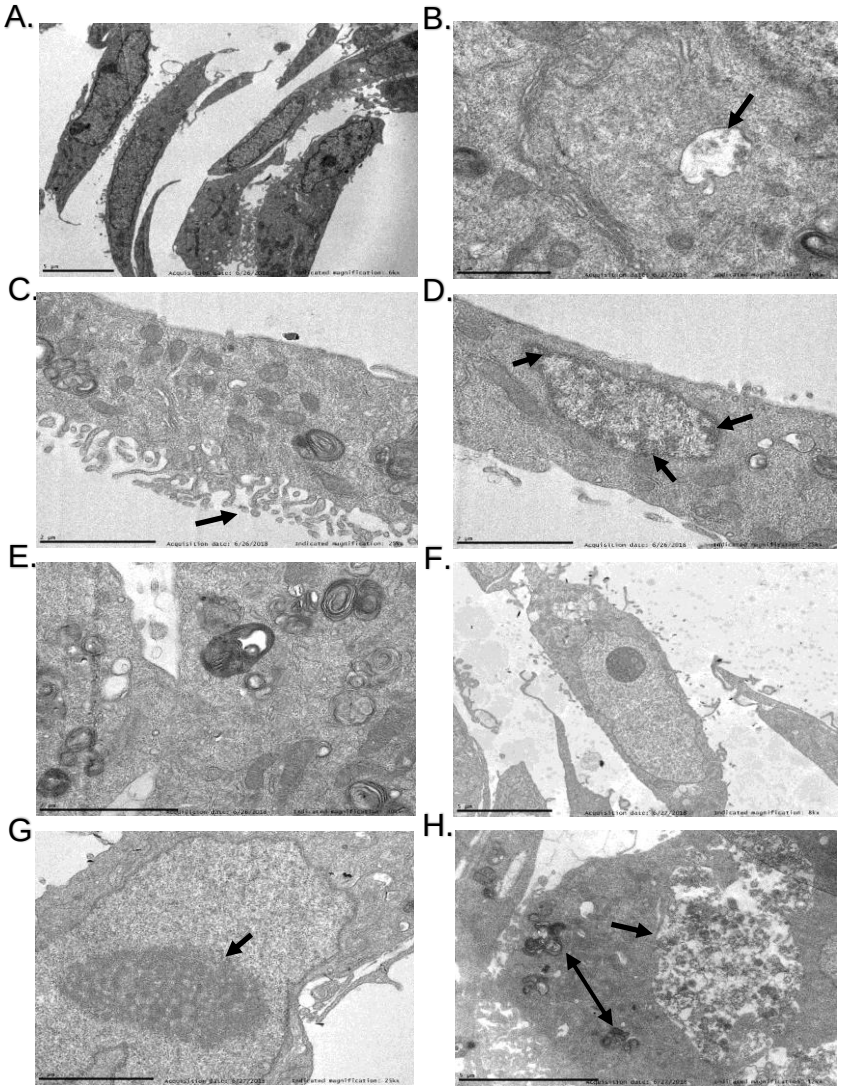

Figure 4.23: MVB presence in PCCL3 cells (A) PCCL3 parental cells **(B)** Multivesicular body (arrow) in cells with H-RAS at GC **(C) (D)** PCCL3 cells expressing mutant H-RAS at ER, heterochromatin is pointed out by arrows **(E)** multilamellar bodies present PCCL3 with active H-RAS at GC **(F)** cells with active H-RAS at LR **(G)** Cells with mutant H-RAS at DM, arrow point out the nucleolus **(H)** Necrotic cell (arrow) and multilamellar bodies (double arrow) in H-RASv12-KDEL expressing cells.

PCCL3 cells expressing H-RAS at LR presented high amount of membrane budding, have lots of free polyribosomes and they are still polarized **(Fig. 4.23 F)**.

PCCL3 cells with H-RAS at DM exhibited i) high membrane activity ii) high amounts of free polyribosomes iii) big and highly condensed nucleolus and iv) little heterochromatin **(Fig. 4.23 G)**. These results coincide with the reduction in the levels of heterochromatin and an increase in nucleolar size in cancer cells (321, 322) pointing out again that cells with H-RAS at DM show characteristics of aggressive cancers.

PCCL3 cells with H-RAS at the GC exhibited i) a hypertrophic GC with some dilated cisterns ii) lots of mitosis and iii) several necrotic cells **(Fig. 4.23 H)**. In addition, as in cells with H-RAS at ER, we saw a high amount of multilamellar bodies, some of them strikingly big **(Fig. 4.23 E)**.

To sum up, H-RAS expressing cells, as well as PCCL3 parental cells, present MVBs, plasma membrane budding known to be related to microvesicles secretion, and high amounts of free polyribosomes. Surprisingly H-RAS signaling from intracellular organelles, ER or the GC, induce multilamellar bodies (MLB) formation, suggesting that H-RAS might be altering cholesterol metabolism and autophagosome trafficking, since these alterations have been related to MLB appearance (323).

4.5.2 H-RAS EXPRESSION IN PCCL3 CELLS AFFECTS EVs CHARACTERISTICS AND SECRETION DEPENDING ON ITS LOCATION

Since we had confirmed MVBs presence inside the cells and some of them never reach the plasma membrane because they are recycled into lysosomes (324), we needed to check whether PCCL3 cells were actually able to secrete EVs. To reach our aim, we isolated EVs by size exclusion chromatography and EVs fractions 3-5, that correspond to the exosome peak, shown in the chromatogram **(Fig. 4.24)**, were analyzed.

Surprisingly, H-RAS activated in the different subcellular locations decreased ALIX-1 EV marker compare to PCCL3 parental cells and EVs secreted by cells expressing H-RASv12 at DM or GC were slightly enriched in SYNTENIN and mostly in TSG-101 **(Fig. 4.25 B)**. Fractions 6-8 are the ones located previous to the protein peak, which is the high peak shown in the chromatogram **(Fig. 4.24)**, and are known to also contain exosomes. Therefore, we also analyzed them by Western blotting and

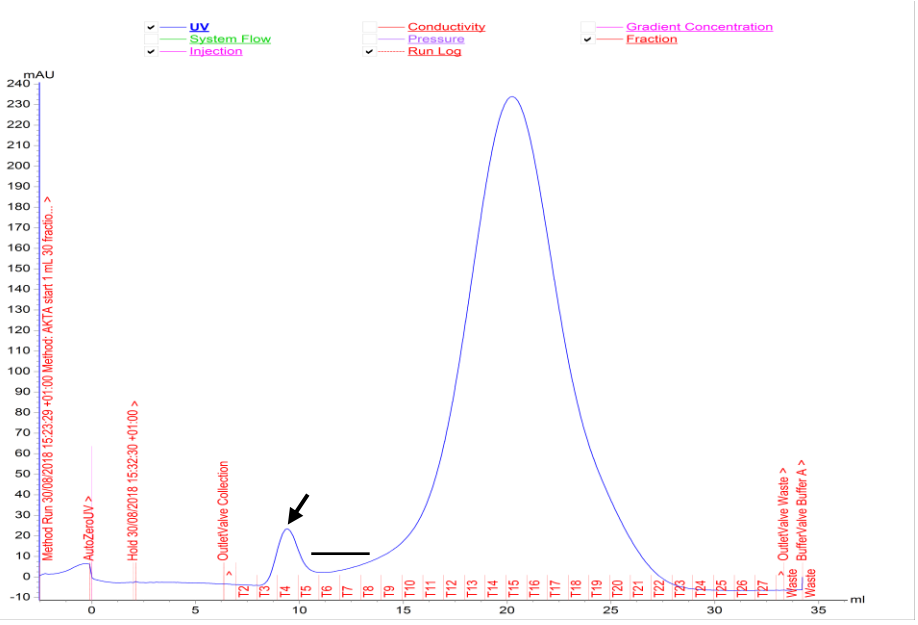

Figure 4.24: Size exclusion chromatogram (PCCL3 parental cells). Fractions T3-T5 (arrow) correspond to the exosome peak. Line shows fractions T6-T8. The 240 mAU peak corresponds to proteins present in supernatants.

we observed that although SYNTENIN and CD63 were all still markedly present in all cell lines, cells expressing HRAS at its different locations had almost undetectable levels of TSG-101 and ALIX-1 but were still strongly present in PCCL3 parental cells **(Fig. 4.25 C)**.

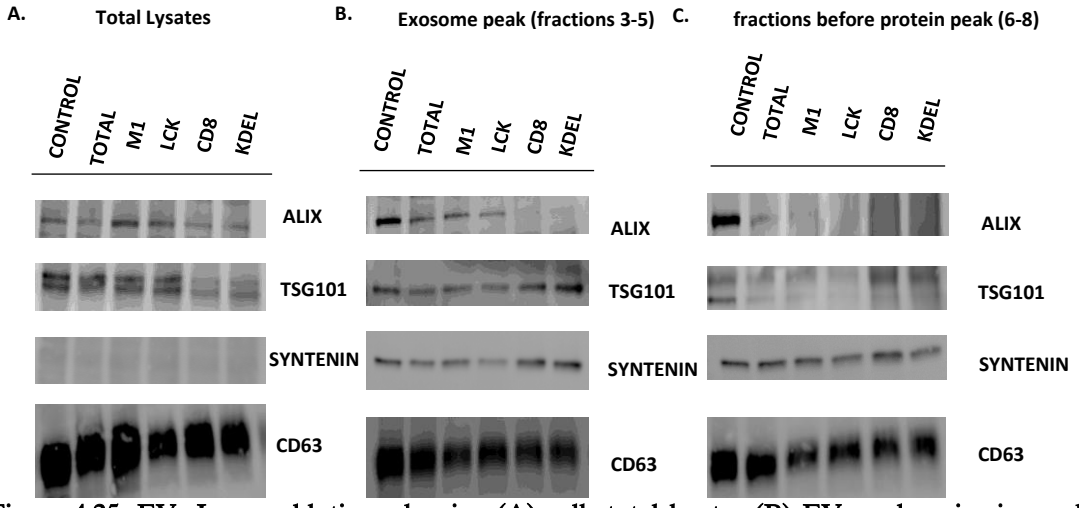

Figure 4.25: EVs Immunoblotings showing (A) cells total lysates (B) EV markers in size exclusion fractions 3-5 (C) EV markers in size exclusion fractions 6-8.

To investigate whether H-RAS was modulating the amount and the size of EVs depending on its sublocalizations, we analyzed EVs concentration by Nanoparticle Tracker Analysis using NanoSight. We saw that PCCL3 parental cells secreted the same amount of EVs as PCCL3 cells with H-RAS at DM and the GC but strikingly more than cells with H-RAS signaling from the ER and LR. Results were similar for both the exosome peak (fractions 3-5) **(Fig. 4.26)** and 6-8 fractions **(Fig. 4.27)**. EVs size was also different between H-RAS sublocalizations and we saw that, like PCCL3 cells, cells with H-RAS at DM and the GC showed bigger EVs in the exosome peak but not in later fractions, when compared to EVs secreted from cells with H-RAS active at ER or LR.

Overall, this data suggests that H-RAS when present at different subcellular locations induce different pools of EVs, that might have distinct cargos.

4.5.3 EVs SECRETED BY CELLS WITH H-RASV AT DM AND GC AFFECT CELL PROLIFERATION

Since we demonstrated that EVs secreted by cells containing H-RAS at DM and GC are different from the ones secreted by cells with H-RAS at ER and LR, we sought to explore if they could have different effects in cell proliferation, in line with our previous findings. To analyze that, we first assessed cellular growth, acquiring live images for three days using the IncuCyte ZOOM® analysis system. This system takes four photos per well every two hours and uses a specific mask to detected cells silhouette, transforming it into a figure. We found that this method showed changes in proliferation that were not detected by AlamarBlue.

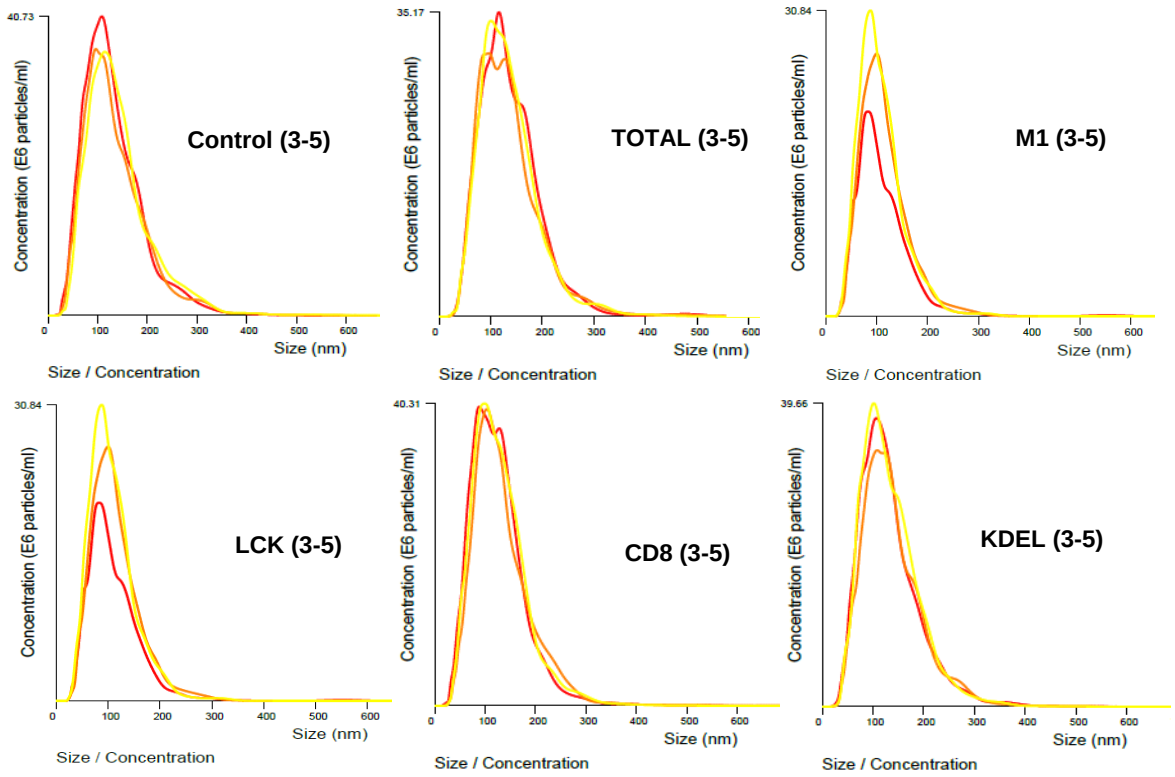

Figure 4.26: NanoSight tracker analysis measurement of particle size distribution and concentration in exosomes from fractions 3-5. (PCCL3 cells transfected with: **Control:** pCEFL; **Total:** H-RASv12; **M1:** H-RASv12 at ER, **LCK:** H-RASv12 at LR; **CD8:** H-RASv12 at DM; **KDEL:** H-RASv12 at GC)

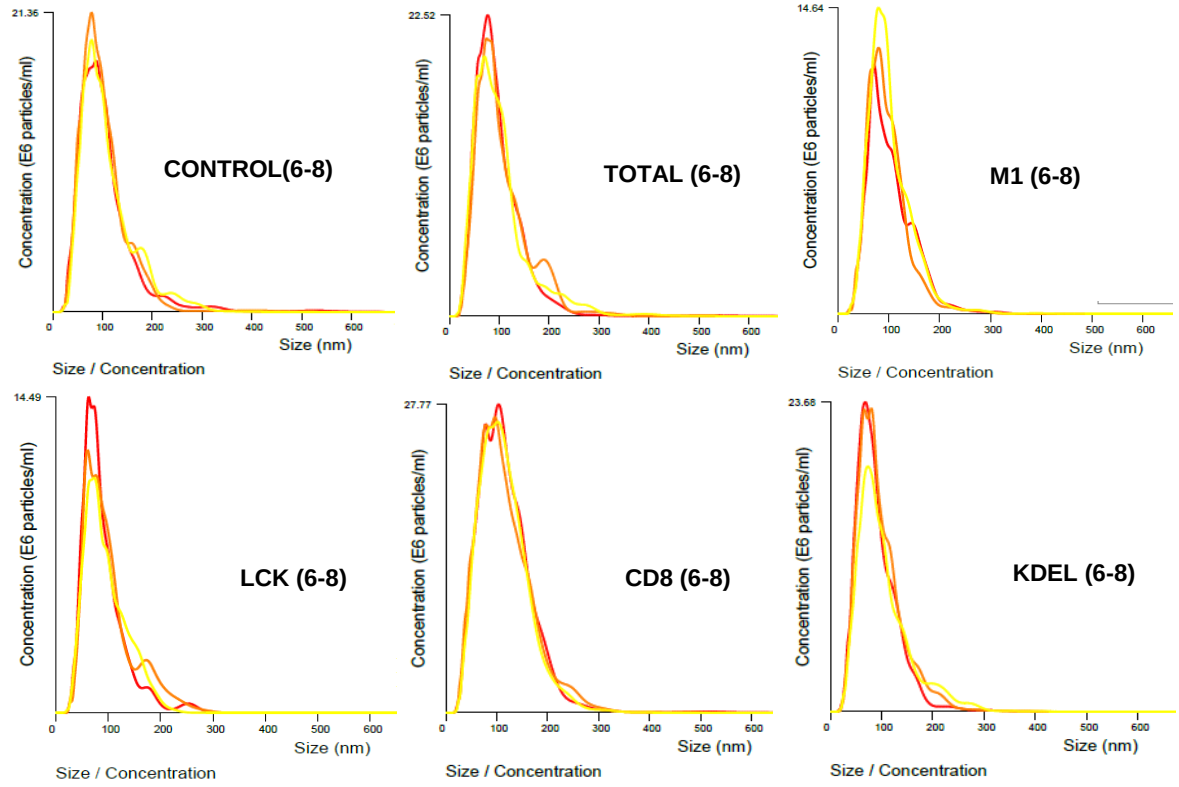

Figure 4.27: NanoSight tracker analysis measurement of particle size distribution and concentration in exosomes from fractions 6-8. (PCCL3 cells transfected with: **Control:** pCEFL; **Total:** H-RASv12; **M1:** H-RASv12 at ER, **LCK:** H-RASv12 at LR; **CD8:** H-RASv12 at DM; **KDEL:** H-RASv12 at GC)

In this case, cells with H-RAS at DM and GC displayed lower levels of proliferation compared to the other cells. However, as seen before, H-RASv12 in ER and LR presented similar proliferation rates as PCCL3 parental cells **(Fig. 4.28 A)**.

To investigate whether EVs secreted by cells containing H-RASv12 tethered to its different subcellular locations could influence cell proliferation differentially, we incubated 3,000 recipient cells with 1,000 EVs (either using 3-5 or 6-8 fractions) collected from the different types of H-RAS-expressing cells for 30 minutes. EVs isolated by size exclusion were utilized and using the IncuCyte ZOOM analysis system we closely followed cell proliferation for 3 days. We found that the EVs secreted by cells with H-RAS at DM and the GC could decrease proliferation of PCCL3 parental cells **(Fig. 28 and 29 B)** and cells containing active H-RAS at ER **(Fig. 28 and 29 C)** or LR **(Fig. 28 and 29 D)** after 24 hours, and more significantly after 72 hours. This effect was more pronounced when exosome peak fractions 3-5 were used **(Fig.28)**. Moreover, EVs secreted by cells with H-RAS at LR also diminished proliferation of PCCL3 parental cells **(Fig. 28 and 29 B)** and of cells with H-RAS at ER **(Fig. 28 and 29 C)**, although to a lesser than the other EVs. In contrast, EVs secreted by cells harboring H-RAS at LR **(Fig. 28 and 29 E and F)** or ER **(Fig. 28 and 29 E and F)** did not promote proliferation of other cells.

These results further indicate that H-RASv12 activated at different subcellular locations generate different EVs.

4.5.4 EVs SECRETED BY PCCL3 CELLS EXPRESSING H-RAS AT DM INCREASE THE METASTATIC POTENTIAL OF CELLS EXPRESSING H-RAS AT ER OR LR AND DECREASE THEIR TUMOR SIZE

Since we demonstrated that EVs isolated from PCCL3 cells expressing H-RASv12 at DM could decrease the proliferation rate of cells expressing H-RAS at other sublocalizations, we hypothesized that these EVs could also decrease their tumor size. To approach it, cells with H-RAS at ER and LR were incubated with EVs secreted from cells harboring H-RAS at DM. After that, cells were grafted onto the CAM of 10-days old chick embryos and after 7 days tumor weight was measured and distal CAM, liver and lungs colonization were analyzed.

It was found that EVs derived from cells expressing H-RAS at DM were capable of reducing tumor growth promoted by H-RAS signals at ER **(Fig. 30 A)** and LR **(Fig. 31 A)** by 50% compared to EVs derived from control cells. More interestingly, these EVs were able to confer cells with H-RAS at ER **(Fig.4.30 B)** and LR **(Fig.4.31 B)** the capacity to intravasate and colonize distant organs as lungs **(Fig.4.30 and 31 F)** and liver **(Fig 4.30 and 31 D)**. These effects were quite outstanding in lungs, where they were capable to almost triplicate H-RAS ER-mediated lung colonization and almost doubled H-RAS LR-mediated one.

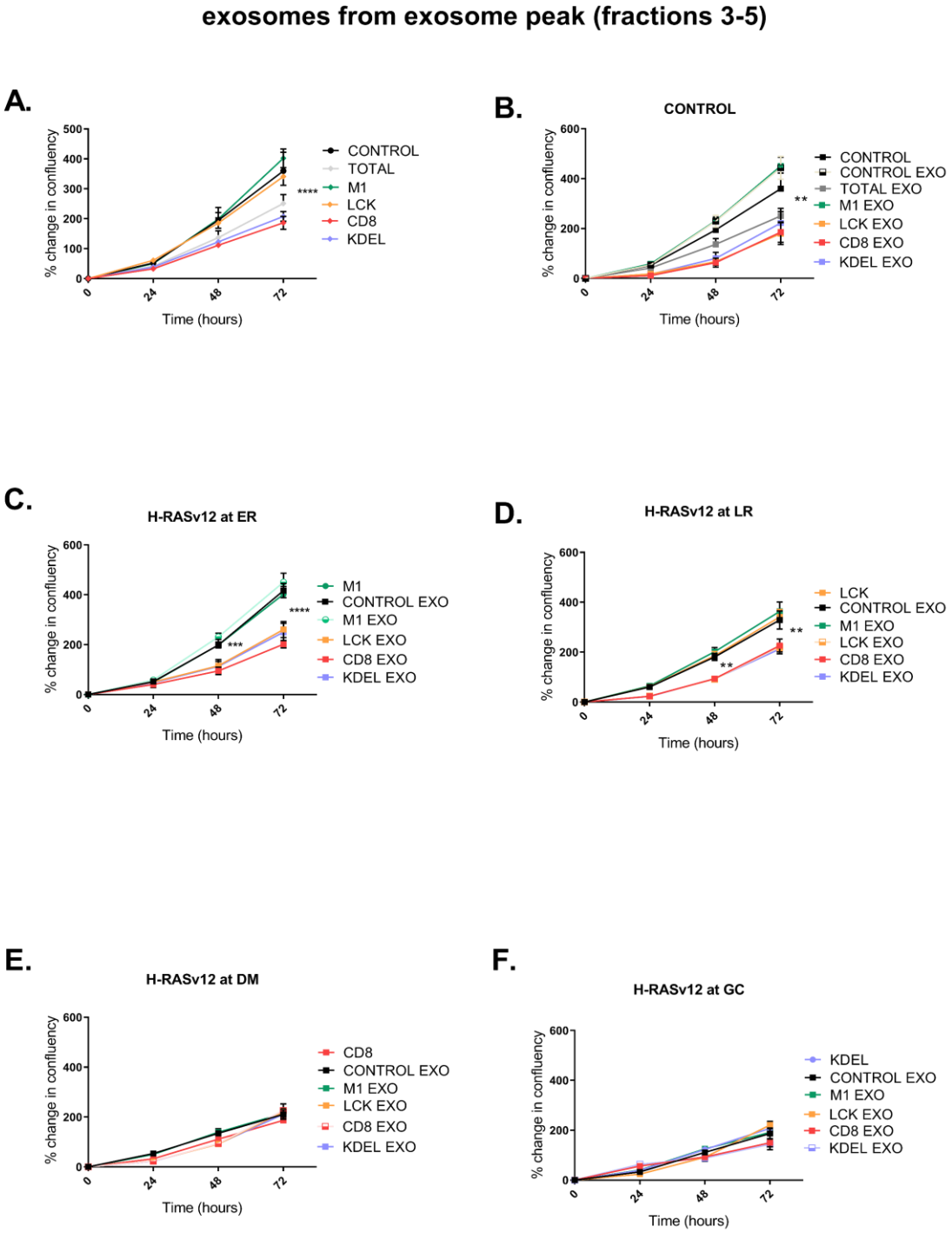

Figure 4.28: Effects of heterologous EVs on cellular proliferation (3-5). The indicated cells lines were incubated with EVs secreted by PCCL3 cells (fractions 3-5) parental or expressing H-RAS at its different localizations. 3,000 PCCL3 cells were incubated with 1x PBS **(A)** or with 1000 EVs/per cell for 30 minutes before seeded and were grown for 72 hours. EVs used were obtained by size exclussion and fractions 3-5, which correspond to the exosome peak. **(B)** PCCL3 parental cells, or PCCL3 with **(C)** H-RASv12 at ER (M1), **(D)** HRASv12 at LR (LCK), **(E)** HRASv12 at DM (CD8) and **(F)** HRASv12 at GC (KDEL) treated with EVs isolated from PCCL3 parental cells or PCCL3 cells expressing H-RASv12 at either ER, LR, DM or GC. Data is from three independent experiments. Statistical significance was determined using a double tailed unpaired Student T-test **p<0.01, ***p<0.001 and ****p<0.0001.

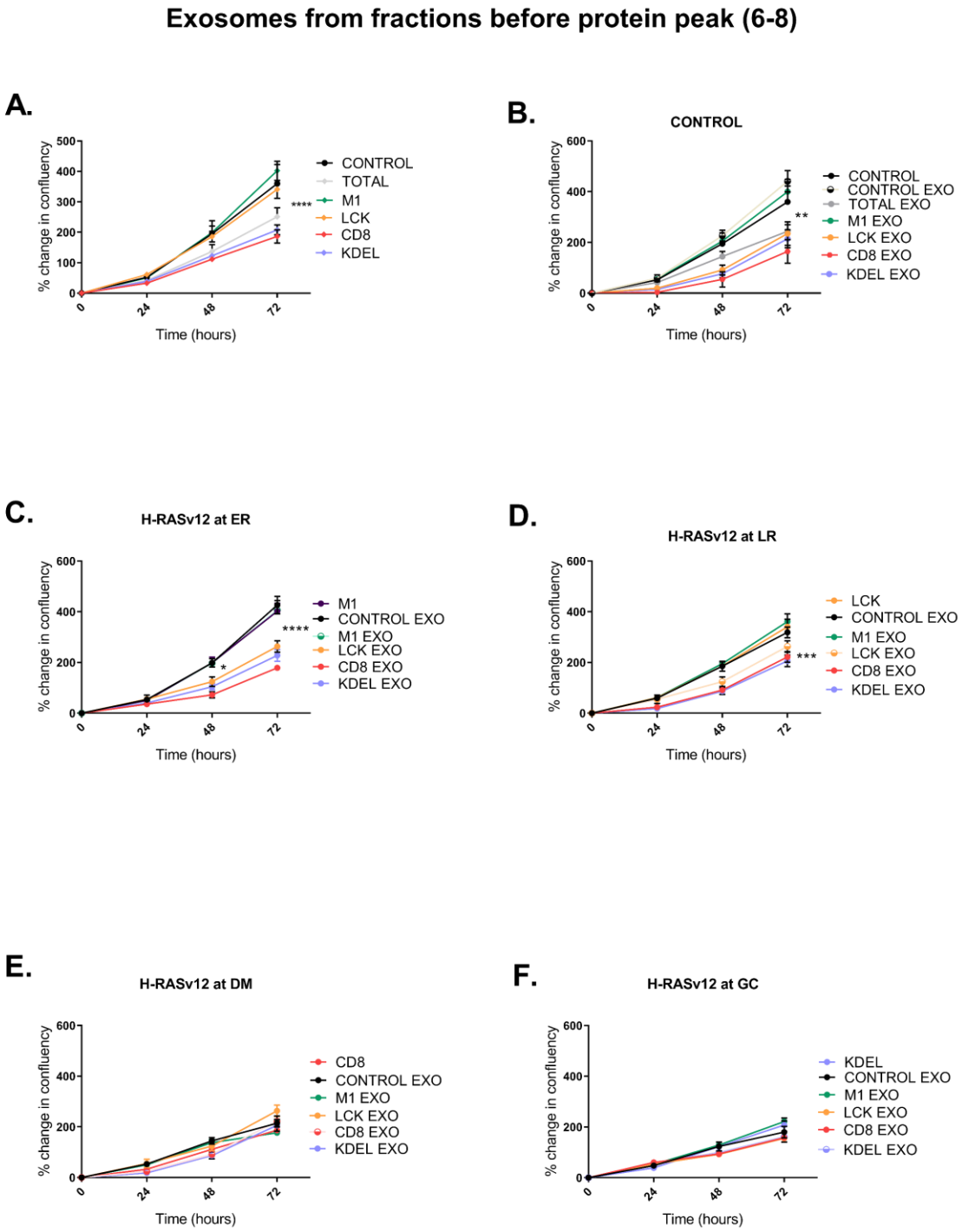

Figure 4.29: Effects of heterologous EVs on cellular proliferation (6-8). The indicated cells lines were incubated with EVs secreted by PCCL3 cells (fractions 6-8) parental or expressing H-RAS at its different localizations. 3,000 PCCL3 cells were incubated with 1x PBS **(A)** or with 1000 EVs/per cell for 30 minutes before seeded and were grown for 72 hours. EVs used were obtained by size exclussion and fractions 6-8, which correspond to the exosome peak. **(B)** PCCL3 parental cells, or PCCL3 with **(C)** H-RASv12 at ER (M1), **(D)** HRASv12 at LR (LCK), **(E)** HRASv12 at DM (CD8) and **(F)** HRASv12 at GC (KDEL) treated with EVs isolated from PCCL3 parental cells or PCCL3 cells expressing H-RASv12 at either ER, LR, DM or GC. data is from three independent experiments. Statistical significance was determined in comparison using a double tailed unpaired Student T a double tailed unpaired T-test **p<0.01, ***p<0.001 and ****p<0.0001.

To sum up, these results suggest that H-RAS at DM can promote the secretion of EVs capable of i) changing tumoral behavior, ii) inducing intravasation and iii) shaping distant tumoral niches allowing cells to extravasate, survive and proliferate, growing micrometastases in these organs.

4.5.5 EVs ISOLATED FROM PCCL3 CELLS EXPRESSING ONCOGENIC H-RAS AT GC MODIFY ER AND LR H-RAS ONCOGENIC POTENTIAL

As EVs isolated from PCCL3 cells with oncogenic H-RAS at GC diminished ER and LR H-RAS mediated proliferation *in vitro,* we sought to explore the possibility that these EVs were also capable of modifying the tumor size and the capacity to invade distant organs displayed by these cells.

To explore this possibility, we incubated $1x10^6$ PCCL3 cells expressing H-RASv12-M1 or H-RASv12-LCK with 1000 EVs/per cell isolated from cells harboring RAS at GC, for 30 minutes. After this time, cells were grafted onto the CAM of 10 days old chick embryos and after 7 days tumoral weight was measured and distal CAM, liver and lungs colonization were analyzed by qPCR. Under these conditions we saw that GC RAS EVs decreased the size of LR H-RAS tumors but not those induced by ER H-RAS one, **(Fig.30 and 31 A)**. Furthermore, GC H-RAS-derived EVs promoted by 2-fold ER H-RAS induced-intravasation **(Fig. 30 B)** and almost tripled its liver and lung colonization in the chick embryo spontaneous metastasis model **(Fig. 30 D and F)**. Regarding LR H-RAS, GC H-RAS-derived EVs increased by 30% their intravasation (Distal CAM colonization) **(Fig. 31 B)**, by a 20% liver colonization **(Fig. 31 D)** and shockingly double their ability to colonize lungs **(Fig. 31 F)**.

All together this data suggests that GC H-RAS-derived EVs and DM H-RAS-derived EVs, besides from being different in terms of the markers they exhibit, are capable to enhance ER and LR H-RAS metastatic potential, presumably by increasing their intravasation rate, by modifying cell organotropism or by preparing the pre-metastatic niche in lungs.

4.5.6 EVs SECRETED BY H-RAS AT ER OR LR DO NOT MODIFY DM OR GC H-RAS METASTATIC POTENTIAL

Although we did not see any changes in proliferation when EVs coming from PCCL3 cells with H-RAS activated in ER or LR were added to cells with H-RAS at DM or GC, we wanted to explore if they were capable of promoting cell intravasation and distant metastasis.

We again followed the same experimental settings as above. However, this time we did not see any changes in tumor size **(Fig. 32 and 33 A)**, intravasation **(Fig. 32 and 33 B)** or distant organs colonization **(Fig. 32 and 33 D and F)** when using EVs derived from cells with H-RAS at ER.

Conversely, we found that EVs isolated from cells with H-RAS active at LR increased GC RAS-promoted tumor size although they did not affect distant organs colonization **(Fig. 4.33 A)**.

To sum up, these results show that extracellular vesicles isolated from cells expressing oncogenic H-RAS exhibit striking different effects, depending on its subcellular locations, that affected other RAS locations-mediated proliferation and metastasis.

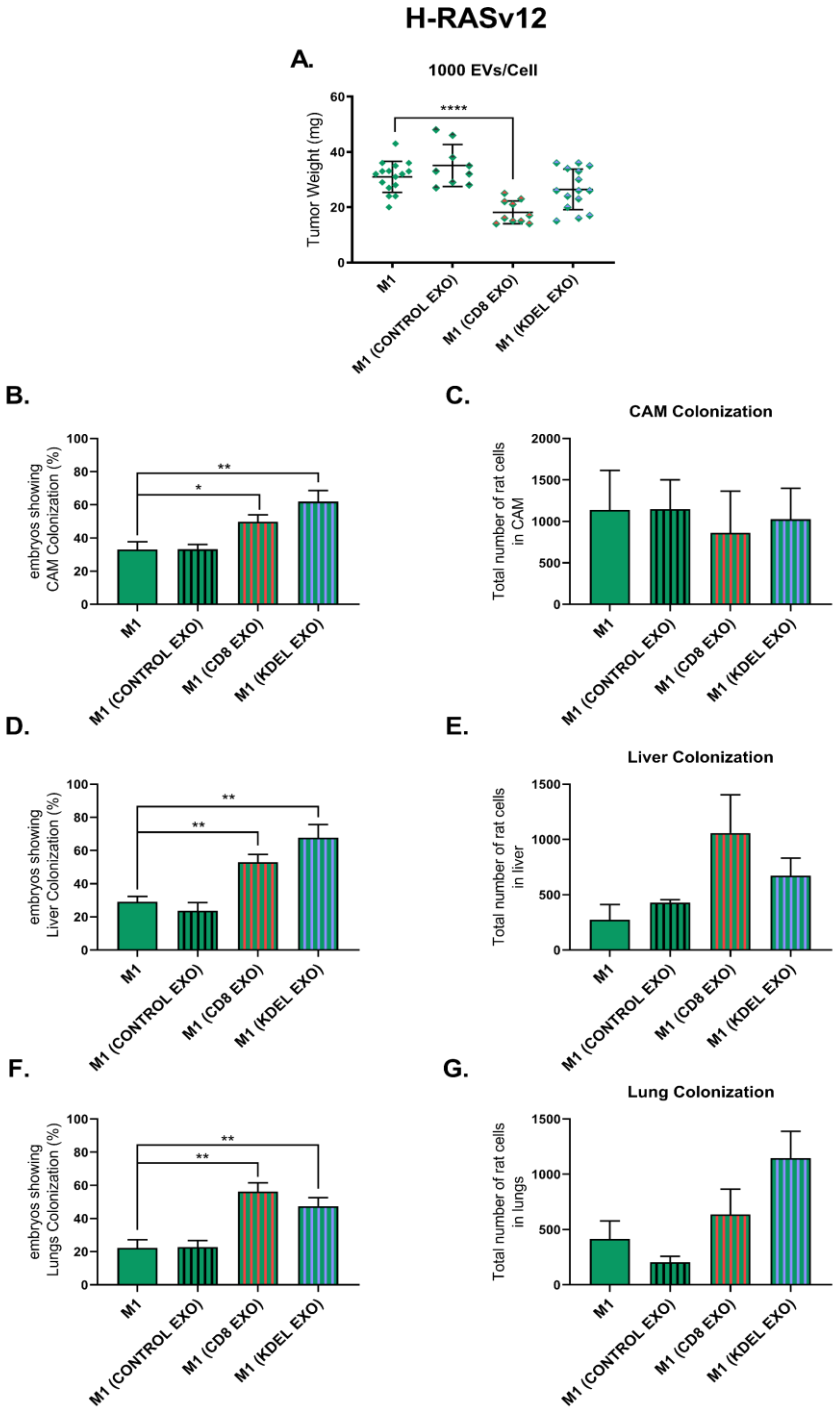

Figure 4.30: Effects of heterologous EVs on the oncogenic potential of cells with H-RASv12 at ER. $1x10^6$ cells expressing H-RASv12 at ER (M1) were incubated with EVs secreted by PCCL3 cells (fractions 3-5 and 6-8 mixed) parental or expressing H-RAS at DM (CD8) or GC (KDEL) and were grafted on 10-days chick embryos. Seven days after, the primary tumors were collected and weighed (mg) **(A)** and the distal portions of the CAM were analyzed by qPCR showing the % of embryos that underwent spontaneous intravasation (distal CAM colonization) **(B)**, liver **(D)** and lung colonization **(F)** allowing us to determine the relative numbers of rat cells per 10^6 chicken cells in CAM **(C)**, liver **(C)** or lungs **(E)**. Error bars shows (Mean ± SD) in **(A)** and in the rest (MEAN ± SEM). Data is from three independent experiments employing from 7 to 12 embryos per cell variant. Statistical significance was determined using a double tailed unpaired student T-test. *p<0.05, **p<0.01, ***p<0.001 and ****p<0.0001.

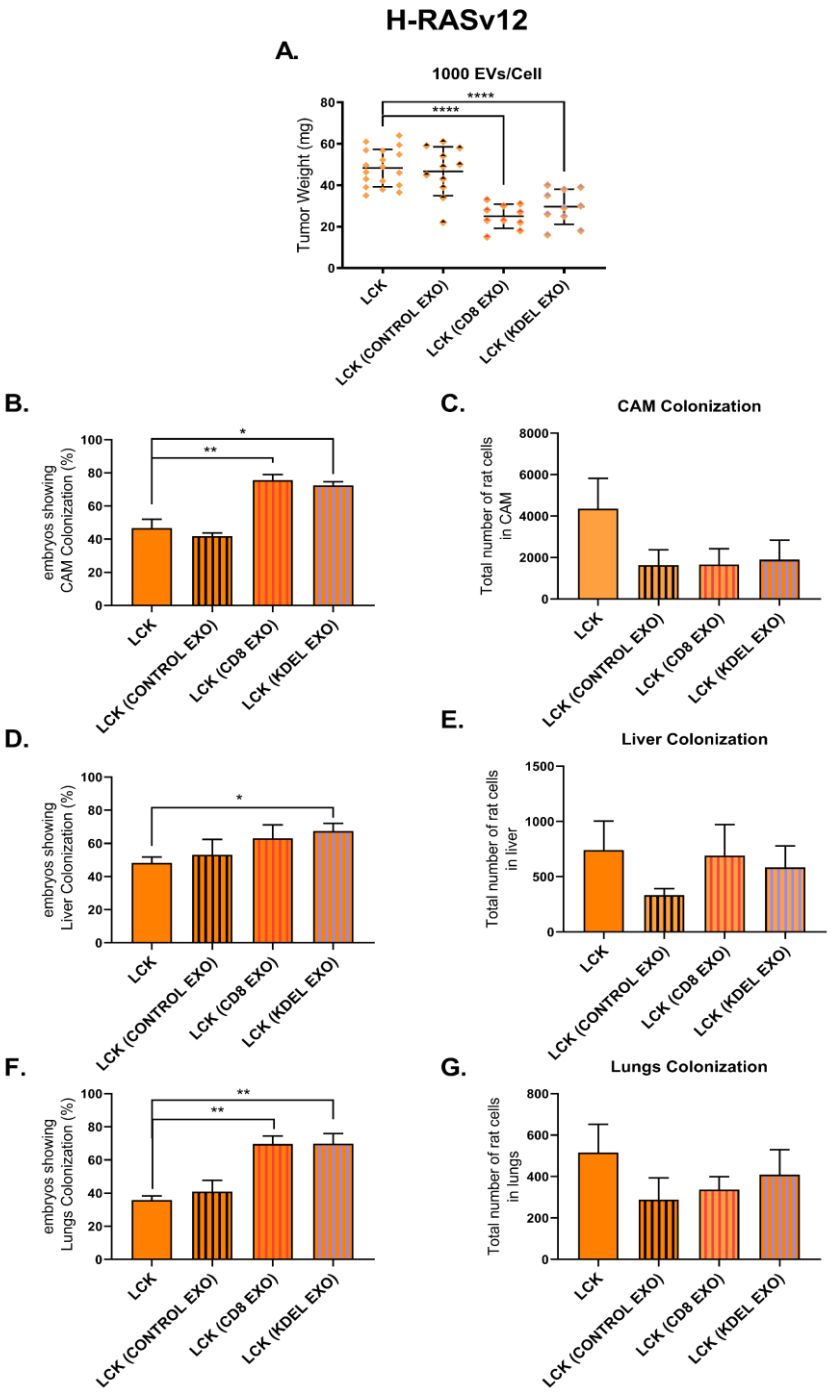

Figure 4.31: Effects of heterologous EVs on the oncogenic potential of cells with H-RASv12 at LR. $1x10^6$ cells expressing H-RASv12 at LR (LCK) were incubated with EVs secreted by PCCL3 cells (fractions 3-5 and 6-8 mixed) parental or expressing H-RAS at DM (CD8) or GC (KDEL) and were grafted on 10-days chick embryos. Seven days after, the primary tumors were collected and weighed (mg) **(A)** and the distal portions of the CAM were analyzed by qPCR showing the % of embryos that underwent spontaneous intravasation (distal CAM colonization) **(B)**, liver colonization **(D)** and lung colonization **(F)** allowing us to determine the relative numbers of rat cells per 10^6 chicken cells in CAM **(C)**, liver **(C)** or lungs **(E)**. Error bars shows (Mean ± SD) in **(A)** and in the rest (MEAN ± SEM). Data is from three independent experiments employing from 7 to 12 embryos per cell variant. Statistical significance was determined using a double tailed unpaired student T-test. *p<0.05, **p<0.01, ***p<0.001 and ****p<0.0001.

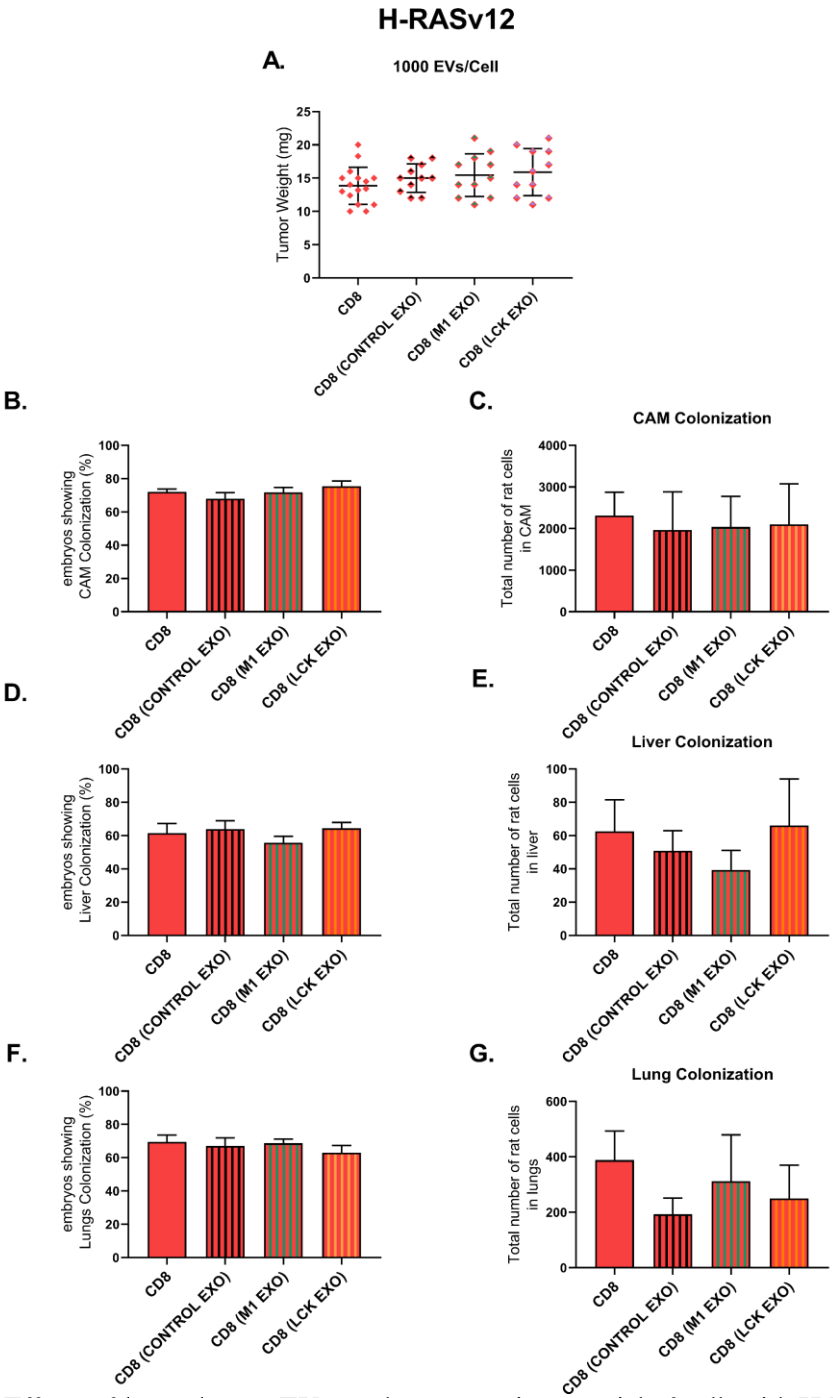

Figure 4.32: Effects of heterologous EVs on the oncogenic potential of cells with H-RASv12 at DM. 1x10^6 cells expressing H-RASv12 at DM (CD) were incubated with EVs secreted by PCCL3 cells (fractions 3-5 and 6-8 mixed) parental or expressing H-RAS at ER (M1) or LR (LCK) and were grafted on 10-days chick embryos. Seven days after, the primary tumors were collected and weighed (mg) **(A)** and the distal portions of the CAM were analyzed by qPCR showing the % of embryos that underwent spontaneous intravasation (distal CAM colonization) **(B)**, liver colonization **(D)** and lung colonization **(F)** allowing us to determine the relative numbers of rat cells per 10^6 chicken cells in CAM **(C),** liver **(C)** or lungs **(E)**. Error bars shows (Mean ± SD) in **(A)** and in the rest (MEAN ± SEM). Data is from three independent experiments employing from 7 to 12 embryos per cell variant. Statistical significance was determined using a double tailed unpaired student T-test. *p<0.05, **p<0.01, ***p<0.001 and ****p<0.0001.

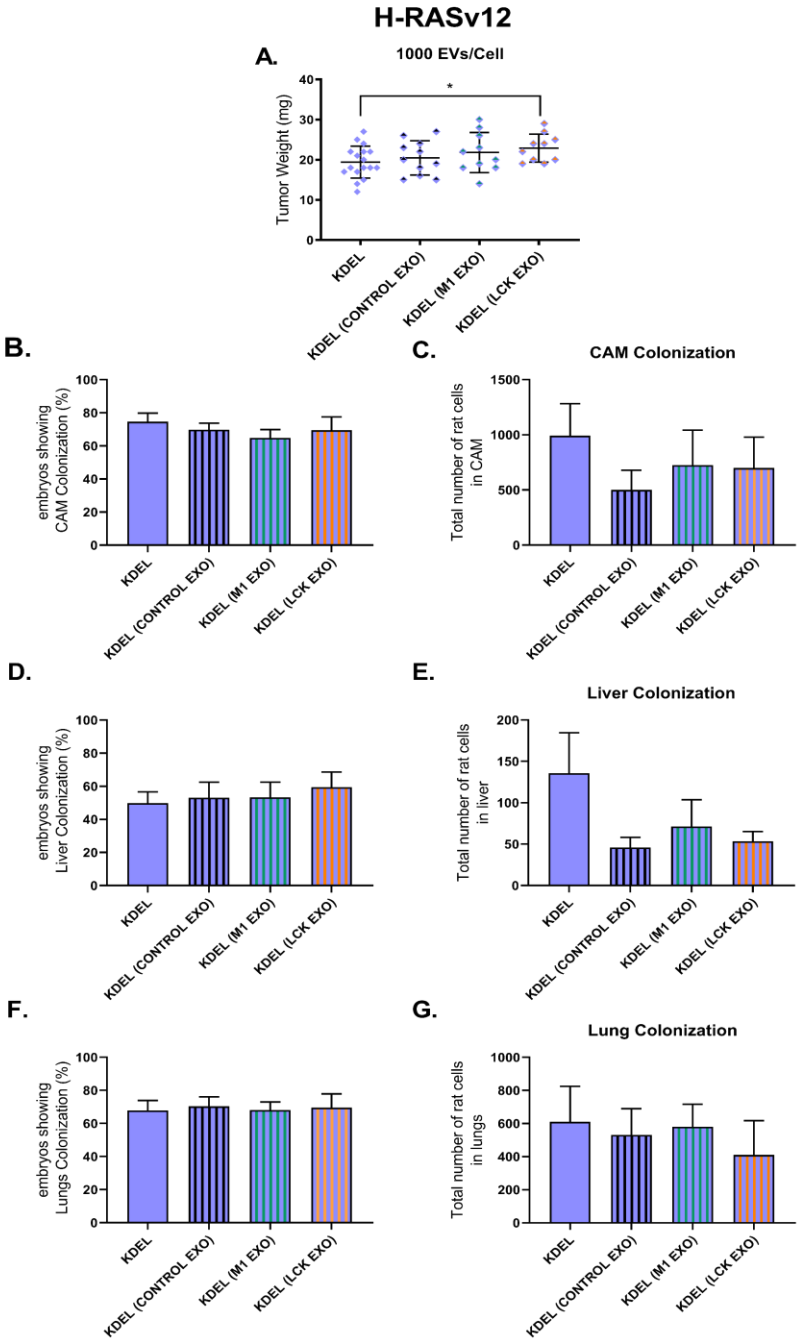

Figure 4.33: Effects of heterologous EVs on the oncogenic potential of cells with H-RASv12 at the GC. $1x10^6$ cells expressing H-RASv12 at the GC (KDEL) were incubated with EVs secreted by PCCL3 cells (fractions 3-5 and 6-8 mixed) parental or expressing H-RAS at ER (M1) or LR (LCK) and were grafted on 10-days chick embryos. Seven days after, the primary tumors were collected and weighed (mg) **(A)** and the distal portions of the CAM were analyzed by qPCR showing the % of embryos that underwent spontaneous intravasation (distal CAM colonization) **(B)**, liver colonization **(D)** and lung colonization **(F)** allowing us to determine the relative numbers of rat cells per 10^6 chicken cells in CAM **(C),** liver **(C)** or lungs **(E)**. Error bars shows (Mean ± SD) in **(A)** and in the rest (MEAN ± SEM). Data is from three independent experiments employing from 7 to 12 embryos per cell variant. Statistical significance was determined using a double tailed unpaired student T-test. *p<0.05, **p<0.01, ***p<0.001 and ****p<0.0001.

5. Discussion

5. DISCUSSION:

More than 50 years have passed since the first RAS protein was discovered but yet, our knowledge on RAS signaling and its role in tumorigenesis is still not fully understood. Today we know that RAS is not exclusively in the inner leaflet of the plasma membrane, where it is present at LR and DM, but it is also present and functional at different subcellular localizations, as in ER and GC, contrasting the initial idea of a single source of RAS signals (101, 104, 325). However, little is known about how RAS sublocalization affects its oncogenic potential. It is well known that *RAS* mutations are found in many human cancers and that thyroid cancer is one of them. For instance, 26% of papillary thyroid carcinoma harbor RAS mutations, follicular thyroid carcinoma around 40% and anaplastic carcinoma about 53% (252). *RAS* mutations also occur in 20–25 % of benign Follicular Thyroid Adenoma (FTA).

However, although in the last decade considerable effort has been made to correlate *RAS* mutations to the clinical management of thyroid nodules and thyroid cancer, most *RAS*-positive thyroid nodules are classified, using the Bethesda system, as indeterminate (326). Moreover, due to RAS uncertain role in the clinical outcome of thyroid cancer, it has been unclear how to appropriately use RAS status to assist the management of thyroid tumors. In consequence, new markers are needed to rule out RAS-positive thyroid nodule malignancy and to predict thyroid cancer aggressiveness and risk for local and distant invasion, since new thyroid cancer guidelines are heading to more conservative approaches.

We therefore hypothesized that the different behavior of thyroid tumors, harboring *RAS* mutations, are related to RAS differential sublocalization in the cell, where it can modulate different proteins and genetic programs. In consequence, the aims of this thesis were to study if RAS sublocalizations modulate RAS oncogenic potential in thyroid cancer and to find new related markers to identify high risk thyroid nodules and cancers.

5.1 Role of RAS sublocalizations in thyroid tumorigenesis

Recently, our group casted some light for the first time *in vivo* on RAS sublocalization-dependent oncogenic effects, demonstrating that RAS at the GC antagonize melanoma formation (121). Moreover, we determined that RAS signals emanating from the GC, and specifically from the cis-Golgi, can induce a potent apoptotic response, endorsing other recent findings that showed GC RAS signals antagonizing proliferation and differentiation (121) (305). However, this was only assessed in one experimental model and in a specific cancer type, melanoma, which makes it risky to extrapolate to other types of cancer.

We generated PCCL3 rat thyroid follicular cell lines stably expressing the three RASv12 isoforms in the different subcellular locations using vectors harboring targeting signals to direct them to ER, LR, DM or GC.

Using these cell lines, we investigated different *in vitro* parameters such as proliferation, apoptosis and migration. A number of important observations were noticed: i) Neither of the RAS isoforms induce PCCL3 cells proliferation, but H-RAS signals from DM and GC slightly decrease it, ii) all H-RAS, N-RAS and K-RAS sublocalizations promote to some extent apoptosis, particularly signals from the GC, iii) H-RAS signals from DM and GC are the most competent for inducing migration.

Therefore, we posit that H-RAS in DM and GC is able to reduce proliferation rates and that H-RAS signals from LRs or ER do not induce proliferation. This could be due to RAS inducing apoptosis. It might be also explained due to a possible need for other type of cells in order to regulate proliferation cues. For instance, it has been seen that oncogenic K-RAS regulates tumor cell signaling via stromal cells dramatically changing tumor cell phosphoproteome resulting in increased cell proliferation and survival (327).

In agreement with our findings regarding RAS inducing apoptosis, other authors have shown that H-RASv12 can induce programmed cell death in PCCL3 *p53* wild-type cells through genome destabilization associated with the disruption of critical cell cycle checkpoints (308).

We also monitored the oncogenic potential of H-RAS, N-RAS and K-RAS sublocalizations *in vivo* using the chick embryo spontaneous metastasis model. Interestingly, our study shows for the first time that, irrespective of its localization, H- and N-RASv12 signals have the same effects in growth and metastasis of thyroid tumor cells. Strikingly, when RAS signals come from DM and the GC they generate smaller tumors, compared to RAS in LRs and ER, but with higher rates of intravasation and distant organ colonization, mostly lungs. However, K-RAS, that is only present in DM and ER, exhibits similar rates of tumor growth at both sublocalizations, although signals from DM were more effective for inducing lung metastasis.

In addition, we demonstrated that DM H-RASv12 signals induce increased nucleolar size and condensation, a feature that has been recognized as a hallmark in a large number of tumor types (322, 328, 329). Also, cells with H-RAS at DM present a tremendous amount of free polyribosomes, that could be a consequence of by RAS induced modification of the nucleolar size. Conversely, data pointing to increased proliferation in cells with bigger nucleoli due to an increment in ribosome synthesis (330, 331), contradict our findings. However, since the nucleolus has recently been assigned a fundamental role in other processes, essential for tumoral cells, such as telomere function, regulation of cell-cycle progression, genome stability or biogenesis of multiple ribonucleoprotein particles (322, 329, 330), it is reasonable to speculate that nucleoli modified by RAS at DM could be relevant for its tumorigenic effects. Therefore, further work needs to be done in this respect to try to unravel how RAS at DM affects nucleoli and what are the consequences.

Intriguingly, our GC results contradict previous findings from our group where it was demonstrated that RAS at the GC antagonizes melanoma progression via induction of PTPRκ that downregulates ERK activity (121). However, when PTPRκ was not present or was present

together with *tp53* mutations, this led to a partial or total rescue of GC RAS transforming potential (121). In consequence, PTPRκ expression and *tp53* status should be investigated in PCCL3. Moreover, PCCL3 cells that have H-RAS in GC exhibit a shocking high amount of mitosis and some necrotic and apoptotic cells. This suggests that GC RAS signals might induce high rates of mitotic catastrophe in our model. Mitotic catastrophe is a regulated antiproliferative process that occurs during defective or failed mitosis. It works by detecting and removing mitotically defective cells to prevent of H-RAS-induced genome instability (332-334). Therefore, mitotic catastrophe could explain, at least in part, GC H-RAS reduced levels of cell proliferation and small tumor size, together with the induction of apoptosis.

For the first time, as far as we know, we have demonstrated in the chick embryo model that GC RAS signals promote thyroid cell metastasis in lungs. However, little is known about how GC RAS could be evoking this effect. Some groups have shown the GC as a key regulator of directional cell migration and invasion (335, 336). Particularly, one study by Bisel and colleagues who showed that ERK activation from the GC, directly phosphorylates the Golgi matrix protein GRASP65, a promigratory signaling event (337). Moreover, previous results from our group demonstrated an increased JNK and RALGDS signals when RAS was present at the GC (110, 338). There are several studies pointing JNK being fundamental for cell migration and invasion (339) in different human cancer cells as pancreatic or gastric (90, 340, 341). In consequence, JNK and RALGDS signaling pathway assessment is necessary and the use of specific inhibitors could give an insight into the role of this pathways in GC mediated thyroid tumorigenesis.

Intriguingly, our results have pointed out that small H- and N-RAS positive tumors, which arise when RAS is present at DM or the GC, are the most invasive and metastatic ones, whereas bigger tumors, which have mutant RAS at LR or ER, shown little or no invasion and metastasis.

This shocking and newfangled results suggest: i) a possible explanation for RAS variable behavior in human thyroid nodules and cancers, based on its sublocalizations, ii) that small thyroid nodules or cancers could be the most metastatic ones, which makes urgent the need for specific markers to predict how RAS-positive thyroid tumors are likely to evolve.

In order to ascertain this last proposal, we analyzed oncogenic H-RAS locations in human anaplastic thyroid cell lines C643 and HTH83 both of which harbor mutant H-RAS. We demonstrate that C643 cells have mutant H-RAS mainly in LRs whereas HTH83 at DM. This differential H-RAS subcellular location is fundamental for their tumorigenic potential. Indeed, HTH83 cells show smaller tumors compared to C643 cells, but promote a more invasive phenotype leading to higher rates of metastasis. Furthermore, they endorse to a large extend to our results with PCCL3 cells expressing H-RAS site-specific constructs, though not completely. For instance, in C643, H-RAS signals from LRs promote higher rates of metastasis than our H-RASv12-LCK construct and H-RAS signals from DM in HTH83 cells

promote bigger tumors than our PCCL3 cells with H-RASv12-CD8. This could be explained by the burden of mutations that these cells contain. For instance, both C643 and HTH83 have mutations in the telomerase reverse transcriptase *TERT* gene promoter. That creates binding sites for E-Twenty-Six (ETS) transcription factors, promoting TERT transcriptional activity resulting in increased telomerase activities. Interestingly, some ETS factors are targets of ERK(342-344), which suggest that *TERT* modulation by H-RAS might be crucial to reduce apoptosis, conferring them a unique survival advantage (345). Moreover, *TERT* promotes cell adhesion and migration, independently of telomerase activity (346) which can to some extend explain C643 higher rates of distant colonization when compared to H-RASv12-LCK expressing PCCL3 cells. In addition, C643 cells are mutated in *p53* which avoids H-RAS induced apoptosis in PCCL3 thyroid cells (291, 306, 307). Furthermore, it is now known that mutant p53 proteins provoke activities that are different to those resulting from the simple loss of wild-type tumor-suppressing p53 function. Many of this newly unveiled functions enable tumor cells to survive, proliferate, invade adjacent tissues and metastasize, which could explain, for instance, HTH83 tumor size (347). Therefore, additional mutations might give C643 and HTH83 cells an advantage compare to our PCCL3 transfected cell lines, that do not harbor any mutations besides the expression of the different RAS constructs.

5.2 APT-1 levels modify thyroid tumoral cells behavior

Due to our results we propose that H-RAS location in different plasma membrane microdomains, a process in part controlled by APT-1, is also of primary importance in anaplastic cells tumorigenesis, as H-RAS lateral diffusion after APT-1 ablation or overexpression modifies tumor growth and distant organ colonization. Moreover, it will be interesting to investigate H-RAS localization at ER and GC in C643 cells and HTH83, since they could be also collaborating in their oncogenicity.

Overall our data suggests that i) small RAS-positive tumors can be highly metastatic, ii) H-RAS subcellular location plays a fundamental role in growth and metastasis iii) APT-1 overexpression is linked to H-RAS location in LRs and recapitulates H-RASv12-LCK effects in PCCL3 cells in the chick embryo metastasis model; and that iiii) APT-1 ablation translocates H-RAS from LRs to DM and APT-1 overexpression leads to H-RAS lateral diffusion from DM to LRs, completely changing cell behavior in tumor formation, cellular intravasation and distal organ colonization.

When we looked for APT-1 alterations in databases of thyroid tumors we found that this protein was mutated only in 0,2% of the 507 samples of papillary thyroid carcinomas(302). However, it displayed had alterations both in DNA, including amplifications, gains, shallow deletions and deep deletions; and in mRNA levels, high and low, in 7% of the cases. When we analyzed survival in samples with alterations that lead to an overexpression in APT-1 (22 cases) we observed 100% survival. When we looked at survival in samples with alterations that

lead to a decrease in APT-1, we did not see changes. However, the low amount of samples, only 5, that showed these alterations preclude us from making any assumptions. Surprinsingly, APT-1 alterations did not co-occurred with H-RAS alterations although they did at some extent with N-RAS suggesting that other depalmytoilases or palmytoilases could be involved in H-RAS and N-RAS, location at its different subcellular locations in thyroid cells, thus affecting its oncogenic potential. We propose that APT-1 even by regulating *wild type* RAS location, could be affecting tumor cells behavior. For instance, we have looked at another tumor type, melanoma, that harbors more alterations in APT-1 in order to get a clearer picture. Indeed, in cBioPortal database of 479 clinical samples we found that APT-1 was amplified in 2.7% of the melanoma cases. When we looked for samples presenting high mRNA levels, gains and amplifications of APT-1 we found that 39% of the samples showed these alterations **(Fig. 5.1)**. We also looked for samples presenting low mRNA levels, shallow and deep deletions of APT-1 and we found that 11% of the samples presented them **(Fig. 5.2)**. We also cheeked for co-occurrences with H-RAS and N-RAS mutations and we saw that almost half of the cases showing H-RAS mutations co-occurred with APT-1 altered mRNA expression. The same was observed for N-RAS **(Fig. 5.3)**.

We then looked for estimate survival and we found that patients exhibiting amplifications, gains or an increase in APT-1 mRNA levels, which, presumably promote the presence of RAS at LR, have a greater overall survival, around 11 months, compare to patients that did not have APT-1 alterations **(Fig. 5.4 A)**. When we looked for the estimate survival of patients showing deletions or low mRNA levels of APT-1 we found that they have a lower overall survival, around 15 months compare to a group without these alterations **(Fig. 5.4 A)**.

Figure 5.1: APT-1 (LYPLA1) gains, amplifications and high mRNA expression levels in skin cutaneous melanoma. Data is been extracted from "cBioPortal for cancer genomics" using a database of 479 samples of skin cutaneous melanoma (TCGA).

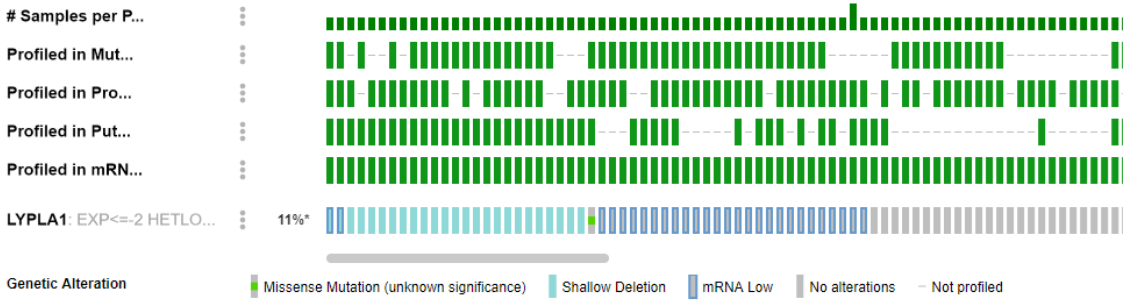

Figure 5.2: APT-1 (LYPLA1) deletions, shallow deletions and low mRNA expression levels in skin cutaneous melanoma. Data is been extracted from "cBioPortal for cancer genomics" using a database of 479 samples of skin cutaneous melanoma (TCGA).

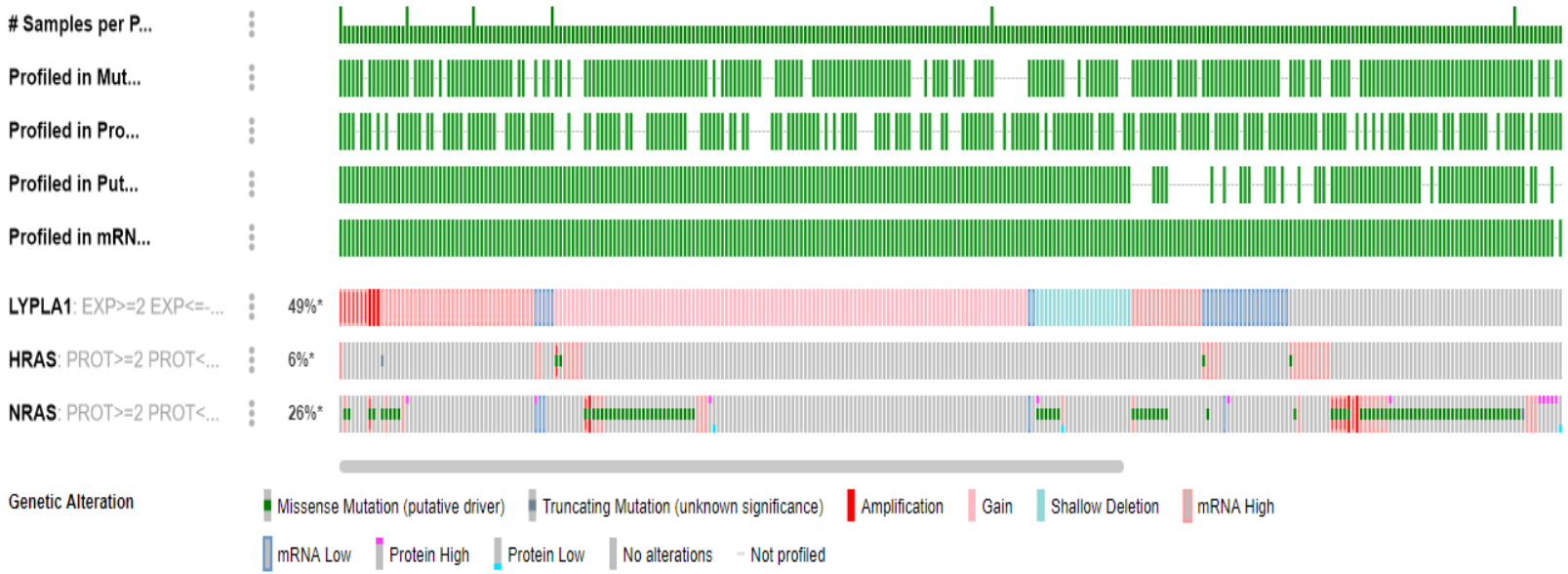

Figure 5.3: APT-1 (LYPLA1), H-RAS and N-RAS mutations, amplifications, gains, deletions and mRNA expression. Data is been extracted from "cBioPortal for cancer genomics" using a database of 479 samples of skin cutaneous melanom (TCGA).

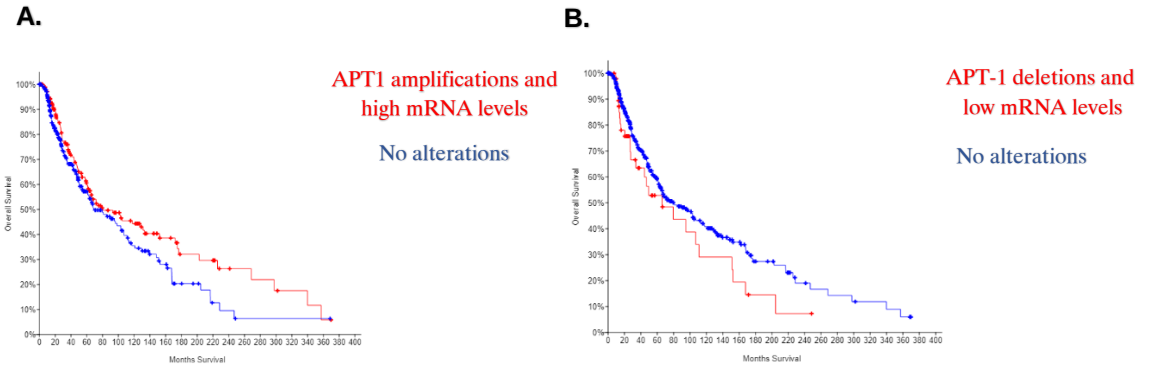

Figure 5.4: Overall survival Kaplan-Meier Estimate. Using data extracted from "cBioPortal for cancer genomics" using a cohort of 479 samples of skin cutaneous melanoma (TCGA) we selected the samples with APT-1 overexpression, amplification and gains (22 samples) and checked for overall survival **(A)** or the samples with low levels of APT-1 mRNA or deletions (6 samples) and checked again for overall survival **(B).**

This data suggests that APT-1 might be crucial for RAS effects by affecting its subcellular location, reinforcing our findings. One explanation for our lack of alterations in APT-1 in thyroid cancer might be that the available database includes only papillary carcinomas and not other types, such as follicular thyroid carcinomas or anaplastic carcinomas, which harbor more RAS mutations. But no mRNA data was available for these tumors. Therefore, we can not conclude that APT-1 is not crucial for RAS driven thyroid tumorigenesis. In addition, we can speculate that APT-1 might also be to some extent modifying tumor behavior by altering wild type RAS subcellular location.

However, APT-1 also has other substrates so we cannot solely attribute the consequences of its alterations to RAS segregation at plasma-membrane microdomains. Nevertheless, it is reasonable to speculate that APT-1 immunohistochemical assessment in FNA samples from RAS positive thyroid nodules might be a potential new marker to better rule out malignancy and risk of locoregional recurrence and distal metastasis. Moreover, it could also be used in other cancers as such as melanoma although more research in this respect is needed.

New American Thyroid Association guidelines controversially recommends not to study nodules <1cm and advice for a partial thyroidectomy in RAS-positive papillary and follicular tumors between 1-4 cm (348). In spite that partial thyroidectomy has been chosen to avoid surgery complications and a life time of hormone supplementations, it worryingly alters the correct follow-up of these patients, which might lead to late diagnosis of locoregional or distant metastasis that otherwise would have been found earlier. However, although, these recommendations have been done due to little changes in overall survival (36), our results suggest that small H- and N-RAS-positive thyroid nodules and cancers could benefit from a total thyroidectomy and closer follow-up. Although it is necessary to work with clinical samples, we suggest that small thyroid nodules could benefit from FNA RAS status analysis. Moreover, we think that until good markers are found, RAS positive thyroid nodules should

not be limited to a partial thyroidectomy as the new 2015 ATA guidelines advice, and that the previous management, that was total thyroidectomy, should be recommended for the possible risks that small H- and N-RAS-positive thyroid nodules have to be cancerous and to metastasize.

5.3 Endomembrane H-RAS signals promote MLB formation

Our results show that cells that present H-RAS active in endomembranes, ER or GC, present a high amount of MLBs. Multilamellar bodies (MLBs) are membrane-bound cellular organelles of lysosomal nature, which vary in size from 100-2400 nm, they are composed of concentric membrane layers, and frequently exhibit an electron-dense core. MLBs are found in numerous cell types, where they participate in lipid storage and secretion (349). Besides, lamellar bodies provide lipids and proteins to form the skin barrier (350). MLBs are also associated with various lysosomal storage diseases such as Fabry´s or Niemman-Pick syndromes, due to deficiencies in various lysosomal degradative enzymes and aberrant lysosomal accumulation of lipids. Multilamellar bodies can be formed from the Golgi Complex (320, 351, 352) or from endoplasmic reticulum (353) although their main way of formation is via autophagy (320). Our results lead us to speculate that H-RAS signals from endomembranes might alter lipid metabolism. leading to their accumulation in lysosomes and giving rise to MLBs. Long term culture of A549 a non-small cell lung cancer cell line, known to be K-RAS mutant, promote MLBs formation (354). We could speculate this is a consequence of mutant K-RAS presence at the ER. Therefore, further work needs to be done in order to relate endomembrane H-RAS signals to lipid disfunction and MLBs formation.

5.4 VEGF-B implications in H-RAS mediated tumorigenesis

Vascular endothelial growth factor B (VEGF-B) controls lipid accumulation in tissues by stimulating fatty acid transport through endothelial cells (137). Given that our frozen sections analysis demonstrates higher levels of fatty acids storages in H-RAS-M1 and H-RAS-LCK evoke tumors we studied the expression of VEGF-B as induced by the different H-RASv12 subcellular locations and its role in tumor growth and metastasis. To date, there are no data with regards to the expression of VEGF-B in thyroid cancer. In the chick embryo model, we found that VEGF-B was highly expressed in cells harboring H-RASv12-M1 and H-RASv12-LCK but not those with H-RASv12-CD8 or H-RASv12-KDEL. In agreement with these results C643 cells, that has H-RAS at LR, presented significantly higher levels of VEGF-B when compare to HTH83 cells with H-RAS at DM. Therefore, it was tempting to speculate that RAS sublocalizations may regulate VEGF-B secretion leading to fatty acids uptake and storage in thyroid cells tumors. Although VEGF-B over expression has been detected in a wide variety of tumors such as breast carcinoma, melanoma (139, 355), colorectal cancer (356),

oral squamous cell carcinomas (357), little is known about its implications. We observed that VEGF-B addition to H-RASv12-CD8 and H-RASv12-KDEL expressing cells, *in vivo*, using the chick embryo metastasis model, increased tumor weight but decreased cell intravasation and lungs colonization. VEGF-B does not induce angiogenesis (126, 134, 135) but it is capable of antagonizing VEGF-A-induced abnormal formation of leaky and permeable vessels (136). Therefore, since H-RAS signals in DM and GC induce high levels of VEGF-A we propose that VEGF-B might be stabilizing abnormal vessel formation, which would lead to organized, stable intra-tumoral vessels, showing less leakage and permeability, leading to high availability of nutrients, increasing cell growth and hindering cell intravasation that, in consequence, decreases metastasis.

Only a few papers have addressed VEGF-B implications in cancer (139, 140, 355, 356) and none of them are in thyroid cancer. Studies using transgenic expression of VEGF-B in the RIP1-Tag2 mouse model of pancreatic neuroendocrine tumorigenesis retarded tumor growth (358). Moreover, another study has observed that colorectal tumors expressing high levels of VEGF-B were more metastatic, although primary tumors growth was largely impaired (356). Similarly, VEGF-B in a VEGF-A–null colorectal tumor resulted in attenuated primary tumor growth but substantial pulmonary metastases (139). Our results show the opposite for thyroid cancer so we can speculate that it is something tissue dependent, although more research is needed in this topic. Moreover, we should use a specific VEGF-B siRNA or shRNA to determine if its knockdown can increase metastasis.

Since VEGF-B is upregulated in the less metastatic tumors we think that its immunohistochemical analysis, together with APT-1, should be assessed in human thyroid cancer samples in order to try to correlate their overexpression with tumor aggressiveness. If confirmed, they could be included in RAS positive thyroid nodules assessment to better stratify and manage patients.

5.5 RAS sublocalizations implications in exosome secretion and its effects

Exosomes are spherical to cup-shaped nanovesicles between 40-100 nm of endocytic origin, that are secreted by many cells including cancer cells. Indeed, H-RAS and K-RAS mutations in kidney cells or colon cancer cells alter exosomes cargo compared to *wt* cells, augmenting invasiveness (183, 186). Furthermore, mutant H-RAS genomic DNA is present in exosomes, relating to higher rates of invasion (177-179). But the most intriguing finding has been RAS co-precipitation with ESCRT-associated proteins ALIX and VSP4A, implicated in exosomes biogenesis, in glioblastoma EVs (181). Although further work needs to be done in that respect, these findings also relate RAS with EVs biogenesis. In consequence, we wanted to explore if RAS subcellular locations affected EV secretion.

Exosome biogenesis starts within the endosomal system; early endosomes mature into late endosomes or multivesicular bodies (MVBs) where intraluminal vesicles ILVs are formed through endosomal membrane invagination (152, 359). To first try to address exosome presence in our different RAS cell lines we looked for MVBs using transmission electron microscopy, which is the only technique that allows to visualize them. Our results show that all PCCL3 cells, parental and transfected with HRASv12 tethered to the different subcellular locations, present MVBs, which suggested that these cells secrete exosomes. However, some MVBs never reach the plasma membrane and are recycled into lysosomes (324). In consequence, exosome isolation by stablished methods such ultracentrifugation or size exclusion chromatography, was necessary to indirectly determine whether our MVBs fused to the membrane and released exosomes.

ESCRT machinery is important in exosome biogenesis. ESCRT consist of four different protein complexes; ESCRT-0, -I, -II, -III and the associated proteins (VPS4, VTA1, ALIX) (152, 359). Some are widely used exosome markers, such as ALIX that can bind SYNTENIN and TSG-101, an ESCRT-I member, among others. Moreover, although not ESCRT related the presence of at least one tetraspanins, such as CD63, CD9 or CD81, is fundamental to define vesicles as exosomes. In our study we checked for these markers in order to confirm exosome secretion. Our results indicate that all cells lines including PCCL3 parental cells secrete exosomes since all, markers, ALIX, TSG-101, SYNTENIN and CD-63, are present. However, some differences between the different cell lines were seen. Parental cells and H-RASv12-M1- and H-RASv12-LCK-expressing cells, which are the less metastatic, showed higher levels of ALIX but lower levels of SYNTENIN and TSG-101, compared to H-RASv12-CD8 and H-RASv12-KDEL expressing cells. It is thus reasonable to speculate that RAS sublocalizations generate heterogeneous exosomes subpopulations. Indeed, the ESCRT biogenesis pathway is not the only one involved in exosome biogenesis since simultaneously silencing of key subunits of all four ESCRT-complexes, ILVs are still formed in MVBs (360). In consequence, it might be possible that H-RAS could be triggering at distinct exosome biogenesis pathways depending on its sublocalization. Interestingly, it has been described that ALIX silencing alters exosome protein composition without affecting their secretion (361). Therefore, one hypothesis that can derived from our last observation is that in H-RASv12-CD8 and H-RASv12-KDEL expressing cells downregulation of ALIX could be affecting their cargo, generating different exosome populations. Therefore, we find of crucial interest to perform transcriptomic and proteomics analysis of the different exosomes in the future in order to confirm it.

TSG-101, although being a ubiquitously-expressed exosome marker, is found at different concentrations among different prostate and breast cancer cell lines EVs, suggesting that that EVs biogenesis, or protein sorting mechanisms, may be different among those cell lines (362). Moreover, since TSG101 depletion reduces exosome secretion (152) we looked at exosome concentration using Nanoparticle Tracking analysis, that also analyzed their size. Our

results match these previous affirmations. Cells with H-RAS at ER and LR, that have lower levels of TSG101, manifest lower exosome secretion. Conversely, PCCL3 cells and H-RASv12-CD8- and H-RAS-KDEL-expressing cells, which presents higher levels of TSG-101, showed higher exosome levels. Again, we can speculate that RAS sublocalizations could be either triggering different exosome biogenesis pathways or/and modifying exosome cargo. To assess so in the future, we could inhibit different biogenesis pathways such as the ESCRT one, and analyze their effects in exosomes. Furthermore, these results again reinforce the urgent need to analyze exosome cargo mainly by transcriptomics and proteomics.miRNA, small non-coding RNA and ribosomal RNA, content could also be investigated as well as lipid composition by lipidomics.

When we looked at the size of the exosome peak EVs (fractions 3-5), we saw that H-RASv12-CD8 and H-RASv12-KDEL expressing cells derived EVs are bigger. This can suggest that we could be having a higher amount of microvesicles in these sets, or that they showed more protein aggregates since Nanoparticle Tracking analysis is not able to distinguish between exosomes, microvesicles or protein aggregates.

Extracellular vesicles are key mediators in cell to cell colonization and have been shown to enhance tumor growth, angiogenesis, immune cell responses, survival, cell migration and invasion (318, 363, 364). To check whether exosomes could modify proliferation or tumor growth in our cells, we tested if EVs isolated form the different RAS-expressing cell lines could alter tumor behavior. Our studies show that DM and GC H-RAS-derived EVs reduce proliferation of cells with H-RAS at ER and LR *in vitro* and tumor growth *in vivo*. However, other cells EVs did not promote proliferation of cells with H-RAS at DM or LR. These findings contradict previous studies pointing EVs to be major tumor enhancers (365). However, little has been done in thyroid cancer in this respect and most findings have only associated thyroid-derived EVs as potent inductors of Epithelial-Mesenchymal Transition (EMT) (319, 366). Indeed, one study has shown that exosomes derived form a papillary thyroid carcinoma cell line, after Transforming Growth factor (TGF) -β1 treatment, transferred to other cells long non coding RNAs with some EMT transcriptional factors such as SLUG or SOX2 (319, 366).

In other cancer types it has been shown that tumor derived exosomes (TDEs) can provide autocrine and paracrine signals programming cancer cells to invade surrounding stromal tissue, to allow intravasation and to enter the circulation (367-370). Moreover, TDEs can educate non-cancer cells in distant organs by metabolic reprogramming, recruiting immune cells and other stromal cells stablishing a supportive microenvironment, also known as metastatic niche formation, that facilitates tumor cell arrest, extravasation and later colonization (364, 371). In consequence, tumor cells organotropism is also shaped by TDEs. For example, EVs from pancreatic ductal adenocarcinoma cells can create an ideal fibrotic liver pre-metastatic niche by transferring Migration Inhibitory Factor (MIF) to Kupffer cells in the liver (170) (372). Another study showed that highly metastatic melanoma cells release

EVs, which increased vascular leakiness and enhanced metastasis of melanoma cells orthotopically injected into mice (373).

To check whether exosomes from the most aggressive H-RAS sublocalization (DM and GC) transferred their ability to colonize lungs to cells wit H-RAS at LR and ER we incubated the corresponding EVs with cells harboring site-specific H-RAS with low metastatic potential. We found that EVs isolated from the most metastatic cells can induce lung colonization of previously low metastatic cells. However, EVs derived from the less metastatic cells could not stop GC or DM H-RAS signals to promote lung colonization, suggesting that EVs derived from LR and ER RAS-expressing cells are not the responsible for these cells inability to colonize distant organs. It is then reasonable to propose that H-RASv12-CD8 or H-RASv12-KDEL expressing cells-derived EVs could be capable of modulating organotropism and shaping of the pre-metastatic niche. In this regard, as EVs in lung can be uptaken by either endothelial cells or fibroblasts (374, 375) new investigations are needed to fully confirm their uptake and its consequences.

Additionally, although mutant K-RAS can be transferred via exosomes in a colon cancer model (186), our model cannot assess RAS transference to other cells since our constructs do not recapitulate physiological conditions. Therefore, we cannot affirm either that thyroid cell exosomes will be able to introduce mutant H-RAS into their EVs or that this possible situation will lead to increase tumor and/or normal cells proliferation.

Besides EVs favoring pre-metastatic niche formation, EVs have also been linked to cancer cells organotropism. It has been shown that priming a mouse with EVs derived from a specific cancer cell line that normally metastasizes to the lungs, can redirect a bone-metastasizing cell to the lungs (171). It has been suggested that integrins were responsible for specific organ colonization. Integrin α6 was linked to lung metastasis, whereas integrins αv and β5 were implicated in liver metastasis (152, 171). For instance, Integrin α 6 shows a 73.3 % homology between *Rattus Norvegicus* and *Gallus Gallus* using BLAST analysis. Although these differences in their sequence, main biding sites might remain unaltered during evolution. Therefore, we think that integrin α 6 expression should be checked among our different EVs to see whether their express it to different levels and if it is implicated in lung tropism and metastasis.

Additionally, we have demonstrated that cells with LRs H-RAS signals have certain tropism to colonize liver, since they exhibit higher rates of colonization compared to other H-RAS sublocalizations. However, when we looked livers by immunohistochemistry small number of cells were present showing only small cells foci. These results can be explained since liver is the first organ that intravasated cells reach once entering chick embryo circulation. In consequence, since all potential metastatic cells will firstly arrive there, and due the permeable nature of liver sinusoids vessels, which facilitate cells extravasation (376, 377), it can be speculated that although H-RASv12-LCK-expressing cells might have a weak tropism to

chicken liver it may not be relevant in humans. Indeed, human thyroid tumors are unlikely to metastasize in liver but mainly invade regional lymph nodes and lungs due to their relative closeness and vascularization (348). Therefore, our results suggest LRs H-RAS signals to not be crucial in liver or lung metastasis in humans and that LRs H-RAS cells-secreted EVs cannot induce higher rates of liver colonization in H-RASv12-CD8 or H-RASv12-KDEL expressing cells.

To sum up, our results suggest for the first time, that RAS sublocalizations have a key role in exosome biogenesis by using different pathways that affect the amount, the size and cargo loading of exosomes. As a result of exosome heterogeneity, EVs released by PCCL3 with mutant H-RAS at GC or DM, display similar characteristics, and can induce a decrease in H-RAS LR and ER mediated proliferation *in vitro* and *in vivo.* More interestingly, these EVs can transfer lung metastatic properties, suggesting that they can be educating the lung pre-metastatic niche although they might also be increasing cell migration and invasion. This part of the project is just currently starting but shows novel and exciting data that needs to be further explored. Moreover, if different cargos are found between EVs secreted by either H-RAS at DM and GC, vs, H-RAS at ER and LR, they could be monitored in patients liquid biopsies which could save patients discomfort and it would possibly help to detect early recurrences and metastasis, even in patients that only undergo a partial thyroidectomy.

6. Conclusions

6. CONCLUSIONS

1. Tumor size in tumors induced by H-RAS and N-RAS site specific signals does not correlate with metastatic potential.

2. The ability to colonize lungs is given by mainly by RAS signals coming from DM

3. APT-1 levels modify thyroid tumor cells behavior with respect to their proliferation and metastatic potential by regulating RAS segregation in plasma-membrane microdomains

4. Tumors with H-RAS at LR and ER accumulate lipids and it relates with high VEGF-B expression levels

5. VEGF-B can alter tumor size and the metastatic potential of cells expressing RAS at DM and GC

6. PCCL3 cells expressing H-RASv12 at its different sublocalizations secrete different populations of EVs

7. Depending on RAS sublocalization, the generated EVs can alter tumor behavior distinctively

7. References

7. REFERENCES

1. Harvey JJ. An Unidentified Virus Which Causes the Rapid Production of Tumours in Mice. Nature. 1964;204:1104-5.

2. Scolnick EM, Maryak JM, Parks WP. Levels of rat cellular RNA homologous to either Kirsten sarcoma virus or rat type-C virus in cell lines derived from Osborne-Mendel rats. J Virol. 1974;14(6):1435-44.

3. Hall A, Marshall CJ, Spurr NK, Weiss RA. Identification of transforming gene in two human sarcoma cell lines as a new member of the ras gene family located on chromosome 1. Nature. 1983;303(5916):396-400.

4. Shimizu K, Goldfarb M, Perucho M, Wigler M. Isolation and preliminary characterization of the transforming gene of a human neuroblastoma cell line. Proc Natl Acad Sci U S A. 1983;80(2):383-7.

5. Gibbs JB, Sigal IS, Poe M, Scolnick EM. Intrinsic GTPase activity distinguishes normal and oncogenic ras p21 molecules. Proc Natl Acad Sci U S A. 1984;81(18):5704-8.

6. McGrath JP, Capon DJ, Goeddel DV, Levinson AD. Comparative biochemical properties of normal and activated human ras p21 protein. Nature. 1984;310(5979):644-9.

7. Sweet RW, Yokoyama S, Kamata T, Feramisco JR, Rosenberg M, Gross M. The product of ras is a GTPase and the T24 oncogenic mutant is deficient in this activity. Nature. 1984;311(5983):273-5.

8. Santos E, Tronick SR, Aaronson SA, Pulciani S, Barbacid M. T24 human bladder carcinoma oncogene is an activated form of the normal human homologue of BALB- and Harvey-MSV transforming genes. Nature. 1982;298(5872):343-7.

9. Boguski MS, McCormick F. Proteins regulating Ras and its relatives. Nature. 1993;366(6456):643-54.

10. Colicelli J. Human RAS superfamily proteins and related GTPases. Sci STKE. 2004;2004(250):RE13.

11. Wennerberg K, Rossman KL, Der CJ. The Ras superfamily at a glance. J Cell Sci. 2005;118(Pt 5):843-6.

12. Etienne-Manneville S, Hall A. Rho GTPases in cell biology. Nature. 2002;420(6916):629-35.

13. Zhou X, Zheng Y. Cell type-specific signaling function of RhoA GTPase: lessons from mouse gene targeting. J Biol Chem. 2013;288(51):36179-88.

14. Pereira-Leal JB, Seabra MC. Evolution of the Rab family of small GTP-binding proteins. J Mol Biol. 2001;313(4):889-901.

15. Bourne HR, Sanders DA, McCormick F. The GTPase superfamily: conserved structure and molecular mechanism. Nature. 1991;349(6305):117-27.

16. Sprang SR. G protein mechanisms: insights from structural analysis. Annu Rev Biochem. 1997;66:639-78.

17. Pai EF, Kabsch W, Krengel U, Holmes KC, John J, Wittinghofer A. Structure of the guanine-nucleotide-binding domain of the Ha-ras oncogene product p21 in the triphosphate conformation. Nature. 1989;341(6239):209-14.

18. Siyang song wC, Shurong Zhou, Yujie Shi, Wenbing Dai, Hua Zhang, Xueqing Wang, Bing He, Qiang Zhang. Small GTPases: Structure, biological function and its interaction with nanoparticles. Asian J Pharm 2018.

19. Antonny B, Beraud-Dufour S, Chardin P, Chabre M. N-terminal hydrophobic residues of the G-protein ADP-ribosylation factor-1 insert into membrane phospholipids upon GDP to GTP exchange. Biochemistry. 1997;36(15):4675-84.

20. Vetter IR, Nowak C, Nishimoto T, Kuhlmann J, Wittinghofer A. Structure of a Ran-binding domain complexed with Ran bound to a GTP analogue: implications for nuclear transport. Nature. 1999;398(6722):39-46.

21. Vetter IR, Wittinghofer A. The Guanine Nucleotide-Binding Switch in Three Dimensions. Science. 2001;294(5545):1299.

22. Milburn MV, Tong L, deVos AM, Brunger A, Yamaizumi Z, Nishimura S, et al. Molecular switch for signal transduction: structural differences between active and inactive forms of protooncogenic ras proteins. Science. 1990;247(4945):939-45.

23. Ryan MB, Corcoran RB. Therapeutic strategies to target RAS-mutant cancers. Nat Rev Clin Oncol. 2018;15(11):709-20.

24. Schmidt A, Hall A. Guanine nucleotide exchange factors for Rho GTPases: turning on the switch. Genes Dev. 2002;16(13):1587-609.

25. Bernards A, Settleman J. GAP control: regulating the regulators of small GTPases. Trends Cell Biol. 2004;14(7):377-85.

26. Garrett MD, Kabcenell AK, Zahner JE, Kaibuchi K, Sasaki T, Takai Y, et al. Interaction of Sec4 with GDI proteins from bovine brain, Drosophila melanogaster and Saccharomyces cerevisiae. Conservation of GDI membrane dissociation activity. FEBS Lett. 1993;331(3):233-8.

27. Goitre L, Trapani E, Trabalzini L, Retta SF. The Ras superfamily of small GTPases: the unlocked secrets. Methods Mol Biol.1120:1-18.

28. Barbacid M. ras genes. Annu Rev Biochem. 1987;56:779-827.

29. Lowy DR, Johnson MR, DeClue JE, Cen H, Zhang K, Papageorge AG, et al. Cell transformation by ras and regulation of its protein product. Ciba Found Symp. 1993;176:67-80; discussion -4.

30. Parker JA, Volmar AY, Pavlopoulos S, Mattos C. K-Ras Populates Conformational States Differently from Its Isoform H-Ras and Oncogenic Mutant K-RasG12D. Structure.26(6):810-20 e4.

31. Parker JA, Mattos C. The K-Ras, N-Ras, and H-Ras Isoforms: Unique Conformational Preferences and Implications for Targeting Oncogenic Mutants. Cold Spring Harb Perspect Med.8(8).

32. Stephanie P. Mo JMC, Ian A. Prior. Ras variant signalling. Biochem Soc Trans. 2018;45(5):1325-32.

33. Willumsen BM, Christensen A, Hubbert NL, Papageorge AG, Lowy DR. The p21 ras C-terminus is required for transformation and membrane association. Nature. 1984;310(5978):583-6.

34. Hancock JF, Magee AI, Childs JE, Marshall CJ. All ras proteins are polyisoprenylated but only some are palmitoylated. Cell. 1989;57(7):1167-77.

35. Boyartchuk VL, Ashby MN, Rine J. Modulation of Ras and a-factor function by carboxyl-terminal proteolysis. Science. 1997;275(5307):1796-800.

36. Clarke S, Vogel JP, Deschenes RJ, Stock J. Posttranslational modification of the Ha-ras oncogene protein: evidence for a third class of protein carboxyl methyltransferases. Proc Natl Acad Sci U S A. 1988;85(13):4643-7.

37. Hrycyna CA, Sapperstein SK, Clarke S, Michaelis S. The Saccharomyces cerevisiae STE14 gene encodes a methyltransferase that mediates C-terminal methylation of a-factor and RAS proteins. EMBO J. 1991;10(7):1699-709.

38. Dai Q, Choy E, Chiu V, Romano J, Slivka SR, Steitz SA, et al. Mammalian prenylcysteine carboxyl methyltransferase is in the endoplasmic reticulum. J Biol Chem. 1998;273(24):15030-4.

39. Zhou Y, Prakash P, Gorfe AA, Hancock JF. Ras and the Plasma Membrane: A Complicated Relationship. Cold Spring Harb Perspect Med. 2017;8(10).

40. Roy S, Plowman S, Rotblat B, Prior IA, Muncke C, Grainger S, et al. Individual palmitoyl residues serve distinct roles in H-ras trafficking, microlocalization, and signaling. Mol Cell Biol. 2005;25(15):6722-33.

41. Mitchell DA, Vasudevan A, Linder ME, Deschenes RJ. Protein palmitoylation by a family of DHHC protein S-acyltransferases. J Lipid Res. 2006;47(6):1118-27.

42. Swarthout JT, Lobo S, Farh L, Croke MR, Greentree WK, Deschenes RJ, et al. DHHC9 and GCP16 constitute a human protein fatty acyltransferase with specificity for H- and N-Ras. J Biol Chem. 2005;280(35):31141-8.

43. Henis YI, Hancock JF, Prior IA. Ras acylation, compartmentalization and signaling nanoclusters (Review). Mol Membr Biol. 2009;26(1):80-92.

44. Laude AJ, Prior IA. Palmitoylation and localisation of RAS isoforms are modulated by the hypervariable linker domain. J Cell Sci. 2008;121(Pt 4):421-7.

45. Ahearn IM, Tsai FD, Court H, Zhou M, Jennings BC, Ahmed M, et al. FKBP12 binds to acylated H-ras and promotes depalmitoylation. Mol Cell. 2011;41(2):173-85.

46. Bivona TG, Quatela SE, Bodemann BO, Ahearn IM, Soskis MJ, Mor A, et al. PKC regulates a farnesyl-electrostatic switch on K-Ras that promotes its association with Bcl-XL on mitochondria and induces apoptosis. Mol Cell. 2006;21(4):481-93.

47. Lander HM, Hajjar DP, Hempstead BL, Mirza UA, Chait BT, Campbell S, et al. A molecular redox switch on p21(ras). Structural basis for the nitric oxide-p21(ras) interaction. J Biol Chem. 1997;272(7):4323-6.

48. Yang MH, Nickerson S, Kim ET, Liot C, Laurent G, Spang R, et al. Regulation of RAS oncogenicity by acetylation. Proc Natl Acad Sci U S A.109(27):10843-8.

49. Ahearn IM, Haigis K, Bar-Sagi D, Philips MR. Regulating the regulator: post-translational modification of RAS. Nat Rev Mol Cell Biol. 2012;13(1):39-51.

50. Thurman R, Siraliev-Perez E, Campbell SL. RAS ubiquitylation modulates effector interactions. Small GTPases. 2017:1-6.

51. Jura N, Scotto-Lavino E, Sobczyk A, Bar-Sagi D. Differential modification of Ras proteins by ubiquitination. Mol Cell. 2006;21(5):679-87.

52. Choi BH, Chen C, Philips M, Dai W. RAS GTPases are modified by SUMOylation. Oncotarget.9(4):4440-50.

53. Lynch SJ, Snitkin H, Gumper I, Philips MR, Sabatini D, Pellicer A. The differential palmitoylation states of N-Ras and H-Ras determine their distinct Golgi subcompartment localizations. J Cell Physiol. 2016;230(3):610-9.

54. Volchuk A, Amherdt M, Ravazzola M, Brugger B, Rivera VM, Clackson T, et al. Megavesicles implicated in the rapid transport of intracisternal aggregates across the Golgi stack. Cell. 2000;102(3):335-48.

55. Glick BS, Luini A. Models for Golgi traffic: a critical assessment. Cold Spring Harb Perspect Biol. 2011;3(11):a005215.

56. Lippincott-Schwartz J, Phair RD. Lipids and cholesterol as regulators of traffic in the endomembrane system. Annu Rev Biophys. 2010

39:559-78.

57. Hancock JF, Parton RG. Ras plasma membrane signalling platforms. Biochem J. 2005;389(Pt 1):1-11.

58. Sugimoto H, Hayashi H, Yamashita S. Purification, cDNA cloning, and regulation of lysophospholipase from rat liver. J Biol Chem. 1996;271(13):7705-11.

59. Duncan JA, Gilman AG. A cytoplasmic acyl-protein thioesterase that removes palmitate from G protein alpha subunits and p21(RAS). J Biol Chem. 1998;273(25):15830-7.

60. Devedjiev Y, Dauter Z, Kuznetsov SR, Jones TL, Derewenda ZS. Crystal structure of the human acyl protein thioesterase I from a single X-ray data set to 1.5 A. Structure. 2000;8(11):1137-46.

61. Yeh DC, Duncan JA, Yamashita S, Michel T. Depalmitoylation of endothelial nitric-oxide synthase by acyl-protein thioesterase 1 is potentiated by Ca(2+)-calmodulin. J Biol Chem. 1999;274(46):33148-54.

62. Flaumenhaft R, Rozenvayn N, Feng D, Dvorak AM. SNAP-23 and syntaxin-2 localize to the extracellular surface of the platelet plasma membrane. Blood. 2007;110(5):1492-501.

63. Veit M, Schmidt MF. Enzymatic depalmitoylation of viral glycoproteins with acyl-protein thioesterase 1 in vitro. Virology. 2001;288(1):89-95.

64. Lin DT, Conibear E. Enzymatic protein depalmitoylation by acyl protein thioesterases. Biochem Soc Trans. 2014;43(2):193-8.

65. Chandra A, Grecco HE, Pisupati V, Perera D, Cassidy L, Skoulidis F, et al. The GDI-like solubilizing factor PDEdelta sustains the spatial organization and signalling of Ras family proteins. Nat Cell Biol. 2012;14(2):148-58.

66. Lin DT, Conibear E. ABHD17 proteins are novel protein depalmitoylases that regulate N-Ras palmitate turnover and subcellular localization. Elife. 2016;4:e11306.

67. Fehrenbacher N, Bar-Sagi D, Philips M. Ras/MAPK signaling from endomembranes. Mol Oncol. 2009;3(4):297-307.

68. Lin DTS, Davis NG, Conibear E. Targeting the Ras palmitoylation/depalmitoylation cycle in cancer. Biochem Soc Trans. 2017;45(4):913-21.

69. Herrmann C. Ras-effector interactions: after one decade. Curr Opin Struct Biol. 2003;13(1):122-9.

70. Castellano E, Downward J. RAS Interaction with PI3K: More Than Just Another Effector Pathway. Genes Cancer. 2011

2(3):261-74.

71. Matallanas D, Birtwistle M, Romano D, Zebisch A, Rauch J, von Kriegsheim A, et al. Raf family kinases: old dogs have learned new tricks. Genes Cancer. 2011;2(3):232-60.

72. Neel NF, Martin TD, Stratford JK, Zand TP, Reiner DJ, Der CJ. The RalGEF-Ral Effector Signaling Network: The Road Less Traveled for Anti-Ras Drug Discovery. Genes Cancer. 2011;2(3):275-87.

73. Cargnello M, Roux PP. Activation and function of the MAPKs and their substrates, the MAPK-activated protein kinases. Microbiol Mol Biol Rev. 2011;75(1):50-83.

74. Quiagen. ERK signaling 2019 [Available from: https://www.qiagen.com/us/shop/genes-and-pathways/pathway-details/?pwid=162.

75. Plotnikov A, Zehorai E, Procaccia S, Seger R. The MAPK cascades: signaling components, nuclear roles and mechanisms of nuclear translocation. Biochim Biophys Acta. 2011;1813(9):1619-33.

76. Li L, Zhao GD, Shi Z, Qi LL, Zhou LY, Fu ZX. The Ras/Raf/MEK/ERK signaling pathway and its role in the occurrence and development of HCC. Oncol Lett. 2016;12(5):3045-50.

77. Subramaniam S, Unsicker K. ERK and cell death: ERK1/2 in neuronal death. FEBS J. 2010;277(1):22-9.

78. Harper SJ, Bates DO. VEGF-A splicing: the key to anti-angiogenic therapeutics? Nat Rev Cancer. 2008;8(11):880-7.

79. Mendoza MC, Er EE, Blenis J. The Ras-ERK and PI3K-mTOR pathways: cross-talk and compensation. Trends Biochem Sci. 2012;36(6):320-8.

80. Cantley LC. The phosphoinositide 3-kinase pathway. Science. 2002;296(5573):1655-7.

81. Alessi DR, James SR, Downes CP, Holmes AB, Gaffney PR, Reese CB, et al. Characterization of a 3-phosphoinositide-dependent protein kinase which phosphorylates and activates protein kinase Balpha. Curr Biol. 1997;7(4):261-9.

82. Castellano E, Downward J. RAS Interaction with PI3K: More Than Just Another Effector Pathway. Genes Cancer. 2011;2(3):261-74.

83. Yamaguchi H, Wang HG. The protein kinase PKB/Akt regulates cell survival and apoptosis by inhibiting Bax conformational change. Oncogene. 2001;20(53):7779-86.

84. Datta SR, Dudek H, Tao X, Masters S, Fu H, Gotoh Y, et al. Akt phosphorylation of BAD couples survival signals to the cell-intrinsic death machinery. Cell. 1997;91(2):231-41.

85. Brunet A, Bonni A, Zigmond MJ, Lin MZ, Juo P, Hu LS, et al. Akt promotes cell survival by phosphorylating and inhibiting a Forkhead transcription factor. Cell. 1999;96(6):857-68.

86. Dibble CC, Cantley LC. Regulation of mTORC1 by PI3K signaling. Trends Cell Biol. 2015;25(9):545-55.

87. Dan HC, Antonia RJ, Baldwin AS. PI3K/Akt promotes feedforward mTORC2 activation through IKKalpha. Oncotarget. 2016

7(16):21064-75.

88. Yang G, Murashige DS, Humphrey SJ, James DE. A Positive Feedback Loop between Akt and mTORC2 via SIN1 Phosphorylation. Cell Rep. 2015;12(6):937-43.

89. Neel NF, Martin TD, Stratford JK, Zand TP, Reiner DJ, Der CJ. The RalGEF-Ral Effector Signaling Network: The Road Less Traveled for Anti-Ras Drug Discovery. Genes Cancer. 2011

2(3):275-87.

90. Gentry LR, Martin TD, Reiner DJ, Der CJ. Ral small GTPase signaling and oncogenesis: More than just 15minutes of fame. Biochim Biophys Acta. 2014;1843(12):2976-88.

91. Willingham MC, Pastan I, Shih TY, Scolnick EM. Localization of the src gene product of the Harvey strain of MSV to plasma membrane of transformed cells by electron microscopic immunocytochemistry. Cell. 1980;19(4):1005-14.

92. Singer SJ, Nicolson GL. The fluid mosaic model of the structure of cell membranes. Science. 1972;175(4023):720-31.

93. Rothman JE, Lenard J. Membrane asymmetry. Science. 1977;195(4280):743-53.

94. Daleke DL. Regulation of transbilayer plasma membrane phospholipid asymmetry. J Lipid Res. 2003;44(2):233-42.

95. Simons K, Ikonen E. Functional rafts in cell membranes. Nature. 1997;387(6633):569-72.

96. Simons K, van Meer G. Lipid sorting in epithelial cells. Biochemistry. 1988;27(17):6197-202.

97. Niv H, Gutman O, Kloog Y, Henis YI. Activated K-Ras and H-Ras display different interactions with saturable nonraft sites at the surface of live cells. J Cell Biol. 2002;157(5):865-72.

98. Prior IA, Muncke C, Parton RG, Hancock JF. Direct visualization of Ras proteins in spatially distinct cell surface microdomains. J Cell Biol. 2003;160(2):165-70.

99. Hancock JF. Ras proteins: different signals from different locations. Nat Rev Mol Cell Biol. 2003;4(5):373-84.

100. Agudo-Ibanez L, Herrero A, Barbacid M, Crespo P. H-ras distribution and signaling in plasma membrane microdomains are regulated by acylation and deacylation events. Mol Cell Biol. 2016;35(11):1898-914.

101. Choy E, Chiu VK, Silletti J, Feoktistov M, Morimoto T, Michaelson D, et al. Endomembrane trafficking of ras: the CAAX motif targets proteins to the ER and Golgi. Cell. 1999;98(1):69-80.

102. Rocks O, Peyker A, Kahms M, Verveer PJ, Koerner C, Lumbierres M, et al. An acylation cycle regulates localization and activity of palmitoylated Ras isoforms. Science. 2005;307(5716):1746-52.

103. Perez de Castro I, Bivona TG, Philips MR, Pellicer A. Ras activation in Jurkat T cells following low-grade stimulation of the T-cell receptor is specific to N-Ras and occurs only on the Golgi apparatus. Mol Cell Biol. 2004;24(8):3485-96.

104. Chiu VK, Bivona T, Hach A, Sajous JB, Silletti J, Wiener H, et al. Ras signalling on the endoplasmic reticulum and the Golgi. Nat Cell Biol. 2002;4(5):343-50.

105. Lynch SJ, Snitkin H, Gumper I, Philips MR, Sabatini D, Pellicer A. The differential palmitoylation states of N-Ras and H-Ras determine their distinct Golgi subcompartment localizations. J Cell Physiol. 2015;230(3):610-9.

106. Gorfe AA, Pellarin R, Caflisch A. Membrane localization and flexibility of a lipidated ras peptide studied by molecular dynamics simulations. J Am Chem Soc. 2004;126(46):15277-86.

107. Misaki R, Morimatsu M, Uemura T, Waguri S, Miyoshi E, Taniguchi N, et al. Palmitoylated Ras proteins traffic through recycling endosomes to the plasma membrane during exocytosis. J Cell Biol. 2011

191(1):23-9.

108. Roy S, Wyse B, Hancock JF. H-Ras signaling and K-Ras signaling are differentially dependent on endocytosis. Mol Cell Biol. 2002;22(14):5128-40.

109. Lu A, Tebar F, Alvarez-Moya B, Lopez-Alcala C, Calvo M, Enrich C, et al. A clathrin-dependent pathway leads to KRas signaling on late endosomes en route to lysosomes. J Cell Biol. 2009;184(6):863-79.

110. Matallanas D, Sanz-Moreno V, Arozarena I, Calvo F, Agudo-Ibanez L, Santos E, et al. Distinct utilization of effectors and biological outcomes resulting from site-specific Ras activation: Ras functions in lipid rafts and Golgi complex are dispensable for proliferation and transformation. Mol Cell Biol. 2006;26(1):100-16.

111. Inder K, Harding A, Plowman SJ, Philips MR, Parton RG, Hancock JF. Activation of the MAPK module from different spatial locations generates distinct system outputs. Mol Biol Cell. 2008;19(11):4776-84.

112. Prior IA, Hancock JF. Ras trafficking, localization and compartmentalized signalling. Semin Cell Dev Biol. 2012;23(2):145-53.

113. Philips MR. Compartmentalized signalling of Ras. Biochem Soc Trans. 2005;33(Pt 4):657-61.

114. Calvo F, Agudo-Ibanez L, Crespo P. The Ras-ERK pathway: understanding site-specific signaling provides hope of new anti-tumor therapies. Bioessays.32(5):412-21.

115. Jun JE, Rubio I, Roose JP. Regulation of ras exchange factors and cellular localization of ras activation by lipid messengers in T cells. Front Immunol. 2013;4:239.

116. Casar B, Crespo P. ERK Signals: Scaffolding Scaffolds? Front Cell Dev Biol. 2016;4:49.

117. Brown MD, Sacks DB. Protein scaffolds in MAP kinase signalling. Cell Signal. 2009;21(4):462-9.

118. Meister G. Argonaute proteins: functional insights and emerging roles. Nat Rev Genet. 2013;14(7):447-59.

119. Agudo-Ibanez L, Herrero A, Barbacid M, Crespo P. H-ras distribution and signaling in plasma membrane microdomains are regulated by acylation and deacylation events. Mol Cell Biol. 2015;35(11):1898-914.

120. Casar B, Pinto A, Crespo P. ERK dimers and scaffold proteins: unexpected partners for a forgotten (cytoplasmic) task. Cell Cycle. 2009;8(7):1007-13.

121. Casar B, Badrock AP, Jimenez I, Arozarena I, Colon-Bolea P, Lorenzo-Martin LF, et al. RAS at the Golgi antagonizes malignant transformation through PTPRkappa-mediated inhibition of ERK activation. Nat Commun. 2018;9(1):3595.

122. Shalaby F, Rossant J, Yamaguchi TP, Gertsenstein M, Wu XF, Breitman ML, et al. Failure of blood-island formation and vasculogenesis in Flk-1-deficient mice. Nature. 1995;376(6535):62-6.

123. Dumont DJ, Jussila L, Taipale J, Lymboussaki A, Mustonen T, Pajusola K, et al. Cardiovascular failure in mouse embryos deficient in VEGF receptor-3. Science. 1998;282(5390):946-9.

124. Holmes DI, Zachary I. The vascular endothelial growth factor (VEGF) family: angiogenic factors in health and disease. Genome Biol. 2005;6(2):209.

125. Chau K, Hennessy A, Makris A. Placental growth factor and pre-eclampsia. J Hum Hypertens. 2017;31(12):782-6.

126. Li X, Lee C, Tang Z, Zhang F, Arjunan P, Li Y, et al. VEGF-B: a survival, or an angiogenic factor? Cell Adh Migr. 2009;3(4):322-7.

127. Carmeliet P, Ferreira V, Breier G, Pollefeyt S, Kieckens L, Gertsenstein M, et al. Abnormal blood vessel development and lethality in embryos lacking a single VEGF allele. Nature. 1996;380(6573):435-9.

128. Ferrara N, Carver-Moore K, Chen H, Dowd M, Lu L, O'Shea KS, et al. Heterozygous embryonic lethality induced by targeted inactivation of the VEGF gene. Nature. 1996;380(6573):439-42.

129. Carmeliet P, Jain RK. Angiogenesis in cancer and other diseases. Nature. 2000;407(6801):249-57.

130. Rosen LS, Jacobs IA, Burkes RL. Bevacizumab in Colorectal Cancer: Current Role in Treatment and the Potential of Biosimilars. Target Oncol. 2017;12(5):599-610.

131. Wenger KJ, Wagner M, You SJ, Franz K, Harter PN, Burger MC, et al. Bevacizumab as a last-line treatment for glioblastoma following failure of radiotherapy, temozolomide and lomustine. Oncol Lett. 2017;14(1):1141-6.

132. Harshman LC, Srinivas S. The bevacizumab experience in advanced renal cell carcinoma. Onco Targets Ther. 2010;3:179-89.

133. Lauro S, Onesti CE, Righini R, Marchetti P. The use of bevacizumab in non-small cell lung cancer: an update. Anticancer Res. 2014;34(4):1537-45.

134. Bellomo D, Headrick JP, Silins GU, Paterson CA, Thomas PS, Gartside M, et al. Mice lacking the vascular endothelial growth factor-B gene (Vegfb) have smaller hearts, dysfunctional coronary vasculature, and impaired recovery from cardiac ischemia. Circ Res. 2000;86(2):E29-35.

135. Li X. VEGF-B: a thing of beauty. Cell Res. 2010;20(7):741-4.

136. Zhang F, Tang Z, Hou X, Lennartsson J, Li Y, Koch AW, et al. VEGF-B is dispensable for blood vessel growth but critical for their survival, and VEGF-B targeting inhibits pathological angiogenesis. Proc Natl Acad Sci U S A. 2009;106(15):6152-7.

137. Hagberg CE, Falkevall A, Wang X, Larsson E, Huusko J, Nilsson I, et al. Vascular endothelial growth factor B controls endothelial fatty acid uptake. Nature. 2010;464(7290):917-21.

138. Hagberg CE, Mehlem A, Falkevall A, Muhl L, Fam BC, Ortsater H, et al. Targeting VEGF-B as a novel treatment for insulin resistance and type 2 diabetes. Nature. 2012;490(7420):426-30.

139. Yang X, Zhang Y, Hosaka K, Andersson P, Wang J, Tholander F, et al. VEGF-B promotes cancer metastasis through a VEGF-A-independent mechanism and serves as a marker of poor prognosis for cancer patients. Proc Natl Acad Sci U S A. 2015;112(22):E2900-9.

140. Gunningham SP, Currie MJ, Han C, Robinson BA, Scott PA, Harris AL, et al. VEGF-B expression in human primary breast cancers is associated with lymph node metastasis but not angiogenesis. J Pathol. 2001;193(3):325-32.

141. Gyorgy B, Szabo TG, Pasztoi M, Pal Z, Misjak P, Aradi B, et al. Membrane vesicles, current state-of-the-art: emerging role of extracellular vesicles. Cell Mol Life Sci. 2011;68(16):2667-88.

142. Huotari J, Helenius A. Endosome maturation. EMBO J. 2011;30(17):3481-500.

143. Raiborg C, Stenmark H. The ESCRT machinery in endosomal sorting of ubiquitylated membrane proteins. Nature. 2009;458(7237):445-52.

144. Hurley JH. The ESCRT complexes. Crit Rev Biochem Mol Biol. 2010;45(6):463-87.

145. van Niel G, D'Angelo G, Raposo G. Shedding light on the cell biology of extracellular vesicles. Nat Rev Mol Cell Biol. 2018;19(4):213-28.

146. Klumperman J, Raposo G. The complex ultrastructure of the endolysosomal system. Cold Spring Harb Perspect Biol. 2014;6(10):a016857.

147. Baietti MF, Zhang Z, Mortier E, Melchior A, Degeest G, Geeraerts A, et al. Syndecan-syntenin-ALIX regulates the biogenesis of exosomes. Nat Cell Biol. 2012;14(7):677-85.

148. Thery C, Zitvogel L, Amigorena S. Exosomes: composition, biogenesis and function. Nat Rev Immunol. 2002;2(8):569-79.

149. Karim MA, Samyn DR, Mattie S, Brett CL. Distinct features of multivesicular body-lysosome fusion revealed by a new cell-free content-mixing assay. Traffic. 2017;19(2):138-49.

150. Savina A, Vidal M, Colombo MI. The exosome pathway in K562 cells is regulated by Rab11. J Cell Sci. 2002;115(Pt 12):2505-15.

151. Han J, Pluhackova K, Bockmann RA. The Multifaceted Role of SNARE Proteins in Membrane Fusion. Front Physiol. 2017

8:5.

152. Hessvik NP, Llorente A. Current knowledge on exosome biogenesis and release. Cell Mol Life Sci. 2018;75(2):193-208.

153. Trajkovic K, Hsu C, Chiantia S, Rajendran L, Wenzel D, Wieland F, et al. Ceramide triggers budding of exosome vesicles into multivesicular endosomes. Science. 2008;319(5867):1244-7.

154. Thery C, Ostrowski M, Segura E. Membrane vesicles as conveyors of immune responses. Nat Rev Immunol. 2009;9(8):581-93.

155. Hurley JH, Boura E, Carlson LA, Rozycki B. Membrane budding. Cell. 2010

143(6):875-87.

156. McConnell RE, Tyska MJ. Myosin-1a powers the sliding of apical membrane along microvillar actin bundles. J Cell Biol. 2007;177(4):671-81.

157. Xu R, Rai A, Chen M, Suwakulsiri W, Greening DW, Simpson RJ. Extracellular vesicles in cancer - implications for future improvements in cancer care. Nat Rev Clin Oncol. 2018;15(10):617-38.

158. Caruso S, Poon IKH. Apoptotic Cell-Derived Extracellular Vesicles: More Than Just Debris. Front Immunol. 2018;9:1486.

159. McKelvey KJ, Powell KL, Ashton AW, Morris JM, McCracken SA. Exosomes: Mechanisms of Uptake. J Circ Biomark. 2015;4:7.

160. Prada I, Meldolesi J. Binding and Fusion of Extracellular Vesicles to the Plasma Membrane of Their Cell Targets. Int J Mol Sci. 2016;17(8).

161. Gonda A, Kabagwira J, Senthil GN, Wall NR. Internalization of Exosomes through Receptor-mediated Endocytosis. Mol Cancer Res. 2018.

162. Escrevente C, Keller S, Altevogt P, Costa J. Interaction and uptake of exosomes by ovarian cancer cells. BMC Cancer. 2011;11:108.

163. Tian T, Zhu YL, Zhou YY, Liang GF, Wang YY, Hu FH, et al. Exosome uptake through clathrin-mediated endocytosis and macropinocytosis and mediating miR-21 delivery. J Biol Chem. 2014;289(32):22258-67.

164. Feng D, Zhao WL, Ye YY, Bai XC, Liu RQ, Chang LF, et al. Cellular internalization of exosomes occurs through phagocytosis. Traffic. 2010;11(5):675-87.

165. Bang C, Thum T. Exosomes: new players in cell-cell communication. Int J Biochem Cell Biol. 2012

44(11):2060-4.

166. Hanahan D, Weinberg RA. Hallmarks of cancer: the next generation. Cell. 2011;144(5):646-74.

167. Hood JL, San RS, Wickline SA. Exosomes released by melanoma cells prepare sentinel lymph nodes for tumor metastasis. Cancer Res. 2011;71(11):3792-801.

168. Grange C, Tapparo M, Collino F, Vitillo L, Damasco C, Deregibus MC, et al. Microvesicles released from human renal cancer stem cells stimulate angiogenesis and formation of lung premetastatic niche. Cancer Res. 2011;71(15):5346-56.

169. Fong MY, Zhou W, Liu L, Alontaga AY, Chandra M, Ashby J, et al. Breast-cancer-secreted miR-122 reprograms glucose metabolism in premetastatic niche to promote metastasis. Nat Cell Biol. 2015;17(2):183-94.

170. Costa-Silva B, Aiello NM, Ocean AJ, Singh S, Zhang H, Thakur BK, et al. Pancreatic cancer exosomes initiate pre-metastatic niche formation in the liver. Nat Cell Biol. 2015;17(6):816-26.

171. Hoshino A, Costa-Silva B, Shen TL, Rodrigues G, Hashimoto A, Tesic Mark M, et al. Tumour exosome integrins determine organotropic metastasis. Nature. 2015;527(7578):329-35.

172. Becker A, Thakur BK, Weiss JM, Kim HS, Peinado H, Lyden D. Extracellular Vesicles in Cancer: Cell-to-Cell Mediators of Metastasis. Cancer Cell. 2016;30(6):836-48.

173. Sexton RE, Mpilla G, Kim S, Philip PA, Azmi AS. Ras and exosome signaling. Semin Cancer Biol. 2019;54:131-7.

174. Garcia-Olmo DC, Dominguez C, Garcia-Arranz M, Anker P, Stroun M, Garcia-Verdugo JM, et al. Cell-free nucleic acids circulating in the plasma of colorectal cancer patients induce the oncogenic transformation of susceptible cultured cells. Cancer Res. 2010;70(2):560-7.

175. Kahlert C, Melo SA, Protopopov A, Tang J, Seth S, Koch M, et al. Identification of double-stranded genomic DNA spanning all chromosomes with mutated KRAS and p53 DNA in the serum exosomes of patients with pancreatic cancer. J Biol Chem. 2015;289(7):3869-75.

176. Melo SA, Luecke LB, Kahlert C, Fernandez AF, Gammon ST, Kaye J, et al. Glypican-1 identifies cancer exosomes and detects early pancreatic cancer. Nature. 2015;523(7559):177-82.

177. Shi Y, Wang W, Yang B, Tian H. ATF1 and RAS in exosomes are potential clinical diagnostic markers for cervical cancer. Cell Biochem Funct. 2017;35(7):477-83.

178. Lee TH, Chennakrishnaiah S, Meehan B, Montermini L, Garnier D, D'Asti E, et al. Barriers to horizontal cell transformation by extracellular vesicles containing oncogenic H-ras. Oncotarget. 2016;7(32):51991-2002.

179. Holmgren L, Bergsmedh A, Spetz AL. Horizontal transfer of DNA by the uptake of apoptotic bodies. Vox Sang. 2002;83 Suppl 1:305-6.

180. Bergsmedh A, Szeles A, Henriksson M, Bratt A, Folkman MJ, Spetz AL, et al. Horizontal transfer of oncogenes by uptake of apoptotic bodies. Proc Natl Acad Sci U S A. 2001;98(11):6407-11.

181. Luhtala N, Aslanian A, Yates JR, 3rd, Hunter T. Secreted Glioblastoma Nanovesicles Contain Intracellular Signaling Proteins and Active Ras Incorporated in a Farnesylation-dependent Manner. J Biol Chem. 2017;292(2):611-28.

182. Clark DJ, Fondrie WE, Yang A, Mao L. Triple SILAC quantitative proteomic analysis reveals differential abundance of cell signaling proteins between normal and lung cancer-derived exosomes. J Proteomics. 2016;133:161-9.

183. Tauro BJ, Mathias RA, Greening DW, Gopal SK, Ji H, Kapp EA, et al. Oncogenic H-ras reprograms Madin-Darby canine kidney (MDCK) cell-derived exosomal proteins following epithelial-mesenchymal transition. Mol Cell Proteomics. 2013;12(8):2148-59.

184. Lin HK, Lin HH, Chiou YW, Wu CL, Chiu WT, Tang MJ. Caveolin-1 down-regulation is required for Wnt5a-Frizzled 2 signalling in Ha-Ras(V12) -induced cell transformation. J Cell Mol Med. 2018;22(5):2631-43.

185. Higginbotham JN, Demory Beckler M, Gephart JD, Franklin JL, Bogatcheva G, Kremers GJ, et al. Amphiregulin exosomes increase cancer cell invasion. Curr Biol. 2011;21(9):779-86.

186. Demory Beckler M, Higginbotham JN, Franklin JL, Ham AJ, Halvey PJ, Imasuen IE, et al. Proteomic analysis of exosomes from mutant KRAS colon cancer cells identifies intercellular transfer of mutant KRAS. Mol Cell Proteomics. 2013;12(2):343-55.

187. Buratta S, Urbanelli L, Sagini K, Giovagnoli S, Caponi S, Fioretto D, et al. Extracellular vesicles released by fibroblasts undergoing H-Ras induced senescence show changes in lipid profile. PLoS One. 2017;12(11):e0188840.

188. Hyenne V, Apaydin A, Rodriguez D, Spiegelhalter C, Hoff-Yoessle S, Diem M, et al. RAL-1 controls multivesicular body biogenesis and exosome secretion. J Cell Biol. 2015;211(1):27-37.

189. Kajimoto T, Mohamed NNI, Badawy SMM, Matovelo SA, Hirase M, Nakamura S, et al. Involvement of Gbetagamma subunits of Gi protein coupled with S1P receptor on multivesicular endosomes in F-actin formation and cargo sorting into exosomes. J Biol Chem. 2018;293(1):245-53.

190. Bhimji EAaSS. Anatomy, Head and Neck, Thyroid: StatPearls Publishing, Treasure Island; 2018

191. Hurlé JG-PaJM. Anatomía humana: McGraw-Hill Interamericana de España S.L; 2003. 1008 p.

192. Barbara Young AS, James S. Lowe and John W. Heath. Wheater´s functional histology: A text and colour atlas: Elsiver; 2007.

193. Dai G, Levy O, Carrasco N. Cloning and characterization of the thyroid iodide transporter. Nature. 1996;379(6564):458-60.

194. Hoermann R, Midgley JE, Larisch R, Dietrich JW. Homeostatic Control of the Thyroid-Pituitary Axis: Perspectives for Diagnosis and Treatment. Front Endocrinol (Lausanne). 2015

6:177.

195. Johansson E, Andersson L, Ornros J, Carlsson T, Ingeson-Carlsson C, Liang S, et al. Revising the embryonic origin of thyroid C cells in mice and humans. Development. 2015

142(20):3519-28.

196. Bliddal S, Nielsen CH, Feldt-Rasmussen U. Recent advances in understanding autoimmune thyroid disease: the tallest tree in the forest of polyautoimmunity. F1000Res. 2017;6:1776.

197. Iddah MA, Macharia BN. Autoimmune thyroid disorders. ISRN Endocrinol. 2013

2013:509764.

198. Sheu SY, Schmid KW. [Inflammatory diseases of the thyroid gland. Epidemiology, symptoms and morphology]. Pathologe. 2003;24(5):339-47.

199. Takano T. Natural history of thyroid cancer [Review]. Endocr J. 2017;64(3):237-44.

200. Society AC. https://www.cancer.org/cancer/thyroid-cancer/about/key-statistics.html 2018 [

201. Cabanillas ME, McFadden DG, Durante C. Thyroid cancer. Lancet. 2016;388(10061):2783-95.

202. Ma J, Huang M, Wang L, Ye W, Tong Y, Wang H. Obesity and risk of thyroid cancer: evidence from a meta-analysis of 21 observational studies. Med Sci Monit. 2015

21:283-91.

203. Cho A, Chang Y, Ahn J, Shin H, Ryu S. Cigarette smoking and thyroid cancer risk: a cohort study. Br J Cancer. 2018

119(5):638-45.

204. Vigneri R, Malandrino P, Vigneri P. The changing epidemiology of thyroid cancer: why is incidence increasing? Curr Opin Oncol. 2015;27(1):1-7.

205. Zhang Y, Zhu Y, Risch HA. Changing incidence of thyroid cancer. JAMA. 2006;296(11):1350; author reply

206. Schlumberger MJ. Papillary and follicular thyroid carcinoma. N Engl J Med. 1998;338(5):297-306.

207. Bryan R. Haugen EKA, Keith C. Bible, Gerard M. Doherty, Susan J. Mandel, Yuri E. Nikiforov, Furio Pacini, Gregory W. Randolph, Anna M. Sawka, Martin Schlumberger, Kathryn Schuff, Steven I. Sherman, Julie Ann Sosa, David L. Steward, R. Michael Tuttle and Leonard Wartofsky. 2015 American thyroid Asocciation Management Guidelines for adult patients with thyroid nodules and differentiated thyroid cancer. American thyroid Asociation. 2015.

208. Gharib H, Papini E. Thyroid nodules: clinical importance, assessment, and treatment. Endocrinol Metab Clin North Am. 2007;36(3):707-35, vi.

209. Cibas ES, Ali SZ. The 2017 Bethesda System for Reporting Thyroid Cytopathology. Thyroid. 2017;27(11):1341-6.

210. Wesola M, Jelen M. Bethesda System in the evaluation of thyroid nodules: Review. Adv Clin Exp Med. 2017;26(1):177-82.

211. Park HJ, Moon JH, Yom CK, Kim KH, Choi JY, Choi SI, et al. Thyroid "atypia of undetermined significance" with nuclear atypia has high rates of malignancy and BRAF mutation. Cancer Cytopathol. 2014;122(7):512-20.

212. Nikiforov YE, Ohori NP, Hodak SP, Carty SE, LeBeau SO, Ferris RL, et al. Impact of mutational testing on the diagnosis and management of patients with cytologically indeterminate thyroid nodules: a prospective analysis of 1056 FNA samples. J Clin Endocrinol Metab. 2011;96(11):3390-7.

213. Alexander EK, Kennedy GC, Baloch ZW, Cibas ES, Chudova D, Diggans J, et al. Preoperative diagnosis of benign thyroid nodules with indeterminate cytology. N Engl J Med. 2012;367(8):705-15.

214. Nikiforov YE, Ohori NP, Hodak SP, Carty SE, LeBeau SO, Ferris RL, et al. Impact of mutational testing on the diagnosis and management of patients with cytologically indeterminate thyroid nodules: a prospective analysis of 1056 FNA samples. J Clin Endocrinol Metab.96(11):3390-7.

215. Nikiforov YE, Steward DL, Robinson-Smith TM, Haugen BR, Klopper JP, Zhu Z, et al. Molecular testing for mutations in improving the fine-needle aspiration diagnosis of thyroid nodules. J Clin Endocrinol Metab. 2009;94(6):2092-8.

216. An JH, Song KH, Kim SK, Park KS, Yoo YB, Yang JH, et al. RAS mutations in indeterminate thyroid nodules are predictive of the follicular variant of papillary thyroid carcinoma. Clin Endocrinol (Oxf). 2014;82(5):760-6.

217. Patel SG, Carty SE, McCoy KL, Ohori NP, LeBeau SO, Seethala RR, et al. Preoperative detection of RAS mutation may guide extent of thyroidectomy. Surgery. 2017;161(1):168-75.

218. Fukahori M, Yoshida A, Hayashi H, Yoshihara M, Matsukuma S, Sakuma Y, et al. The associations between RAS mutations and clinical characteristics in follicular thyroid tumors: new insights from a single center and a large patient cohort. Thyroid. 2012;22(7):683-9.

219. Suarez HG, du Villard JA, Severino M, Caillou B, Schlumberger M, Tubiana M, et al. Presence of mutations in all three ras genes in human thyroid tumors. Oncogene. 1990;5(4):565-70.

220. Vasko V, Ferrand M, Di Cristofaro J, Carayon P, Henry JF, de Micco C. Specific pattern of RAS oncogene mutations in follicular thyroid tumors. J Clin Endocrinol Metab. 2003;88(6):2745-52.

221. Esapa CT, Johnson SJ, Kendall-Taylor P, Lennard TW, Harris PE. Prevalence of Ras mutations in thyroid neoplasia. Clin Endocrinol (Oxf). 1999;50(4):529-35.

222. Nikiforov YE, Ohori NP, Hodak SP, Carty SE, LeBeau SO, Ferris RL, et al. Impact of mutational testing on the diagnosis and management of patients with cytologically indeterminate thyroid nodules: a prospective analysis of 1056 FNA samples. J Clin Endocrinol Metab. 2011

96(11):3390-7.

223. Borowczyk M, Szczepanek-Parulska E, Olejarz M, Wieckowska B, Verburg FA, Debicki S, et al. Evaluation of 167 Gene Expression Classifier (GEC) and ThyroSeq v2 Diagnostic Accuracy in the Preoperative Assessment of Indeterminate Thyroid Nodules: Bivariate/HROC Meta-analysis. Endocr Pathol. 2018.

224. Sumana BS, Shashidhar S, Shivarudrappa AS. Galectin-3 Immunohistochemical Expression in Thyroid Neoplasms. J Clin Diagn Res. 2015;9(11):EC07-11.

225. Sherman SI. Thyroid carcinoma. Lancet. 2003;361(9356):501-11.

226. Stamatakos M, Paraskeva P, Stefanaki C, Katsaronis P, Lazaris A, Safioleas K, et al. Medullary thyroid carcinoma: The third most common thyroid cancer reviewed. Oncol Lett. 2011;2(1):49-53.

227. Grimm D. Current Knowledge in Thyroid Cancer-From Bench to Bedside. Int J Mol Sci. 2017;18(7).

228. Lubitz CC, Sosa JA. The changing landscape of papillary thyroid cancer: Epidemiology, management, and the implications for patients. Cancer. 2016;122(24):3754-9.

229. Cameselle-Teijeiro JM, Sobrinho-Simoes M. New WHO classification of thyroid tumors: a pragmatic categorization of thyroid gland neoplasms. Endocrinol Diabetes Nutr. 2018;65(3):133-5.

230. Qubain SW, Nakano S, Baba M, Takao S, Aikou T. Distribution of lymph node micrometastasis in pN0 well-differentiated thyroid carcinoma. Surgery. 2002;131(3):249-56.

231. Arturi F, Russo D, Giuffrida D, Ippolito A, Perrotti N, Vigneri R, et al. Early diagnosis by genetic analysis of differentiated thyroid cancer metastases in small lymph nodes. J Clin Endocrinol Metab. 1997;82(5):1638-41.

232. Parameswaran R, Shulin Hu J, Min En N, Tan WB, Yuan NK. Patterns of metastasis in follicular thyroid carcinoma and the difference between early and delayed presentation. Ann R Coll Surg Engl. 2017;99(2):151-4.

233. Ahmadi S, Stang M, Jiang XS, Sosa JA. Hurthle cell carcinoma: current perspectives. Onco Targets Ther. 2016;9:6873-84.

234. Bhattacharyya N. Survival and prognosis in Hurthle cell carcinoma of the thyroid gland. Arch Otolaryngol Head Neck Surg. 2003;129(2):207-10.

235. Matsuzu K, Sugino K, Masudo K, Nagahama M, Kitagawa W, Shibuya H, et al. Thyroid lobectomy for papillary thyroid cancer: long-term follow-up study of 1,088 cases. World J Surg. 2014;38(1):68-79.

236. Barney BM, Hitchcock YJ, Sharma P, Shrieve DC, Tward JD. Overall and cause-specific survival for patients undergoing lobectomy, near-total, or total thyroidectomy for differentiated thyroid cancer. Head Neck. 2011;33(5):645-9.

237. Mendelsohn AH, Elashoff DA, Abemayor E, St John MA. Surgery for papillary thyroid carcinoma: is lobectomy enough? Arch Otolaryngol Head Neck Surg. 2010;136(11):1055-61.

238. Haigh PI, Urbach DR, Rotstein LE. Extent of thyroidectomy is not a major determinant of survival in low- or high-risk papillary thyroid cancer. Ann Surg Oncol. 2005;12(1):81-9.

239. Tuttle RM. Controversial Issues in Thyroid Cancer Management. J Nucl Med. 2018;59(8):1187-94.

240. Patel KN, Shaha AR. Poorly differentiated and anaplastic thyroid cancer. Cancer Control. 2006;13(2):119-28.

241. Xu B, Ghossein R. Genomic Landscape of poorly Differentiated and Anaplastic Thyroid Carcinoma. Endocr Pathol. 2016;27(3):205-12.

242. LLoyd. WHO Classification of Tumours of Endocrine Organs, 4th Edition2017.

243. Besic N, Gazic B. Sites of metastases of anaplastic thyroid carcinoma: autopsy findings in 45 cases from a single institution. Thyroid. 2013;23(6):709-13.

244. Cabanillas ME, Zafereo M, Gunn GB, Ferrarotto R. Anaplastic Thyroid Carcinoma: Treatment in the Age of Molecular Targeted Therapy. J Oncol Pract.12(6):511-8.

245. Landa I, Ibrahimpasic T, Boucai L, Sinha R, Knauf JA, Shah RH, et al. Genomic and transcriptomic hallmarks of poorly differentiated and anaplastic thyroid cancers. J Clin Invest. 2016;126(3):1052-66.

246. Wiseman SM, Loree TR, Hicks WL, Jr., Rigual NR, Winston JS, Tan D, et al. Anaplastic thyroid cancer evolved from papillary carcinoma: demonstration of anaplastic transformation by means of the inter-simple sequence repeat polymerase chain reaction. Arch Otolaryngol Head Neck Surg. 2003;129(1):96-100.

247. Takano T, Amino N. Fetal cell carcinogenesis: a new hypothesis for better understanding of thyroid carcinoma. Thyroid. 2005;15(5):432-8.

248. Network CGAR. Integrated genomic characterization of papillary thyroid carcinoma. Cell. 2014;159(3):676-90.

249. Kunstman JW, Juhlin CC, Goh G, Brown TC, Stenman A, Healy JM, et al. Characterization of the mutational landscape of anaplastic thyroid cancer via whole-exome sequencing. Hum Mol Genet. 2015;24(8):2318-29.

250. Riesco-Eizaguirre G, Santisteban P. ENDOCRINE TUMOURS: Advances in the molecular pathogenesis of thyroid cancer: lessons from the cancer genome. Eur J Endocrinol. 2016;175(5):R203-17.

251. Nikiforov YE. Thyroid carcinoma: molecular pathways and therapeutic targets. Mod Pathol. 2008;21 Suppl 2:S37-43.

252. Howell GM, Hodak SP, Yip L. RAS mutations in thyroid cancer. Oncologist. 2013;18(8):926-32.

253. Insilla AC, Proietti A, Borrelli N, Macerola E, Niccoli C, Vitti P, et al. TERT promoter mutations and their correlation with BRAF and RAS mutations in a consecutive cohort of 145 thyroid cancer cases. Oncol Lett. 2018;15(3):2763-70.

254. Krishnamoorthy GP, Davidson NR, Leach SD, Zhao Z, Lowe SW, Lee G, et al. EIF1AX and RAS mutations cooperate to drive thyroid tumorigenesis through ATF4 and c-MYC. Cancer Discov. 2018.

255. Lakshmanan A, Scarberry D, Shen DH, Jhiang SM. Modulation of sodium iodide symporter in thyroid cancer. Horm Cancer. 2014;5(6):363-73.

256. Hong D, Ye L, Gagel R, Chintala L, El Naggar AK, Wright J, et al. Medullary thyroid cancer: targeting the RET kinase pathway with sorafenib/tipifarnib. Mol Cancer Ther. 2008;7(5):1001-6.

257. Santoro M, Melillo RM, Carlomagno F, Vecchio G, Fusco A. Minireview: RET: normal and abnormal functions. Endocrinology. 2004;145(12):5448-51.

258. Finn SP, Smyth P, O'Leary J, Sweeney EC, Sheils O. Ret/PTC chimeric transcripts in an Irish cohort of sporadic papillary thyroid carcinoma. J Clin Endocrinol Metab. 2003;88(2):938-41.

259. Ishizaka Y, Kobayashi S, Ushijima T, Hirohashi S, Sugimura T, Nagao M. Detection of retTPC/PTC transcripts in thyroid adenomas and adenomatous goiter by an RT-PCR method. Oncogene. 1991;6(9):1667-72.

260. Greco A, Miranda C, Pierotti MA. Rearrangements of NTRK1 gene in papillary thyroid carcinoma. Mol Cell Endocrinol. 2010;321(1):44-9.

261. Chou A, Fraser S, Toon CW, Clarkson A, Sioson L, Farzin M, et al. A detailed clinicopathologic study of ALK-translocated papillary thyroid carcinoma. Am J Surg Pathol. 2015;39(5):652-9.

262. Raman P, Koenig RJ. Pax-8-PPAR-gamma fusion protein in thyroid carcinoma. Nat Rev Endocrinol. 2014;10(10):616-23.

263. Placzkowski KA, Reddi HV, Grebe SK, Eberhardt NL, McIver B. The Role of the PAX8/PPARgamma Fusion Oncogene in Thyroid Cancer. PPAR Res. 2008;2008:672829.

264. Garnett MJ, Marais R. Guilty as charged: B-RAF is a human oncogene. Cancer Cell. 2004;6(4):313-9.

265. Roskoski R, Jr. RAF protein-serine/threonine kinases: structure and regulation. Biochem Biophys Res Commun. 2010;399(3):313-7.

266. Lee SE, Hwang TS, Choi YL, Han HS, Kim WS, Jang MH, et al. Prognostic Significance of TERT Promoter Mutations in Papillary Thyroid Carcinomas in a BRAF(V600E) Mutation-Prevalent Population. Thyroid. 2013;26(7):901-10.

267. Liu X, Bishop J, Shan Y, Pai S, Liu D, Murugan AK, et al. Highly prevalent TERT promoter mutations in aggressive thyroid cancers. Endocr Relat Cancer. 2013;20(4):603-10.

268. Landa I, Ganly I, Chan TA, Mitsutake N, Matsuse M, Ibrahimpasic T, et al. Frequent somatic TERT promoter mutations in thyroid cancer: higher prevalence in advanced forms of the disease. J Clin Endocrinol Metab. 2013;98(9):E1562-6.

269. Afkhami M, Karunamurthy A, Chiosea S, Nikiforova MN, Seethala R, Nikiforov YE, et al. Histopathologic and Clinical Characterization of Thyroid Tumors Carrying the BRAF(K601E) Mutation. Thyroid. 2016;26(2):242-7.

270. Trovisco V, Vieira de Castro I, Soares P, Maximo V, Silva P, Magalhaes J, et al. BRAF mutations are associated with some histological types of papillary thyroid carcinoma. J Pathol. 2004;202(2):247-51.

271. Hou P, Liu D, Shan Y, Hu S, Studeman K, Condouris S, et al. Genetic alterations and their relationship in the phosphatidylinositol 3-kinase/Akt pathway in thyroid cancer. Clin Cancer Res. 2007;13(4):1161-70.

272. Garcia-Rostan G, Costa AM, Pereira-Castro I, Salvatore G, Hernandez R, Hermsem MJ, et al. Mutation of the PIK3CA gene in anaplastic thyroid cancer. Cancer Res. 2005;65(22):10199-207.

273. Sastre-Perona A, Santisteban P. Role of the wnt pathway in thyroid cancer. Front Endocrinol (Lausanne). 2012;3:31.

274. Manzella L, Stella S, Pennisi MS, Tirro E, Massimino M, Romano C, et al. New Insights in Thyroid Cancer and p53 Family Proteins. Int J Mol Sci. 2017;18(6).

275. Malumbres M, Barbacid M. RAS oncogenes: the first 30 years. Nat Rev Cancer. 2003;3(6):459-65.

276. Garcia-Rostan G, Zhao H, Camp RL, Pollan M, Herrero A, Pardo J, et al. ras mutations are associated with aggressive tumor phenotypes and poor prognosis in thyroid cancer. J Clin Oncol. 2003;21(17):3226-35.

277. Wright PA, Lemoine NR, Mayall ES, Wyllie FS, Hughes D, Williams ED, et al. Papillary and follicular thyroid carcinomas show a different pattern of ras oncogene mutation. Br J Cancer. 1989;60(4):576-7.

278. Challeton C, Bounacer A, Du Villard JA, Caillou B, De Vathaire F, Monier R, et al. Pattern of ras and gsp oncogene mutations in radiation-associated human thyroid tumors. Oncogene. 1995;11(3):601-3.

279. Ricarte-Filho JC, Ryder M, Chitale DA, Rivera M, Heguy A, Ladanyi M, et al. Mutational profile of advanced primary and metastatic radioactive iodine-refractory thyroid cancers reveals distinct pathogenetic roles for BRAF, PIK3CA, and AKT1. Cancer Res. 2009;69(11):4885-93.

280. Volante M, Rapa I, Gandhi M, Bussolati G, Giachino D, Papotti M, et al. RAS mutations are the predominant molecular alteration in poorly differentiated thyroid carcinomas and bear prognostic impact. J Clin Endocrinol Metab. 2009;94(12):4735-41.

281. Karga H, Lee JK, Vickery AL, Jr., Thor A, Gaz RD, Jameson JL. Ras oncogene mutations in benign and malignant thyroid neoplasms. J Clin Endocrinol Metab. 1991;73(4):832-6.

282. Basolo F, Pisaturo F, Pollina LE, Fontanini G, Elisei R, Molinaro E, et al. N-ras mutation in poorly differentiated thyroid carcinomas: correlation with bone metastases and inverse correlation to thyroglobulin expression. Thyroid. 2000;10(1):19-23.

283. Herrero A, Reis-Cardoso M, Jimenez-Gomez I, Doherty C, Agudo-Ibanez L, Pinto A, et al. Characterisation of HRas local signal transduction networks using engineered site-specific exchange factors. Small GTPases. 2017:1-13.

284. Arozarena I, Matallanas D, Berciano MT, Sanz-Moreno V, Calvo F, Munoz MT, et al. Activation of H-Ras in the endoplasmic reticulum by the RasGRF family guanine nucleotide exchange factors. Mol Cell Biol. 2004;24(4):1516-30.

285. Swift AM, Machamer CE. A Golgi retention signal in a membrane-spanning domain of coronavirus E1 protein. J Cell Biol. 1991;115(1):19-30.

286. Townsley FM, Wilson DW, Pelham HR. Mutational analysis of the human KDEL receptor: distinct structural requirements for Golgi retention, ligand binding and retrograde transport. EMBO J. 1993;12(7):2821-9.

287. Littman DR, Thomas Y, Maddon PJ, Chess L, Axel R. The isolation and sequence of the gene encoding T8: a molecule defining functional classes of T lymphocytes. Cell. 1985;40(2):237-46.

288. Einhauer A, Jungbauer A. The FLAG peptide, a versatile fusion tag for the purification of recombinant proteins. J Biochem Biophys Methods. 2001;49(1-3):455-65.

289. Schembri L, Dalibart R, Tomasello F, Legembre P, Ichas F, De Giorgi F. The HA tag is cleaved and loses immunoreactivity during apoptosis. Nat Methods. 2007;4(2):107-8.

290. Fusco A, Berlingieri MT, Di Fiore PP, Portella G, Grieco M, Vecchio G. One- and two-step transformations of rat thyroid epithelial cells by retroviral oncogenes. Mol Cell Biol. 1987;7(9):3365-70.

291. Saavedra HI, Knauf JA, Shirokawa JM, Wang J, Ouyang B, Elisei R, et al. The RAS oncogene induces genomic instability in thyroid PCCL3 cells via the MAPK pathway. Oncogene. 2000;19(34):3948-54.

292. Sastre-Perona A, Riesco-Eizaguirre G, Zaballos MA, Santisteban P. beta-catenin signaling is required for RAS-driven thyroid cancer through PI3K activation. Oncotarget. 2016;7(31):49435-49.

293. Puxeddu E, Knauf JA, Sartor MA, Mitsutake N, Smith EP, Medvedovic M, et al. RET/PTC-induced gene expression in thyroid PCCL3 cells reveals early activation of genes involved in regulation of the immune response. Endocr Relat Cancer. 2005;12(2):319-34.

294. Garg M, Okamoto R, Nagata Y, Kanojia D, Venkatesan S, M TA, et al. Establishment and characterization of novel human primary and metastatic anaplastic thyroid cancer cell lines and their genomic evolution over a year as a primagraft. J Clin Endocrinol Metab. 2015;100(2):725-35.

295. Lee JJ, Foukakis T, Hashemi J, Grimelius L, Heldin NE, Wallin G, et al. Molecular cytogenetic profiles of novel and established human anaplastic thyroid carcinoma models. Thyroid. 2007;17(4):289-301.

296. Rampersad SN. Multiple applications of Alamar Blue as an indicator of metabolic function and cellular health in cell viability bioassays. Sensors (Basel). 2012;12(9):12347-60.

297. Subauste MC, Kupriyanova TA, Conn EM, Ardi VC, Quigley JP, Deryugina EI. Evaluation of metastatic and angiogenic potentials of human colon carcinoma cells in chick embryo model systems. Clin Exp Metastasis. 2009;26(8):1033-47.

298. Liu M, Scanlon CS, Banerjee R, Russo N, Inglehart RC, Willis AL, et al. The Histone Methyltransferase EZH2 Mediates Tumor Progression on the Chick Chorioallantoic Membrane Assay, a Novel Model of Head and Neck Squamous Cell Carcinoma. Transl Oncol. 2017;6(3):273-81.

299. Crespo P, Casar B. The Chick Embryo Chorioallantoic Membrane as an in vivo Model to Study Metastasis. Bio-protocol. 2016;6(20):e1962.

300. Tham E, Gielen AW, Khademi M, Martin C, Piehl F. Decreased expression of VEGF-A in rat experimental autoimmune encephalomyelitis and in cerebrospinal fluid mononuclear cells from patients with multiple sclerosis. Scand J Immunol. 2006;64(6):609-22.

301. Vestad B, Llorente A, Neurauter A, Phuyal S, Kierulf B, Kierulf P, et al. Size and concentration analyses of extracellular vesicles by nanoparticle tracking analysis: a variation study. J Extracell Vesicles. 2017;6(1):1344087.

302. Cancer Genome Atlas Research N. Integrated genomic characterization of papillary thyroid carcinoma. Cell. 2014;159(3):676-90.

303. Zhou D, Li Z, Bai X. BRAFV600E and RET/PTC Promote Proliferation and Migration of Papillary Thyroid Carcinoma Cells In Vitro by Regulating Nuclear Factor-kappaB. Med Sci Monit. 2017;23:5321-9.

304. Riesco-Eizaguirre G, Rodriguez I, De la Vieja A, Costamagna E, Carrasco N, Nistal M, et al. The BRAFV600E oncogene induces transforming growth factor beta secretion leading to sodium iodide symporter repression and increased malignancy in thyroid cancer. Cancer Res. 2009;69(21):8317-25.

305. Herrero A, Casar B, Colon-Bolea P, Agudo-Ibanez L, Crespo P. Defined spatiotemporal features of RAS-ERK signals dictate cell fate in MCF-7 mammary epithelial cells. Mol Biol Cell. 2016;27(12):1958-68.

306. Daum JR, Gorbsky GJ. Casein kinase II catalyzes a mitotic phosphorylation on threonine 1342 of human DNA topoisomerase IIalpha, which is recognized by the 3F3/2 phosphoepitope antibody. J Biol Chem. 1998;273(46):30622-9.

307. Shirokawa JM, Elisei R, Knauf JA, Hara T, Wang J, Saavedra HI, et al. Conditional apoptosis induced by oncogenic ras in thyroid cells. Mol Endocrinol. 2000;14(11):1725-38.

308. Pylayeva-Gupta Y, Grabocka E, Bar-Sagi D. RAS oncogenes: weaving a tumorigenic web. Nat Rev Cancer. 2011;11(11):761-74.

309. Tajiri H, Uruno T, Shirai T, Takaya D, Matsunaga S, Setoyama D, et al. Targeting Ras-Driven Cancer Cell Survival and Invasion through Selective Inhibition of DOCK1. Cell Rep. 2017;19(5):969-80.

310. Buchanan FG, McReynolds M, Couvillon A, Kam Y, Holla VR, Dubois RN, et al. Requirement of phospholipase D1 activity in H-RasV12-induced transformation. Proc Natl Acad Sci U S A. 2005;102(5):1638-42.

311. Herrero A, Pinto A, Colon-Bolea P, Casar B, Jones M, Agudo-Ibanez L, et al. Small Molecule Inhibition of ERK Dimerization Prevents Tumorigenesis by RAS-ERK Pathway Oncogenes. Cancer Cell. 2015;28(2):170-82.

312. Deryugina EI, Zijlstra A, Partridge JJ, Kupriyanova TA, Madsen MA, Papagiannakopoulos T, et al. Unexpected effect of matrix metalloproteinase down-regulation on vascular intravasation and metastasis of human fibrosarcoma cells selected in vivo for high rates of dissemination. Cancer Res. 2005;65(23):10959-69.

313. Menen R, Pinney E, Hassanein MK, Kolostova K, Bobek V, Suetsugu A, et al. Inhibition of metastasis of circulating human prostate cancer cells in the chick embryo by an extracellular matrix produced by foreskin fibroblasts in culture. Anticancer Res. 2012;32(5):1573-7.

314. Deryugina EI, Quigley JP. Chick embryo chorioallantoic membrane model systems to study and visualize human tumor cell metastasis. Histochem Cell Biol. 2008;130(6):1119-30.

315. Herrmann A, Moss D, See V. The Chorioallantoic Membrane of the Chick Embryo to Assess Tumor Formation and Metastasis. Methods Mol Biol. 2016;1464:97-105.

316. Ribatti D. The chick embryo chorioallantoic membrane (CAM). A multifaceted experimental model. Mech Dev. 2016;141:70-7.

317. Morrison JA, Pike LA, Lund G, Zhou Q, Kessler BE, Bauerle KT, et al. Characterization of thyroid cancer cell lines in murine orthotopic and intracardiac metastasis models. Horm Cancer. 2015;6(2-3):87-99.

318. Maia J, Caja S, Strano Moraes MC, Couto N, Costa-Silva B. Exosome-Based Cell-Cell Communication in the Tumor Microenvironment. Front Cell Dev Biol. 2018;6:18.

319. Luo D, Zhan S, Xia W, Huang L, Ge W, Wang T. Proteomics study of serum exosomes from papillary thyroid cancer patients. Endocr Relat Cancer. 2018;25(10):879-91.

320. Lajoie P, Guay G, Dennis JW, Nabi IR. The lipid composition of autophagic vacuoles regulates expression of multilamellar bodies. J Cell Sci. 2005;118(Pt 9):1991-2003.

321. Carone DM, Lawrence JB. Heterochromatin instability in cancer: from the Barr body to satellites and the nuclear periphery. Semin Cancer Biol. 2013;23(2):99-108.

322. Orsolic I, Jurada D, Pullen N, Oren M, Eliopoulos AG, Volarevic S. The relationship between the nucleolus and cancer: Current evidence and emerging paradigms. Semin Cancer Biol. 2016;37-38:36-50.

323. Garcia-Sanz P, Orgaz L, Fuentes JM, Vicario C, Moratalla R. Cholesterol and multilamellar bodies: Lysosomal dysfunction in GBA-Parkinson disease. Autophagy. 2018;14(4):717-8.

324. Eitan E, Suire C, Zhang S, Mattson MP. Impact of lysosome status on extracellular vesicle content and release. Ageing Res Rev. 2016;32:65-74.

325. Fehrenbacher N, Philips M. Intracellular signaling: peripatetic Ras. Curr Biol. 2009;19(11):R454-7.

326. Xing M. Clinical utility of RAS mutations in thyroid cancer: a blurred picture now emerging clearer. BMC Med. 2016;14:12.

327. Tape CJ, Ling S, Dimitriadi M, McMahon KM, Worboys JD, Leong HS, et al. Oncogenic KRAS Regulates Tumor Cell Signaling via Stromal Reciprocation. Cell. 2016;165(7):1818.

328. Montanaro L, Trere D, Derenzini M. Nucleolus, ribosomes, and cancer. Am J Pathol. 2008;173(2):301-10.

329. Lindstrom MS, Jurada D, Bursac S, Orsolic I, Bartek J, Volarevic S. Nucleolus as an emerging hub in maintenance of genome stability and cancer pathogenesis. Oncogene. 2018;37(18):2351-66.

330. Diesch J, Hannan RD, Sanij E. Perturbations at the ribosomal genes loci are at the centre of cellular dysfunction and human disease. Cell Biosci. 2014;4:43.

331. Derenzini M, Trere D, Pession A, Govoni M, Sirri V, Chieco P. Nucleolar size indicates the rapidity of cell proliferation in cancer tissues. J Pathol. 2000;191(2):181-6.

332. Galluzzi L, Vitale I, Abrams JM, Alnemri ES, Baehrecke EH, Blagosklonny MV, et al. Molecular definitions of cell death subroutines: recommendations of the Nomenclature Committee on Cell Death 2012. Cell Death Differ. 2012;19(1):107-20.

333. Vitale I, Galluzzi L, Castedo M, Kroemer G. Mitotic catastrophe: a mechanism for avoiding genomic instability. Nat Rev Mol Cell Biol. 2011;12(6):385-92.

334. Mc Gee MM. Targeting the Mitotic Catastrophe Signaling Pathway in Cancer. Mediators Inflamm. 2015;2015:146282.

335. Yadav S, Puri S, Linstedt AD. A primary role for Golgi positioning in directed secretion, cell polarity, and wound healing. Mol Biol Cell. 2009;20(6):1728-36.

336. Farhan H, Wendeler MW, Mitrovic S, Fava E, Silberberg Y, Sharan R, et al. MAPK signaling to the early secretory pathway revealed by kinase/phosphatase functional screening. J Cell Biol. 2010;189(6):997-1011.

337. Bisel B, Wang Y, Wei JH, Xiang Y, Tang D, Miron-Mendoza M, et al. ERK regulates Golgi and centrosome orientation towards the leading edge through GRASP65. J Cell Biol. 2008;182(5):837-43.

338. Agudo-Ibanez L, Nunez F, Calvo F, Berenjeno IM, Bustelo XR, Crespo P. Transcriptomal profiling of site-specific Ras signals. Cell Signal. 2007;19(11):2264-76.

339. Sun Y, Zhang D, Guo X, Li W, Li C, Luo J, et al. MKK3 modulates JNK-dependent cell migration and invasion. Cell Death Dis. 2019;10(3):149.

340. Cai J, Du S, Wang H, Xin B, Wang J, Shen W, et al. Tenascin-C induces migration and invasion through JNK/c-Jun signalling in pancreatic cancer. Oncotarget. 2017;8(43):74406-22.

341. Li Y, Zhang M, Dorfman RG, Pan Y, Tang D, Xu L, et al. SIRT2 Promotes the Migration and Invasion of Gastric Cancer through RAS/ERK/JNK/MMP-9 Pathway by Increasing PEPCK1-Related Metabolism. Neoplasia. 2018;20(7):745-56.

342. Janknecht R, Ernst WH, Nordheim A. SAP1a is a nuclear target of signaling cascades involving ERKs. Oncogene. 1995;10(6):1209-16.

343. Whitmarsh AJ, Shore P, Sharrocks AD, Davis RJ. Integration of MAP kinase signal transduction pathways at the serum response element. Science. 1995;269(5222):403-7.

344. Strahl T, Gille H, Shaw PE. Selective response of ternary complex factor Sap1a to different mitogen-activated protein kinase subgroups. Proc Natl Acad Sci U S A. 1996;93(21):11563-8.

345. Cao Y, Li H, Deb S, Liu JP. TERT regulates cell survival independent of telomerase enzymatic activity. Oncogene. 2002;21(20):3130-8.

346. Liu H, Liu Q, Ge Y, Zhao Q, Zheng X, Zhao Y. hTERT promotes cell adhesion and migration independent of telomerase activity. Sci Rep. 2016;6:22886.

347. Muller PA, Vousden KH. p53 mutations in cancer. Nat Cell Biol. 2013;15(1):2-8.

348. Pitoia F, Miyauchi A. 2015 American Thyroid Association Guidelines for Thyroid Nodules and Differentiated Thyroid Cancer and Their Implementation in Various Care Settings. Thyroid. 2016;26(2):319-21.

349. Schmitz G, Muller G. Structure and function of lamellar bodies, lipid-protein complexes involved in storage and secretion of cellular lipids. J Lipid Res. 1991;32(10):1539-70.

350. Feingold KR. Lamellar bodies: the key to cutaneous barrier function. J Invest Dermatol. 2012;132(8):1951-3.

351. Polenov AL, Garlov PE. The hypothalamo-hypophysial system in Acipenseridae. I. Ultrastructural organization of large neurosecretory terminals (Herring bodies) and axoventricular contacts. Z Zellforsch Mikrosk Anat. 1971;116(3):349-74.

352. Rothman JE, Wieland FT. Protein sorting by transport vesicles. Science. 1996;272(5259):227-34.

353. Spanel-Borowski K, Nowicki M, Borlak J, Trapphoff T, Eichenlaub-Ritter U. Endoplasmic reticulum-derived multilamellar bodies in oocytes of mouse follicle cultures under oxidized low-density lipoprotein treatment. Cells Tissues Organs. 2013;197(1):77-88.

354. Cooper JR, Abdullatif MB, Burnett EC, Kempsell KE, Conforti F, Tolley H, et al. Long Term Culture of the A549 Cancer Cell Line Promotes Multilamellar Body Formation and Differentiation towards an Alveolar Type II Pneumocyte Phenotype. PLoS One. 2016;11(10):e0164438.

355. Maae E, Nielsen M, Steffensen KD, Jakobsen EH, Jakobsen A, Sorensen FB. Estimation of immunohistochemical expression of VEGF in ductal carcinomas of the breast. J Histochem Cytochem. 2011;59(8):750-60.

356. Choi MR, Yoo NJ, Lee SH, An CH. Frameshift mutation of an angiogenesis factor VEGFB and its mutational heterogeneity in colorectal cancers. Pathol Oncol Res. 2015;21(3):853-5.

357. Shintani S, Li C, Ishikawa T, Mihara M, Nakashiro K, Hamakawa H. Expression of vascular endothelial growth factor A, B, C, and D in oral squamous cell carcinoma. Oral Oncol. 2004;40(1):13-20.

358. Albrecht I, Kopfstein L, Strittmatter K, Schomber T, Falkevall A, Hagberg CE, et al. Suppressive effects of vascular endothelial growth factor-B on tumor growth in a mouse model of pancreatic neuroendocrine tumorigenesis. PLoS One. 2010;5(11):e14109.

359. Colombo M, Moita C, van Niel G, Kowal J, Vigneron J, Benaroch P, et al. Analysis of ESCRT functions in exosome biogenesis, composition and secretion highlights the heterogeneity of extracellular vesicles. J Cell Sci. 2013;126(Pt 24):5553-65.

360. Stuffers S, Sem Wegner C, Stenmark H, Brech A. Multivesicular endosome biogenesis in the absence of ESCRTs. Traffic. 2009;10(7):925-37.

361. Sun S, Zhou X, Zhang W, Gallick GE, Kuang J. Unravelling the pivotal role of Alix in MVB sorting and silencing of the activated EGFR. Biochem J. 2015;466(3):475-87.

362. Yoshioka Y, Konishi Y, Kosaka N, Katsuda T, Kato T, Ochiya T. Comparative marker analysis of extracellular vesicles in different human cancer types. J Extracell Vesicles. 2013;2.

363. Skog J, Wurdinger T, van Rijn S, Meijer DH, Gainche L, Sena-Esteves M, et al. Glioblastoma microvesicles transport RNA and proteins that promote tumour growth and provide diagnostic biomarkers. Nat Cell Biol. 2008;10(12):1470-6.

364. Weidle UH, Birzele F, Kollmorgen G, Ruger R. The Multiple Roles of Exosomes in Metastasis. Cancer Genomics Proteomics. 2017;14(1):1-15.

365. Lindoso RS, Collino F, Vieyra A. Extracellular vesicles as regulators of tumor fate: crosstalk among cancer stem cells, tumor cells and mesenchymal stem cells. Stem Cell Investig. 2017;4:75.

366. Hardin H, Helein H, Meyer K, Robertson S, Zhang R, Zhong W, et al. Thyroid cancer stem-like cell exosomes: regulation of EMT via transfer of lncRNAs. Lab Invest. 2018;98(9):1133-42.

367. Aga M, Bentz GL, Raffa S, Torrisi MR, Kondo S, Wakisaka N, et al. Exosomal HIF1alpha supports invasive potential of nasopharyngeal carcinoma-associated LMP1-positive exosomes. Oncogene. 2014;33(37):4613-22.

368. You Y, Shan Y, Chen J, Yue H, You B, Shi S, et al. Matrix metalloproteinase 13-containing exosomes promote nasopharyngeal carcinoma metastasis. Cancer Sci. 2015;106(12):1669-77.

369. Soldevilla B, Rodriguez M, San Millan C, Garcia V, Fernandez-Perianez R, Gil-Calderon B, et al. Tumor-derived exosomes are enriched in DeltaNp73, which promotes

oncogenic potential in acceptor cells and correlates with patient survival. Hum Mol Genet. 2014;23(2):467-78.

370. Syn N, Wang L, Sethi G, Thiery JP, Goh BC. Exosome-Mediated Metastasis: From Epithelial-Mesenchymal Transition to Escape from Immunosurveillance. Trends Pharmacol Sci. 2016;37(7):606-17.

371. Lobb RJ, Lima LG, Moller A. Exosomes: Key mediators of metastasis and pre-metastatic niche formation. Semin Cell Dev Biol. 2017;67:3-10.

372. Boelens MC, Wu TJ, Nabet BY, Xu B, Qiu Y, Yoon T, et al. Exosome transfer from stromal to breast cancer cells regulates therapy resistance pathways. Cell. 2014;159(3):499-513.

373. Peinado H, Aleckovic M, Lavotshkin S, Matei I, Costa-Silva B, Moreno-Bueno G, et al. Melanoma exosomes educate bone marrow progenitor cells toward a pro-metastatic phenotype through MET. Nat Med. 2012;18(6):883-91.

374. Shentu TP, Huang TS, Cernelc-Kohan M, Chan J, Wong SS, Espinoza CR, et al. Thy-1 dependent uptake of mesenchymal stem cell-derived extracellular vesicles blocks myofibroblastic differentiation. Sci Rep. 2017;7(1):18052.

375. Zheng Y, Liu L, Chen C, Ming P, Huang Q, Li C, et al. The extracellular vesicles secreted by lung cancer cells in radiation therapy promote endothelial cell angiogenesis by transferring miR-23a. PeerJ. 2017;5:e3627.

376. Vidal-Vanaclocha F. The prometastatic microenvironment of the liver. Cancer Microenviron. 2008;1(1):113-29.

377. Braet F, Nagatsuma K, Saito M, Soon L, Wisse E, Matsuura T. The hepatic sinusoidal endothelial lining and colorectal liver metastases. World J Gastroenterol. 2007;13(6):821-5.